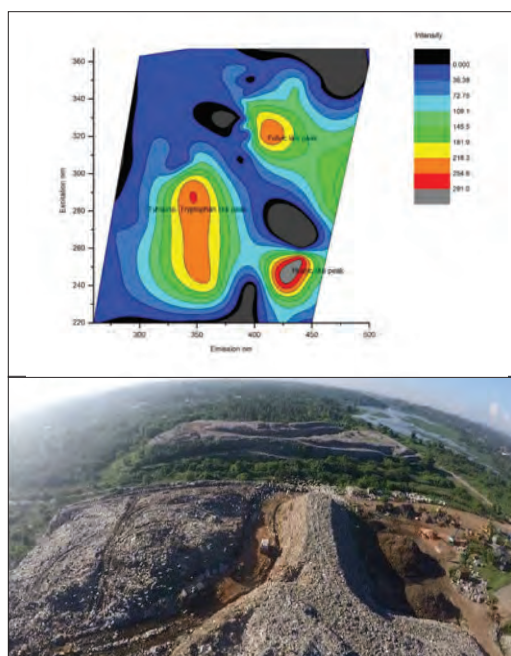




Journal of the National Science Foundation of Sri Lanka





NATIONAL
SCIENCE
FOUNDATION

JOURNAL OF THE NATIONAL SCIENCE FOUNDATION OF SRI LANKA

Editorial Board

Ajit Abeysekera (Editor in Chief)

A. Atputharajah

J.K.D.S. Jayanetti

L.P. Jayatissa

P. Prasad M. Jayaweera

Jagath Manatunge

S.S.N. Perera

Rohini de A. Seneviratne

Saman Seneweera

P. Wijekoon

M.J.S. Wijeyaratne

Language Editor

R.D. Guneratne

Editorial Office

Nadeeja Wickramarachchi (Principal Scientific Officer)

Uthpala T. Karunaratne (Senior Scientific Officer)

Upuli Ratnayake (Scientific Officer)

International Editorial Advisory Board

Chamil Abeykoon, UK

Dilanthi Amaratunga, UK

Dilantha Fernando, Canada

Leslie Gunatilaka, USA

Saman K. Halgamuge, Australia

Kithsiri W. Jayasena, Australia

Vassilios Kapaklis, Sweden

Wah Yun Low, Malaysia

Thomas Mathew, USA

Shanthi Mendis, Switzerland

Javier Francisco Ortega, USA

Malik Peiris, Hong Kong

Kamal Premaratne, USA

Nalin Samarasingha, USA

Ravi Silva, UK

Christopher C. Steel, Australia

Impact Factor : **0.515**

Publication : Published quarterly (March, June, September and December) by the National Science Foundation of Sri Lanka.

Subscription : Foreign : US \$ 75 (SAARC countries)
US \$ 150 (other countries) } inclusive
Local : Rs. 2000 } of airmail
postage

Accepted as standing orders or on a calendar year basis.
Single issues - Available on request;
Rs. 600 per copy

Payment must accompany all orders. Remittances in favour of the National Science Foundation of Sri Lanka.

Manuscripts : Research Articles, Research Communications, Reviews and Correspondence in all fields of Science and Technology may be submitted for consideration for publication. A guide to the preparation of manuscripts is provided in each issue. The guidelines may also be obtained by visiting the NSF website.

No responsibility is assumed by the National Science Foundation of Sri Lanka for statements and opinions expressed by contributors to this Journal.

Manuscripts and all correspondence relating to them should be sent to the Editorial Office, National Science Foundation, 47/5, Maitland Place, Colombo 07, Sri Lanka.

Fax: 94-11- 2694754

E-mail: jnsf@nsf.gov.lk

JNSF home page: <http://www.nsf.gov.lk/index.php/nsf-science-magazine>

Publication : A publication fee of US\$ 150 will be levied for each manuscript except when the corresponding author is affiliated to a Sri Lankan institution.

Copyright : © National Science Foundation of Sri Lanka

Articles in the Journal of the National Science Foundation of Sri Lanka are Open Access articles published under the Creative Commons CC-BY-ND License (<http://creativecommons.org/licenses/by/4.0/>). This license permits use, distribution and reproduction, commercial and non-commercial, provided that the original work is properly cited and is not changed anyway.

Indexing : The JNSF is indexed in Science Citation Index Expanded, Journal Citation Reports/Science Edition, BIOSIS Previews, Zoological Record, Biological Abstracts, Chemical Abstracts, Scopus, TEEAL, Ulrich's, AGRICOLA and EBSCOhost

**JOURNAL OF THE
NATIONAL SCIENCE FOUNDATION
OF SRI LANKA**

Volume 50 Number 1

March 2022

C O N T E N T S

EDITORIAL

- 01 Functions of the review article within scientific discourse**
Ajit Abeysekera
-

RESEARCH ARTICLES

- 03 Micropropagation of *Stevia rebaudiana* (Bertoni) Bertoni using nutrient water of *Cocos nucifera* var. *aurantiaca* (King coconut) as a natural growth enhancer**
HGMK Karunaratna, K Medagama, S Wijesundara and MCM Iqbal
- 13 Estimation of mean considering the joint influence of measurement errors and non-response in two-phase sampling designs**
S Sabir, A Sanaullah and S Gupta
- 27 Induction of somatic embryogenesis from leaf explants of *Exacum trinervium* (L.) Druce (Binara)**
V de Silva and JP Eeswara
- 35 Meta-QTL analysis identified stable quantitative trait loci (QTLs) and associated resistance gene analogues in rice**
HED Shashiprabha, SP Abeyundara and CK Ariyaratna
- 53 Tropical cyclones in the Arabian Sea and the Bay of Bengal: comparison of environmental factors**
G Pathirana and K Priyadarshani
- 65 Determination of safe zone of the mandible for implant and bone harvesting (using CBCT) of mandible in a group of Sri Lankan subjects**
RMAU Dharmapala, DM Satharasinghe, SPI Silva and J Jeyasugiththan
- 73 Increasing the effectiveness of T-junctions with an innovative geometrical and phasing arrangement**
NK Jayasooriya, HLK Perera and JMSJ Bandara
- 87 Vegetative and reproductive phenology of *Cinnamomum verum* J. Presl grown in intermediate climatic zone of Sri Lanka**
ASH Kodikara and AS Kodikara
- 101 Novel nebulizer design with adaptive flow regulation**
U Dampage and M Ariyasinghe

- 111 **Characterization of landfill leachate at the Karadiyana open dumpsite, Sri Lanka, and assessment of water pollution in its vicinity**
PA Koliyabandara, AT Cooray, S Liyanage and C Siriwardhana
- 125 **Optimization of high solids batch anaerobic co-digestion of lignocellulosic biomass and cow dung under mesophilic temperature conditions**
HGMK Karunarathna, K Medagama, S Wijesundara and MCM Iqbal
- 137 **Predominance of phylogenetic group B2 among commensal *Escherichia coli* in humans from Kandy District, Sri Lanka**
BNLD Rangama, CL Abayasekara and DM Gordon
- 151 **Sonication-assisted water extract of *Dendronephthya gigantea* exhibits anti-fine dust effects; attenuation of MAPK phosphorylation in macrophages**
TU Jayawardena, IPS Fernando, DP Nagahawatta, L Wang, HW Yang, JY Oh, KKA Sanjeewa and Y Jeon
- 161 **A novel approach for energy and exergy analysis of a flat plate solar collector with energy storage**
M Hanif, M K Khattak, I Ul Haq, R Uddin and K Ullah-

Guidelines for Contributors



Cover: Fluorescence excitation-emission matrix for Karadiyana leachate dissolved organic matter (top), and bird's-eye view of the Karadiyana Dumpsite (bottom)
See *J.Natn.Sci. Foundation Sri Lanka* 2022 50(1): 111–124

EDITORIAL

Functions of the review article within scientific discourse

In the pre-digital/pre-internet age, when access to primary and secondary sources of scientific literature was not so facile as it is today, the type of Review Article which mainly presented a description of published research on a selected topic, classified in an appropriate manner with a commentary by the author, served an important purpose in enabling entrants to a particular field of research, to obtain a good overview of the topic. This type of article was more in the nature of a survey than a review.

With the availability of search engines such as Google Scholar and Science Direct among others, this type of Review Article has lost much of its value. However, it has to be conceded that they continue to be written by scientists and published by some journals.

The type of Review Article that is of most value today, is one written by an expert in the specific area of the review, who would not only direct the reader to the important primary literature on the topic, but also provide critical insights into the current state of knowledge, relating it to fundamental scientific principles,

particularly highlighting/resolving contradictory or opposing points of view in the literature, and also focus on gaps in knowledge that would be fruitful areas for research in the future.

An important difference in the decision-making process of an editorial board with regard to Review Articles versus Research Articles is that not only the content, but the standing of the authors with respect to their expertise is also evaluated. In other words, the Review Article needs to be *authoritative*. Thus, in order to evaluate their expertise, some journals require the authors to list a specified number of papers published by them which are related most closely to the topic under review, along with their proposal to write a Review Article for the journal. Similarly, the JNSF requires authors of Review Articles to have had a substantial leadership in research supported by a publication track record in the areas covered by the review. It is to be noted that the term “areas covered by the review” is interpreted here in a narrow sense, as being closely related to the topic of the review.

Ajit Abeysekera

RESEARCH ARTICLE

Plant Tissue Culture

Micropropagation of *Stevia rebaudiana* (Bertoni) Bertoni using nutrient water of *Cocos nucifera* var. *aurantiaca* (King coconut) as a natural growth enhancer

HGMK Karunarathna, K Medagama, S Wijesundara and MCM Iqbal*

National Institute of Fundamental Studies, Hanthana Road, Kandy.

Submitted: 15 January 2021; Revised: 22 June 2021; Accepted: 03 August 2021

Abstract: *Stevia rebaudiana* (Bertoni) Bertoni is a herb producing zero-calorie diterpene glycosides in its leaves, which are extensively used as a substitute for sugar since they are about 200 – 400 times sweeter than sucrose. It is an economically important plant in the food and beverage industry around the world. The drawbacks associated with the conventional propagation through seeds and cuttings impede its mass production. Thus, effective *in vitro* micropropagation is advantageous on an industrial scale. Partial media replacement was done to the Murashige and Skoog (MS) medium with water from immature (6 – 7 months from flowering) *Cocos nucifera* var. *aurantiaca* (King coconut). Sterilized young nodal cuttings cultured on the MS medium with 10 % (v/v) coconut water (CW), without any hormones, induced 93.3 % bud break or shoot initiation from the nodes with a mean shoot length of 41.86 ± 0.85 mm. Increasing the CW to 30 % with 0.2 mg/L 6-benzylamino purine (BAP) produced the highest mean number of shoots (9.44 ± 0.51) and the highest number of leaves (8.28 ± 0.81) in three weeks. Modified rooting media incorporating only macronutrients, 0.2 mg/L of indole-3-butyric acid (IBA) and 5 % CW without micronutrients showed the earliest rooting (6.6 days). The highest number of root initiations (13.5) was with $\frac{1}{2}$ MS + 0.2 mg/L IBA + 5 % CW. Regenerated plantlets were successfully hardened and acclimatized in glass jars with compost and sand (1:3 ratio) covered with polypropylene caps under greenhouse conditions. Our results suggest that *Stevia* can be propagated effectively with CW incorporated media and in the future, this could be used in small-scale commercial cultivations.

Keywords: Acclimatization, coconut water, nodal segments, rooting, shooting, *Stevia rebaudiana*.

INTRODUCTION

Stevia rebaudiana (Bertoni) Bertoni is a member of the family Asteraceae that produces zero-calorie diterpene glycosides in its leaves, which can be used as a substitute for sucrose (Megeji *et al.*, 2005; Goyal *et al.*, 2010). According to the reports, sweetness in *Stevia* comes from six compounds: stevioside, rebaudiosides A, D and E and dulcosides A and B (Kohda *et al.*, 1976; Kennelly, 2001) where stevioside acts as the prominent sweetener (Chang *et al.*, 1983). Studies have indicated that these glycosides are 200-400 times sweeter than sucrose (Wölwer-Rieck, 2012; Gupta *et al.*, 2013; Czinkóczy *et al.*, 2018; Chughtai *et al.*, 2020). The plant shows zero glycemic index since the human body is unable to breakdown these glycosides (Brandle *et al.*, 1992; Chughtai *et al.*, 2020). Although, most artificial sweeteners are known to have neurological or renal side effects, *Stevia* is known to have no side effects and is recommended for diabetes patients and has been extensively tested on animals (Megeji *et al.*, 2005). Additionally, it possesses anti-fungal and anti-bacterial properties, and can safely be used in herbal medicine, tonics for diabetic patients, and daily usage since mild *Stevia* leaf offers excellent relief for stomach problems (Momtazi-Borojeni *et al.*, 2017). *Stevia* has recently attained better awareness owing to its superior sweetness and curative values for restraining the deposition of fat and lowering blood pressure in humans (Singh *et al.*, 2005; Kalpana *et al.*, 2009; Chughtai *et al.*,

* Corresponding author (Iqbal.mo@nifs.ac.lk  <https://orcid.org/0000-0002-4862-5099>)



This article is published under the Creative Commons CC-BY-ND License (<http://creativecommons.org/licenses/by-nd/4.0/>). This license permits use, distribution and reproduction, commercial and non-commercial, provided that the original work is properly cited and is not changed in anyway.

2020). Although the plant is native to Paraguay and Southern Brazil, it is now cultivated on a commercial scale for food, beverage, and pharmaceutical products in other countries such as Japan, Taiwan, Korea, Thailand, and Indonesia (Perera *et al.*, 2014). However, it will become a major source of high potency sweetener for the growing natural food market in the future.

Conventional propagation through seeds and cuttings has become unproductive due to inefficient sexual reproduction from self-incompatibility and insufficient pollination (Yadav *et al.*, 2011; Khalil *et al.*, 2014). Cross-pollination promotes heterogeneity in *Stevia* resulting in variability in chemical composition (glycoside) in plant parts (Sakaguchi *et al.*, 1982; Loc *et al.*, 2005; Ramírez-Mosqueda *et al.*, 2016). In addition, seeds lose viability within a short period and the presence of immature embryos result in germination problems (Khalil *et al.*, 2014). Vegetative propagation is limited by the smaller number of plants that can be obtained simultaneously from a single plant due to pathogen accumulation in the tissues (Sakaguchi *et al.*, 1982). Thus, under this scenario, stem cuttings and seed germination are not considered as effective methods to cater to the demand for commercial cultivation.

Micropropagation using plant tissue culture technology is a better option since it is capable of producing large numbers of genetically similar, disease-free plants in a short time under limited space. It is a conventional method of *in vitro* propagation where plants are grown in artificial nutrient media consisting of essential macronutrients, micronutrients, vitamins, amino acids, hormones, and sucrose. *Stevia* has been previously micropropagated with direct organogenesis through shoot tips (Ibrahim *et al.*, 2008; Seema *et al.*, 2011; Pawar *et al.*, 2015), leaves (Jain *et al.*, 2009; Kalpana *et al.*, 2010), nodal segments (Ma *et al.*, 2008; Seema *et al.*, 2011; Pawar *et al.*, 2015), and thin layer sections of hypocotyl (Ramírez-Mosqueda *et al.*, 2016).

When moving from traditional practices to novel techniques, such as plant tissue culture, the synthetic chemicals used in media preparation are expensive. The present study suggests the use of naturally available substitutes for synthetic chemicals in the tissue culture medium.

Coconut water (CW) is known to be a good source of nutrients, consisting of the unique chemical composition of sugar, vitamins, minerals, amino acids, and phytohormones (Yong *et al.*, 2009). It has been reported in many studies as an alternative source of nutrients for

media preparation in plant tissue culture (Al-Khayri *et al.*, 1992; Dornelas *et al.*, 1994). Cytokinin is known to be the significant and most useful component in CW (Kende *et al.*, 1997) and together with auxins play a major role in plant morphology by controlling the growth of shoots, roots and overall growth of the plant. Though few studies have used CW in *Stevia* micropropagation (Ahmed *et al.*, 2016; Herath *et al.*, 2017), the nutrient composition of CW varies with climatic, environmental and geographical regions (Yong *et al.*, 2009). King coconut (*Cocos nucifera* var. *aurantiaca*) was recognized as an intermediate type of coconut among Sri Lankan varieties. According to Perera *et al.* (2014), king coconut belongs to the category with highest bunches per tree (annual average bunches is 16.5). Here, this variety was selected to extract CW due to its higher distribution around the country and nutritional composition (Herath *et al.*, 2017).

In this study, we investigated the effectiveness of using CW to replace synthetic chemicals (micronutrients, vitamins, and amino acids) in *in vitro* cultures of *S. rebaudiana*. CW was incorporated from the culture initiating step until rooting.

MATERIALS AND METHODS

Plant material preparation

Shoots were taken from three-month-old *S. rebaudiana* plants grown in the greenhouse. Explants with 3 - 4 nodes (6-10 cm) were washed in running tap water for 10 -15 min and sequentially rinsed with liquid detergent (Teepol 1 % (v/v)) for 3-5 min to remove superficial dust particles, microorganisms and their spores. Explants were transferred to a laminar flow hood, washed with 5 % NaOCl with Tween 20® for 5 min and washed three times with sterile double distilled water. The same procedure was practised for another 5 min, followed by three rinses with sterile distilled water.

Preparation of CW and MS media

Young nuts (*Cocos nucifera* var. *aurantiaca*) at age of 6 - 7 months after flowering were collected from Kandy. The nuts were washed with tap water thoroughly to remove dust and dirt from the outside, and surface sterilized with 1 % Teepol (v/v) followed by a wipe with 70 % ethanol (v/v) before transfer into the laminar flow hood. The nuts were cut inside the laminar flow hood to collect the nutrient water. This solution was not autoclaved, and freshly mixed with pre-autoclaved

MS media at the time of media preparation to avoid the destruction of thermolabile compounds which are unique and vital for CW.

Full MS (Murashige *et al.*, 1962) media composed of macronutrients, vitamins and amino acids was mixed with 30 g/L of sucrose (commercial sugar). Sequentially, different levels of hormones (BAP and IBA) were added according to different plant development stages. The pH of the medium was adjusted to 5.8 ± 0.2 with 1 N NaOH and 1 N HCl, before adding 0.8 % Bacto agar as the gelling agent. The media were autoclaved in Erlenmeyer flasks at 1.06 kg/cm² and 121 °C for 20 min, mixed with the different levels of fresh CW, and poured into containers in the sterile bench.

Shoot initiation and multiplication

Nodal explants (1-1.5 cm) with a single axillary bud were cultured vertically under aseptic conditions on full MS (Murashige *et al.*, 1962) media fortified with different levels of CW (0, 10, 20, 30, and 40 %) (v/v), and the phytohormone BAP (0, 0.2, 0.5 mg/L) for shoot initiation and multiplication (Table 1). The experiment was arranged in a complete randomized design (CRD) with ten replicates for each treatment. Cultures were incubated at a constant temperature of 25 ± 1 °C with a 16 h photoperiod (2000 lux). Final data were recorded after three weeks on the number of explants showing shoot initiation, the number of days for shoot initiation, the average number of shoots per culture, the average length of shoots per culture and the average number of leaves per culture to identify best-performing media. Subcultures were done every three weeks after collecting the data. Nodal segments from the proliferated shoots were subcultured again in a medium which gave the highest shoot multiplication for further shoot production.

Rooting

Multiple shoots regenerated from the nodal segments were separated into individual shoots and cultured on MS medium (Full MS and ½ MS) with different concentrations of indole butyric acid (IBA) and CW. Different IBA levels (0, 0.2 mg/L) were used to promote rooting. Basal media were full strength MS and ½ strength MS with the incorporation of macro-elements and different concentrations of CW (0, 5, 10, 20 %). Since CW is a good source of micro-elements and vitamins, they were not added to the rooting media. The experiment was arranged in a (CRD) with ten replicates for each treatment.

Acclimatization

After 4 wks, well-rooted plantlets were separated from the cultures and sub-cultured on ½ MS media with 10 g/L of sucrose and without any growth hormones for 1 week. Before transferring to the soil, all the MS media around the roots were removed by rinsing gently with warm water under aseptic conditions. The plantlets were transferred to different hardening media inside glass bottles with compost and sand mixed in different ratios (compost : sand in 2:1, 1:1, 1:2 and 1:3) and covered with a transparent polythene cap for another 1 week. They were then kept in a propagator with 100 % relative humidity by spraying with water. The relative humidity was gradually reduced, and the light intensity gradually increased. After another 2 wks, the plantlets were transferred to larger pots. Survival rate was observed every week.

Data Analysis

The data were analysed by Analysis of Variance (ANOVA) and significant differences among the treatments determined with Tukey multiple range test at 5 % level of significance using the Minitab 17.0.1 statistical package.

RESULTS AND DISCUSSION

Number of days to initiate shoots and % of bud break

Shoots were initiated in all the treatments within 4 to 8 days showing its higher bud break potential as a herbaceous species. In the absence of CW and BAP, the explants required the maximum number of days to initiate shoots (around 7-8 days). However, a small amount of CW (10 %) made no significant change at $p < 0.05$ (7.50 ± 0.33 days) in the number of days, but showed the highest percentage of response in shoots (93.33 %). The rate was higher than that obtained with the media with BAP, showing that a small incorporation of CW can induce bud break regardless of the presence of artificial cytokinin (BAP) (Table 1). Another fact identified was that 10 % CW with 0, 0.2 and 0.5 mg/L of BAP gave the highest rates of bud breaks (93.33 %, 90.67 % and 89.33 %, respectively) showing that 10 % of CW is best to induce bud break in *Stevia*. Further, the results suggest that with a higher concentration of CW (40 %) and BAP (0.5 mg/L), bud break was faster (4.16 ± 0.35 ds). However, at this concentration, the number of explants developing shoots declined to 70 - 72 % (Table 1). Altogether, with CW, more than

50 % of the explants initiated shoots, in its absence, it was 49 %, either with (0.2, 0.5 mg/L) or without BAP (Table 1). Although the percentage of explants initiating shoots was highest in the absence of BAP, its presence in the medium sustained shoot initiation at over 80 % (Table 1). Even though the present study reported a positive response with CW, studies by Ahmed *et al.* (2016); Wahyono *et al.* (2021) and Asmono *et al.* (2017) explained the inefficiency of CW in shoot induction of *Stevia*; the lowest duration was taken by the media that excluded CW.

In this study, CW from young nuts was selected, since they have more nutrients than mature nuts. Previously, autoclaved CW was used in experiments (Al-Kayri *et al.*, 1992; Dornelas *et al.*, 1994; Ahmed *et al.*, 2016), while we used fresh CW and observed no media contamination. The cytokinin zeatin and the auxin IAA present in CW, which are known to be heat-sensitive, would have their efficiency altered if autoclaved (Yong *et al.*, 2009). Further, in contrast to the previous findings by Ahmed *et al.* (2016), Asmono *et al.* (2017) and Wahyono *et al.* (2021), we could observe positive results with CW for *Stevia*. It may be due to preserving nutrients that are not being destroyed by autoclaving. The quality of the CW or the nutritional composition depends on the maturity, variety, location, soil conditions, climate conditions, and other environmental conditions (Hall *et al.*, 2000). Therefore, nuts in the same maturity stage were collected from the same ecological zone to avoid the influence on the nutritional composition.

Vegetative growth (number of shoots, average length of shoots and average number of leaves per culture)

Vegetative growth determines the amount of active compounds that can be extracted from the *Stevia* plant. Hence, commercially, vegetative production is very important. In *Stevia*, the highest number of shoots were observed in the media with 20 % and 30 % of CW with 0.2 mg/L BAP (9.00 and 9.44) and the results are significantly higher ($p < 0.05$) than those of all the used concentrations (Table 1). A sudden drop in shoot number to 2.28 with 40 % of CW, shows the inhibitory effect of CW at higher concentrations even though BAP was present at lower concentration (0.2 mg/L). The results suggest that there is a considerable effect from CW on shoot multiplication. In the absence of BAP, shoot number was reduced to 2 to 3 (Table 1). A contrasting observation was that in the absence of CW, shoot production was higher in the treatments T14 and T15 (5.78 and 5.47, respectively). However, the presence of BAP (0.2 and 0.5 mg/L) has retrieved that effect of CW.

Hence, the optimum conditions were identified as little incorporation of BAP (0.2 mg/L) with 20-30 % of CW.

Previously, Ahmed *et al.* (2016) obtained highest shoot multiplication with 10 % CW with BAP (2.0 mg/L), Kinetin (0.5 mg/L) and NAA (0.1 mg/L). However, Asmono *et al.* (2017), Herath *et al.* (2017), and Naranjo *et al.* (2016) found contrasting results with no significant growth in *Stevia* with CW or in combination with BAP, while higher concentrations inhibited the growth. Even though the findings of Ahmed *et al.* (2016) are compatible with our results, where a small supplementation of CW enhanced the shoot multiplication whilst increased concentration inhibited the growth, they have applied around 4-8 % of CW to enhance vegetative growth.

The average length of *Stevia* shoots were taken as a parameter since higher internodal distance is advantageous in subculturing as well as in initiation of new shoots by bud break. The highest length was observed with 10 % CW without BAP (41.86 mm) and in the media with only 10 % CW and 0.2 mg/L BAP (34.99 mm) showing that a lower amount of CW shows the highest growth rate even if the shoot number is lower (2.52). At the same time, shoot growth was significantly lower ($p < 0.05$) in the media with highest amount of BAP (0.5 mg/L) (11.38 mm) and the result was the same at 40 % CW. These results indicated that, when the number of shoots increase, leaves also increase. The highest number of leaves was observed as 8.28 in the media with 30 % CW and 0.2 mg/L BAP; the same media showed the highest number of shoots (Table 1). In the absence of CW, the cultures developed the least number (4 to 5) of leaves. Similar to our results, studies on *Passiflora* species by Dornelas *et al.* (1994) found that MS + 2.0 mg/L, and BA + 10 % CW induced the highest bud break while growth was suppressed with higher levels of CW. *Gloriosa superba* L. and *Dendrobium fimbriatum* Hook also have shown improved results compared to those without CW (Roy *et al.*, 2003; Ibrahim *et al.*, 2008).

In an experiment with olive, Peixe *et al.* (2007) showed the effect of CW in combination with BAP was similar to the more expensive cytokinin, zeatin. In *G. superba*, the addition of 15 % (v/v) CW to MS basal medium with BA, NAA and activated charcoal increased the number of shoots in *in vitro* cultures (Ibrahim *et al.*, 2008). Shoot induction and multiplication in *Curcuma zedoaria* Roxb. was also successful with 20 % CW (v/v) in combination with BA and kinetin (Roy *et al.*, 2003). In addition, CW has been successfully used for *in vitro* propagation of passion fruit (Hall *et al.*, 2000), coffee (Ismail *et al.*, 2003) and orchids (Santos-Hernández *et al.*,

2005). Similar to our results with *Stevia*, CW alone was not sufficient to promote satisfactory shoot multiplication in all the above mentioned species; a blend of CW with BAP was necessary (Peixe *et al.*, 2007).

Callus development in *in vitro* cultures is undesired since nutrients in the culture medium are diverted to this undifferentiated mass of cells at the expense of shoot and leaf development. In this study, cultures with callus at the base of the explant retarded the development of shoots (Figure 1c). High levels of CW (20 %, 30 %, and 40 %)

in combination with 0.5 mg/L BAP induced callusing in *Stevia* after three weeks of culture (Table 1). In the process of keeping the clonality of a species, avoiding callus-phase is advantageous. Thus, it is important to determine the optimum concentrations of CW and BAP for efficient micropropagation of *Stevia* without the proliferation of calluses. In the process of somatic embryogenesis, the induction of callus is an important stage. However, a study by Naranjo *et al.* (2016) described the inefficiency and the inhibiting activity of CW in the somatic embryogenesis of *Stevia*.

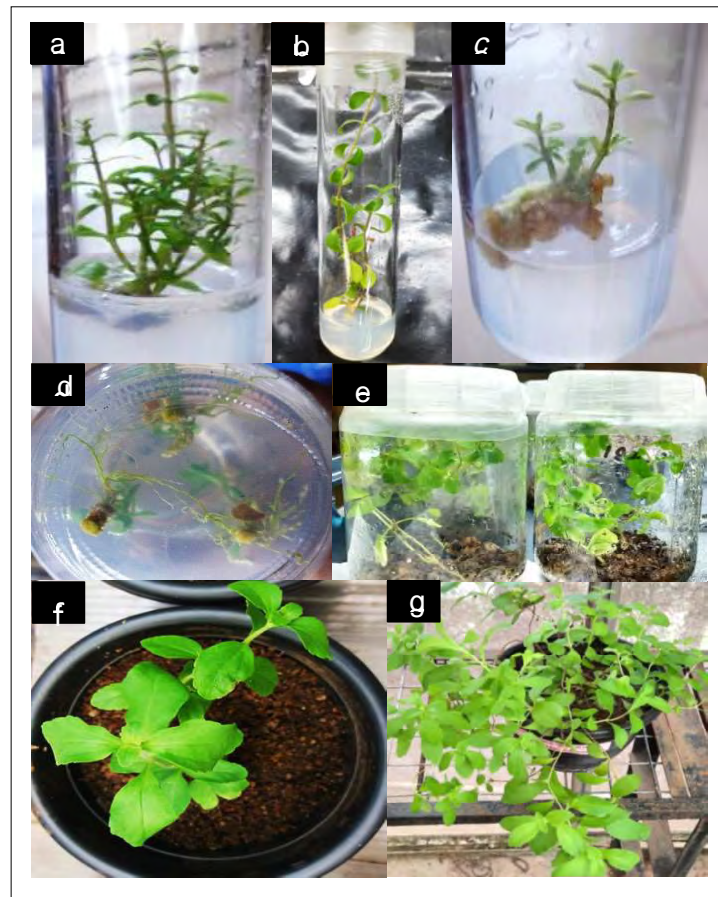


Figure 1: Different stages of *in vitro* growth of the *Stevia* plant (a). shoot multiplication (T7 – 30 % CW+0.2 mg/L BAP), (b). highest shoot length (T5 - 10% CW+0.2 mg/L BAP), (c). cuttings with callus initiation at the base showed retarded growth (T12 - 40% CW+0.5 mg/L) (d). rooting in media with $\frac{1}{2}$ MS+ 5% CW+ 0.2 mg/L IBA, (e). acclimatization of plants under *in vitro* conditions, (f). *Stevia* plants after training to the natural environment, (g). fully grown plant after 2 months

Table 1: Effects of different concentrations of coconut water (CW) in MS medium with cytokinin (BAP) on in vitro shoot proliferation from nodal segments of *Stevia*. Data were recorded after three weeks of culture (-: no callus, +: very little callus, ++: moderate callus, +++: profuse callus)

Experiment	Amount of CW (%) (v/v) with full MS	BAP (mg/L)	% of bud break	Number of days for shoot initiation	Average number of shoots per culture	Average length of shoots per culture (mm)	Average number of leaves per culture	Callus growth at the base of the shoots (after 3 weeks)
T1	10	0	93.33	7.50 ± 0.33 ^{ab}	2.52 ± 0.65 ^{def}	41.86 ± 0.85 ^a	5.29 ± 0.42 ^{efgh}	-
T2	20	0	70.67	6.82 ± 0.48 ^{bcd}	2.78 ± 0.69 ^{def}	22.37 ± 0.46 ^d	6.82 ± 0.48 ^{bcd}	-
T3	30	0	54.67	6.06 ± 0.89 ^{def}	3.00 ± 0.33 ^{cdef}	19.91 ± 0.82 ^e	7.93 ± 1.13 ^{ab}	+
T4	40	0	68.00	5.28 ± 0.42 ^{fg}	2.80 ± 0.50 ^{def}	27.00 ± 0.59 ^c	6.06 ± 0.89 ^{cdefg}	++
T5	10	0.2	90.67	7.11 ± 0.31 ^{abc}	6.00 ± 0.88 ^b	34.99 ± 0.66 ^b	6.37 ± 0.25 ^{cdef}	-
T6	20	0.2	82.67	6.65 ± 0.39 ^{bcd}	9.00 ± 0.25 ^a	22.22 ± 0.92 ^d	7.96 ± 0.68 ^{ab}	+
T7	30	0.2	69.33	6.37 ± 0.25 ^{cde}	9.44 ± 0.51 ^a	21.40 ± 0.99 ^{de}	8.28 ± 0.81 ^a	++
T8	40	0.2	49.33	5.16 ± 0.16 ^{gh}	2.28 ± 0.26 ^{ef}	15.50 ± 0.66 ^g	5.17 ± 0.17 ^{gh}	+++
T9	10	0.5	89.33	7.34 ± 0.23 ^{abc}	4.44 ± 0.51 ^{bade}	17.71 ± 0.83 ^f	6.65 ± 0.39 ^{bade}	+
T10	20	0.5	86.67	5.10 ± 0.83 ^{gh}	4.80 ± 0.64 ^{bcd}	16.82 ± 0.67 ^{fg}	7.11 ± 0.32 ^{bce}	+++
T11	30	0.5	72.00	4.60 ± 0.16 ^{gh}	5.39 ± 0.92 ^{bc}	16.80 ± 0.61 ^{fg}	5.10 ± 0.83 ^{gh}	+++
T12	40	0.5	70.67	4.16 ± 0.35 ^h	1.92 ± 0.36 ^f	12.47 ± 0.34 ^h	4.70 ± 0.92 ^{gh}	+++
T13	0	0	48.00	7.77 ± 0.29 ^a	3.65 ± 0.10 ^{bade}	21.33 ± 0.89 ^{de}	5.41 ± 0.21 ^{defgh}	-
T14	0	0.2	49.33	5.41 ± 0.20 ^{fg}	5.78 ± 0.84 ^b	18.07 ± 0.84 ^f	4.60 ± 0.17 ^h	++
T15	0	0.5	49.33	5.07 ± 0.69 ^{gh}	5.47 ± 0.81 ^b	11.38 ± 0.63 ^h	5.07 ± 0.69 ^{gh}	+++

Numbers represent the mean ± SE (standard error). Means with different letters are significantly different (Tukey, $p \leq 0.05$)

Table 2: Effect of different concentrations of coconut water (CW) in MS medium with auxin (IBA) on *in vitro* rooting of *Stevia*. Data were recorded after four weeks of culture

Basal media (MS)	Amount of CW (%)	IBA concentration (mg/L)	Days for root initiation	Mean number of roots
Full	0	0	0.00 ± 0.00 ^e	0.00 ± 0.00 ^f
Full	0	0.2	0.00 ± 0.00 ^e	0.00 ± 0.00 ^f
½	0	0	20.83 ± 0.40 ^a	2.75 ± 0.61 ^d
½	0	0.2	20.16 ± 0.75 ^a	8.33 ± 1.33 ^b
Full	5	0	6.66 ± 0.51 ^d	9.83 ± 0.52 ^b
Full	10	0	20.00 ± 0.54 ^a	3.00 ± 0.79 ^d
Full	20	0	18.00 ± 1.09 ^b	1.33 ± 0.52 ^d
Full	5	0.2	20.58 ± 0.49 ^a	3.16 ± 0.68 ^d
Full	10	0.2	20.91 ± 0.66 ^a	1.00 ± 0.00 ^{ef}
Full	20	0.2	0.00 ± 0.00 ^e	0.00 ± 0.00 ^f
½	5	0	20.75 ± 0.60 ^a	2.75 ± 0.61 ^d
½	10	0	20.75 ± 0.61 ^a	6.25 ± 0.68 ^c
½	20	0	20.16 ± 0.75 ^a	3.33 ± 0.41 ^d
½	5	0.2	12.75 ± 1.47 ^c	13.53 ± 0.51 ^a
½	10	0.2	20.25 ± 0.88	1.51 ± 0.55 ^f
½	20	0.2	0.00 ± 0.00 ^e	0.00 ± 0.00 ^f

Numbers represent the mean ± SE (standard error). Means with different superscripts shows significantly different values (Tukey, $p \leq 0.05$)

Rooting

The number of days to induce roots ranged from 6 to 20 days. Earliest rooting was observed after six days in a medium with MS + 5 % CW, which also produced the maximum mean number of roots (9.83 ± 0.52) (Table 2). The combination of ½ MS with 5 % CW and 0.2 mg/L IBA induced roots after 12 days (Table 2). The induction of roots was suppressed with the increasing levels of CW (20 %) in the medium (Table 2). The presence of CW with ½ MS medium did not promote early rooting.

According to the previous studies, different auxins have promoted root initiation and development of *Stevia*. Addition of 1.0 mg/L NAA with full MS achieved 63.2 % rooting within 12.3 days (Pawar *et al.*, 2015). Root growth of 4.4 cm was achieved in ½ MS with 1 mg/L IBA (Seema *et al.*, 2011). The full MS medium with 0.25 mg/L IAA produced 100 % rooting (7.6 roots per explant) within 3 weeks (Yücesan *et al.*, 2016), while ½ MS with 0.5 mg/L IBA produced 92 % rooting (Puneet *et al.*, 2018). Full MS with 0.2 mg/L IBA produced 93.33 % rooting (Majumder *et al.*, 2016), while full MS with 1.0 mg/L IBA or 1.0 mg/L NAA produced 66.67 % rooting (Ahmed *et al.*, 2016). CW has been used

as a media enhancer for rooting in limited species (Roy *et al.*, 2003). Even though the researchers have studied shoot proliferation of *Stevia* with CW (Ahmed *et al.*, 2016; Asmona *et al.*, 2017; Wahyono *et al.*, 2021), they have not applied CW for root induction or root growth. According to Yong *et al.* (2009), CW from immature nuts contains 150 nM of IAA, which is an important auxin for root formation. Since the CW in the present study was not autoclaved, heat-sensitive IAA may be retained in the media in its natural form and induce roots.

Aman *et al.* (2013) observed that the rooting response decreases with the addition of IAA, NAA and IBA to full MS-medium. Full strength MS + 20 % CW + 0.2 mg/L IBA did not produce roots; indirectly, high nutrients in the culture medium encouraged callus growth at the base of the shoots which suppressed the development of roots. Recent studies have confirmed that a low concentration of MS salts without PGRs contributed to 90-100 % rooting of *S. rebaudiana* (Seema *et al.*, 2011; Gantait *et al.*, 2015; Ramírez-Mosqueda *et al.*, 2016). The above results indicate that *Stevia* is a plant, which needs a smaller amount of nutrients for its growth *in vitro* and the addition of minimum CW can stimulate the growth of shoots as well as roots. It was noted that growth

parameters were highly influenced by the addition of CW since their performance was very high when compared with controls without CW.

Acclimatization

The prerequisites for successful acclimatization were healthy *in vitro* plantlets with thick stems (high stem diameter), a large number of leaves and well-developed roots. Early subcultures of the shoots should be selected to induce roots since the survival of later subcultures was poor. Media composed of ½ strength MS without any hormones and reduced sugar content was used to encourage photosynthesis. The rooted plantlets were transferred to ½ strength MS media with a sugar content of 10 g/L and then shifted to soil media.

Accordingly, of the four treatments, compost: sand in 1:3 ratio showed the highest survival rate (93.33%) while increase of compost resulted in a reduced level of plant survival. Compost : sand in 2:1, 1:1, and 1:2 ratios showed a gradual increase in survival after three weeks (40.0 %, 60.0 %, and 66.7 %, respectively). The results suggest that under greenhouse conditions, *Stevia* requires well-drained soil to survive. When considering the survival of the *in vitro* cultured plants, hardening appears to be crucial and the most difficult part.

Morpho-physiological studies have noted the importance of controlling the water loss for the survival of cultured plants since they consist of little epicuticular wax and guard cells that are highly variable in morphology and size (Ziv *et al.*, 1987), and lacked starch grains in their cells (Ibrahim *et al.*, 2008). During hardening, the appearance of starch grains precedes the normalization of mesophyll cells. Hence, maintenance of microclimatic conditions is a must for a higher survival rate. The internal environment of the propagators, covered with polythene was gradually changed by increasing the temperature and light intensity (moving plantlets from culture room to greenhouse) and decreasing the humidity by opening the polythene. In a previous study of *in vitro* grown Carnation plantlet, the reduced humidity inside the culture tubes and higher agar concentration induced the stomatal development by increasing the survival percentage (Ziv *et al.*, 1987). When calluses were present at the base, plantlets did not survive. *Stevia* is a delicate plant and needs to be carefully monitored through the process of hardening. Under good conditions, plantlets can be hardened in six weeks.

CONCLUSION

Nodal cuttings of *S. rebaudiana* cultured on MS medium with 10 % CW induced 93.3 % bud break. Increasing the coconut water to 30 % with 0.2 mg/L BAP produced the highest mean number of shoots (8.44) and the highest number of leaves (8.28) in three weeks. Modified rooting media incorporating only MS macronutrients, IBA and 5 % CW, without micronutrients, showed earliest rooting (6.6 days). The highest number of root initiation (13.5) was with ½ MS+ 0.2 mg/L IBA and 5% CW. Regenerated plantlets were successfully hardened and acclimatized in glass jars with compost and sand with 3:1 ratio under greenhouse conditions. Our results suggest that *Stevia* plants can be propagated effectively with CW incorporated media and can be potentially adapted for small to medium scale commercial cultivation.

Conflicts of interest

The authors declare that they have no conflict of interest regarding the publication of this paper.

Acknowledgement

The authors thank Ms Shirani Perera and Mr Hapukotuwa for helping them in the laboratory.

REFERENCES

- Ahmed S.R., Howlader M.M.S., Sutradhar P. & Yasmin S. (2016). An efficient protocol for *in vitro* regeneration of *Stevia rebaudiana*. *Asian Journal of Medical Biological Research* **2**(1): 95–106.
DOI: <https://doi.org/10.3329/ajmbr.v2i1.27574>
- Al-Khayri J.M., Huang F.H., Morelock T.E. & Busharar T.A. (1992). Spinach tissue culture improved with coconut water. *HortScience* **27**(4): 357–358.
DOI: <https://doi.org/10.21273/HORTSCI.27.4.357>
- Aman N., Hadi F., Khalil S.A., Zamir R. & Ahmad N. (2013). Efficient regeneration for enhanced steviol glycosides production in *Stevia rebaudiana* (Bertoni). *Comptes Rendus Biologies* **336**(10): 486–492.
DOI: <https://doi.org/10.1016/j.crv.2013.10.002>
- Asmono L.S., Sari K.V. & Wardana R. (2017). *In vitro* propagation response of *Stevia rebaudiana* Bertoni in different types of cytokinin and coconut water concentration. *Jurnal Penelitian Pertanian* **21**(2): 146–154.
- Brandle J. & Rosa N. (1992). Heritability for yield, leaf: stem ratio and stevioside content estimated from a landrace cultivar of *Stevia rebaudiana*. *Canadian Journal of Plant*

- Science* **72**(4): 1263–1266.
DOI: <https://doi.org/10.4141/cjps92-159>
- Chang S.S. & Cook J.M. (1983). Stability studies of stevioside and rebaudioside A in carbonated beverages. *Journal of Agricultural Food Chemistry* **31**(2): 409–412.
DOI: <https://doi.org/10.1021/jf00116a056>
- Chughtai M.F.J., Pasha I., Zahoor T., Khaliq A., Ahsan S., Wu Z., Nadeem M., Mehmood T., Amir R.M. & Yasmin I. (2020). Nutritional and therapeutic perspectives of *Stevia rebaudiana* as emerging sweetener; a way forward for sweetener industry. *CYTA-Journal of Food* **18**(1): 164–177.
DOI: <https://doi.org/10.1080/19476337.2020.1721562>
- Czinkóczy R. & Németh Á. (2018). Investigations into enzymatic bioconversion to form Rebaudioside A from Stevioside. *Periodica Polytechnica Chemical Engineering* **62**(4): 396–402.
DOI: <https://doi.org/10.3311/PPch.12673>
- Dornelas M.C. & Carneiro Vieira M.L. (1994). Tissue culture studies on species of *Passiflora*. *Plant Cell, Tissue and Organ Culture* **36**(2): 211–217.
DOI: <https://doi.org/10.1007/BF00037722>
- Gantait S., Das A. & Mandal N. (2015). Stevia: a comprehensive review on ethnopharmacological properties and *in vitro* regeneration. *Sugar Tech* **17**(2): 95–106.
DOI: <https://doi.org/10.1007/s12355-014-0316-3>
- Goyal S., Samsher & Goyal R. (2010). Stevia (*Stevia rebaudiana*) a bio-sweetener: a review. *International Journal of Food Sciences Nutrition* **61**(1): 1–10.
DOI: <https://doi.org/10.3109/09637480903193049>
- Gupta E., Purwar S., Sundaram S. & Rai G. (2013). Nutritional and therapeutic values of *Stevia rebaudiana*: A review. *Journal of Medicinal Plants Research* **7**(46): 3343–3353.
DOI: <https://doi.org/10.5897/JMPR2013.5276>
- Hall R.M., Drew R.A., Higgins C.M. & Dietzgen R.G. (2000). Efficient organogenesis of an Australian passionfruit hybrid (*Passiflora edulis* x *Passiflora edulis* var. *flavicarpa*) suitable for gene delivery. *Australian Journal of Botany* **48**(5): 673–680.
DOI: <https://doi.org/10.1071/BT99067>
- Herath H. & Wijebandara D. (2017). Potential use of king coconut husk as a nutrient source for organic coconut cultivation. *Journal of Food and Agriculture* **10**(1–2): 1–7.
DOI: <http://doi.org/10.4038/jfa.v10i1-2.5207>
- Ibrahim I.A., Nasr M.I., Mohammed B.R. & El-Zefzafi M.M. (2008). Plant growth regulators affecting *in vitro* cultivation of *Stevia rebaudiana*. *Sugar Tech* **10**(3): 254–259.
DOI: <https://doi.org/10.1007/s12355-008-0045-6>
- Ismail S., Naqvi B., Anwar N. & Zuberi R. (2003). *In vitro* multiplication of *Coffea arabica*. *Pakistan Journal of Botany* **35**(5): 829–834.
- Jain P., Kachhwaha S. & Kothari S. (2009). Improved micropropagation protocol and enhancement in biomass and chlorophyll content in *Stevia rebaudiana* (Bert.) Bertonii by using high copper levels in the culture medium. *Scientia Horticulturae* **119**(3): 315–319.
DOI: <https://doi.org/10.1016/j.scienta.2008.08.015>
- Kalpana M., Anbazhagan M., Natarajan V. & Dhanavel D. (2009). Improved micropropagation method for the enhancement of biomass in *Stevia rebaudiana* Bertoni. *Recent Research in Science Technology* **2**(1): 8–13.
- Kende H. & Zeevaart J. (1997). The five” Classical” plant hormones. *The Plant Cell* **9**(7): 1197.
DOI: <https://doi.org/10.1105/tpc.9.7.1197>
- Kennelly E.J. (2001). Sweet and non-sweet constituents of *Stevia rebaudiana*. In: *Stevia, the Genus Stevia* (ed. A.D. Kinghorn), pp. 68–85. Taylor and Francis, London, UK.
- Khalil S.A., Zamir R. & Ahmad N. (2014). Selection of suitable propagation method for consistent plantlets production in *Stevia rebaudiana* (Bertonii). *Saudi Journal of Biological Sciences* **21**(6): 566–573.
DOI: <https://doi.org/10.1016/j.sjbs.2014.02.005>
- Kohda H., Kasai R., Yamasaki K., Murakami K. & Tanaka O.J.P. (1976). New sweet diterpene glucosides from *Stevia rebaudiana* **15**(6): 981–983.
DOI: [https://doi.org/10.1016/S0031-9422\(00\)84384-8](https://doi.org/10.1016/S0031-9422(00)84384-8)
- Loc N.H., Duc D.T., Kwon T.H. & Yang M.S. (2005). Micropropagation of zedoary (*Curcumazedoaria* Roscoe)—a valuable medicinal plant. *Plant Cell, Tissue Organ Culture* **81**(1): 119–122.
DOI: <https://doi.org/10.1007/s11240-004-3308-2>
- Ma Z., Ge L., Lee A.S., Yong J.W.H., Tan S.N. & Ong E.S. (2008). Simultaneous analysis of different classes of phytohormones in coconut (*Cocos nucifera* L.) water using high-performance liquid chromatography and liquid chromatography–tandem mass spectrometry after solid-phase extraction. *Analytica Chimica Acta* **610**(2): 274–281.
DOI: <https://doi.org/10.1016/j.aca.2008.01.045>
- Majumder S. & Rahman M.M. (2016). Micropropagation of *Stevia rebaudiana* Bertoni. through direct and indirect organogenesis. *Journal of Innovations in Pharmaceuticals Biological Sciences* **3**(3): 47–56.
DOI: <https://doi.org/10.1016/j.aca.2008.01.045>
- Megeji N., Kumar J., Singh V., Kaul V. & Ahuja P.S. (2005). Introducing *Stevia rebaudiana*, a natural zero-calorie sweetener. *Current Science* **88**(5): 801–804.
- Momtazi-Borojeni A. A., Esmaceli S.-A., Abdollahi E. & Sahebkar A. (2017). A review on the pharmacology and toxicology of steviol glycosides extracted from *Stevia rebaudiana*. *Current Pharmaceutical Design* **23**(11): 1616–1622.
DOI: <https://doi.org/10.2174/1381612822666161021142835>
- Murashige T. & Skoog F. (1962). A revised medium for rapid growth and bio assays with tobacco tissue cultures. *Physiologia Plantarum* **15**(3): 473–497.
DOI: <https://doi.org/10.1111/j.1399-3054.1962.tb08052.x>
- Naranjo E.J., Fernandez O.B. & Urrea A.I.T. (2016). Effect of genotype on the *in vitro* regeneration of *Stevia rebaudiana* via somatic embryogenesis. *Acta Biológica Colombiana* **21**(1): 87–98.
DOI: <http://dx.doi.org/10.15446/abc.v21n1.47382>
- Pawar S., Khandagale V., Jambhale V., Jadhav A. & Pawar B. (2015). *In vitro* regeneration studies in *Stevia* through nodal segment and shoot tip. *The BioScan* **10**(3): 1007–1010.

- Peixe A., Raposo A., Lourenço R., Cardoso H. & Macedo E. (2007). Coconut water and BAP successfully replaced zeatin in olive (*Olea europaea* L.) micropropagation. *Scientia Horticulturae* **113**(1): 1–7.
DOI: <https://doi.org/10.1016/j.scienta.2007.01.011>
- Perera S., Dissanayaka H., Herath H., Meegahakumbura M. & Perera L. (2014). Quantitative characterization of nut yield and fruit components in indigenous coconut germplasm in Sri Lanka. *International Journal of Biodiversity* **2014**: Article ID 740592.
DOI: <http://dx.doi.org/10.1155/2014/740592>
- Puneet B., Priyanka S., Beniwal V. & Vikas H. (2018). Micropropagation of *Stevia rebaudiana* using shoot tip explants-a magical sweetener and medicinal plant. *Annals of Biology* **34**(1): 4–11.
- Ramírez-Mosqueda M., Iglesias-Andreu L., Ramírez-Madero G. & Hernández-Rincón E. (2016). Micropropagation of *Stevia rebaudiana* Bert. in temporary immersion systems and evaluation of genetic fidelity. *South African Journal of Botany* **106**: 238–243.
DOI: <https://doi.org/10.1016/j.sajb.2016.07.015>
- Ramírez-Mosqueda M.A. & Iglesias-Andreu L.G. (2016). Direct organogenesis of *Stevia rebaudiana* Bertoni using thin cell layer (TCL) method. *Sugar Tech* **18**(4): 424–428.
DOI: <https://doi.org/10.1007/s12355-015-0391-0>
- Roy J. & Banerjee N. (2003). Induction of callus and plant regeneration from shoot-tip explants of *Dendrobium fimbriatum* Lindl. var. *oculatum* Hk. f. *Scientia Horticulturae* **97**(3–4): 333–340.
DOI: [https://doi.org/10.1016/S0304-4238\(02\)00156-5](https://doi.org/10.1016/S0304-4238(02)00156-5)
- Sakaguchi M. & Kan T. (1982). Japanese researches on *Stevia rebaudiana* (Bert.) Bertoni and stevioside. *Ciencia e Cultura* **34**: 235–248.
- Santos-Hernández L., Martínez-García M., Campos J.E. & Aguirre-Leon E. (2005). *In vitro* propagation of *Laelia albida* (Orchidaceae) for conservation and ornamental purposes in Mexico. *HortScience* **40**(2): 439–442.
DOI: <https://doi.org/10.21273/HORTSCI.40.2.439>
- Seema T., Arnold R., Tiwari A., Mishra R. & Chauhan U. (2011). Cyanobacterial extract and MS media as a novel tool for *in vitro* regeneration of *Stevia rebaudiana* Bertoni. *Journal of Algal Biomass Utilization* **2**(2): 24–40.
- Singh S. & Rao G. (2005). *Stevia*: The herbal sugar of 21st Century. *Sugar Tech* **7**(1): 17–24.
DOI: <https://doi.org/10.1007/BF02942413>
- Wahyono N.D., Hasanah N. & Nurprahastani N. (2021). Optimization of sterilization techniques and effects of coconut water for the induction of Shoots of stevia (*Stevia rebaudiana* Bertoni). *Proceedings of the 3rd International Conference on Food and Agriculture*. 7–8 November, Indonesia. **3**(1): 10–18
- Wölwer-Rieck U. (2012). The leaves of *Stevia rebaudiana* (Bertoni), their constituents and the analyses thereof: a review. *Journal of Agricultural Food Chemistry* **60**(4): 886–895.
DOI: <https://doi.org/10.1021/jf2044907>
- Yadav A.K., Singh S., Dhyani D. & Ahuja P.S. (2011). A review on the improvement of stevia [*Stevia rebaudiana* (Bertoni)]. *Canadian Journal of Plant Science* **91**(1): 1–27.
DOI: <https://doi.org/10.4141/cjps1008691>
- Yong J.W., Ge L., Ng Y.F. & Tan S.N. (2009). The chemical composition and biological properties of coconut (*Cocos nucifera* L.) water. *Molecules* **14**(12): 5144–5164.
DOI: <https://doi.org/10.3390/molecules14125144>
- Yücesan B., Mohammed A., Büyükgöçmen R., Altuğ C., Kavas Ö., Gürel S. & Gürel E. (2016). *In vitro* and *ex vitro* propagation of *Stevia rebaudiana* Bertoni with high Rebaudioside-A content-A commercial scale application. *Scientia Horticulturae* **203**: 20–28.
DOI: <https://doi.org/10.1016/j.scienta.2016.03.008>
- Ziv M., Schwartz A. & Fleminger D. (1987). Malfunctioning stomata in vitreous leaves of carnation (*Dianthus caryophyllus*) plants propagated *in vitro*; implications for hardening. *Plant Science* **52**(1–2): 127–134.
DOI: [https://doi.org/10.1016/0168-9452\(87\)90114-2](https://doi.org/10.1016/0168-9452(87)90114-2)

RESEARCH ARTICLE

Survey Sampling

Estimation of mean considering the joint influence of measurement errors and non-response in two-phase sampling designs

S Sabir¹, A Sanaullah^{1*} and S Gupta²

¹ Department of Statistics, COMSATS University Islamabad, Lahore Campus, Pakistan.

² Department of Mathematics and Statistics, The University of North Carolina at Greensboro, USA.

Submitted: 06 August 2020; Revised: 19 April 2021; Accepted: 27 August 2021

Abstract: Recently, a few studies have presented the problem of estimation of the mean for a finite homogenous population considering the joint influence of non-response and measurement errors and following the assumption that population mean of auxiliary variable is available. However, in real situations the population under observation may not be homogeneous and population mean of the auxiliary variable may also not be available. Therefore, in this study, we present new estimators which are the generalized form of the difference-cum-exponential type estimator of the finite population mean in the presence of non-response and measurement errors in two-phase simple random sampling and stratified random sampling. The expressions for mean square error and bias of the proposed estimators are shown under the first order approximation in each sampling design. Theoretically, it has been shown that the proposed estimators are more efficient than some existing estimators in both sampling designs. A numerical study has also been carried out using two different simulated populations under simple random sampling designs as well as under stratified random sampling design to support the theoretical results. Numerical results show that the proposed estimators perform more efficiently than some modified versions of the existing estimators in both sampling designs.


Keywords: Auxiliary variable, exponential estimator, mean square error, measurement error, ratio estimator, regression estimator.

INTRODUCTION

Survey errors arise when a difference is found between the true and recorded values. In practice, it is observed that researchers face the problem of measurement

error and/or non-response while collecting information from the samples. For example, in surveys regarding agriculture, the households are asked to report a total area of their holdings, which may vary from the cadastral data. Many researchers have studied the problem of mean estimation considering only measurement errors like Shalabh (1997), Wang (2002), Shukla *et al.* (2012) Sharma *et al.* (2013) and Khalil *et al.* (2017). Hansen and Hurwitz (1946) considered the problem of non-response only while estimating the population mean. They recommended that the questionnaires are mailed to all the respondents included in the sample and as the deadline is passed, a list of non-respondents is prepared in order to draw a sub-sample from the list of non-respondents and the necessary information is collected by direct interview. Many researchers have discussed this issue following Hansen and Hurwitz's sub-sampling plan, including Cochran (1977), Rao (1986), Singh and Kumar (2010), Kumar and Bhogal (2011), Kumar (2015), Sanaullah *et al.* (2015; 2018), Riaz *et al.* (2014; 2016), and Saleem *et al.* (2018).

Many authors who have studied non-response have neglected the measurement errors whereas many of those who have studied measurement errors have ignored the presence of non-response. However, Azeem (2014) and Kumar (2015; 2016) considered both the presence of non-response and measurement errors simultaneously. Azeem (2014) and Kumar (2015) considered only the situation where population is homogeneous and the population mean of the auxiliary variable is available, which may not be true for many practical situations.

* Corresponding author (chaamirsanaullah@yahoo.com;  <https://orcid.org/0000-0001-8114-0678>)



This article is published under the Creative Commons CC-BY-ND License (<http://creativecommons.org/licenses/by-nd/4.0/>). This license permits use, distribution and reproduction, commercial and non-commercial, provided that the original work is properly cited and is not changed in anyway.

Sabir and Sanaullah (2019) examined the mean estimator introduced by Kumar (2016) and provided corrected expressions for the mean square error. Zahid and Shabbir (2018) provided estimators for mean considering the joint presence of non-response and measurement errors in stratified simple random sampling. Irfan *et al.* (2018) studied how to optimize the estimation of mean if non-response and measurement errors are jointly present in a simple random sample.

Deviating from Azeem (2014) and Kumar (2015; 2016), this study is aimed at providing some improved estimators for population mean considering the situation when the population mean of an auxiliary variable may not be readily available. Further, the proposed estimators are compared with the modified ratio, exponential and regression estimators in both simple random sampling and stratified random sampling designs.

Notations and sampling methodology:

Let $\Phi = \{\Phi_1, \Phi_2, \dots, \Phi_N\}$ be a finite population of N homogeneous units which is divided into two mutually exclusive groups say the respondent group of size $N_{(1)}$ and the non-respondent group of size $N_{(2)} = N - N_{(1)}$. Some basic notations to be used in Sections 1 and 2 are defined as given below.

n' : 1st-phase sample size

n'' : sub-sample \ 2nd-phase sample size to be selected from

$n''_{(1)}$: number of respondents in 2nd-phase sample

$n''_{(2)}$: number of non-respondents in 2nd-phase sample

r : size of sub-sample to be selected for interview from $n''_{(2)}$

$Y_i \setminus X_i$: True values on Y and X for the i^{th} unit

$\mu_Y \setminus \mu_X$: Population mean of Y given population mean of X

$\mu_{Y(1)}, \mu_{X(1)}$: Population means of Y and X groups of respondents

$\mu_{Y(2)}, \mu_{X(2)}$: Population means of Y and X groups of non-respondents

σ_Y^2, σ_X^2 : Population variances of Y and X , respectively

$\sigma_{Y(1)}^2, \sigma_{X(1)}^2$: Population variances for Y and X groups of respondents

$\sigma_{Y(2)}^2, \sigma_{X(2)}^2$: Population variances for Y and X groups of non-respondents

$C_{Y(1)} = \frac{\sigma_{Y(1)}}{\mu_{Y(1)}}, C_{X(1)} = \frac{\sigma_{X(1)}}{\mu_{X(1)}}$: Coefficient of variations for Y and X groups of respondents

$C_{Y(2)} = \frac{\sigma_{Y(2)}}{\mu_{Y(2)}}, C_{X(2)} = \frac{\sigma_{X(2)}}{\mu_{X(2)}}$: Coefficient of variation for Y and X groups of non-respondents

$y_i \setminus x_i$: reported values on Y and X for the i^{th} unit

$U_i = y_i - Y_i$: measurement error on the study variable associated with i^{th} unit in h^{th} stratum

$V_i = x_i - X_i$: measurement error on the auxiliary variable associated with i^{th} unit in h^{th} stratum

$U_i^* = y_i^* - Y_i^*$: measurement error and non-response on Y associated with i^{th} unit in h^{th} stratum

$V_i^* = x_i^* - X_i^*$: measurement error and non-response on X associated with i^{th} unit in h^{th} stratum

$\sigma_{U(2)}^2$ and $\sigma_{V(2)}^2$: Population variances of U and V groups of non-respondents

$\rho_{YX(1)}$ and $\rho_{YX(2)}$: Coefficients of correlation between the study and auxiliary variables

μ_y' and μ_x' : Sample mean estimator for y and x based on units

$\mu_{y(1)}'', \mu_{x(1)}''$: sample mean estimators for y and x based on units

$\mu_{y(2)r}'', \mu_{x(2)r}''$: sample mean estimators for y and x based on units

$\mu_{y'}^{**}, \mu_{x'}^{**}$: sample mean estimators for y and x following Hansen and Hurwitz (1946)

The measurement errors are assumed to have means zero and the variances $\sigma_{u(2)}^2 = \frac{1}{N_2-1} \sum_{i=1}^{N_2} (U_i - \bar{U}_{(2)})^2$ and $\sigma_{v(2)}^2 = \frac{1}{N_2-1} \sum_{i=1}^{N_2} (V_i - \bar{V}_{(2)})^2$ for the non-respondent group. Let $\mu_{Y(1)} = \frac{1}{N_1} \sum_{i=1}^{N_1} Y_i$ and $\mu_{X(1)} = \frac{1}{N_1} \sum_{i=1}^{N_1} X_i$ be the means and, $\sigma_{Y(1)}^2 = \frac{1}{N_1-1} \sum_{i=1}^{N_1} (Y_i - \mu_{Y(1)})^2$ and $\sigma_{X(1)}^2 = \frac{1}{N_1-1} \sum_{i=1}^{N_1} (X_i - \mu_{X(1)})^2$ be the variances of the study and the auxiliary variables from the respondent group. Similarly, let $\mu_{Y(2)} = \frac{1}{N_2} \sum_{i=1}^{N_2} Y_i$ and $\mu_{X(2)} = \frac{1}{N_2} \sum_{i=1}^{N_2} X_i$ be the means and $\sigma_{Y(2)}^2 = \frac{1}{N_2-1} \sum_{i=1}^{N_2} (Y_i - \mu_{Y(2)})^2$ and $\sigma_{X(2)}^2 = \frac{1}{N_2-1} \sum_{i=1}^{N_2} (X_i - \mu_{X(2)})^2$ be the variances for the non-respondent group. Let $\rho_{XY(1)} = \frac{\sigma_{XY(1)}}{\sigma_{X(1)} \sigma_{Y(1)}}$ and

$\rho_{XY(2)} = \frac{\sigma_{XY(2)}}{\sigma_{X(2)}\sigma_{Y(2)}}$ be the coefficients of correlation between X and Y in the populations of respondent and non-respondent groups, respectively.

In the presence of non-response and measurement errors, we can define the population mean by

$$\mu_Y = W_1\mu_{Y(1)} + W_2\mu_{Y(2)}, \text{ where } W_1 = \frac{N_1}{N} \text{ and } W_2 = \frac{N_2}{N}.$$

At first phase, we select a large sample of size n' ($n' < N$) by simple random sampling without replacement (SRSWOR) to estimate μ_X and a sub-sample of size n'' is taken on 2nd phase by SRSWOR to observe the study variable Y . It is assumed that $n''_{(1)}$ of these units respond and $n''_{(2)} = (n'' - n''_{(1)})$ do not. Let $r \left(= \frac{n''_{(2)}}{k}; k > 1 \right)$ be a sub-sample of the individuals who do not respond to the mailed questionnaire but respond when they are contacted again for their personal interviews, where k is the inverse sampling ratio. It is further assumed that all units respond while interviewing them for the study variable y .

Now, the unbiased sample estimators of μ_Y following the first-phase and second-phase samples, respectively are

$$\mu'_y = \frac{1}{n_1} \sum_{i=1}^{n_1} y_i,$$

and $t_0 = \mu_{y''}^* = \frac{n_1''}{n''} \mu_{y(1)}'' + \frac{n_2''}{n''} \mu_{y(2)r}''$, where

$$\mu_{y(1)}'' = \frac{1}{n_1''} \sum_{i=1}^{n_1''} y_i \text{ and } \mu_{y(2)r}'' = \frac{1}{r} \sum_{i=1}^r y_i^*,$$

with their variances given respectively by

$$\text{Var}(\mu'_y) = \lambda' \mu_Y^2 C_Y^2, \text{ where } \lambda' = \frac{1}{n} - \frac{1}{N} \text{ and}$$

$$\text{Var}(t_0) = \text{Var}(\mu_{y''}^*) = \lambda'' \mu_Y^2 \left(C_Y^2 + \frac{\sigma_{U_1}^2}{\mu_Y^2} \right) + \theta'' \mu_Y^2 \left(C_{Y(2)}^2 + \frac{\sigma_{U_2}^2}{\mu_Y^2} \right),$$

where $\lambda'' = \frac{1}{n''} - \frac{1}{N}$ and $\theta'' = \frac{W_2(r-1)}{n''}$.

Similarly, let $\mu_{x(1)}'' = \frac{1}{n_1''} \sum_{i=1}^{n_1''} x_i$ and $\mu_{x(2)r}'' = \frac{1}{r} \sum_{i=1}^r x_i^*$ denote the means of responding units and the r sub-sampled units for the auxiliary variable.

We modify the usual ratio estimator, usual exponential ratio estimator and usual regression estimator to cover the case of non-response and measurement errors in two-phase sampling. The modified estimators are given respectively by,

$$t_1 = \frac{\mu_{y''}^*}{\mu_{x''}^*} \mu_{x'}', \quad \dots(1)$$

$$t_2 = \mu_{y''}^* \exp \left(\frac{\mu_{x'}' - \mu_{x''}^*}{\mu_{x'}' + \mu_{x''}^*} \right), \quad \dots(2)$$

and

$$t_3 = \mu_{y''}^* + b^* (\mu_{x'}' - \mu_{x''}^*), \quad \dots(3)$$

with the Mean Square Errors (MSE) of t_1, t_2 and t_3 respectively, upto the first order approximation, given by

$$\begin{aligned} \text{MSE}(t_1) = & \lambda'' \mu_Y^2 \left((C_Y^2 + C_X^2 - 2\rho_{yx} C_Y C_X) \left(\frac{\sigma_u^2}{\mu_Y^2} + \frac{\sigma_v^2}{\mu_X^2} \right) \right) \\ & + \theta'' \mu_Y^2 \left((C_{Y(2)}^2 + C_{X(2)}^2 - 2\rho_{yx(2)} C_{Y(2)} C_{X(2)}) \right. \\ & \left. + \left(\frac{\sigma_{u(2)}^2}{\mu_Y^2} + \frac{\sigma_{v(2)}^2}{\mu_X^2} \right) \right) - \lambda' \mu_Y^2 (2\rho_{yx} C_Y C_X - C_X^2), \end{aligned} \quad \dots(4)$$

$$\begin{aligned} \text{MSE}(t_2) = & \lambda'' \mu_Y^2 \left((C_Y^2 + \frac{C_X^2}{4} - \rho_{yx} C_Y C_X) + \left(\frac{\sigma_u^2}{\mu_Y^2} + \frac{\sigma_v^2}{4\mu_X^2} \right) \right) \\ & + \theta'' \mu_Y^2 \left((C_{Y(2)}^2 + \frac{C_{X(2)}^2}{4} - \rho_{yx(2)} C_{Y(2)} C_{X(2)}) \right. \\ & \left. + \left(\frac{\sigma_{u(2)}^2}{\mu_Y^2} + \frac{\sigma_{v(2)}^2}{4\mu_X^2} \right) \right) - \lambda' \mu_Y^2 \left(\rho_{yx} C_Y C_X - \frac{C_X^2}{4} \right), \end{aligned} \quad \dots(5)$$

$$\text{MSE}(t_3) = \mu_Y^2 \left(\lambda'' (C_Y^2 + \frac{\sigma_u^2}{\mu_Y^2}) + \theta'' (C_{Y(2)}^2 + \frac{\sigma_{u(2)}^2}{\mu_Y^2}) \{1 - \theta_0''\} \right), \quad \dots(6)$$

where

$$\theta_0'' = \frac{(\lambda'' \rho_{yx} \sigma_Y \sigma_X + \theta'' \rho_{yx(2)} \sigma_{Y(2)} \sigma_{X(2)} - \lambda' \rho_{yx} C_Y C_X)^2}{\lambda'' \left(C_Y^2 + C_X^2 + \left(\frac{\sigma_u^2}{\mu_Y^2} + \frac{\sigma_v^2}{\mu_X^2} \right) \right) + \theta'' \left(C_{Y(2)}^2 + C_{X(2)}^2 + \left(\frac{\sigma_{u(2)}^2}{\mu_Y^2} + \frac{\sigma_{v(2)}^2}{\mu_X^2} \right) \right) - \lambda' C_X^2}$$

The expression of MSE() is obtained iff

$$b^* = \frac{\lambda'' \rho_{yx} \sigma_Y \sigma_X + \theta'' \rho_{yx(2)} \sigma_{Y(2)} \sigma_{X(2)}}{R \left(\lambda'' (C_X^2 + \frac{\sigma_v^2}{\mu_X^2}) + \theta'' (C_{X(2)}^2 + \frac{\sigma_{v(2)}^2}{\mu_X^2}) \right)}, \quad \text{and } R = \frac{\mu_Y}{\mu_X}.$$

The proposed improved generalized class of estimator (IGCE):

In survey sampling, the surveys often yield biased estimates because of the non-response and/or the measurement errors. Many estimators have been used to deal with the non-response and the measurement errors independently. In this section, we propose an IGCE considering the presence of both the non-response and the measurement errors together on the study variable as well as on the auxiliary variable. We are considering the situation when the population mean of the auxiliary variable is not available.

The proposed IGCE in two-phase sampling considering the non-response and measurement errors is given by

$$t_{4(a)} = (H + \omega_1(\mu'_x - \mu^{*''}_x) + \omega_2\mu^{*''}_y) \exp\left(\frac{\mu'_x - \mu^{*''}_x}{\mu_x + \mu^{*''}_x}\right), \quad \dots(7)$$

$$\text{where } H = \frac{\mu^{*''}_y}{2} \left(\exp\left(\frac{\left(\frac{1}{a}\right)^{*''} \mu^{*''}_x - \left(\frac{1}{a}\right)^{*''} \mu^{*''}_x}{\left(\frac{1}{a}\right)^{*''} \mu^{*''}_x + \left(\frac{1}{a}\right)^{*''} \mu^{*''}_x}\right) + \exp\left(\frac{\left(\frac{1}{a}\right)^{*''} \mu^{*''}_x - \left(\frac{1}{a}\right)^{*''} \mu^{*''}_x}{\left(\frac{1}{a}\right)^{*''} \mu^{*''}_x + \left(\frac{1}{a}\right)^{*''} \mu^{*''}_x}\right) \right),$$

ω_1 and ω_2 are constants which need to be optimized to get minimum mean square error of $t_{4(a)}$, and a is a generalizing constant to get different estimators under the a^{th} root transformation.

For example, for $a=1$, the proposed estimator $t_{4(a)}$ is reduced to the form

$$t_{4(1)} = \left(\frac{\mu^{*''}_y}{2} \left(\exp\left(\frac{\mu'_x - \mu^{*''}_x}{\mu_x + \mu^{*''}_x}\right) + \exp\left(\frac{\mu^{*''}_x - \mu'_x}{\mu^{*''}_x + \mu_x}\right) \right) + \omega_1^{opt(1)} (\mu'_x - \mu^{*''}_x) + \omega_2^{opt(1)} \mu^{*''}_y \right) \exp\left(\frac{\mu'_x - \mu^{*''}_x}{\mu_x + \mu^{*''}_x}\right),$$

and for $a=2$, the proposed estimator is reduced to the form

$$t_{4(2)} = \left(\frac{\mu^{*''}_y}{2} \left(\exp\left(\frac{\left(\frac{1}{2}\right)^{*''} \mu^{*''}_x - \left(\frac{1}{2}\right)^{*''} \mu^{*''}_x}{\left(\frac{1}{2}\right)^{*''} \mu^{*''}_x + \left(\frac{1}{2}\right)^{*''} \mu^{*''}_x}\right) + \exp\left(\frac{\left(\frac{1}{2}\right)^{*''} \mu^{*''}_x - \left(\frac{1}{2}\right)^{*''} \mu^{*''}_x}{\left(\frac{1}{2}\right)^{*''} \mu^{*''}_x + \left(\frac{1}{2}\right)^{*''} \mu^{*''}_x}\right) \right) + \omega_1^{opt(2)} (\mu'_x - \mu^{*''}_x) + \omega_2^{opt(2)} \mu^{*''}_y \right) \exp\left(\frac{\mu'_x - \mu^{*''}_x}{\mu_x + \mu^{*''}_x}\right).$$

The bias and MSE of IGCE $t_{4(a)}$

In order to obtain the expressions for the bias and MSE of $t_{4(a)}$ let us consider,

$$W_X^* = \sum_{i=1}^n (x_i^{*''} - \mu_X), \quad W_U^* = \sum_{i=1}^n U_i^*, \quad W_V^* = \sum_{i=1}^n V_i^*,$$

$$\text{and } W_X = \sum_{i=1}^n (x_i' - \mu_X). \quad \dots(8)$$

Now from (8), the errors due to sampling in the presence of non-response and measurement errors may be written as

$$e_0^{*''} = \frac{1}{n} (W_Y^* + W_U^*), \quad e_1^{*''} = \frac{1}{n} (W_X^* + W_V^*), \text{ and } e_1' = \frac{1}{n} (x_i' - \mu_X), \text{ or alternatively } \mu_y^{*''} = \mu_Y(1 + e_0^{*''}), \mu_x^{*''} = \mu_X(1 + e_1^{*''}), \text{ and } \mu_x' = \mu_X(1 + e_1'),$$

such that $E(e_0^{*''}) = E(e_1^{*''}) = E(e_1') = 0$, and

$$E(e_0^{*''})^2 = \left(\lambda'' \left(C_Y^2 + \frac{\sigma_u^2}{\mu_Y^2} \right) + \theta'' \left(C_{Y(2)}^2 + \frac{\sigma_{u(2)}^2}{\mu_Y^2} \right) \right) = V_{02},$$

$$E(e_1^{*''})^2 = \left(\lambda'' \left(C_X^2 + \frac{\sigma_v^2}{\mu_X^2} \right) + \theta'' \left(C_{X(2)}^2 + \frac{\sigma_{v(2)}^2}{\mu_X^2} \right) \right) = V_{20},$$

$$E(e_0^{*''} e_1^{*''}) = (\lambda'' \rho_{YX} C_Y C_X + \theta'' \rho_{YX(2)} C_{Y(2)} C_{X(2)}) = V_{11},$$

$$E(e_1')^2 = E(e_1^{*''} e_1') = \lambda' C_X^2 = V_{20}, \text{ and}$$

$$E(e_0^{*''} e_1') = \lambda' \rho_{YX} C_Y C_X = V_{11}.$$

Now $t_{4(a)}$ can be rewritten as below:

$$t_{4(a)} = \left(\frac{\mu_Y(1+e_0^{*''})}{2} \left(\exp\left(\frac{\left(\frac{1}{a}\right)^{*''} \mu_X^{*''}(1+e_1') - \left(\frac{1}{a}\right)^{*''} \mu_X^{*''}(1+e_1^{*''})}{\left(\frac{1}{a}\right)^{*''} \mu_X^{*''}(1+e_1') + \left(\frac{1}{a}\right)^{*''} \mu_X^{*''}(1+e_1^{*''})}\right) + \exp\left(\frac{\left(\frac{1}{a}\right)^{*''} \mu_X^{*''}(1+e_1^{*''}) - \left(\frac{1}{a}\right)^{*''} \mu_X^{*''}(1+e_1')}{\left(\frac{1}{a}\right)^{*''} \mu_X^{*''}(1+e_1^{*''}) + \left(\frac{1}{a}\right)^{*''} \mu_X^{*''}(1+e_1')}\right) \right) + \omega_1(\mu_X - \mu_X(1+e_1')) + \omega_2\mu_Y(1+e_0^{*''}) \right) \exp\left(\frac{\mu_X(1+e_1') - \mu_X(1+e_1^{*''})}{\mu_X(1+e_1') + \mu_X(1+e_1^{*''})}\right). \quad \dots(9)$$

Simplifying the above expression up to the order $O(n^{-1})$ we can write (9) as

$$t_{4(a)} - \mu_Y \cong \mu_Y \left(e_0'' + \frac{e_1'}{2} - \frac{e_1''}{2} - \frac{e_1'^2}{8} + \frac{3e_1''^2}{8} - \frac{e_1'e_1''}{4} + \right. \\ \left. \frac{e_1'e_0''}{2} - \frac{e_1''e_0''}{2} + \frac{e_1'^2}{8a^2} + \frac{e_1'^2}{8a^2} - \frac{e_1'e_1''}{4a^2} + w_2e_0'' + \omega_2\frac{e_1'}{2} - \right. \\ \left. w_2\frac{e_1''}{2} - w_2\frac{e_1'^2}{8} + \frac{3w_2e_1''^2}{8} - w_2\frac{e_1'e_1''}{4} + w_2\frac{e_1'e_0''}{2} - \right. \\ \left. w_2\frac{e_1''e_0''}{2} \right) + \omega_1\mu_X \left(e_1' - e_1'' + \frac{e_1'^2}{2} + \frac{e_1''^2}{2} - e_1'e_1'' \right). \quad \dots(10)$$

The expressions for the bias and MSE of $t_{4(a)}$, up to the order $O(n^{-1})$, are given respectively by

$$\text{Bias}(t_{4(a)}) \cong \mu_Y \left(-\frac{V_{20}'}{8} + \frac{3V_{20}''}{8} - \frac{V_{20}'}{4} + \frac{V_{11}'}{2} - \frac{V_{11}''}{2} + \frac{V_{20}''}{8a^2} \right. \\ \left. + \frac{V_{20}'}{8a^2} - \frac{V_{20}''}{4a^2} + \omega_2 - \omega_2\frac{V_{20}'}{8} + \frac{3\omega_2V_{20}''}{8} - \omega_2\frac{V_{20}'}{4} \right. \\ \left. + \omega_2\frac{V_{11}'}{2} - \omega_2\frac{V_{11}''}{2} \right) + \omega_1\mu_X \left(\frac{V_{20}'}{2} + \frac{V_{20}''}{2} - V_{20}' \right), \quad \dots(11)$$

and

$$MSE(t_{4(a)}) \cong \mu_Y^2 \left(V_{02}'' - Y_{11} + \frac{1}{4}Y_{20} + \omega_2^2(1 + V_{02}'' - 2Y_{11} + Y_{20}) + \omega_2(2V_{02}'' - 3Y_{11} + \right. \\ \left. \frac{5}{4}Y_{20} + \frac{1}{4a^2}Y_{20}) \right) + \omega_1^2\mu_X^2Y_{20} \\ + 2\mu_Y\mu_X\omega_1 \left(\omega_2(Y_{20} - Y_{11}) - Y_{11} + \frac{1}{2}Y_{20} \right), \quad \dots(12)$$

where, $Y_{20} = V_{20}'' - V_{20}'$, and $Y_{11} = V_{11}'' - V_{11}'$.

Or alternatively, the MSE of $t_{4(a)}$ can also be given by

$$MSE(t_{4(a)}) \cong \bar{V}_0 + \omega_2^2\bar{V}_1 + \omega_2\bar{V}_2 + \omega_1^2\bar{V}_3 + \omega_1\omega_2\bar{V}_4 + \omega_1\bar{V}_5, \quad \dots(13)$$

where,

$$\bar{V}_0 = \mu_Y^2 \left(V_{02}'' + \frac{1}{4}V_{20} - Y_{11} \right), \\ \bar{V}_1 = \mu_Y^2 (1 + V_{02}'' + Y_{20} - 2Y_{11}), \\ \bar{V}_2 = \mu_Y^2 \left(2V_{02}'' - 3Y_{11} + \frac{5}{4}Y_{20} + \frac{1}{4a^2}Y_{20} \right), \\ \bar{V}_3 = \mu_X^2 Y_{20}, \\ \bar{V}_4 = -2\mu_Y\mu_X (Y_{11} - Y_{20}), \text{ and} \\ \bar{V}_5 = -2\mu_Y\mu_X \left(Y_{11} - \frac{1}{2}Y_{20} \right).$$

Now, to get the optimum values, (13) is differentiated partially with respect to ω_1 and ω_2 and then equating each of the first derivatives with zero. This gives two normal equations which are then solved simultaneously to get the optimum values. Finally, the optimum values are shown by,

$$\omega_1^{opt} = \frac{\bar{V}_2\bar{V}_4 - 2\bar{V}_1\bar{V}_5}{4\bar{V}_1\bar{V}_3 - \bar{V}_4^2} \quad \text{and} \quad \omega_2^{opt} = \frac{\bar{V}_4\bar{V}_5 - 2\bar{V}_2\bar{V}_3}{4\bar{V}_1\bar{V}_3 - \bar{V}_4^2}. \quad \dots(14)$$

Substituting the optimum values ω_1^{opt} and ω_2^{opt} in (13), the expression of the minimum $MSE(t_{4(a)})$ may be obtained as

$$\min MSE(t_{4(a)}) = \bar{V}_0 - \frac{(\bar{V}_2\bar{V}_4\bar{V}_5 - \bar{V}_2^2\bar{V}_3 - \bar{V}_1\bar{V}_5^2)}{\bar{V}_4^2 - 4\bar{V}_1\bar{V}_3}. \quad \dots(15)$$

Theoretical comparisons:

In this section, the proposed estimator IGCE is compared for its efficiency based on the MSE criterion under two-phase sampling with ratio estimator and exponential estimator.

i) The proposed estimator IGCE is more efficient than ratio estimator if $MSE(t_1) - MSE(t_{4(a)}) > 0$, and this gives

$$\frac{1}{V_{02}''Y_{20}} - 2\frac{Y_{11}}{V_{02}''Y_{20}} > \frac{1}{Y_{20}} - \frac{MSE(t_{4(a)})}{Y_{20}Var t_0},$$

$$\text{or alternatively, } \varphi_0 > \frac{\varphi_2}{2} + \varphi_2 \frac{MSE(t_{4(a)})}{2Var t_0} - \frac{1}{2},$$

$$\text{where } \varphi_0 = \frac{Y_{11}}{V_{02}''Y_{20}}, \varphi_1 = \frac{1}{V_{02}''Y_{20}}, \text{ and } \varphi_2 = \frac{1}{Y_{20}}.$$

ii) The proposed estimator IGCE is more efficient than exponential ratio estimator if

$$MSE(t_2) - MSE(t_{4(a)}) > 0, \text{ and this gives}$$

$$\frac{1}{4V_{02}''Y_{20}} - \frac{Y_{11}}{V_{02}''Y_{20}} > \frac{1}{Y_{20}} - \frac{MSE(t_{4(a)})}{Y_{20}Var t_0},$$

or alternatively,

$$\varphi_0 > \frac{\varphi_3}{4} + \varphi_2 \frac{MSE(t_{4(a)})}{2Var t_0} - \varphi_2, \quad \text{where } \varphi_3 = \frac{1}{V_{02}''Y_{20}}.$$

iii) The proposed estimator IGCE is more efficient than regression estimator if

$MSE(t_3) - MSE(t_{4(a)}) > 0$, and this gives

$$\varphi_0 > 1 - \frac{MSE(t_{4(a)})}{Var t_0}.$$

RESULTS AND DISCUSSION

In this section, we examine the performance of the proposed estimators in comparison to the modified estimators. We have generated two populations by using normal, and lognormal distributions with different parameter values using R statistical software. The description of each population is given below.

Population I: [normal population]

$X=N(5000, 5, 15)$; $z=N(5000, 0, 1)$; $Y=50X+15z$;
 $y=Y+N(1, 3)$; $x=X+N(1, 3)$; $\mu_Y = 248.67$; $\mu_X = 4.97$;
 $\sigma_y^2=583685.70$; $\sigma_x^2=242.30$; $\sigma_U^2=9.25$; $\sigma_V^2=9.25$;
 $\rho_{yx}=0.98$; $N=5000$; $N_1=3500$; $N_2=1500$; $n'=500$;
 $\sigma_{y(2)}^2=599476.60$; $\sigma_{x(2)}^2=239.94$; $\sigma_{U(2)}^2=9.14$;
 $\sigma_{V(2)}^2=8.81$; $\rho_{yx(2)}=0.99$;

Population II: [lognormal population]

$X=\log N(5000, \log(4), \log(6))$; $z=N(5000, 0, 1)$;
 $Y=50X+15z$; $y=Y+N(1, 3)$; $x=X+N(1, 3)$; $\mu_Y = 703.27$;
 $\mu_X = 14.07$; $\sigma_y^2=5871164.00$; $\sigma_x^2=2363.44$; $\sigma_U^2=9.03$;
 $\sigma_V^2=8.69$; $\rho_{yx}=0.99$; $N=5000$; $N_1=3500$; $N_2=1500$;
 $n'=500$; $\sigma_{y(2)}^2=9035398.00$; $\sigma_{x(2)}^2=3615.41$;
 $\sigma_{U(2)}^2=8.72$; $\sigma_{V(2)}^2=8.85$; $\rho_{yx(2)}=0.99$;

The MSE s and the bias of proposed and some available estimators are presented in Tables A1-A4 in appendix A.

The bold numbers in Tables A1 and A2, represents the lowest two $MSE t_{4(a)}$ as compared to the MSE s,

of t_0 , t_1 , t_2 and t_3 . From Tables A1 and A2, one can observe that the proposed class of estimators provides estimators which have less MSE values than the MSE 's of all of the modified estimators. We observe that the best performance is for $a=1$. However, the performance of the modified estimator for $a=2$ still shows smaller MSE than the MSE s of all other estimators. Tables A3 and A4 display the absolute relative bias. It can be observed that the proposed estimators are slightly more biased than the existing estimators, but the biases are not notable. Therefore, still the proposed estimators can be preferred over other existing estimators.

The proposed improved generalized class of estimator in stratified two-phase sampling (IGCEStr)

Let a population be divided into L homogenous strata with N_h units ($h=1, 2, \dots, L$) such that $\sum_{h=1}^L N_h = N$. At first-phase, a large sample of size n'_h is selected from h^{th} stratum such that $\sum_{h=1}^L n'_h = n'$ and a sub-sample of size n''_h ($n''_h < n'_h$) from each stratum is taken on 2nd phase such that $\sum_{h=1}^L n''_h = n''$ by *SRSWOR*. Let (y_{hi}, x_{hi}) be the observed values instead of true values (Y_{hi}, X_{hi}) of the two characteristic (Y, X) , respectively associated with i^{th} unit of h^{th} stratum, where $i=1, 2, \dots, N_h$ and $h=1, 2, \dots, L$. It is assumed that only $n''_{h(1)}$ units respond and $n''_{h(2)} = (n''_h - n''_{h(1)})$ do not. Following Hansen and Hurwitz (1946), another sub-sample of size r_h ($r_h = \frac{n''_{h(2)}}{k_h}$; $k_h > 1$) is taken from $n''_{h(2)}$ ($r_h < n''_{h(2)}$) and the subjects are interviewed. It is further assumed that all r_h units respond while interviewing them for the study variable Y .

In addition, let $\mu_Y = \sum_{i=1}^L P_h \mu_{Yh}$ and $\mu_X = \sum_{i=1}^L P_h \mu_{Xh}$, where $\mu_{Yh} = \frac{1}{N_h} \sum_{i=1}^{N_h} Y_{hi}$, $\mu_{Xh} = \frac{1}{N_h} \sum_{i=1}^{N_h} X_{hi}$, are the population means of the study and the auxiliary variables respectively and $P_h = N_h/N$ is the weight of h^{th} stratum in the presence of non-response on the study variable as well as the auxiliary variable in h^{th} stratum. Let (X_{hi}^*, Y_{hi}^*) be the observed values and (X_{hi}^*, Y_{hi}^*) be the true values for the two characteristics (x_{hi}, y_{hi}) respectively associated with i^{th} ($i=1, 2, \dots$) sample unit of h^{th} stratum. The measurement error in the presence of non-response for h^{th} stratum may

be taken as $U_{hi}^* = y_{hi} - Y_{hi}$ and $V_{hi}^* = x_{hi} - X_{hi}$ with mean zero and variances $\sigma_{U_h}^2$ and $\sigma_{V_h}^2$, respectively. Let $(\mu_{Yh(1)}, \mu_{Xh(1)})$ and $(\sigma_{Yh(1)}^2, \sigma_{Xh(1)}^2)$ respectively be the means and variances of the study and the auxiliary variables in h^{th} stratum for respondent group. Similarly, let $(\mu_{Yh(2)}, \mu_{Xh(2)})$ and $(\sigma_{Yh(2)}^2, \sigma_{Xh(2)}^2)$ respectively be the means and variances for non-respondent group. Further, let $(C_{Yh(1)}, C_{Xh(1)})$ and $(C_{Yh(2)}, C_{Xh(2)})$ respectively be the coefficient of variations for the respondent and the non-respondent group respectively. Let $\rho_{xyh(1)}$ and $\rho_{xyh(2)}$ be the correlations from the populations of respondents and non-respondents, respectively.

Now, usual unbiased mean estimators assuming non-response and measurement error in stratified first-phase and stratified two-phase sampling are defined respectively by

$$\mu'_{y(st)} = \sum_{h=1}^L P_h \mu'_{yh}, \text{ and } t_{01} = \mu^{*''}_{y(st)} = \frac{n_{h(1)}''}{n_h''} \mu''_{yh(1)} + \frac{n_{h(2)}''}{n_h''} \mu''_{y(2)k_h},$$

where $\mu'_{yh} = \frac{1}{n_h} \sum_{i=1}^{n_h} y_{hi}$, $\mu''_{yh(1)} = \frac{1}{n_{h(1)}''} \sum_{i=1}^{n_{h(1)}''} y_{hi}$ and

$$\mu''_{y(2)r_h} = \frac{1}{r_h} \sum_{i=1}^{r_h} y_{hi}^*.$$

The expressions for the variances of $\mu'_{y(st)}$ and $\mu^{*''}_{y(st)}$ are given respectively by

$$\text{var}(\mu'_{y(st)}) = \mu_Y^2 \sum_{h=1}^L P_h^2 \lambda_h' C_{Yh}^2,$$

and

$$\text{var}(t_{01}) = \text{var}(\mu^{*''}_{y(st)}) = \mu_Y^2 \sum_{h=1}^L P_h^2 \lambda_h'' \left(C_{Yh}^2 + \frac{\sigma_{uh}^2}{\mu_Y^2} \right) + \mu_Y^2 \sum_{h=1}^L P_h^2 (C_{Yh(2)}^2 + \frac{\sigma_{uh(2)}^2}{\mu_Y^2}),$$

where $\lambda_h'' = \left(\frac{1}{n_h''} - \frac{1}{N_h} \right)$, $\lambda_h' = \left(\frac{1}{n_h} - \frac{1}{N_h} \right)$,

$$\theta_h'' = \frac{W_{h(2)}(k_h-1)}{n_h''}, \text{ and } W_{h(2)} = \frac{N_{h(2)}}{N_h}.$$

Similarly, let $\mu''_{xh(1)} = \frac{1}{n_{h(1)}''} \sum_{i=1}^{n_{h(1)}''} x_{ih}$ and $\mu''_{x(2)r_h} = \frac{1}{r_h} \sum_{i=1}^{r_h} x_{ih}^*$ denote the means of the

responding units, and r_h sub-sampled units for the auxiliary variable.

We modify the usual ratio, exponential ratio and regression estimators to the case of non-response and measurement error in two-phase sampling respectively as

$$t_5 = \frac{\mu_{y(st)}^{*''}}{\mu_{x(st)}^{*''}} \mu'_{x(st)}, \quad \dots(16)$$

$$t_6 = \mu_{y(st)}^{*''} \exp \left(\frac{\mu'_{x(st)} - \mu_{x(st)}^{*''}}{\mu_{x(st)}^{*''} + \mu_{x(st)}^{*''}} \right), \quad \dots(17)$$

and

$$t_7 = (\mu_{y(st)}^{*''} + b^{**}(\mu'_{x(st)} - \mu_{x(st)}^{*''})). \quad \dots(18)$$

The MSEs of t_5 , t_6 and t_7 , respectively are given by,

$$\begin{aligned} \text{MSE}(t_5) = & \lambda_h'' \mu_Y^2 \sum_{h=1}^L P_h^2 \left((C_{Yh}^2 + C_{Xh}^2 - 2\rho_{yxh} C_{Yh} C_{Xh}) \right. \\ & + \left(\frac{\sigma_{uh}^2}{\mu_Y^2} + \frac{\sigma_{vh}^2}{\mu_X^2} \right) \Big) + \theta_h'' \mu_Y^2 \sum_{h=1}^L P_h^2 \left((C_{Yh(2)}^2 + C_{Xh(2)}^2 - \right. \\ & 2\rho_{yxh(2)} C_{Yh(2)} C_{Xh(2)}) + \left(\frac{\sigma_{uh(2)}^2}{\mu_Y^2} + \frac{\sigma_{vh(2)}^2}{\mu_X^2} \right) \Big) \\ & - \lambda_h' \mu_Y^2 \sum_{h=1}^L P_h^2 (2\rho_{yxh} C_{Yh} C_{Xh} - C_{Xh}^2), \quad \dots(19) \end{aligned}$$

$$\begin{aligned} \text{MSE}(t_6) = & \lambda_h'' \mu_Y^2 \sum_{h=1}^L P_h^2 \left(\left(C_{Yh}^2 + \frac{C_{Xh}^2}{4} - \rho_{yxh} C_{Yh} C_{Xh} \right) \right. \\ & + \left(\frac{\sigma_{uh}^2}{\mu_Y^2} + \frac{\sigma_{vh}^2}{4\mu_X^2} \right) \Big) + \theta_h'' \mu_Y^2 \sum_{h=1}^L P_h^2 \left((C_{Yh(2)}^2 + \right. \\ & \frac{C_{Xh(2)}^2}{4} - \rho_{yxh(2)} C_{Yh(2)} C_{Xh(2)}) + \left(\frac{\sigma_{uh(2)}^2}{\mu_Y^2} + \frac{\sigma_{vh(2)}^2}{4\mu_X^2} \right) \Big) - \\ & \lambda_h' \mu_Y^2 \sum_{h=1}^L P_h^2 \left(\rho_{yxh} C_{Yh} C_{Xh} - \frac{C_{Xh}^2}{4} \right), \quad \dots(20) \end{aligned}$$

and

$$\begin{aligned} \text{MSE}(t_7) = & \mu_Y^2 \sum_{h=1}^L P_h^2 \left(\lambda_h'' \left(C_{Yh}^2 + \frac{\sigma_{uh}^2}{\mu_Y^2} \right) \right. \\ & + \theta_h'' \left(C_{Yh(2)}^2 + \frac{\sigma_{uh(2)}^2}{\mu_Y^2} \right) \{1 - \theta_0''\} \Big), \quad \dots(21) \end{aligned}$$

where

$$\theta_0'' = \frac{\sum_{h=1}^L P_h^2 (\lambda_h'' \rho_{YXh} \sigma_{Yh} \sigma_{Xh} + \theta_h'' \rho_{YXh(2)} \sigma_{Yh(2)} \sigma_{Xh(2)} - \lambda_h' \rho_{YXh} C_{Yh} C_{Xh})^2}{\sum_{h=1}^L P_h^2 \left(\lambda_h'' \left(C_{Yh}^2 + C_{Xh}^2 + \left(\frac{\sigma_{uh(2)}^2}{\mu_Y^2} + \frac{\sigma_{vh(2)}^2}{\mu_X^2} \right) \right) + \theta_h'' \left(C_{Yh(2)}^2 + C_{Xh(2)}^2 + \left(\frac{\sigma_{uh(2)}^2}{\mu_Y^2} + \frac{\sigma_{vh(2)}^2}{\mu_X^2} \right) \right) \right) - \lambda_h' \sum_{h=1}^L P_h^2 C_{Xh}^2}$$

The expression of $MSE(t_7)$ is obtained if

$$b^{**} = \frac{\sum_{h=1}^L P_h^2 (\lambda_h'' \rho_{YXh} \sigma_{Yh} \sigma_{Xh} + \theta_h'' \rho_{YXh(2)} \sigma_{Yh(2)} \sigma_{Xh(2)})}{R \sum_{h=1}^L P_h^2 \left(\lambda_h'' \left(C_{Xh}^2 + \frac{\sigma_{vh}^2}{\mu_X^2} \right) + \theta_h'' \left(C_{Xh(2)}^2 + \frac{\sigma_{vh(2)}^2}{\mu_X^2} \right) \right)},$$

$$\text{and } R = \frac{\mu_Y}{\mu_X}.$$

Now following (16) to (18), we propose another generalized estimator in two-phase sampling considering non-response and measurement error on 2nd phase only, as given by

$$t_{8(a)} = (H^* + \alpha_1 (\mu_{x(st)}' - \mu_{x(st)}^{*''}) + \alpha_2 \mu_{y(st)}^{*''}) \exp \left(\frac{\mu_{x(st)}' - \mu_{x(st)}^{*''}}{\mu_{x(st)}' + \mu_{x(st)}^{*''}} \right), \quad \dots(22)$$

where

$$H^* = \frac{\mu_{y(st)}^{*''}}{2} \left(\exp \left(\frac{\mu_{x(st)}' - \mu_{x(st)}^{*''}}{\mu_{x(st)}' + \mu_{x(st)}^{*''}} \right) + \exp \left(\frac{\mu_{x(st)}^{*''} - \mu_{x(st)}'}{\mu_{x(st)}^{*''} + \mu_{x(st)}'} \right) \right),$$

and α_1 and α_2 are the optimizing constants and a is a generalizing constant. For different choices of a , different estimators are obtained. For example, for $a=1$, the proposed estimator is reduced to the form

$$t_{8(1)} = \left(\frac{\mu_{y(st)}^{*''}}{2} \left(\exp \left(\frac{\mu_{x(st)}' - \mu_{x(st)}^{*''}}{\mu_{x(st)}' + \mu_{x(st)}^{*''}} \right) + \exp \left(\frac{\mu_{x(st)}^{*''} - \mu_{x(st)}'}{\mu_{x(st)}^{*''} + \mu_{x(st)}'} \right) \right) + \alpha_1^{opt(1)} (\mu_{x(st)}' - \mu_{x(st)}^{*''}) + \alpha_2^{opt(1)} \mu_{y(st)}^{*''} \right) \exp \left(\frac{\mu_{x(st)}' - \mu_{x(st)}^{*''}}{\mu_{x(st)}' + \mu_{x(st)}^{*''}} \right),$$

and for $a=2$, the proposed estimator $t_{4(a)}$ is reduced to the form

$$t_{8(2)} = \left(\frac{\mu_{y(st)}^{*''}}{2} \left(\exp \left(\frac{\mu_{x(st)}^{*(1/2)} - \mu_{x(st)}^{*(1/2)}}{\mu_{x(st)}^{*(1/2)} + \mu_{x(st)}^{*(1/2)}} \right) + \exp \left(\frac{\mu_{x(st)}^{*(1/2)} - \mu_{x(st)}^{*(1/2)}}{\mu_{x(st)}^{*(1/2)} + \mu_{x(st)}^{*(1/2)}} \right) \right) + \alpha_1^{opt(2)} (\mu_{x(st)}' - \mu_{x(st)}^{*''}) \right)$$

$$+ \alpha_2^{opt(2)} \mu_{y(st)}^{*''} \exp \left(\frac{\mu_{x(st)}' - \mu_{x(st)}^{*''}}{\mu_{x(st)}' + \mu_{x(st)}^{*''}} \right).$$

The bias and MSE of $t_{8(a)}$

In order to obtain the expressions for the bias and MSE of $t_{8(a)}$ let us consider

$$W_{Yh}^* = \sum_{i=1}^{n_h} (y_{hi}^{*''} - \mu_{Yh}), W_{Xh}^* = \sum_{i=1}^{n_h} (x_{hi}^{*''} - \mu_{Xh}),$$

$$W_{Uh}^* = \sum_{i=1}^{n_h} U_{hi}^*, W_{Vh}^* = \sum_{i=1}^{n_h} V_{hi}^*,$$

$$\text{and } W_{Xh} = \sum_{i=1}^{n_h} (x_{hi}' - \mu_{Xh}). \quad \dots(23)$$

Now the sampling errors, assuming the presence of non-response and measurement errors in stratified two-phase random sampling, may be given by

$$e_{0(st)}^{*''} = \frac{1}{\mu_Y} \sum_{h=1}^L \frac{P_h}{n_h} (W_{Yh}^* + W_{Uh}^*),$$

$$e_{1(st)}^{*''} = \frac{1}{\mu_X} \sum_{h=1}^L \frac{P_h}{n_h} (W_{Xh}^* + W_{Vh}^*), \text{ and}$$

$$e_{1(st)}' = \frac{1}{\mu_X} \sum_{h=1}^L \frac{P_h}{n_h} (x_{hi}' - \mu_{Xh}), \text{ or alternatively by,}$$

$$\mu_{y(st)}^{*''} = \mu_Y (1 + e_{0(st)}^{*''}), \mu_{x(st)}^{*''} = \mu_X (1 + e_{1(st)}^{*''}), \text{ and}$$

$$\mu_{x(st)}' = \mu_X (1 + e_{1(st)}'),$$

such that $E(e_{0(st)}^{*''}) = E(e_{1(st)}^{*''}) = E(e_{1(st)}') = 0$, and

$$E(e_{0(st)}^{*''})^2 = \sum_{h=1}^L P_h^2 \left(\lambda_h'' (C_{Yh}^2 + \frac{\sigma_{uh}^2}{\mu_Y^2}) + \theta_h'' (C_{Yh(2)}^2 + \frac{\sigma_{uh(2)}^2}{\mu_Y^2}) \right) = V_{02(st)}^{*''},$$

$$E(e_{1(st)}^{*''})^2 = \sum_{h=1}^L P_h^2 \left(\lambda_h'' (C_{Xh}^2 + \frac{\sigma_{vh}^2}{\mu_X^2}) + \theta_h'' (C_{Xh(2)}^2 + \frac{\sigma_{vh(2)}^2}{\mu_X^2}) \right) = V_{20(st)}^{*''},$$

$$E(e_{0(st)}^{*''} e_{1(st)}^{*''}) = \sum_{h=1}^L P_h^2 (\lambda_h'' \rho_{YXh} C_{Yh} C_{Xh} + \theta_h'' \rho_{YXh(2)} C_{Yh(2)} C_{Xh(2)}) = V_{11(st)}^{*''},$$

$$E(e'_{1(st)})^2 = E(e'^{*''}_{1(st)} e'_{1(st)}) = \sum_{h=1}^L P_h^2 \lambda'_h C_{Xh}^2 = V'_{20(st)},$$

$$E(e'^{*''}_{0(st)} e'_{1(st)}) = \sum_{h=1}^L P_h^2 (\lambda'_h \rho_{YXh} C_{Yh} C_{Xh}) = V'_{11(st)}.$$

Now we may express $t_{8(a)}$ in terms of e, s by

$$\begin{aligned} t_{8(a)} = & \left(\frac{\mu_Y (1 + e'^{*''}_{0(st)})}{2} \right) \left(\exp \left(\frac{\mu_X^{\frac{1}{a}} (1 + e'_{1(st)})^{\frac{1}{a}} - \mu_X^{\frac{1}{a}} (1 + e'^{*''}_{1(st)})^{\frac{1}{a}}}{\mu_X^{\frac{1}{a}} (1 + e'_{1(st)})^{\frac{1}{a}} + \mu_X^{\frac{1}{a}} (1 + e'^{*''}_{1(st)})^{\frac{1}{a}}} \right) + \right. \\ & \left. \exp \left(\frac{\mu_X^{\frac{1}{a}} (1 + e'^{*''}_{1(st)})^{\frac{1}{a}} - \mu_X^{\frac{1}{a}} (1 + e'_{1(st)})^{\frac{1}{a}}}{\mu_X^{\frac{1}{a}} (1 + e'^{*''}_{1(st)})^{\frac{1}{a}} + \mu_X^{\frac{1}{a}} (1 + e'_{1(st)})^{\frac{1}{a}}} \right) \right) + \\ & \alpha_1 (\mu_X - \mu_X (1 + e'_{1(st)})) + \alpha_2 \mu_Y (1 + e'^{*''}_{0(st)}) \\ & \exp \left(\frac{\mu_X (1 + e'_{1(st)}) - \mu_X (1 + e'^{*''}_{1(st)})}{\mu_X (1 + e'_{1(st)}) + \mu_X (1 + e'^{*''}_{1(st)})} \right). \end{aligned} \quad \dots(24)$$

Simplifying the above expression up to the order $O(n^{-1})$, we get

$$\begin{aligned} t_{8(a)} - \mu_Y \cong & \mu_Y \left(e'^{*''}_{0(st)} + \frac{e'_{1(st)}}{2} - \frac{e'^{*''}_{1(st)}}{2} - \frac{e'^2_{1(st)}}{8} + \frac{3e'^{*''2}_{1(st)}}{8} \right. \\ & - \frac{e'_{1st} e'^{*''}_{1(st)}}{4} + \frac{e'_{1(st)} e'^{*''}_{0(st)}}{2} - \frac{e'^{*''}_{1(st)} e'^{*''}_{0(st)}}{2} + \frac{e'^{*''2}_{1(st)}}{8a^2} \\ & + \frac{e'^2_{1(st)}}{8a^2} - \frac{e'_{1(st)} e'^{*''}_{1(st)}}{4a^2} + \alpha_2 + \alpha_2 e'^{*''}_{0(st)} + \alpha_2 \frac{e'_{1(st)}}{2} \\ & - \alpha_2 \frac{e'^{*''}_{1(st)}}{2} - \alpha_2 \frac{e'^2_{1(st)}}{8} + \frac{3\alpha_2 e'^{*''}_{1(st)}}{8} - \alpha_2 \frac{e'_{1(st)} e'^{*''}_{1(st)}}{4} \\ & + \alpha_2 \frac{e'_{1(st)} e'^{*''}_{0(st)}}{2} - \alpha_2 \frac{e'^{*''}_{1(st)} e'^{*''}_{0(st)}}{2} \Big) \\ & + \alpha_1 \mu_X \left(e'_{1(st)} - e'^{*''}_{1(st)} + \frac{e'^2_{1(st)}}{2} + \frac{e'^{*''2}_{1(st)}}{2} - e'_{1(st)} e'^{*''}_{1(st)} \right). \end{aligned} \quad \dots(25)$$

The expressions for the bias and MSE of $t_{8(a)}$, upto the order $O(n^{-1})$, may be obtained from (25) as

$$Bias(t_{8(a)}) \cong \mu_Y \left(-\frac{V'_{20(st)}}{8} + \frac{3V'^{*''}_{20(st)}}{8} - \frac{V'_{20(st)}}{4} + \frac{V'_{11(st)}}{2} \right.$$

$$\begin{aligned} & - \frac{V'^{*''}_{11(st)}}{2} + \frac{V'^{*''}_{20(st)}}{8a^2} + \frac{V'_{20(st)}}{8a^2} - \frac{V'_{20(st)}}{4a^2} + \alpha_2 - \\ & \alpha_2 \frac{V'_{20(st)}}{8} + \frac{3\alpha_2 V'^{*''}_{20(st)}}{8} - \alpha_2 \frac{V'_{20(st)}}{4} + \alpha_2 \frac{V'_{11(st)}}{2} - \alpha_2 \frac{V'^{*''}_{11(st)}}{2} \Big) \\ & + \alpha_1 \mu_X \left(\frac{V'_{20(st)}}{2} + \frac{V'^{*''}_{20(st)}}{2} - V'_{20(st)} \right), \end{aligned} \quad \dots(26)$$

and

$$\begin{aligned} MSE(t_{8(a)}) \cong & \mu_Y^2 \left(V'^{*''}_{02(st)} - \mathbb{Y}_{11} + \frac{1}{4} \mathbb{Y}_{20} + \alpha_2^2 \right. \\ & + \alpha_2^2 (1 + V'^{*''}_{02(st)} - 2\mathbb{Y}_{11} + \mathbb{Y}_{20}) + \alpha_2 (2V'^{*''}_{02(st)} - \\ & 3\mathbb{Y}_{11} + \frac{5}{4} \mathbb{Y}_{20} + \frac{1}{4a^2} \mathbb{Y}_{20}) + \alpha_1^2 \mu_X^2 \mathbb{Y}_{20} \\ & + 2\mu_Y \mu_X \alpha_1 \left(\alpha_2 (\mathbb{Y}_{20} - \mathbb{Y}_{11}) - \mathbb{Y}_{11} + \frac{1}{2} \mathbb{Y}_{20} \right), \end{aligned} \quad \dots(27)$$

where, $\mathbb{Y}_{20} = V'^{*''}_{20(st)} - V'_{20(st)}$, and

$$\mathbb{Y}_{11} = V'^{*''}_{11(st)} - V'_{11(st)}.$$

Or alternatively,

$$MSE(t_{8(a)}) \cong \nabla_0 + \alpha_2^2 \nabla_1 + \alpha_2 \nabla_2 + \alpha_1^2 \nabla_3 + \alpha_1 \alpha_2 \nabla_4 + \alpha_1 \nabla_5, \quad \dots(28)$$

where,

$$\nabla_0 = \mu_Y^2 \left(V'^{*''}_{02(st)} + \frac{1}{4} \mathbb{Y}_{20} - \mathbb{Y}_{11} \right),$$

$$\nabla_1 = \mu_Y^2 \left(1 + V'^{*''}_{02(st)} + \mathbb{Y}_{20} - 2\mathbb{Y}_{11} \right),$$

$$\nabla_2 = \mu_Y^2 \left(2V'^{*''}_{02(st)} - 3\mathbb{Y}_{11} + \frac{5}{4} \mathbb{Y}_{20} + \frac{1}{4a^2} \mathbb{Y}_{20} \right),$$

$$\nabla_3 = \mu_X^2 \mathbb{Y}_{20},$$

$$\nabla_4 = -2\mu_Y \mu_X (\mathbb{Y}_{11} - \mathbb{Y}_{20}),$$

$$\text{and } \nabla_5 = -2\mu_Y \mu_X \left(\mathbb{Y}_{11} - \frac{1}{2} \mathbb{Y}_{20} \right).$$

Now, to get the optimum values, equation (28) is differentiated partially with respect to α_1 , and α_2 , and then equating each of the first derivatives with zero. This gives two normal equations which are then solved simultaneously to get the optimum values. Finally, the optimum values are shown by,

$$\alpha_1^{(opt)} = \frac{\nabla_2 \nabla_4 - 2 \nabla_1 \nabla_5}{4 \nabla_1 \nabla_3 - \nabla_4^2} \text{ and } \alpha_2^{(opt)} = \frac{\nabla_4 \nabla_5 - 2 \nabla_2 \nabla_3}{4 \nabla_1 \nabla_3 - \nabla_4^2}. \quad \dots(29)$$

Substituting the optimum values of α_1 and α_2 in (28), the expression for the minimum $MSE(t_{8(a)})$ may be obtained as

$$\min MSE(t_{8(a)}) = \nabla_0 - \frac{(\nabla_2 \nabla_4 \nabla_5 - \nabla_2^2 \nabla_3 - \nabla_1 \nabla_5^2)}{\nabla_4^2 - 4 \nabla_1 \nabla_3}. \quad \dots(30)$$

Theoretical comparisons

In this section, the proposed estimator IGCEStr is compared for its efficiency based on the MSE criterion under stratified two-phase sampling with ratio estimator and exponential estimator.

- i) The proposed estimator IGCEStr is more efficient than ratio estimator under stratified two-phase sampling if $MSE(t_5) - MSE(t_{8(a)}) > 0$, and this gives

$$\frac{1}{V_{02(st)}'' \bar{y}_{20}} - 2 \frac{\bar{y}_{11}}{V_{02(st)}'' \bar{y}_{20}} > \frac{1}{\bar{y}_{20}} - \frac{MSE(t_{8(a)})}{\bar{y}_{20} Var t_{0(st)}},$$

$$\text{or alternatively, } \tau_0 > \frac{\tau_2}{2} + \tau_2 \frac{MSE(t_{8(a)})}{2 Var t_{0(st)}} - \frac{1}{2},$$

$$\text{where } \tau_0 = \frac{\bar{y}_{11}}{V_{02(st)}'' \bar{y}_{20}}, \tau_1 = \frac{1}{V_{02(st)}'' \bar{y}_{20}}, \text{ and } \tau_2 = \frac{1}{\bar{y}_{20}}.$$

- ii) The proposed estimator IGCEStr is more efficient

than exponential ratio estimator under stratified two-phase sampling if $MSE(t_6) - MSE(t_{8(a)}) > 0$, and this gives

$$\frac{1}{4 V_{02(st)}'' \bar{y}_{20}} - \frac{\bar{y}_{11}}{V_{02(st)}'' \bar{y}_{20}} > \frac{1}{\bar{y}_{20}} - \frac{MSE(t_{8(a)})}{\bar{y}_{20} var t_{0(st)}},$$

or alternatively,

$$\tau_0 > \frac{\tau_3}{4} + \tau_2 \frac{MSE(t_{8(a)})}{2 var t_{0(st)}} - \tau_2, \text{ where } \tau_3 = \frac{1}{V_{02(st)}'' \bar{y}_{20}}.$$

- iii) The proposed estimator IGCEStr is more efficient than regression estimator under stratified two-phase sampling if $MSE(t_3) - MSE(t_{4(a)}) > 0$, and this gives

$$\tau_0 > 1 - \frac{MSE(t_{8(a)})}{Var t_{0(st)}}.$$

Empirical results and discussion using stratified populations:

In order to compare performance of the proposed estimators $t_{8(a)}$ for $a=1,2$, from the proposed class of IGCEStr with $t_{0(st)}$ t_5 , t_6 , and t_7 , we consider two different simulated stratified populations. The description on parameters of each stratified population is given respectively as below;

Stratified population I: [Normal Population]

Stratum-1 $X_1 = N(5000, 4, 15)$; $z_1 = N(5000, 0, 1)$; $Y_1 = 50X + 15z$; $y_1 = Y + N(1, 3)$; $x_1 = X + N(1, 3)$;
 Stratum-2 $X_2 = N(5000, 5, 15)$; $z_2 = N(5000, 0, 1)$; $Y_2 = 50X + 15z$; $y_2 = Y + N(1, 3)$; $x_2 = X + N(1, 3)$;
 Stratum-3 $X_3 = N(5000, 6, 15)$; $z_3 = N(5000, 0, 1)$; $Y_3 = 50X + 15z$; $y_3 = Y + N(1, 3)$; $x_3 = X + N(1, 3)$;

stratum	N_h	ρ_{yxh}	μ_{yh}	μ_{xh}	σ_{Uh}^2	σ_{Vh}^2	σ_{yh}^2	σ_{xh}^2
1	5000	0.98	183.62	3.67	9.19	9.32	543610.50	227.16
2	5000	0.98	248.67	4.97	9.19	9.25	583685.70	242.30
3	5000	0.98	301.68	6.04	9.10	9.18	578114.50	240.50
stratum	n_h'	n_h''	$\sigma_{yh(2)}^2$	$\sigma_{xh(2)}^2$	$\sigma_{Uh(2)}^2$	$\sigma_{Vh(2)}^2$	$\rho_{yxh(2)}$	
1	500	300	575428.90	230.66	9.15	9.75	0.99	
2	500	300	599476.60	239.94	9.14	8.80	0.99	
3	500	300	577044.10	230.86	9.32	8.63	0.99	

Stratified population II: [Lognormal Population]

Stratum-1 $X_1 = \log N(5000, \log(2), \log(6))$; $z_1 = N(5000, 0, 1)$; $Y_1 = 50X + 15z$; $y_1 = Y + N(1, 3)$; $x_1 = X + N(1, 3)$;
 Stratum-2 $X_2 = \log N(5000, \log(3), \log(6))$; $z_2 = N(5000, 0, 1)$; $Y_2 = 50X + 15z$; $y_2 = Y + N(1, 3)$; $x_2 = X + N(1, 3)$;
 Stratum-3 $X_3 = \log N(5000, \log(4), \log(6))$; $z_3 = N(5000, 0, 1)$; $Y_3 = 50X + 15z$; $y_3 = Y + N(1, 3)$; $x_3 = X + N(1, 3)$;

stratum	N_h	ρ_{yjh}	μ_{yh}	μ_{xh}	σ_{yh}^2	σ_{xh}^2	σ_{yjh}^2	σ_{xjh}^2
1	5000	0.99	703.27	14.07	9.03	8.69	5871164.00	2363.44
2	5000	0.99	915.35	18.31	8.73	9.16	8522645.00	3424.65
3	5000	0.99	1221.84	24.44	8.94	9.03	20392993.00	8165.68

stratum	n'_h	n''_h	$\sigma_{yh(2)}^2$	$\sigma_{xh(2)}^2$	$\sigma_{yjh(2)}^2$	$\sigma_{xjh(2)}^2$	$\rho_{yjh(2)}$
1	500	300	9035398.00	3615.41	8.72	8.85	0.99
2	500	300	5158451.00	2063.84	8.65	9.15	0.99
3	500	300	17392184.00	6956.91	8.85	8.88	0.9

We have computed the mean squared error (*MSEs*) and bias of the proposed and some available estimators and the results are presented in Tables 5 – 8.

In this section the relative performance of the proposed *IGCEStr* with some modified estimators is observed taking different values of k_h ($=2, 3, 4, \& 5$). It can be observed from Tables 5 – 6 that the proposed performs better than $t_{0(st)}, t_5, t_6$ and t_7 . We note that performance of the estimator $t_{8(a)}$ is the best for $a=1$, however for $a=2$ the estimator is showing relatively large *MSE*. Therefore, we note that the square root transformation is not working better than the case $a=1$ for . Further, we can note that *MSEs* of for $a=2$ are smaller than the *MSEs* of the all the other modified estimators and it is therefore $t_{8(a)}$ may be considered as the best estimator for both $a=2$ and $a=1$. Tables 7 – 8 display the absolute relative bias. It can be observed that the proposed estimators are slightly more biased than the existing estimators, but the biases are not notable. Therefore, still the proposed estimators can be preferred over other existing estimators.

CONCLUSION

In this study, we have proposed *IGCE* $t_{4(a)}$ for estimating population mean in the presence of joint influence of non-response and measurement error using simple random sampling assuming that the population mean of the auxiliary variable is not available. The performance of *IGCE* $t_{4(a)}$ is compared with some modified estimators t_1, t_2 and t_3 and it is observed that $t_{4(a)}$ provides the more efficient class of estimators $t_{4(1)}$, and $t_{4(2)}$ as these estimators have shown less *MSE* values than the

MSE values of t_0, t_1, t_2 and t_3 . We have also proposed another *IGCEStr* $t_{8(a)}$ estimator in stratified two-phase sampling for estimating population mean in the joint presence of non-response and measurement error. The performance of the *IGCEStr* $t_{8(a)}$ is compared with some modified estimators and it is observed that $t_{8(a)}$ is the most efficient class of estimators as some estimators from this class such as $t_{8(1)}$, and $t_{8(2)}$ have shown less *MSE* values than the *MSE* values of $t_{0(st)}, t_5, t_6$ and t_7 . Finally, the study is supported by three simulated populations in both, simple random sampling and stratified random sampling. Based on numerical results presented in Tables 2 – 3 and Tables 5 – 6, we conclude that *IGCE* $t_{4(a)}$ and *IGCEStr* $t_{8(a)}$ to be more efficient for estimating the population mean if non-response and measurement error are jointly present. We observe that in both simple random and stratified sampling, a reasonable choice for a is 1 or 2 although $a=1$ may be preferred.

REFERENCES

- Azeem M. (2014). On estimation of population mean in the presence of measurement error and non-response. *PhD thesis*, National College of Business Administration and Economics, Lahore, India.
- Azeem M. & Hanif M. (2017). Joint influence of measurement error and non-response on estimation of population mean. *Communications in Statistics- Theory and Methods* **46**(4): 1679–1693.
DOI: <https://doi.org/10.1080/03610926.2015.1026992>.
- Hanan M.H. & Hurwitz W.N. (1946). The problem of non-response in sample surveys. *Journal of American Statistical Association* **41**: 517–29.
DOI: <https://doi.org/10.1080/01621459.1946.10501894>.

- Irfan M., Javed M. & Lin Z. (2018). Optimized estimation for population mean using conventional and non-conventional measures under the joint influence of measurement error and non-response. *Journal of Statistical Computation and Simulation* **88**(12): 2385–2403.
DOI: <https://doi.org/10.1080/00949655.2018.1464571>.
- Khalil S. Gupta S. & Hanif M. (2017). A generalized estimator for finite population mean in the presence of measurement errors in stratified sampling. *Journal of Statistical Theory and Practice* **12**(2): 311–324.
DOI: <https://doi.org/10.1080/15598608.2017.1370621>.
- Kumar S. (2015). Efficient use of auxiliary information in estimating the population ratio, product and mean in the presence of non-response. *Journal of Advanced Computing* **4**(2): 59–67.
DOI: <https://doi.org/10.15446/rce.v38n1.48807>.
- Kumar S. (2016). Improved estimation of population mean in presence of non-response and measurement error. *Journal of Statistical Theory and Practice* **10**(4): 707–720.
DOI: <https://doi.org/10.1080/15598608.2016.1216488>.
- Rao P.S.R.S. (1986). Ratio estimation with sub sampling the non-respondents. *Survey Methodology* **12**(2): 217–230.
DOI: <https://doi.org/10.12001-x198600214463>.
- Riaz S. & Darda A.M. (2016). Some class of estimators in the presence of non-response using auxiliary attribute. *Springer Plus* **5**: 1271.
DOI: <https://doi.org/10.1186/s40064-016-2922-x>.
- Riaz S., Diana G. & Shabbir J. (2014). Improved classes of estimators for population mean in presence of non-response. *Pakistan Journal of Statistics* **30**(1): 83–100.
- Sabir S. & Sanaullah A. (2019). A note on Kumar (2016): Improved estimation of population mean in the presence of measurement error and non-response. *Journal of Statistical Theory and Practice* **13**(1): 25.
DOI: <https://doi.org/10.1007/s42519-018-0025-4>.
- Saleem I., Sanaullah A. & Hanif M. (2018). A generalized class of estimators for estimating population mean in the presence of non-response. *Journal of Statistical Theory and Applications* **17**(4): 32–40.
DOI: <https://doi.org/10.2991/jsta.2018.17.4.4>.
- Sanaullah A., Ali H.A. Noor-ul-amin A. & Hanif M. (2014). Generalized exponential chain ratio estimators under stratified two-phase random sampling. *Applied Mathematics and Computation* **26**(5): 2419–2428.
DOI: <https://doi.org/10.1016/j.amc.2013.10.088>.
- Sanaullah A., Noor-ul-amin A. & Hanif M. (2015). Generalized exponential-type ratio-cum-ratio and product-cum-product estimators for population mean in the presence of non-response under stratified two-phase random sampling. *Pakistan Journal of Statistics* **31**(1): 71–94.
- Sanaullah A., Noor-ul-amin A., Hanif M. & Koyuncu N. (2018). Generalized exponential-type estimators for population mean taking two auxiliary variables for unknown means in stratified sampling with sub-sampling the non-respondents. *International Journal of Applied and Computational Mathematics* **4**: 56.
DOI: <https://doi.org/10.1007/s40819-018-0489-7>.
- Singh P.H. & Kumar S. (2010). Estimation of mean in presence of non-response using two phase sampling scheme. *Springer Verlag* **51**: 559–582.
DOI: <https://doi.org/10.1007/s00362-008-0140-5>.
- Wang L. (2002). A simple adjustment for measurement errors in some dependent variable models. *Statistics and Probability Letters* **58**: 427–33.
DOI: [https://doi.org/10.1016/S0167-7152\(02\)00165-7](https://doi.org/10.1016/S0167-7152(02)00165-7).
- Zahid E. & Shabbir J. (2018). Estimation of population mean in the presence of measurement error and non-response under stratified random sampling. *PLoS ONE* **13**(2): e0191572.
DOI: <https://doi.org/10.1371/journal.pone.0191572>.

Appendix A

Table A1: MSE at different values of k using Normal Distribution

Estimators	$1/k$			
	$\frac{1}{2}$	$\frac{1}{3}$	$\frac{1}{4}$	$\frac{1}{5}$
t_0	2428.39	3027.88	3627.37	4226.85
t_1	1176.62	1198.90	1221.17	1243.44
t_2	1426.71	1581.99	1737.29	1892.58
t_3	1166.11	1188.55	1210.54	1232.33
$t_{4(1)}$	1128.37	1141.62	1153.43	1164.07
$t_{4(2)}$	1134.96	1151.86	1167.89	1183.28

Table A2: MSE at different values of k using Log Normal Distribution

Estimators	$1/k$			
	$\frac{1}{2}$	$\frac{1}{3}$	$\frac{1}{4}$	$\frac{1}{5}$
t_0	27431.75	36467.16	45502.56	54537.97
t_1	10687.62	10709.97	10732.32	10754.67
t_2	14807.86	17071.51	19335.17	21598.82
t_3	10686.60	10709.04	10731.40	10753.73
$t_{4(1)}$	10244.96	10121.80	9977.86	9813.21
$t_{4(2)}$	10334.20	10276.60	10210.75	10136.69

Table A3: Bias at different values of k using Normal Distribution

Estimators	$1/k$			
	$\frac{1}{2}$	$\frac{1}{3}$	$\frac{1}{4}$	$\frac{1}{5}$
t_1	0.1446	0.1748	0.2004	0.2232
t_2	0.1293	0.1554	0.1776	0.1974
$t_{4(1)}$	0.1452	0.1752	0.2009	0.2236
$t_{4(2)}$	0.1473	0.1775	0.2032	0.2262

Table A4: Bias at different values of k using Log Normal Distribution

Estimators	$1/k$			
	$\frac{1}{2}$	$\frac{1}{3}$	$\frac{1}{4}$	$\frac{1}{5}$
t_1	0.1366	0.1695	0.1969	0.2209
t_2	0.1186	0.1470	0.1708	0.1916
$t_{4(1)}$	0.1366	0.1695	0.1969	0.2210
$t_{4(2)}$	0.1384	0.1714	0.1990	0.2233

Table A5: MSE at different values of k using Normal Distribution

Estimators	$1/k_h=1/k$			
	$\frac{1}{2}$	$\frac{1}{3}$	$\frac{1}{4}$	$\frac{1}{5}$
t_5	888.44	1109.37	1330.31	1551.24
t_6	559.45	599.27	639.08	678.90
t_7	554.61	620.15	685.70	751.25
t_8	514.66	550.71	585.83	620.53
$t_{8(1)}$	506.91	540.51	572.88	604.51
$t_{8(2)}$	508.28	542.66	575.95	608.64

Table A6: MSE at different values of k using Lognormal Distribution

Estimators	$1/k_h=1/k$			
	$\frac{1}{2}$	$\frac{1}{3}$	$\frac{1}{4}$	$\frac{1}{5}$
t_5	14748.44	18344.68	21940.93	25537.17
t_6	7037.73	7189.29	7340.86	7492.42
t_7	8651.65	9589.94	10528.23	11466.52
t_8	6993.81	7141.86	7288.81	7435.28
$t_{8(1)}$	6899.41	7024.02	7144.98	7262.88
$t_{8(2)}$	6915.81	7049.66	7181.26	7311.20

Table 7: Bias at different values of k using Normal Distribution

Estimators	$1/k_h=1/k$			
	$\frac{1}{2}$	$\frac{1}{3}$	$\frac{1}{4}$	$\frac{1}{5}$
t_5	0.07294	0.090825	0.105727	0.118773
t_6	0.073475	0.088946	0.1021	0.113741
$t_{8(1)}$	0.077747	0.09505	0.109724	0.122683
$t_{8(2)}$	0.078549	0.095913	0.110675	0.123734

Table 8: Bias at different values of k using Log Normal Distribution

Estimators	$1/k_h=1/k$			
	$\frac{1}{2}$	$\frac{1}{3}$	$\frac{1}{4}$	$\frac{1}{5}$
t_5	0.124861	0.150183	0.171813	0.191009
t_6	0.111027	0.133045	0.151905	0.168669
$t_{8(1)}$	0.125216	0.150502	0.172119	0.191311
$t_{8(2)}$	0.125975	0.151291	0.172961	0.19222

RESEARCH ARTICLE

Plant Tissue Culture

Induction of somatic embryogenesis from leaf explants of *Exacum trinervium* (L.) Druce (Binara)

V de Silva and JP Eeswara*

Department of Crop Science, Faculty of Agriculture, University of Peradeniya, Peradeniya.

Submitted: 09 March 2021; Revised: 17 June 2021; Accepted: 27 August 2021

Abstract: *Exacum trinervium*, commonly known as *Binara*, produces dark blue violet flowers with contrasting bright yellow anthers that have a very high potential as commercial flowering, potted, or bedding plants. Lack of planting materials is one of the major constraints for popularizing it and therefore, development of planting materials through *in vitro* somatic embryogenesis would be a viable solution. The possibility of producing somatic embryos of *E. trinervium* using *in vitro* grown leaf explants was investigated. The effect of five concentrations (0, 1, 2, 3 and 5 mg L⁻¹) of 2, 4 - Dichlorophenoxyacetic acid (2,4-D) and 1 - Naphthaleneacetic acid (NAA) on somatic embryogenesis was investigated under dark and light with a photoperiod of 16 hours. The highest percentage of leaf explants (72 %) that produced calli was observed when cultured on the medium supplemented with 1 mg/L 2,4-D. Embryogenic stages could be observed only in calli originating from media supplemented with 1 mg/L and 2 mg/L 2,4-D after transferring to MS medium without growth regulators and incubated both in the light and the complete darkness. Leaf explants cultured on media containing NAA produced heavily rooted calli and did not produce any embryos. The highest number of embryos (15 ± 6 per/mL) was observed in the calli originating from the MS medium containing 1 mg/L 2,4-D. Further development of embryos up to plantlet with 60 % regeneration efficiency could be achieved on MS medium without plant growth regulators.

Keywords: *Binara*, *exacum trinervium*, somatic embryogenesis

INTRODUCTION

Exacum trinervium (Trimen) Cramer, commonly known as *Binara*, belongs to family Gentianaceae and tribe Exaceae, is an endemic and near threatened species in

Sri Lanka (MOE, 2012). The tribe Exaceae consists of 64 species, dispersed around the Indian Ocean Basin, Africa, Madagascar, India, Sri Lanka, and Australia (Yuan *et al.*, 2005). The highest diversity of genus *Exacum* has been reported in India, Sri Lanka and Madagascar (Klackenberg, 1983).

Exacum trinervium, which produces dark blue violet flowers (4 - 7 cm in diameter) with contrasting bright yellow anthers and attractive glossy foliage has a very high potential as commercial flowering, potted, or bedding plant for the floriculture industry (Riseman & Chennareddy, 2004). However, it is not popular as an ornamental plant in Sri Lanka due to lack of planting materials. Even though *E. trinervium* produces a large number of seeds, the low germination percentage, reduction of seed viability, time consumption, and high cost of production hindered them from being used as a planting material (Riseman *et al.*, 2006). Furthermore, propagation of *Exacum* by stem cutting is rather slow and time consuming (Elangomathavan *et al.*, 2003). Thus, there is a need for introducing efficient propagation methods to overcome these problems.

Tissue culture methods are effective at producing a large number of disease free plants within a short time period, compared to conventional methods. Several protocols for micropropagation of different *Exacum* species such as *E. travancoricum* (Elangomathavan *et al.*, 2003; Kannan *et al.*, 2007; Janarthanam *et al.*, 2009), *E. affine* (Torres & Ntarell, 1984; Ballal 1990; Ornstrup

* Corresponding author (jpe@pdn.ac.lk;  <https://orcid.org/0000-0002-8877-331X>)



This article is published under the Creative Commons CC-BY-ND License (<http://creativecommons.org/licenses/by-nd/4.0/>). This license permits use, distribution and reproduction, commercial and non-commercial, provided that the original work is properly cited and is not changed in anyway.

et al., 1993) and *Exacum styre* group (Unda *et al.*, 2007) have been reported. Micropropagation protocols existing for commercially available *E. affine* was not effective for *E. trinervium* (Riseman & Chennareddy, 2004). *Exacum* hybrids originating from Sri Lankan taxa showed a high level of genetic variation, with resulting modification of medium composition for different genotypes (Riseman & Chennareddy, 2004). A complete protocol for propagating *E. trinervium* through multiplication of single nodal cuttings, direct and indirect organogenesis from leaf explants has been reported (Tennakoon *et al.*, 2015). However, an efficient somatic embryogenesis protocol for the species is yet to be developed.

Somatic embryogenesis is an efficient clonal propagation technique, which can be used for synthetic seed production (Haque & Ghosh, 2014), and as a model to study the initial events of zygotic embryogenesis in higher plants (Méndez-Hernández *et al.*, 2019). Furthermore, somatic embryogenesis is very useful technique in regenerating plants from selected single cells with desirable genetic characters. Thus, development of somatic embryos would pave a path to improve *E. trinervium* through biotechnological approaches such as integration of genes to change the plant architecture to develop it as a potted ornamental plant.

Therefore, in the present study, the production of plantlets through somatic embryogenesis of *E. trinervium* was investigated with the final objective of introducing it into the floriculture industry.

MATERIALS AND METHODS

Immature leaves from *in vitro* cultured *E. trinervium* plants were excised and approximately 1 cm² pieces with a portion of the main vein were cultured on full strength Murashige and Skoog (1969) semi solid medium (MS) with 5 concentrations (0, 1, 2, 3 and 5 mg/L) of 2,4-D and NAA. The media were supplemented with 30 g/L sucrose and solidified with 2.0 g/L phytagel. The pH of the media were adjusted to 5.8 before autoclaving. The cultures were incubated at 20 °C in complete dark to induce callus production. Each treatment was replicated 3 times and each replicate consisted of an average of 20 leaf explants cultured on 25 mL culture tubes. Each culture tube contained a single piece of leaf explant (1 cm²) on 10 mL of the medium. Cultures were observed for 8 weeks and the number of leaf explants producing calli in each treatment were counted at the time of sub culturing.

Eight weeks after establishment, whole leaf explants with initiated calli from different media were separately transferred to full strength MS solid medium supplemented with 2.0 g/L phytagel without any plant growth regulator (PGR). Part of the cultures were incubated continuously at 25 °C in complete dark conditions while other part was transferred to light (1300 lux, 16 h photoperiod). The callus lines were maintained separately based on the composition of the original medium where the callus was initiated, to identify the effect of type and concentration of auxin in the original medium for somatic embryogenesis. Growth of the callus or roots was measured by weighing at the time of transferring under aseptic conditions inside the laminar flow cabinet, using a Mettler Analytical balance (Mettler, Germany). Calli were observed using a dissecting microscope (XT-Series-Alltion) at 2 wks interval for the production of somatic embryos.

Then 16 wks after establishment of cultures, calli originating from MS media supplemented with 1 and 2 mg/L 2,4-D and transferred to MS solid medium without growth regulators were again transferred to full strength MS liquid and solid media without any plant growth regulators. These two callus lines were incubated only in light to identify the effect of liquid medium for separation of somatic embryos. Cultures were observed under a dissecting microscope (XT-Series-Alltion) at 2 wks intervals by taking destructive samples for the production of somatic embryos. The number of embryos present was counted by taking 1 mL of the sample by using a micro pipette (Gilsons - 5 mL) with sterile tips inside the laminar flow cabinet and observing through a dissecting microscope (XT-Series-Alltion). Different stages of somatic embryogenesis were also documented by using photographs.

The initiated somatic embryos were transferred to MS medium without growth regulators for germination and the number of regenerated plantlets was counted. Regenerated plantlets were taken out from culture jars and washed by using warm water to remove adhesive agar and the medium. Then the plants were acclimatized by placing inside culture jars containing 1 cm layers of gravel, coir dust and sand. These jars were sterilized by autoclaving before placing the plantlets under sterile conditions inside a laminar flow cabinet. The plantlets were kept two weeks in culture room prior to transferring into the plant house. Jars were opened gradually to exposed plants to the open environment inside the plant house. Then the acclimatized plantlets were transferred to soil and grown up to flowering in the plant house (Tennakoon *et al.*, 2015).

Data analysis

All the experiments were arranged in completely randomized design. The number of explants producing calli/roots at different concentrations of 2, 4-D and NAA were analyzed using the Chi-Square test. The effect of dark and light on the growth of the callus after transferring to growth regulator free media was analyzed by using ANOVA considering the light condition as one factor and the concentrations of 2, 4-D and NAA present in the medium where calli was originated from leaf explants as the second factor. Numbers of somatic embryos initiated on different media were compared using the Chi-Square test.

RESULTS AND DISCUSSION

Selection of the correct development stage of the explant is important for somatic embryogenesis. Young and fast dividing parts of the plant with least microbial infections are considered as the most favourable explants for embryogenic callus formation (Ornstrup *et al.*, 1993). In the present study somatic embryogenesis of *E. trinervium* was achieved by using immature leaf explants. The risk of contaminations could be minimized and immature leaves could be obtained easily since *in vitro* plants were

used as the mother plants. Hamidah *et al.* (1997) also identified leaf pieces obtained from micropropagated plants as the best explant for the induction of somatic embryogenesis of *Anthurium scherianum*.

Calli initiation from the cut margins of the leaf explants (Figure 1a) started 3-4 wks after establishing the cultures on media supplemented with 2,4-D and NAA. Calli initiated from explants cultured on MS media supplemented with 2,4-D gradually became yellowish and further multiplied (Figure 1b and 1c) while the explants producing calli on MS media supplemented with NAA produced white colour roots and rapid multiplication of roots was observed (Figure 1d and 1e). Medium without auxins produced neither calli nor roots (Figure 1f).

Eight weeks after establishment of cultures, the highest percentage (72 %) of explants had produced calli on the medium supplemented with 1 mg/L 2,4 D concentration and it was significantly ($p < 0.05$) higher compared to all the other growth regulator concentrations (Figure 2). However, at this stage calli or roots were difficult to separate from the explants and therefore, whole explants with initiated calli or roots were transferred to MS media without plant growth regulators.

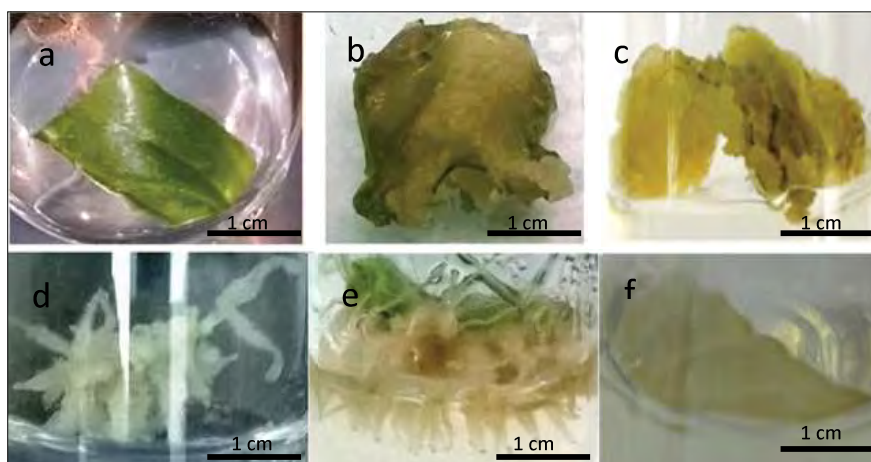


Figure 1: Effect of 2,4-D and NAA on callus/root initiation from leaf explants: (a) Leaf explant at the time of establishment. (b) Soft light yellow callus on edges of leaf explant in 2,4-D media. (c) Multiplication of callus initiated on 1 mg/L 2,4-D after transferring to growth regulator free MS. (d) Root initiated callus in NAA media. (e) Multiplication of white colour rooted callus initiated on 1 mg/L NAA after transferring to growth regulator free MS medium in the dark. (f) Leaf explant cultured in the dark on medium without auxin.

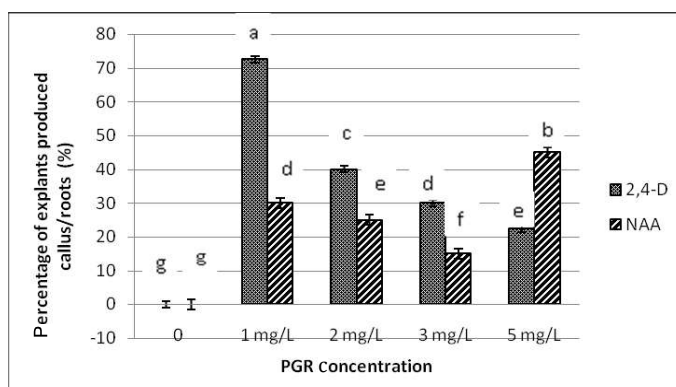


Figure 2: Production of callus on immature leaf explants after eight weeks from the establishment of cultures on MS media supplemented with different concentrations of 2,4 -D and NAA, (Note: Bars indicated by same letters are not significantly different)

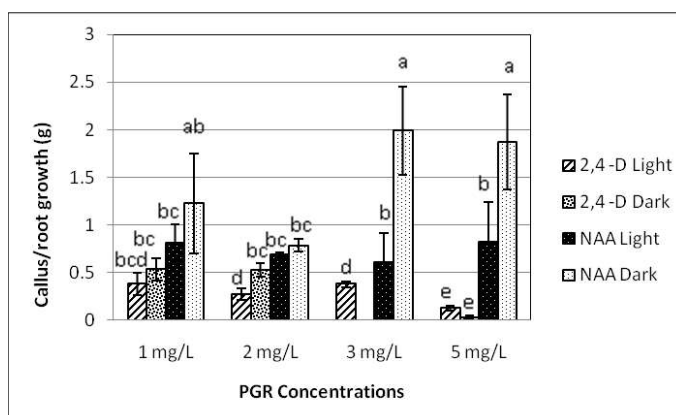


Figure 3: Effect of light conditions, 2,4-D and NAA on callus/root weight (Note: Bars indicated by same letters are not significantly different)

Calli initiated on media supplemented with 2,4-D produced more calli under both conditions, the complete darkness and the light (16 h light / 8 h dark at 1300 lux) when they were transferred to MS medium without growth regulators. Furthermore, calli incubated in the dark produced yellowish, friable calli (Figure 1c) while yellowish green colour friable calli were produced by cultures incubated under light conditions. Calli originated from MS medium supplemented with NAA produced more roots under both light and dark conditions, after transferring to MS medium without growth regulators (Figure 1e).

After 16 weeks of establishment (8 weeks after transferring to growth regulator free medium) calli/root

weight were taken to determine the effect of growth regulators (2,4-D/NAA) present in the original medium and light on calli/root growth. A significant difference ($\alpha = 0.05$) could be observed between dark and light conditions and between composition of 2,4-D and NAA in the callus initiating medium on further growth of callus and roots after transferring to MS medium without growth regulators (Figure 3). MS media supplemented with NAA have shown a higher weight increase compared to MS media supplemented with 2,4-D and this was mainly due to rapid root production (Figure 3). Furthermore, significant increase in callus/root growth was observed when the cultures were maintained under dark conditions irrespective of the type of the growth regulators.

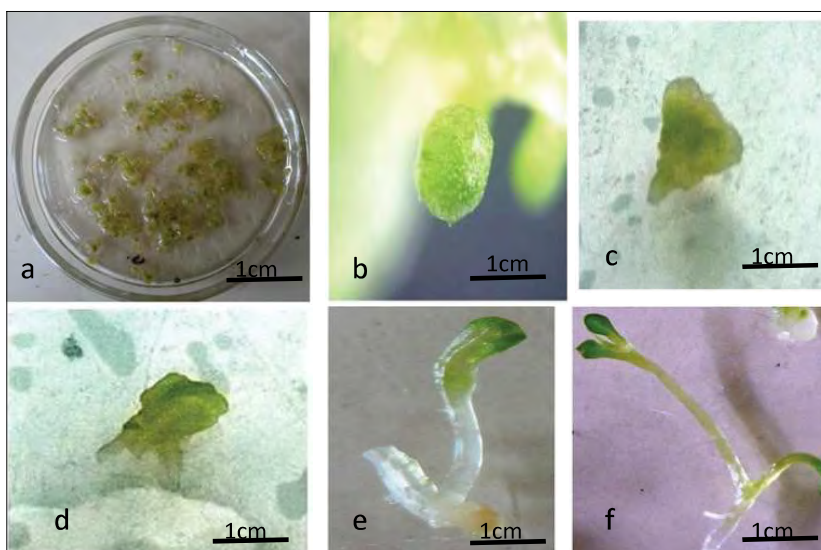


Figure 4: Different embryogenic stages in liquid MS medium: (a) Development of somatic embryos in liquid medium-[x1(normal eye)] (different stages of somatic embryos isolated from the same culture observed using a dissecting microscope are shown in Figure 4b-f). (b) Globular stage (x40). (c) Heart stage (x40). (d) Torpedo stage (x40). (e) Torpedo stage with root initials (x40). (f) Plantlets [x1(normal eye)] at 20 weeks of establishment.

Two weeks and four weeks after transferring (10 and 12 weeks after establishment) to plant growth regulator free MS media, different embryogenic stages could be observed in calli which were initiated in MS media with 1 mg/L and 2 mg/L 2,4-D concentrations and incubated under both light and dark conditions (Figure 4). However no somatic embryogenesis was observed from a callus originating from any explants cultured on MS media containing NAA. The role of growth regulators is very important for cultured cells and tissues in developing a specific mode of growth. Auxins such as NAA promote *in vitro* plant rooting (Ngomuo *et al.*, 2013). Furthermore, Lazzaeri *et al.* (1987) have reported that when similar concentrations of 2,4-D and NAA were compared, 2,4-D produced a larger number of somatic embryos in soybean. Four weeks after transferring (12 wks after establishment) of calli to MS media without growth regulators, further development of embryogenic stages could be observed.

Two weeks after transferring to liquid medium, different developmental stages of somatic embryos could be easily identified since they were well separated from each other in the liquid medium. A higher number of somatic embryos (15 ± 6 per mL) were produced by calli originated on MS solid medium supplemented with 1 mg/L 2,4 D compared to that of 2 mg/L 2,4-D)

(10 ± 5 per mL). However, results were not significantly different. Four weeks after transferring to liquid medium (20 weeks after establishment) development of plantlets could be observed (Figure 4).

Auxin plays a major role in induction of embryogenesis in cultures and further development of embryos (Li *et al.*, 1999; Nurazah *et al.*, 2009). In the initial media, tissues get the ability to synthesize all the gene products required to complete the globular stage of embryogenesis (Komamine *et al.*, 1992). Once embryogenesis has been induced embryos start to produce endogenous auxin and the role of auxin changes (Fan *et al.*, 2012). The cultures have to be transferred to a medium with reduced or free of auxin (Zimmerman, 1993). In accordance with that in the present study the calli that were induced in the initial MS medium supplemented with auxin were transferred to full strength MS medium without growth regulators 8 weeks after establishment to induce embryogenic ability. However Gawel *et al.* (1986) have transferred the calli initiated on leaf disc explants of *Gossypium hirsutum* L. two weeks after establishment. Furthermore, calli initiated on leaf explants of *Anthurium scherzerianum* have been transferred 4 weeks after establishment (Hamidah *et al.*, 1997). This implies that the time of transferring of calli to auxin free media varies with the plant species.

In this study the transferring time was decided according to the callus formation percentage. The transferring was done when the majority (75%) of the explants produced calli. Transferring time should be carefully decided since a longer or shorter time period of cultures in initial media may result in the loss of the embryogenic ability of the cultures (Nurul *et al.*, 2016)

According to the results of the present study 2,4-D was the most effective plant growth regulator on induction of somatic embryogenesis of *E. trinervium*. Although explants in the initial MS medium supplemented with different concentrations of 2,4-D and NAA produced different percentages of calli, only 1 mg/L and 2 mg/L 2,4-D was effective in producing embryogenic calli from immature leaf explants. The presence of higher concentrations of 2,4-D has showed an inhibitory effect on callus formation of *E. trinervium* (Tennakoon *et al.*, 2015). Ornstrup *et al.* (1993) have reported that 2,4-D was essential in achieving somatic embryogenesis of *Exacum affine*.

Somatic embryogenesis is a useful method especially as a solution for issues related to plant breeding such as problems with floral morphology, sterility, and time consumption. This is also useful as a method of genetic improvement of plant species and multiplication of valuable germplasm. In the case of *E. trinervium*, somatic embryogenesis can be used to overcome problems regarding commercialization of the plant.

CONCLUSION

Somatic embryogenesis of *E. trinervium* could be achieved by culturing immature leaf explants on MS media supplemented with 1 mg/L 2,4-D, under both conditions, total darkness and light, followed by transferring to solid MS medium without plant growth regulators, and finally transferring to liquid MS medium without growth regulators.

REFERENCES

- Ballal S.K. (1990). Morphogenetic potential of *Exacum affine* and *Eustoma grandiflorum* in tissue culture. *Journal of Plant Growth Regulations* **18**: 73–76.
- Elangomathavan R., Prakash S., Kathiravan K., Seshadri S. & Ignaciimuthu S. (2006). Plant regeneration through micropropagation from nodal explants of critically endangered and endemic plant *Exacum travancoricum*. *Journal of Plant Biotechnology* **8**: 52–55.
- Fan M., Xu C., Xu K. & Xu Y. (2012) Lateral organ boundaries domain transcription factors direct callus formation in *Arabidopsis* regeneration. *Cell Research* **22**: 1169–1180. DOI: <https://doi.org/10.1038/cr.2012.63>.
- Gawel J.N., Rao A.P. & Robacker C.D. (1986). Somatic embryogenesis from leaf and petiole callus cultures of *Gossypium hirsutum* L. *Plant Cell Reports* **5**: 457–459. DOI: <https://doi.org/10.1007/BF00269641>
- Hamidah M., Karim A.G.A. & Debergh P. (1997). Somatic embryogenesis and plant regeneration in *Anthurium scherzerianum*. *Plant Cell Tissue and Organ Culture* **48**: 189–193. DOI: <https://doi.org/10.1023/A:1005834131478>
- Haque S.M. & Ghosh B. (2014). Somatic embryogenesis and synthetic seed production-a biotechnological approach for true-to-type propagation and in vitro conservation of an ornamental bulbaceous plant *Drimiopsis kirkii* Baker *Applied Biocheistry and Biotechnology* **172**(8): 4013–4024. DOI: <https://doi.org/10.1007/s12010-014-0817-2>.
- Janarthanam B., Goplakrishnan M. & Sekar T. (2009). In vitro shoot regeneration from nodal explants of *Exacum travancoricum*. *Journal of Tropical Medicinal Plants* **10**(2): 205–207.
- Kannan P.P.A. & Ignaciimuthu S. (2007). Thidiazuron induced shoot regeneration in the endangered species, *Exacum travancoricum* Beedi. *Indian Journal of Biotechnology* (6): 564–566.
- Klackenberg J. (1983). A reevaluation of the genus *Exacum* (Gentianaceae) in Ceylon. *Nordic Journal of Botany* **3**(30): 355–370. DOI: <https://doi.org/10.1111/j.1756-1051.1983.tb01951.x>
- Komamin A. *et al.* (12 authors) (1992). Mechanisms of somatic embryogenesis in cell cultures: physiology, biochemistry and molecular biology. *In vitro Cell Developmental Biology* **28**: 11–14. DOI: <https://doi.org/10.1007/BF02632185>
- Lazzaeri P.A., Hildebrand D.F. & Collins G.B. (1987). Soybean somatic embryogenesis: Effect of hormones and culture manipulations. *Plant Cell Tissue and Organ Culture* **10**: 197–208. DOI: <https://doi.org/10.1007/BF00037304>
- Li J.R., Liu M.X., Chen H.R., Wu Z.B. & Wang J.J. (1999) Callus induction and sub-culture of *Taxus chinensis*. *Journal of Forestry Research* **10**(1): 11–14. DOI: <https://doi.org/10.1007/BF02855471>
- Méndez-Hernández H.A.N., Juárez-Gómez Y.L., Skeete A., Avilez-Montalvo J., De-la-Peña C. & Loyola-Vargas V.M. (2019). Signaling overview of plant somatic embryogenesis. *Frontiers in Plant Science* **10** (Article 77). DOI: 10.3389/fpls.2019.00077
- MOE (2012). *The National Red List 2012 of Sri Lanka; Conservation Status of the Fauna and Flora*. Ministry of Environment, Colombo, Sri Lanka.
- Murashige T. & Skoog F. (1962). A revised medium for rapid growth and bioassay with tobacco tissue cultures. *Physiolgia Plantarum* **15**: 473–497. DOI: <https://doi.org/10.1111/j.1399-3054.1962.tb08052.x>
- Ngomuo M., Mneney E. & Ndakidemi P. (2013). The effects of auxins and cytokinin on growth and development of (*Musa*

- sp.) Var. “Yangambi” explants in tissue culture. *American Journal of Plant Sciences* **4**: 2174–2180.
DOI: <http://dx.doi.org/10.4236/ajps.2013.411269>
- Nurazah Z., Radzali M., Syahida A. & Maziah M., (2009). Effects of plant growth regulators on callus induction from *Cananga odorata* flower petal ex-plants. *African Journal of Biotechnology* **8**(12): 2740–2743.
DOI: <https://doi.org/10.5897/AJB09.203>
- Nurul I.O., Jaafar S.N. & Awal A. (2016). Effects of variations in culture media and hormonal treatments upon callus induction potential in endosperm explant of *Barringtonia racemosa* L. *Asian Pacific Journal of Tropical Biomedicine* **6**(2): 145–147.
DOI: <http://dx.doi.org/10.1016/J.APJTb.2015.10.007>
- Ørnstrup H., Mølgaard J.P. & Farestveit B. (1993) Somatic embryogenesis and plant regeneration from cell suspensions of *Exacum affine*. *Plant Cell Tissue and Organ Culture* **35**: 37–41.
DOI: <https://doi.org/10.1007/BF00043937>
- Riseman A. & Chennareddy S. (2004). Genotypic variation in the micropropagation of Sri Lankan *Exacum* Hybrids. *Journal of American Society of Horticulture Science* **129**(5): 698–703.
DOI: <https://doi.org/10.21273/JASHS.129.5.0698>
- Riseman A., Sumanasinghe V.A. & Craig R. (2006). Cytology, crossability, and pollen fertility of Sri Lankan *Exacum* (Gentianaceae) and their hybrids. *International Journal of Plant Sciences* **167**(2): 191–199.
DOI: <https://doi.org/10.1086/499610>
- Tennakoon S., Peiris S.E. & Eeswara J.P. (2015). *In vitro* regeneration of *Exacum trinervium*. *Acta Horticulture* **1104** 237–244. Published by International Horticultural Society.
DOI: <https://doi.org/10.17660/ActaHortic.2015.1104.36>
- Torres K.C. & Ntarella N.J. (1984). *In vitro* propagation of *Exacum*. *Hortscience* **19**: 224–225.
- Unda F., Kalynyak P. & Riseman A. (2007). Organogenesis plant regeneration from leaf explants of *Exacum styer* group. *Plant Cell Tissue and Organ Culture* **89**: 105–111.
DOI: <https://doi.org/10.1007/s11240-007-9218-3>
- Yuan Y.M., Wohlhauser S., Moller S.M., Klackenberg J., Callmender M. & Upfer P.K (2005). Phylogeny and biogeography of *Exacum* (Gentianaceae): a disjunctive distribution in the Indian ocean basin resulted from long distance dispersal and extensive radiation. *Systemic Biology* **54**(1): 21–34.
DOI: <https://doi.org/10.1080/10635150590905867>
- Zimmerman J.L. (1993). Somatic embryogenesis: a model for early development in higher plants. *The Plant Cell* **5**: 1411–1423.
DOI: <https://doi.org/10.1105/tpc.5.10.1411>

RESEARCH ARTICLE

Molecular Plant Sciences

Meta-QTL analysis identified stable quantitative trait loci (QTLs) and associated resistance gene analogues in rice

HED Shashiprabha¹, SP Abeysundara¹ and HACK Ariyaratna^{2*}

¹ Department of Statistics and Computer Science, Faculty of Science, University of Peradeniya, Peradeniya.

² Department of Botany, Faculty of Science, University of Peradeniya, Peradeniya.


Submitted: 18 January 2021; Revised: 06 July 2021; Accepted: 27 August 2021

Abstract: Disease resistant rice varieties are mandatory for sustainable rice production to ensure the global food supply. This study aimed to identify meta-QTLs and associated with disease resistance and candidate R-genes. A consensus map was constructed by merging 9 QTL mapping studies, 115 QTLs and 943 markers. The consensus map was 1554.71 cM in length with a 1.65 cM-1 average marker density. Totally, 24 meta-QTLs were projected on the consensus chromosome maps except on chromosomes 5, 6, and 10. Larger effect meta-QTLs ($R^2 \geq 25$ to 56 %) were reported on chromosomes 1, 2, 3, 4, 8, and 11. Three or more meta-QTLs were predicted on 1, 2, 7, 8, and 9 chromosomes. More than 62 % of the meta-QTLs were contributed by 3 or more mapping studies. Furthermore, 6 of the putative meta-QTLs collocated with 11 meta-QTLs from previous studies, and 23 resistance loci that are used in existing resistance breeding programs indicating robust expression. Nine meta-QTLs were associated with blast (BL) resistance whereas 14 were associated with both BL and sheath blight (SHB) resistance. Candidate gene mining identified 79 disease resistance gene analogues (RGAs) of which 74 % were complete putative R genes. Nine of the meta-QTLs predicted clusters of RGAs. Out of these, expression of LOC_Os11g12340 was cross-validated using publicly available expression data in tissues infected with *M. oryzae*, indicating a functional role of this gene in the disease cycle. The outcome clearly exposed genomic abundance of R-genes and their potential functional redundancy. Further, these findings provide potential resources for rice breeding for disease resistance.

Keywords: BioMercator, Gramene, meta-QTLs, PRGdb, resistance genes, *Rice Genome Annotation Project*.

INTRODUCTION

Rice, the staple food for more than half of the global population provides 20 % of the daily human calorie intake (<http://rice.plantbiology.msu.edu/>), and is an integral component of global food and nutrition security. Rice is susceptible to over 70 pests and diseases that collectively cause 37 % yield reduction (<http://www.knowledgebank.irri.org/>). The impact is significant in food-deficit regions and food security hotspots in tropical Asia, where over 90 % of the total global rice is produced and consumed (Sharma *et al.*, 2012). Blast (BL), bacterial blight (BB), and sheath blight (SHB) are the most destructive diseases in rice worldwide (Gnanamanickam, 2009). BL, a fungal disease caused by *Magnaporthe oryzae*, infects all parts of the rice plant and can result in yield reductions of 10 - 60 % (Wang *et al.*, 2014). BB is due to infection by *Xanthomonas oryzae*. The disease causes yield losses up to 50 % and also affects rice grain quality (Liu *et al.*, 2014). Losses due to SHB, a disease caused by the soil-born fungus *Rhizoctonia solani*, can be as high as 10 to 30 % in severely infected fields (Banniza *et al.*, 2001; Sreenivasaprasad, 2004; Boukaew & Prasertsan, 2014; Liu *et al.*, 2014). Application of synthetic fungicides for the management of these diseases incurs both economic and environmental losses (Nalley *et al.*, 2016). Developing host resistance in elite cultivars provides cost-effective solutions to increase

* Corresponding author (chandimaariyaratna@pdn.ac.lk;  <https://orcid.org/0000-0002-1860-7754>)



This article is published under the Creative Commons CC-BY-ND License (<http://creativecommons.org/licenses/by-nd/4.0/>). This license permits use, distribution and reproduction, commercial and non-commercial, provided that the original work is properly cited and is not changed in anyway.

rice production and profits at minimal cost and damage to the environment. Disease-resistant varieties are vital components of sustainable rice cultivation to ensure global food supply and therefore genetic improvement for host resistance to BL, BB, and SHB is among the priority objectives of rice breeding programmes worldwide.

Genes and QTLs associated with the multilayers of innate defence mechanisms are potential resources for resistance/tolerance breeding of crops. Over 350 resistance loci that are associated with BL were mapped on rice (Miah *et al.*, 2013; Su *et al.*, 2015; Xiao *et al.*, 2017). Among these 27 allelic QTLs have been fully sequenced; *Pib*, *pb1*, *Pita*, *Pi9*, *Pi2*, *Pizt*, *Pid2*, *Pi33*, *Pii*, *Pi36*, *Pi37*, *Pikm*, *Pit*, *Pi5*, *Pid3*, *Pid3-A4*, *Pi54*, *Pish*, *Pik*, *Pikp*, *Pia*, *PiCO39*, *Pi25*, *Pi1*, *Pi21*, *P50* and *Pi650* (Miah *et al.*, 2013; Liu *et al.*, 2014; Su *et al.*, 2015). Moreover, up to 200 QTLs that are associated with SHB resistance and 14 QTLs associated with BB are reported (Zarbafti & Ham, 2019). While some of these were discovered in isolated research, others were discovered in a variety of settings and experiments (Zarbafti & Ham, 2019). Rice breeding schemes, in which major effect resistance QTLs such as *Pib*, *Pita*, *Pia*, *Pi1*, *Pikh*, *Pi2* and *Pi4*, or minor effect resistance QTL alleles including *Pi-1*, *Pi2*, *Pi9*, *Pi20*, *Pi27*, *Pi39*, *Pi40* and *Pikh* were deployed in gene pyramids, were successful in producing race-specific or broad-spectrum resistance (Narayanan *et al.*, 2002; Ballini *et al.*, 2008; Gnanamanickam *et al.*, 2009; Djan- Caporalino *et al.*, 2014; Ellis *et al.*, 2014; Ordon & Kühne, 2014; Jia *et al.*, 2019; Zarbafti & Ham, 2019). However, shifts in strains of the pathogen populations due to mutations result in frequent “resistance breakdown.” Therefore, continuous searching and stacking of multiple loci or genes that are associated with disease resistance through strategic breeding schemes are important to sustain breeding activities for steady delivery of disease-resistant rice varieties.

Resistance genes (R-genes) interact with pathogen avirulence genes (*Avr*) and initiate signaling cascades to activate defence mechanisms. R-genes are vital elements of the host resistance mechanisms and are successfully used in cereal resistance breeding programmes (Miah *et al.*, 2013; Bouktila *et al.*, 2014; Zhang *et al.*, 2015). Conserved structural motifs and protein domains enable computational identification of R-genes by peptide sequence alignments and searching for structural similarity (Michelmore & Meyers, 1998). Thereby a large class of potential R-genes, known as Resistance Gene Analogs (RGAs), were predicted and mapped in rice (Miah *et al.*, 2013; Sekhwal *et al.*, 2015) and the orthologs of the rice RGAs were identified in wheat

(Bouktila *et al.*, 2014), maize (Xiao *et al.*, 2007), rye (Dracatos *et al.*, 2010) and finger millet (Reddy *et al.*, 2011; Babu *et al.* 2014). The annotated rice genome and transcriptome data provide opportunities for the discovery of novel RGAs and these resources are increasingly investigated in search of RGAs as gene candidates for disease resistance.

Meta-analysis of QTLs integrates information from multiple QTL mapping studies into a single consensus map to enable contraction of QTL intervals and identification of robust and reliable QTLs. Thereby meta-QTLs identify consensus QTLs that are expressed across different environments, and genetic backgrounds and these stable QTLs are highly desired for their applicability in breeding (Goudemand *et al.*, 2013; Hamon *et al.*, 2013). Meta-QTL analysis identified genetic determinants of complex traits in a variety of crops, including yield, fiber quality, drought tolerance, and disease resistance in rice (Khowaja *et al.*, 2009), cotton (*Gossypium hirsutum* L.) (Said *et al.*, 2013), maize (*Zea mays* L.) (Semagn *et al.*, 2013), pea (*Pisum sativum* L.) (Hamon *et al.*, 2013), wheat (*Triticum aestivum* L.) (Griffiths *et al.*, 2009) and mustard (*Brassica juncea* L.) (Yadava *et al.*, 2012). This study aimed to predict meta-QTLs associated with BL, BB, and SHB resistance in rice. A consensus genetic map with high marker density was constructed to identify meta-QTLs with narrow genomic intervals. Candidate genes that collocate with the meta-QTL regions were predicted and cross-validated using genomic, and transcriptomic data available in the public domain. The findings of the study will aid in increasing precision of QTL mapping, the identification of candidate genes, and the generation of markers for effective marker-assisted selection (MAS) programs.

MATERIALS AND METHODS

QTL studies used for meta-QTL analysis

Rice QTLs associated with BL, BB, and SHB resistance were mined in the Gramene QTL database (<https://archive.gramene.org/qtl/>). In total, 9 mapping studies for disease resistance were selected from the Gramene QTL database (Table 1). The 95 % confidence interval (CI) of the QTLs predicted on backcross or F2 mapping population was estimated using the equation $95\% \text{ CI} = 530/(NR^2)$ (Darvasi, 1997), whereas the equation $95\% \text{ CI} = 163/(NR^2)$ was used for QTLs predicted on recombinant inbred line mapping population (Guo *et al.*, 2006). Here N is the population size and R^2 is the proportion of phenotypic variance explained by the QTLs. R (version 3.5.3) language was used for data web scrapping and preprocessing.

Table 1: Details of the nine rice QTL maps accessed through Gramene QTL database (<https://archive.gramene.org/qtl/>) and used in the meta-analysis of QTLs associated with resistance to blast, bacterial blight and sheath blight diseases in rice

Population	Population size	No. of markers on the map	Number of disease resistance QTLs mapped on each chromosome												Reference
			1	2	3	4	5	6	7	8	9	10	11	12	
Lemont × Teqing	284	244	-	2	2	2	-	2	1	-	2	-	-	2	(Tabien <i>et al.</i> , 2002)
Jasmine × Lemont	128	76	-	2	1	-	-	-	1	-	2	-	2	-	(Zou <i>et al.</i> , 2000)
IR64 × Azucena	116	170	-	-	-	-	1	-	-	1	-	-	-	-	(Ramalingam <i>et al.</i> , 2003)
Lemont × Teqing	255	111	-	3	3	-	-	-	-	3	3	-	-	3	(Li <i>et al.</i> , 1995)
Nipponbare × Owarihatamochi	146	110	-	-	-	2	-	-	-	-	1	-	-	1	(Fukuoka and Okuno, 2001)
Bala × Azucena	205	114	2	1	-	2	-	-	4	-	1	3	3	-	(Talukder <i>et al.</i> , 2005)
IR64 × Azucena	105	322	-	-	-	-	-	1	-	1	-	1	-	3	(Sallaud <i>et al.</i> , 2003)
Moroberekan × CO39	281	125	2	-	1	-	1	2	1	1	-	-	-	1	(Wang <i>et al.</i> , 1994)
Zhenshan Minghui	241	234	17	11	1	-	-	-	4	4	5	-	-	-	(Chen <i>et al.</i> , 2003)

Construction of consensus map & QTL projection

A consensus map was constructed using BioMercator v4.2 (<http://moulon.inrae.fr/logiciels/biomercator/>) with default parameters. Nine selected rice mapping studies were projected on the map. The method implemented in BioMercator applies a classical weighted least square (WLS) strategy. Chromosomes that share less than two common markers between the mapping studies were excluded. The QTLs were projected on the consensus map using a simple scaling rule between the original QTL flanking marker interval and the corresponding one on the consensus chromosome. Projection of the initial QTLs on the high-density consensus map was based on LOD scores, phenotypic variation explained by each QTL, 95 % CIs, and QTL flanking marker positions. The 95 % CI of the QTLs that were projected on the consensus map were approximated using Gaussian distribution.

Meta-QTL analysis

The meta-analysis of QTLs was performed using the QTL clustering-based approach proposed by Veyrieras *et al.* (2007) using BioMercator v4.2. The distribution of QTLs is viewed as a Gaussian mixture model and parameter estimates were obtained using the Expectation-Maximization algorithm. The lowest Akaike-Information Criterion (AIC) was used to determine the best model for each chromosome. The accuracy of QTL model selection using AIC was studied by a simulation in the Veyrieras

method (Veyrieras *et al.*, 2007). The meta-QTLs thereby predicted were compared with meta-QTLs and QTLs associated with BL, SHB, and BB resistance, available in the public domain.

Identification of candidate genes

The nearest markers of 95 % CI of meta-QTLs were identified. Physical positions of the nearest markers were retrieved from the Gramene marker database (<https://archive.gramene.org/markers/>). The Rice Genome Annotation Project (<http://rice.plantbiology.msu.edu/>) was studied for the putative genes, the encoded proteins, and the functional annotation of the genes associated with the meta-QTLs, based on physical locations of the nearest markers.

The sequences of the putative R-genes were web scraped from Rice Genome Annotation Project and then used in BLAST search in the PRGdb (<http://prgdb.org/prgdb/>) to predict the domain types. The expression of the R-genes was studied in the susceptible and resistant varieties using expression libraries available from NCBI Sequence Read Archives: SRR074129, SRX032224, SRR074133, SRR074134, SRR074135, and SRR074136. Genes were reported 'expressed' when at least one sequence read mapped uniquely within an exon of the target gene. All steps of identification of candidate R-genes were carried out using R (version 3.5.3) language.

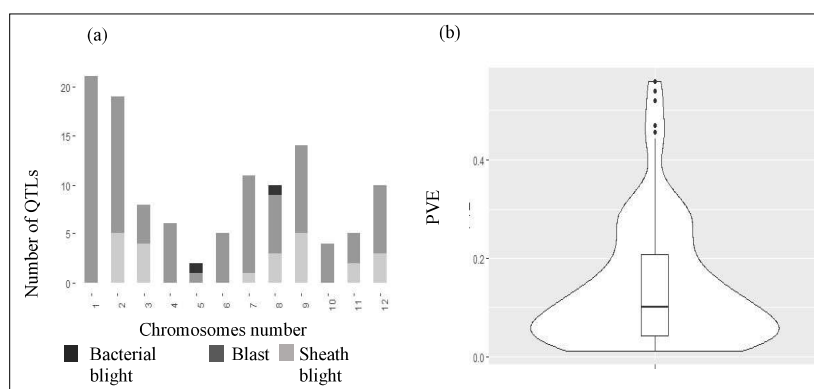


Figure 1: Overview of QTLs used in this study. (a) Total number of QTLs identified on the 12 rice chromosomes. (b) QTL density for phenotypic variance explained (PVE) by QTLs. Area of the graph demonstrate the QTL density

Table 2: Details of the consensus map

Chromosome	Number of markers	Map length (cM)	Marker density (Markers/cM)	Average distance between two adjacent markers (cM)
1	113	128.47	1.14	1.15
2	96	72.93	0.756	0.77
3	115	168.95	1.47	1.48
4	77	142.38	1.85	1.87
5	49	135.24	2.76	2.81
6	76	217.50	2.86	2.90
7	69	116.65	1.69	1.72
8	60	205.13	3.42	3.48
9	75	54.01	0.72	0.73
10	59	113.86	1.93	1.96
11	96	125.65	1.31	1.32
12	58	73.94	1.27	1.30
Total	943	1554.71		

RESULTS AND DISCUSSION

Overview of initial QTLs

Novel genetic resources are constantly required as inputs into the continuing process of crop improvement for disease resistance. The 9 maps predicted altogether 143 QTLs including 111, 26, and 6 QTLs that were associated with BL, SHB, and BB resistance, respectively (Figure 1-a). Out of the 143, a detailed analysis was available in the literature for 115 QTLs. The phenotypic variance explained by those 115 QTLs ranged from 1.2 % to 55.9 % (Figure 1-b). More than 80 % of the QTLs contributed to less than 30 % of the

phenotypic variance of target traits indicating that the majority of the QTLs had minor to moderate effects on the phenotype (Figure 1-b). Furthermore, 95 % CI of the QTLs varied from 1.3 cM to 93.18 cM, indicating widely spread QTL intervals, thereby reducing plausibility of application of the mapping results in candidate gene and marker search.

Constructing a consensus map, QTL projection and meta-QTL analysis

A consensus map was generated by merging the 9 rice maps by BioMercator v4.2 using default parameters. The 115 QTLs along with 943 markers were projected on the

consensus map (Table 2). The total length of the consensus map was 1554.71 cM with 1.65 cM⁻¹ average marker density. The average distance between adjacent markers across chromosomes ranged from 0.73 to 3.48 cM. A total of 24 meta-QTLs were projected on the consensus map on all except 5, 6, and 10 rice chromosomes (Table 3 and Figure 2). Out of the 24 meta-QTLs, 23 were clustered by two or more QTLs. More than 62 % of the meta-QTLs were common to more than 3 QTL mapping studies.

Larger effect meta-QTLs (where $R^2 \geq 25$ to 56 %) were reported on chromosomes 1, 2, 3, 4, 8, and 11. Out of the 24 meta-QTLs, 22 showed 95 % CI estimates narrower than those of their clustered QTLs. Meta-QTL intervals varied from 0.18 cM to 12.09 cM. Meta-analysis resulted in a QTL length reduction of 1.07 % on the minimum and 91.61 % on the maximum, thereby attaining a more accurate prediction of chromosomal regions associated with phenotypic variability for the target traits.

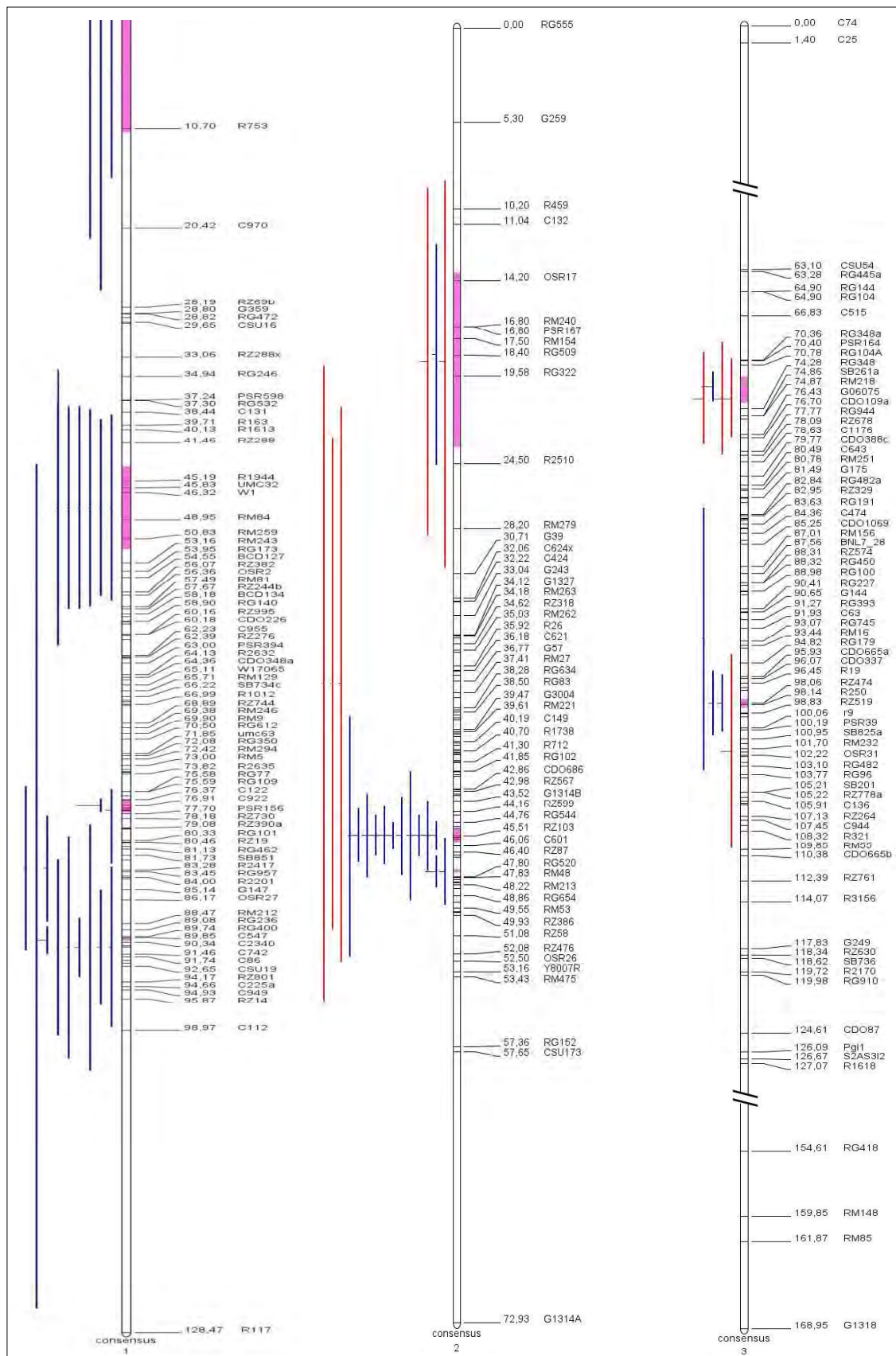
Table 3: Details of the predicted meta-QTLs

Meta-QTL	¹ No. of clustered QTLs ¹	² LOD max	³ R ² max	⁴ Chrom	Model	AIC value	Meta-QTL position cM	Meta-QTL CI (95%) cM	Meta-QTL left markers	Meta-QTL right marker	Associated traits
<i>MQTL011</i>	1	2	3.3				5.35	11.39	C161	R753	BL
<i>MQTL012</i>	2	3.5	3.9	1	4	166.87	47.85	8.05	R1944	RM259	BL
<i>MQTL013</i>	3	22.5	52				77	1.29	C122	PSR156	BL
<i>MQTL014</i>	3	11.9	25				90.03	0.34	C547	C2340	BL
<i>MQTL021</i>	3	5.07	21.2	2	3	92.56	18.68	9.82	OSR17	R2510	BL, SHB
<i>MQTL022</i>	4	27.8	44.2				45.53	0.79	RZ531	C601	BL, SHB
<i>MQTL023</i>	3	13.8	31.7				47.46	0.18	RG520	RG520	BL, SHB
<i>MQTL031</i>	2	17.61	32.3	3	2	44.31	72.77	2.11	RG104A	RG348	BL, SHB
<i>MQTL032</i>	3	6.86	26.5				98.11	0.73	RZ474	R250	BL, SHB
<i>MQTL041</i>	3	19.3	45.7	4	1	39.11	120.9	1.78	RG190	G379	BL
<i>MQTL071</i>	2	6.02	22.2	7	3	86.82	51.09	6.04	G338	RG769	BL, SHB
<i>MQTL072</i>	3	6.02	22.2				65.64	12.09	CSU109	RZ471	BL
<i>MQTL073</i>	3	6.8	19				88.18	0.73	CDO418	R1245	BL
<i>MQTL081</i>	2	3.45	55.9	8	3	111.51	49.53	3.59	RM25	RM25	BL, SHB
<i>MQTL082</i>	3	10	29				59.43	2.29	RG333	RZ562	BL, SHB
<i>MQTL083</i>	2	6.3	22				72.19	7.13	C1121	C483	BL
<i>MQTL091</i>	4	4.2	12.2	9	3	102.71	24.84	6.56	RM105	RG463	BL, SHB
<i>MQTL092</i>	5	4.2	13				36.68	5.69	RZ422	RZ228	BL, SHB
<i>MQTL093</i>	3	4.08	13				46.49	3.65	RM215	C506	BL, SHB
<i>MQTL111</i>	1	4.4	14.5	11	2	41.18	0	4.91	R642	R642	BL
<i>MQTL112</i>	2	7.17	31.2				56.24	7.82	R2918	r2	BL, SHB
<i>MQTL121</i>	4	9.8	28	12	2	55.14	47.27	7.49	RM19	L102	BL, SHB
<i>MQTL122</i>	4	19.43	54				54.64	3.41	RG869	C443	BL, SHB

¹ Number of different initial QTL studies (detailed in Table 1) contributed to the meta-QTL

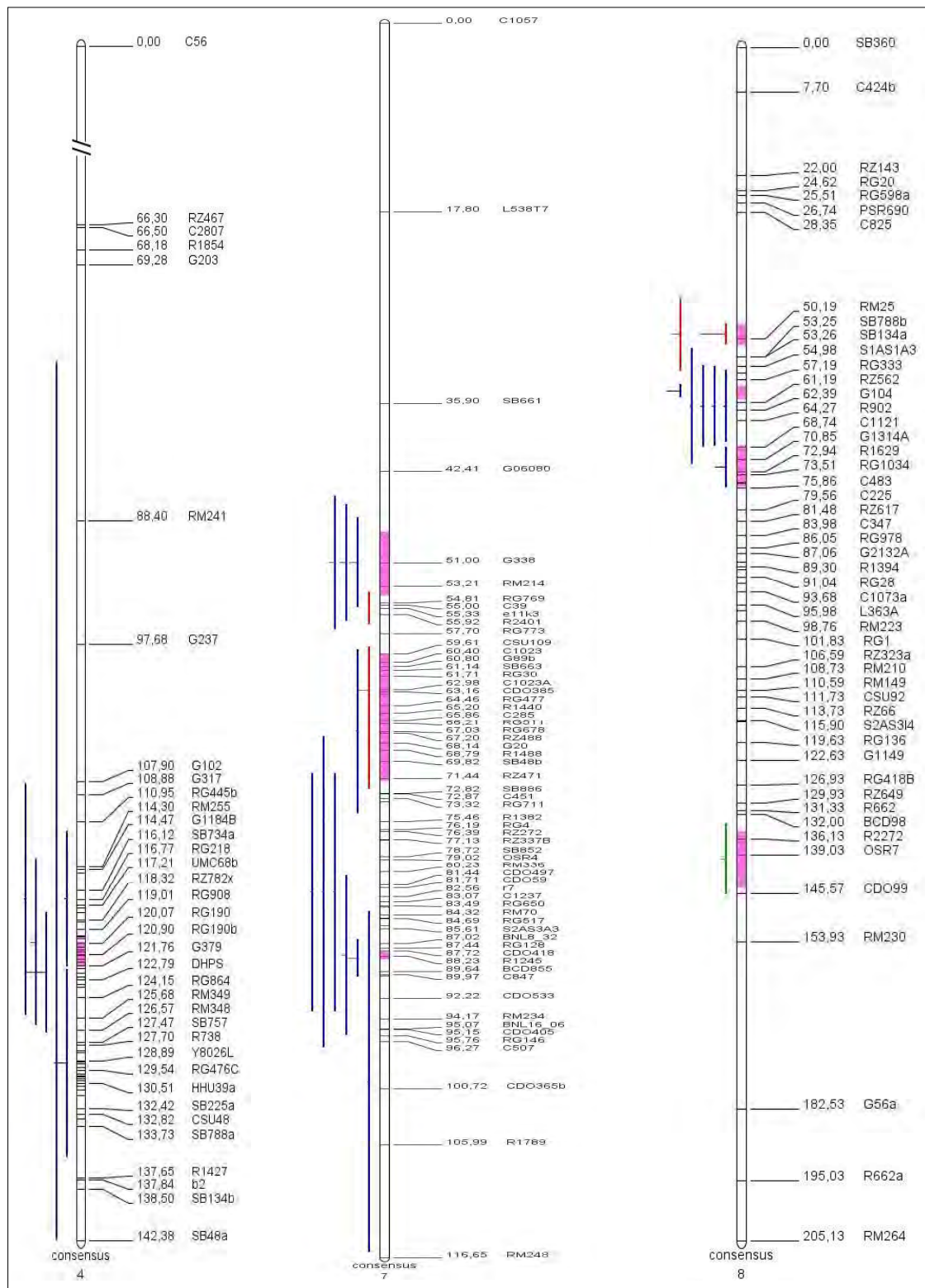
^{2,3} Out of the clustered QTLs for a given meta-QTL, QTL that expressed highest LOD and/or R² were considered. The LOD and/or R² were extracted from the original references given in Table 1

⁴ Chromosome where the meta-QTL is located



Continued -

- continued from page 40-



Continued -

- continued from page 41 -

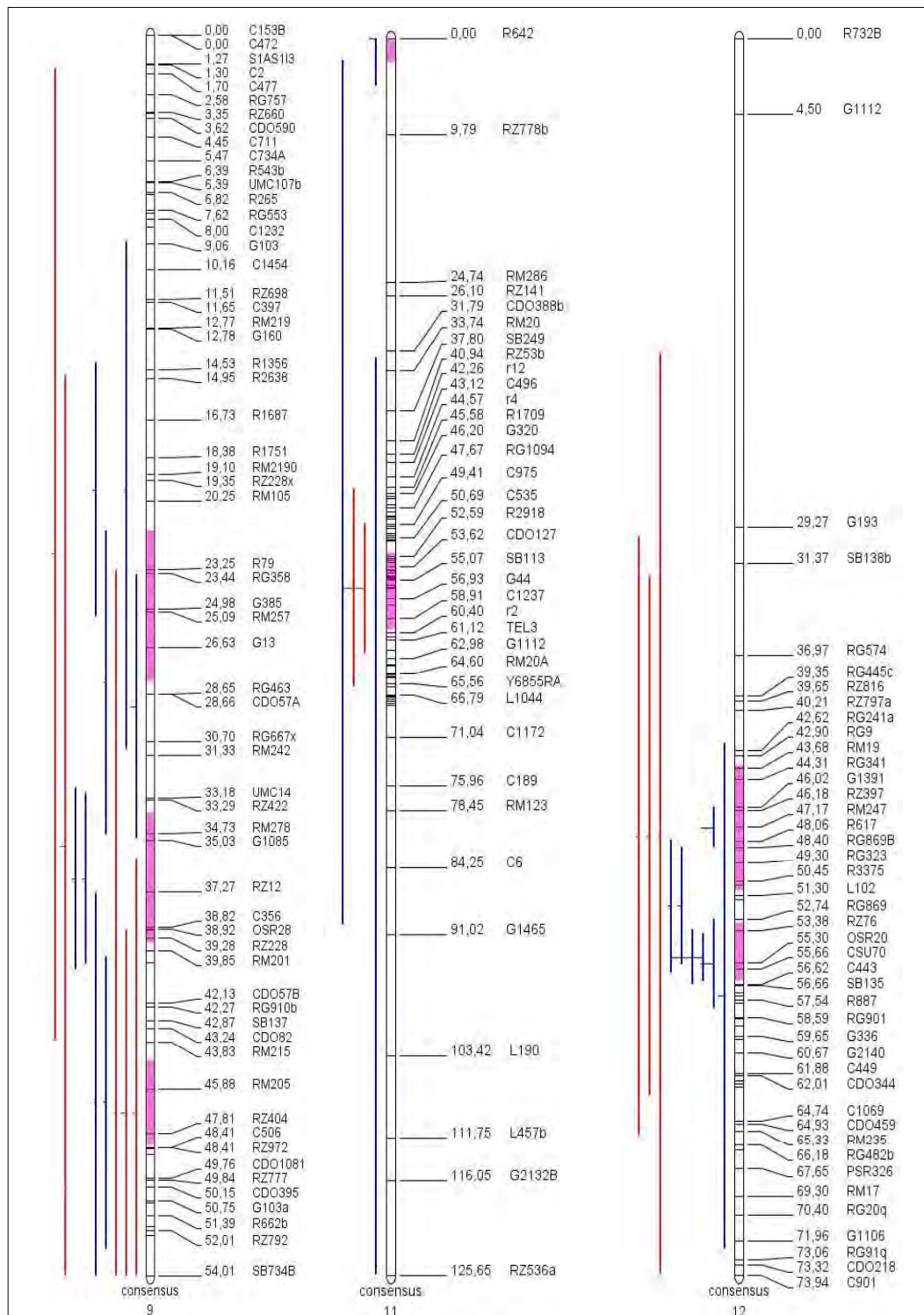


Figure 2: Meta-QTLs predicted on chromosome 1, 2, 3, 4, 7, 8, 9, 11, and 12. The chromosome number is given on the bottom of each map. Vertical lines to the left of each chromosome represent the 95 % Confidence Interval of clustered QTLs. QTLs associated with blast, bacterial blight and sheath blight are represented in blue, green and red lines. The meta-QTLs are represented by purple bars on the body of the chromosome.

Out of the 24 meta-QTLs, 9 were associated with BL resistance whereas 14 were associated with both BL and SHB resistance. This study did not identify meta-QTLs associated with BB resistance (Figure 2). Figure 3 is a graphical representation of physical positions (in Mbp) of the meta-QTLs predicted in this study, meta-QTLs identified in previous studies, and resistance QTLs that are successfully utilized in existing resistance breeding programmes. Interestingly, 6 of the meta-QTLs predicted herein collocate with 11 meta-QTLs from previous studies, and 23 resistance QTLs that are successfully utilized in existing resistance breeding programmes (Miah *et al.*, 2013; Liu *et al.*, 2014; Su *et al.*, 2015) providing further confirmation of their stable expression and significant contribution in resistant phenotypes.

The QTLs associated with the predicted 24 meta-QTLs contributed phenotypic effects ranging from 1.2 % to 55.9 %. Major effect loci expressing dominant and clear resistant phenotypes are prone to “resistance break-down” due to rapid virulence formation within pathogen populations. On the other hand, quantitative resistance resulting from combinations of QTLs and QTLs specific to one or several isolates (Calenge *et al.*, 2004; Rocherieux *et al.* 2004; Ellis *et al.*, 2014; Wiesner-Hanks and Nelson, 2016) can provide partial resistance (Poland *et al.*, 2009; St. Clair, 2010). Stable expression of the meta-QTLs under differential strains and inoculum pressure of the same and /or different pathogens indicates broad-spectrum resistance and is highly desirable in developing durable resistance in crops. The 14 meta-QTLs that expressed resistant phenotypes for both BL and SHB presumably predicted Multiple Disease Resistance (MDR) loci or multiple disease susceptibility (MDS) loci, or loci associated with loss of baseline levels of resistance. Meta-QTLs predicted herein there by expressed a broad spectrum of disease resistance in rice and provide assorted targets for resistance breeding.

Identification of candidate genes

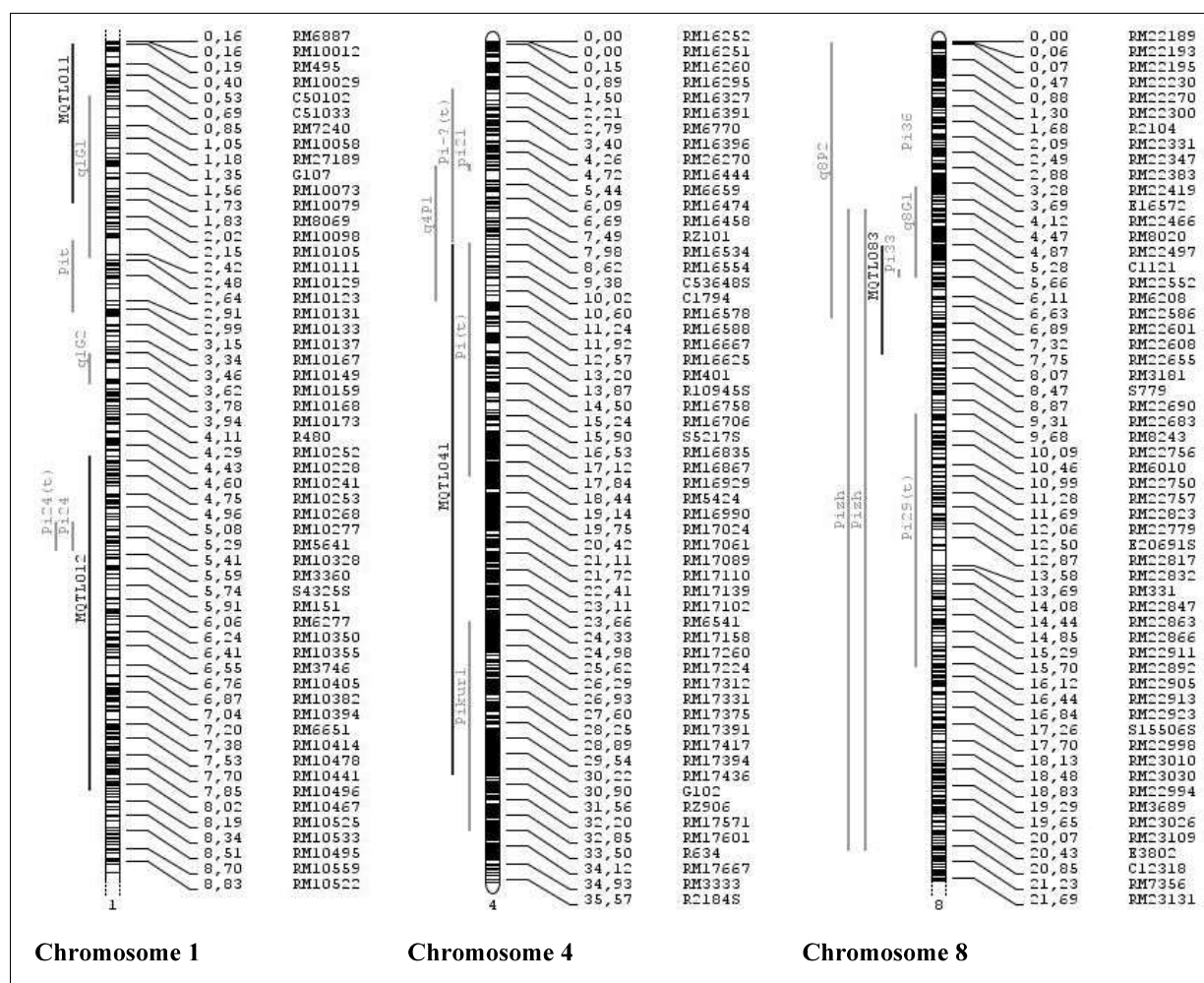
More than 3 meta-QTLs were predicted on the 1, 2, 7, 8, and 9 chromosomes where the meta-QTLs were tightly linked within 40 % to 50 % of the total length of the chromosome. Over 64 % of the QTLs associated with BL resistance that is reported in the literature were clustered on 6, 11, and 12 rice chromosomes (Ashkani *et al.*, 2016). These include, 15 loci including *Pi1*, *Pi7*, *Pi18*, *Pif*, *Pi34*, *Pi38*, *Pi44(t)*, *PBR*, *Pilm2* and *Pik* on the long arm of the rice chromosome 11, and 17 including *Pita*, *Pita-2*, *Pitq6*, *Pi6(t)*, *Pi12(t)*, *Pi12(t)*, *Pi19(t)*, *Pi20(t)*, *Pi21(t)*, *Pi24(t)*, *Pi31(t)*, *Pi32(t)*, *Pi39(t)*, *Pi62(t)*, *Pi157(t)*, *IPi*, and *IPi3* loci on the centromere region

of chromosome 12 (<http://www.ricedata.cn/gene/>) (Liu *et al.*, 2005; Tanweer, *et al.* 2015). These chromosome segments associated with clusters of QTLs are hotspots for identifying gene candidates and genetic/genomic resources for resistance breeding.

A total of 79 candidate Resistance gene analogues (RGAs) that collocate with the meta-QTLs were predicted (Table 4). Over 73 % of those were complete RGAs consisting of CC/NBS/LRR/TM domains. The rest were partial RGAs with NBS / TM (1.25 %), NBS/LRR/ CC (5 %), or NBS/ LRR/ TM (20 %) domain types. Indeed, a large fraction of resistance QTLs in crops collocate with NBS-LRR genes, altered forms (*e.g.*, *Pi35*), or loss-of-function susceptibility alleles (*e.g.*, *Pi21*) of NBS-LRR genes (Poland *et al.*, 2009). For an example over 80 % out of 180 rice RGAs that were associated with BL resistance (<http://www.ricedata.cn/ontology>) were NBS-LRR candidates (Ballini *et al.*, 2008). Interestingly, 9 of the meta-QTLs collocated with clusters of RGAs. For example, meta-QTL, MQTL112 collocated with 45 RGAs. Tandem repeats of the NBS-LRR genes are a regular feature in plant genomes, whereby 50 % of the NBS-LRR genes in the rice genome are clustered tandem repeats (Yang *et al.*, 2006). Some of these NBS-LRR clusters evolve under diversifying selection and contribute to functional redundancy of R-genes and enhance the potential to cope with rapidly evolving pathogens like *M. oryzae* (Zhong *et al.*, 2016). Interestingly, the variability of NBS-LRR gene sequences among paralogs within clusters can provide resistance against distantly related pathogen taxa, resulting in MDR loci (Stiekema *et al.*, 1999; Narusaka *et al.*, 2009). Based on transcriptome data available in the public domain (<http://rice.plantbiology.msu.edu/expression.shtml>), except one, none of the RGAs that collocate with the 24 meta-QTLs was expressed when rice is infected with *M. oryzae*. Out of the 79 RGAs, *RPR1h* (LOC_Os11g12340), a disease resistance gene in NB-LRR family is expressed in tissues of resistant Nipponbare genotypes, 12 hours after infection of *M. oryzae*, indicating a functional role of the gene in the disease cycle. The same gene is differentially expressed in resistant genotypes compared to susceptibility when infected with different fungal pathogens (Wamishe *et al.*, 2018; Salvador-Guirao *et al.*, 2019). This indicates complex and rigid regulation of the RGAs. Genomic abundance of R-genes that enable functional redundancy in the ability to recognize potential pathogens is widely studied in the rice-blast patho-system. For example, a given pathogen isolate can be recognized by approximately 8 % of the R-genes selected from a genome-wide NBS-LRR gene pool (Zhang *et al.*, 2015). Therefore, it is evident that the pool

integrated into a target host genetic background a given R-gene has to be (i) effective against the repertoire of *Avr* genes retained in the local pathogen pool, (ii) not already present or inherent in the host genetic background, and also (iii) functionally non-redundant in the host-pathogen system. Therefore, a systematic screening of the RGA pool for the above three criteria is a prerequisite for their effective use. Nonetheless the number of RGAs predicted herein that collocate with meta-QTLs identify putative R genes that significantly contribute to phenotypic expression of disease resistance in multiple locations and multiple genetic backgrounds and therefore are potential, stable genomic resources for breeding host resistance.

The 24 meta-QTLs including 6 previously known and 18 novel ones, the high resolution maps, and the RGAs made available herein are important additions to the existing genetic and genomic resources available for resistance breeding for BL and SHB. However, functional redundancy is a challenge when R-genes/RGAs are selectively targeted in resistance breeding programmes to improve host resistance. Because to be effective when



Journal of the National Science Foundation of Sri Lanka 50(1)

- continued from page 44

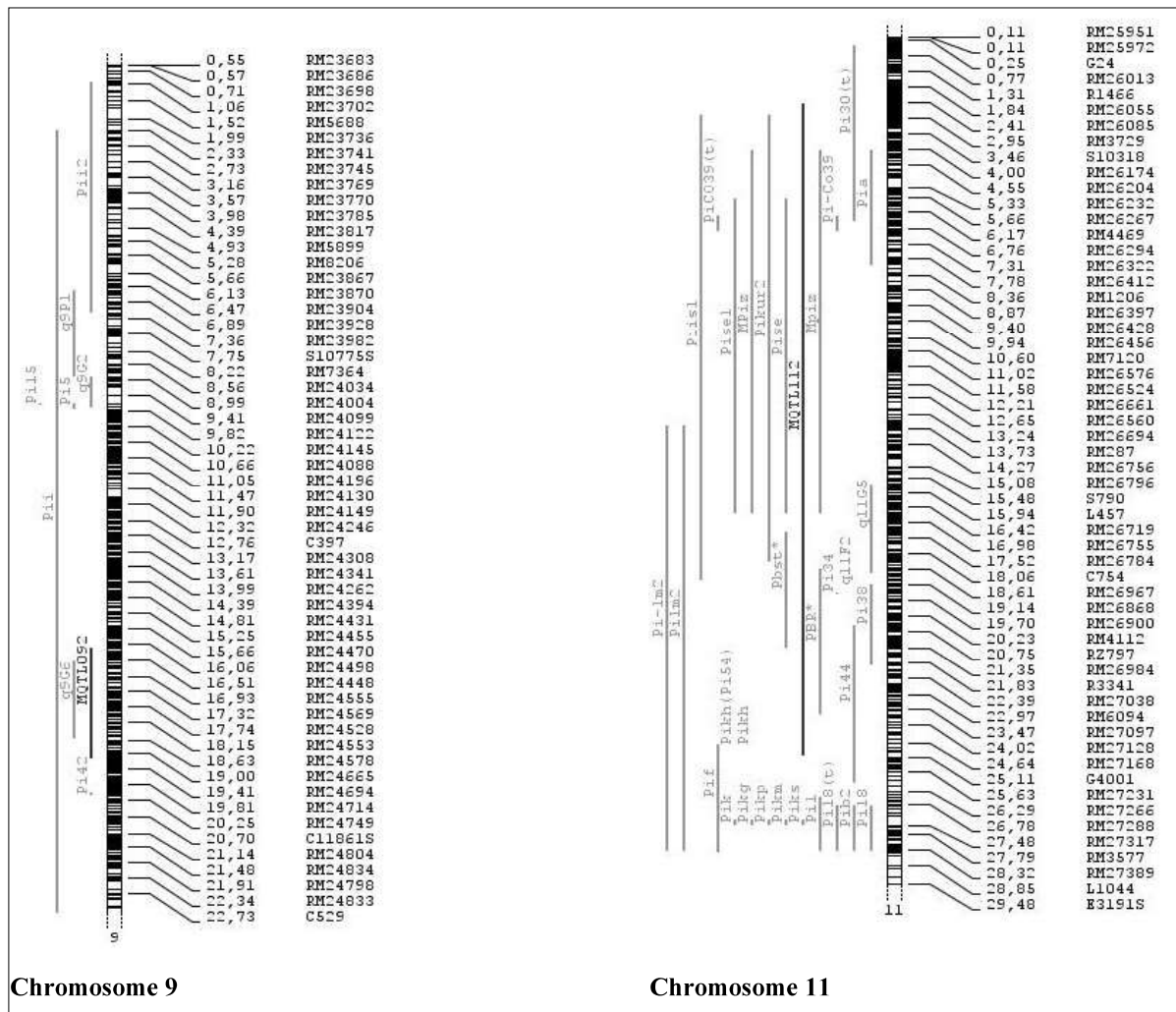


Figure 3: Collocation of meta-QTLs predicted herein with known meta-QTLs and resistance QTLs from previous studies. The dark vertical lines represent meta-QTLs predicted in this study. Light vertical lines represent meta-QTLs and QTLs from previous studies. Meta-QTLs reported in previous studies: *q1G2*, *q1G1*, *q4P1*, *q8P2*, *q9G2*, *q9P1* (Wang & Valent, 2009), *q8G1*, *q8G8*, *q9G6*, *q11G5*, *q11F2* (Ballini *et al.*, 2008) and QTLs reported in previous studies: *Pi24*, *Pi-2(t)*, *Pi24(t)*, *Pi33*, *Pi29(t)*, *Pi30(t)* (Sallaud *et al.*, 2003), *Pi-Co39*, *PiCO39(t)* (Chauhan *et al.*, 2002), *Pit*, *Pikp* (Hayashi *et al.*, 2006), *pi21* (Fukuoka & Okuno, 2001), *Pi36* (Liu *et al.*, 2005), *Pizh* (Causse *et al.*, 1994; Tanksley, 1993), *Pi5* (Wang *et al.*, 1994), *Pi-lm2* (Tabien *et al.*, 2000), *Pikm* (Ashikawa *et al.*, 2008), *Piks* (Fjellstrom *et al.*, 2003), *Pil* (Yu *et al.*, 1991), *Pi18(t)* (Ahn *et al.*, 2000), *Pisel*, *MPiz*, *Pikur1*, *Pikur2*, *Piis1*, *Pise*, *Pia* (GOTO, 1970), *Pikh* (Sharma *et al.*, 2005), *Pii2* (Kinoshita and Kiyosawa, 1997), *Pi44* (Chen *et al.*, 1999), *Pi38* (Gowda *et al.*, 2006), *Pi34* (Zenbayashi *et al.*, 2002), *Pik* (L. Wang *et al.*, 2009), *Pif* (Toriyama, 1972), *Pikg* (Sharma *et al.*, 2012), *Pib2* (Tabien *et al.*, 1996) *PBR*, *Pbst* (Fujii *et al.*, 1995), *Pi18* (Nagato, 1998), *Pii* (Ise, 1991), *Pi15* (Qing-Hua *et al.*, 2003), *Pi42* (Ballini *et al.*, 2008). Physical position of the markers are given in Mbp.

Table 4: Putative resistance genes that collocate with the meta-QTLs

Meta-QTL	Meta-QTL start (bp)	Meta-QTL stop (bp)	Gene ID	Gene start (bp)	Gene stop (bp)	Gene domain structure
MQTL014	41820536	43337474 ¹	LOC_Os01g72390	41986078	41988856	NBS, CC, LRR, TM
			LOC_Os01g72680	42169412	42172204	NBS, CC, LRR
MQTL022	31163706	36444094	LOC_Os02g57305	35108829	35110107	CC, NBS, TM, LRR
MQTL041	8667054	31213886	LOC_Os04g21890	12396117	12398915	NBS, CC, TM, LRR
			LOC_Os04g30530	18247444	18250388	NBS, CC, LRR, TM
			LOC_Os04g30610	18279293	18281498	NBS, CC, LRR, TM
			LOC_Os04g30660	18318639	18322459	NBS, CC, LRR, TM
			LOC_Os04g30690	18340866	18344512	NBS, CC, LRR, TM
			LOC_Os04g39460	23506845	23509631	NBS, LRR, TM
			LOC_Os04g43340	25631835	25636842	CC, NBS, LRR, TM
			LOC_Os04g46300	27430842	27434629	NBS, CC, TM, LRR
			LOC_Os04g51172	30297864	30305606	NBS, TM
			LOC_Os07g17220	10142289	10145916	CC, NBS, LRR, TM
MQTL071	7157274	11393756 ²	LOC_Os07g17250	10173157	10176827	NBS, CC, LRR, TM
			LOC_Os07g17250	10173157	10176827	NBS, CC, LRR, TM
MQTL072	10115789 ³	19502523	LOC_Os07g17220	10142289	10145916	CC, NBS, LRR, TM
			LOC_Os07g17250	10173157	10176827	NBS, CC, LRR, TM
			LOC_Os07g29810	17524037	17528680	CC, NBS, TM, LRR
			LOC_Os07g29820	17529552	17535086	CC, NBS, TM, LRR
MQTL073	2350101 ⁴	24954614	LOC_Os07g08890	4618666	4622813	NBS, CC, TM, LRR
			LOC_Os07g09900	5263409	5267310	CC, NBS, TM, LRR
			LOC_Os07g09940	5292921	5293886	NBS, LRR, TM
			LOC_Os07g17220	10142289	10145916	CC, NBS, LRR, TM
			LOC_Os07g17250	10173157	10176827	NBS, CC, LRR, TM
			LOC_Os07g29810	17524037	17528680	CC, NBS, TM, LRR
			LOC_Os07g29820	17529552	17535086	CC, NBS, TM, LRR
			LOC_Os07g33690	20129648	20135321	CC, NBS, TM, LRR
			LOC_Os07g33720	20157460	20160904	CC, NBS, LRR, TM
			LOC_Os07g40810	24456130	24459910	NBS, LRR, TM
MQTL083	5326953	8156813	LOC_Os08g09430	5466374	5469304	NBS, CC, TM, LRR
			LOC_Os08g10260	5964410	5967847	NBS, CC, TM, LRR
			LOC_Os08g10430	6127418	6131390	NBS, CC, TM, LRR
			LOC_Os08g10440	6137622	6141505	CC, NBS, LRR, TM
			LOC_Os08g12740	7539941	7551989	NBS, LRR, TM
MQTL092	16201951	19168603	LOC_Os09g30220	18391869	18397839	NBS, CC, TM, LRR
			LOC_Os09g30230	18402208	18404264	NBS, CC, TM, LRR
MQTL112	2435497	25125119 ⁵	LOC_Os11g10550	5777015	5787839	CC, NBS, LRR, TM
			LOC_Os11g10570	5797007	5801720	NBS, TM, LRR
			LOC_Os11g10610	5820833	5826729	CC, NBS, LRR, TM
			LOC_Os11g10620	5828343	5828674	CC, NBS, LRR, TM
			LOC_Os11g10760	5907950	5911943	CC, NBS, LRR, TM
			LOC_Os11g10770	5911937	5919029	NBS, LRR, TM
			LOC_Os11g11550	6419845	6424350	NBS, LRR, TM
			LOC_Os11g11770	6532861	6535926	CC, NBS, LRR, TM
			LOC_Os11g11790	6541924	6546026	NBS, LRR, TM
			LOC_Os11g11810	6554514	6561687	NBS, CC, TM, LRR
			LOC_Os11g11950	6631958	6634662	CC, NBS, LRR, TM
			LOC_Os11g11960	6638262	6640922	CC, NBS, LRR, TM
			LOC_Os11g12000	6668507	6681159	CC, NBS, LRR, TM
			LOC_Os11g12020	6690417	6690681	CC, NBS, LRR, TM
			LOC_Os11g12040	6692025	6697566	CC, NBS, LRR, TM

Continued -

- continued from page 47 -

Meta-QTL	Meta-QTL start (bp)	Meta-QTL stop (bp)	Gene ID	Gene start (bp)	Gene stop (bp)	Gene domain structure
			LOC_Os11g12050	6703120	6709237	CC, NBS, LRR, TM
			LOC_Os11g12300	6872037	6873056	CC, NBS, LRR, TM
			LOC_Os11g12320	6875946	6877418	CC, NBS, LRR, TM
			LOC_Os11g12330	6878608	6884945	CC, NBS, LRR, TM
			LOC_Os11g12340	6888057	6896357	CC, NBS, LRR, TM
			LOC_Os11g12350	6896964	6898774	CC, NBS, LRR, TM
			LOC_Os11g13940	7712006	7717010	CC, NBS, TM, LRR
			LOC_Os11g15670	8883111	8885768	CC, NBS, TM, LRR
			LOC_Os11g16510	9136895	9137837	NBS, LRR, TM
			LOC_Os11g17110	9505035	9505904	NBS, TM, LRR
			LOC_Os11g17120	9508232	9509376	NBS, CC, TM, LRR
			LOC_Os11g29030	16807964	16809227	NBS, LRR, TM
			LOC_Os11g29050	16821579	16826538	NBS, LRR, TM
			LOC_Os11g29520	17126630	17132216	CC, NBS, TM, LRR
			LOC_Os11g29980	17425545	17429007	NBS, CC, LRR, TM
			LOC_Os11g29990	17434258	17438286	NBS, CC, LRR, TM
			LOC_Os11g30060	17484860	17489555	CC, NBS, TM, LRR
			LOC_Os11g30110	17508573	17509867	NBS, CC, LRR, TM
			LOC_Os11g30210	17561346	17565177	NBS, CC, LRR, TM
			LOC_Os11g35580	20859839	20862861	NBS, CC, TM, LRR
			LOC_Os11g36410	21468751	21472160	NBS, CC, LRR
			LOC_Os11g38480	22799288	22802116	NBS, CC, LRR
			LOC_Os11g38580	22862447	22867268	NBS, CC, LRR
			LOC_Os11g39160	23305866	23313424	NBS, LRR, TM
			LOC_Os11g39260	23377646	23378368	NBS, LRR, TM
			LOC_Os11g39280	23389785	23391708	NBS, CC, TM, LRR
			LOC_Os11g40780	24387280	24390444	CC, NBS, TM, LRR
			LOC_Os11g41170	24670967	24674338	NBS, TM, LRR
			LOC_Os11g41210	24712661	24719904	NBS, TM, LRR
			LOC_Os11g41540	24911501	24917050	NBS, CC, TM, LRR

¹ RG331; ² C39; ³ C1023; ⁴ RG128; ⁵ G4001

a, b, c, d, e Second nearest marker was used due to the unavailability of physical position of the first nearest marker

Conflict of interest statement

The authors declare that they have no competing interests.

Acknowledgement

The authors acknowledge the National Research Council Investigator Driven Grants for financial assistance.

REFERENCES

Ashkani S., Rafii M.Y., Shabanmofrad M., Ghasemzadeh A., Ravanfar S.A. & Latif M.A. (2016). Molecular progress on the mapping and cloning of functional genes for blast disease in rice (*Oryza sativa* L.): current status and future

considerations. *Critical Reviews in Biotechnology* **36**(2): 353–367.

DOI: <https://doi.org/10.3109/07388551.2014.961403>

Ahn S.-N., Kim Y.-K., Hong H.-C., Han S.-S., Kwon S.-J., Choi H.-C., Moon H.-P. & McCouch S. (2000). Molecular mapping of a new gene for resistance to rice blast (*Pyricularia grisea* Sacc.). *Euphytica* **116**: 17–22.

DOI: <https://doi.org/10.1023/A:1004045812357>

Ashikawa I., Hayashi N., Yamane H., Kanamori H., Wu J., Matsumoto T., Ono K. & Yano M. (2008). Two adjacent nucleotide-binding site-leucine-rich repeat class genes are required to confer pikm-specific rice blast resistance. *Genetics* **180**: 2267–2276.

DOI: <https://doi.org/10.1534/genetics.108.095034>

Babu B.K., Dinesh P., Agrawal P.K., Sood S., Chandrashekara C., Bhatt J.C. & Kumar A. (2014). Comparative genomics

- and association mapping approaches for blast resistant genes in finger millet using SSRs. *PloS One* **9**(6): e99182. DOI: <https://doi.org/10.1371/journal.pone.0099182>
- Ballini E., Morel J.B., Droc G., Price A., Courtois B., Nottoghem J.L. & Tharreau D. (2008). A genome-wide meta-analysis of rice blast resistance genes and quantitative trait loci provides new insights into partial and complete resistance. *Molecular Plant-Microbe Interactions* **21**(7): 859–868. DOI: <https://doi.org/10.1094/MPMI-21-7-0859>
- Banniza S. & Holderness M. (2001). Rice sheath blight-pathogen biology and diversity. In: *Major Fungal Diseases of Rice*, pp. 201–211. Springer, Dordrecht, Germany. DOI: https://doi.org/10.1007/978-94-017-2157-8_14
- Boukaew S. & Prasertsan P. (2014). Suppression of rice sheath blight disease using a heat stable culture filtrate from *Streptomyces philanthi* RM-1-138. *Crop Protection* **61**: 1–10. DOI: <https://doi.org/10.1016/j.cropro.2014.02.012>
- Bouktila D., Khalfallah Y., Habachi-Houimli Y., Mezghani-Khemakhem M., Makni M. & Makni H. (2014). Large-scale analysis of NBS domain-encoding resistance gene analogs in Triticeae. *Genetics and Molecular Biology* **37**(3): 598–610. DOI: <https://doi.org/10.1590/S1415-47572014000400017>
- Calenge F., Faure A., Goerre M., Gebhardt C., Van de Weg W.E., Parisi L. & Durel C.E. (2004). Quantitative trait loci (QTL) analysis reveals both broad-spectrum and isolate-specific QTL for scab resistance in an apple progeny challenged with eight isolates of *Venturia inaequalis*. *Phytopathology* **94**(4): 370–379. DOI: <https://doi.org/10.1094/PHYTO.2004.94.4.370>
- Causse M.A. et al. (13 authors) (1994). Saturated molecular map of the rice genome based on an interspecific backcross population. *Genetics* **138**(4): 1251–1274. <https://doi.org/10.1093/genetics/138.4.1251>
- Chauhan R., Farman M., Zhang H.-B. & Leong S. (2002). Genetic and physical mapping of a rice blast resistance locus, Pi-CO39(t), that corresponds to the avirulence gene AVR1-CO39 of *Magnaporthe grisea*. *Molecular Genetics and Genomics* **267**(5): 603–612. DOI: <https://doi.org/10.1007/s00438-002-0691-4>
- Chen D., Viña M., Inukai T., Mackill D., Ronald P. & Nelson R. (1999). Molecular mapping of the blast resistance gene, Pi44(t), in a line derived from a durably resistant rice cultivar. *Theoretical and Applied Genetics* **98**: 1046–1053. DOI: <https://doi.org/10.1007/s001220051166>
- Chen H., Wang S., Xing Y., Xu C., Hayes P.M. & Zhang Q. (2003). Comparative analyses of genomic locations and race specificities of loci for quantitative resistance to *Pyricularia grisea* in rice and barley. *Proceedings of the National Academy of Sciences USA* **100**(5): 2544. DOI: <https://doi.org/10.1073/pnas.0437898100>
- Darvasi A. & Soller M. (1997). A simple method to calculate resolving power and confidence interval of QTL map location. *Behavior Genetics* **27**(2): 125–132. DOI: <https://doi.org/10.1023/A:1025685324830>
- Djian-Caporalino C. et al. (12 authors) (2014). Pyramiding, alternating or mixing: comparative performances of deployment strategies of nematode resistance genes to promote plant resistance efficiency and durability. *BMC Plant Biology* **14**(1): 53. DOI: <https://doi.org/10.1186/1471-2229-14-53>
- Dracatos P.M., Cogan N.O.I., Keane P.J., Smith K.F. & Forster J.W. (2010). Biology and genetics of crown rust disease in ryegrasses. *Crop Science* **50**(5): 1605–1624. DOI: <https://doi.org/10.2135/cropsci2010.02.0085>
- Ellis J.G., Lagudah E.S., Spielmeier W. & Dodds P.N. (2014). The past, present and future of breeding rust resistant wheat. *Frontiers in Plant Science* **5**: 641. DOI: <https://doi.org/10.3389/fpls.2014.00641>
- Fjellstrom R., Conaway-Bormans C.A., McClung A.M., Marchetti M.A., Shank A.R. & Park W.D. (2004). Development of DNA markers suitable for marker assisted selection of three Pi genes conferring resistance to multiple *Pyricularia grisea* pathotypes. *Crop Science* **44**(5): 1790–1795. DOI: <https://doi.org/10.2135/cropsci2004.1790>
- Fujii K., Hayano-Saito Y., Shumiya A. & Inoue M. (1995). Genetical mapping based on the RFLP analysis for the panicle blast resistance derived from a rice parental line St. No. 1. *Breed Science* **45**(Suppl 1): 209.
- Fukuoka S. & Okuno K. (2001). QTL analysis and mapping of pi21, a recessive gene for field resistance to rice blast in Japanese upland rice. *Theoretical and Applied Genetics* **103**(2): 185–190. DOI: <https://doi.org/10.1007/s001220100611>
- Goto I. (1970). Genetic studies on the resistance of rice plant to the blast fungus. *Japanese Journal of Phytopathology* **36**(5): 304–312. DOI: <https://doi.org/10.3186/jjphytopath.36.304>
- Gnanamanickam S.S. (2009). Major diseases of rice. In: *Biological Control of Rice Diseases*, pp. 13–42. Springer, Dordrecht, Germany. DOI: https://doi.org/10.1007/978-90-481-2465-7_2
- Goudemand E., Laurent V., Duchalais L., Ghaffary S.M.T., Kema G.H., Lonnet P., Margalé E. & Robert O. (2013). Association mapping and meta-analysis: two complementary approaches for the detection of reliable *Septoria tritici* blotch quantitative resistance in bread wheat (*Triticum aestivum* L.). *Molecular Breeding* **32**(3): 563–584. DOI: <https://doi.org/10.1007/s11032-013-9890-4>
- Griffiths S. et al. (14 authors) (2009). Meta-QTL analysis of the genetic control of ear emergence in elite European winter wheat germplasm. *Theoretical and Applied Genetics* **119**(3): 383–395. DOI: <https://doi.org/10.1007/s00122-009-1046-x>
- Guo B., Sleper D.A., Lu P., Shannon J.G., Nguyen H.T. & Arelli P.R. (2006). QTLs associated with resistance to soybean cyst nematode in soybean: Meta-analysis of QTL locations. *Crop Science* **46**(2): 595–602. DOI: <https://doi.org/10.2135/cropsci2005.04-0036-2>
- Gowda M., Roy-Barman S. & Chattoo B. (2006). Molecular mapping of a novel blast resistance gene Pi38 in rice using SSLP and AFLP markers. *Plant Breeding* **125**: 596–599. DOI: <https://doi.org/10.1111/j.1439-0523.2006.01248.x>

- Hamon C. *et al.* (15 authors) (2013). QTL meta-analysis provides a comprehensive view of loci controlling partial resistance to *Aphanomyces euteiches* in four sources of resistance in pea. *BMC Plant Biology* **13**(1): 45.
DOI: <https://doi.org/10.1186/1471-2229-13-45>
- Hayashi K., Yoshida H. & Ashikawa I. (2006). Development of PCR-based allele-specific and InDel marker sets for nine rice blast resistance genes. *Theoretical and Applied Genetics* **113**(2): 251–260.
DOI: <https://doi.org/10.1007/s00122-006-0290-6>
- Ise K. (1991). Linkage analysis of some blast resistance gene in rice, *Oryza sativa* L. *Japanese Journal of Breeding* **42**: 388–389.
- Jia Y., Jia M.H., Wang X. & Zhao H. (2019). A toolbox for managing blast and sheath blight diseases of rice in the United States of America. In: *Protecting Rice Grains in the Post-Genomic Era*. IntechOpen.
DOI: <https://doi.org/10.5772/intechopen.86901>
- Khowaja F.S., Norton G.J., Courtois B. & Price A.H. (2009). Improved resolution in the position of drought-related QTLs in a single mapping population of rice by meta-analysis. *BMC Genomics* **10**(1): 276.
DOI: <https://doi.org/10.1186/1471-2164-10-276>
- Kinoshita T. & Kiyosawa S. (1997). Some considerations on linkage relationships between Pii and Piz in the blast resistance of rice. *Rice Genetics Newsletter* **14**: 57–59.
- Li Z., Pinson S.R.M., Marchetti M.A., Stansel J.W. & Park W.D. (1995). Characterization of quantitative trait loci (QTLs) in cultivated rice contributing to field resistance to sheath blight (*Rhizoctonia solani*). *Theoretical and Applied Genetics* **91**(2): 382–388.
DOI: <https://doi.org/10.1007/BF00220903>
- Liu W., Liu J., Triplett L., Leach J.E. & Wang G.L. (2014). Novel insights into rice innate immunity against bacterial and fungal pathogens. *Annual Review of Phytopathology* **52**: 213–241.
DOI: <https://doi.org/10.1146/annurev-phyto-102313-045926>
- Liu X.Q., Wang L., Chen S., Lin F. & Pan Q.H. (2005). Genetic and physical mapping of Pi36(t), a novel rice blast resistance gene located on rice chromosome 8. *Molecular Genetics and Genomics* **274**(4): 394–401.
DOI: <https://doi.org/10.1007/s00438-005-0032-5>
- Miah G., Rafii M.Y., Ismail M.R., Puteh A.B., Rahim H.A., Asfaliza R. & Latif M.A. (2013). Blast resistance in rice: a review of conventional breeding to molecular approaches. *Molecular Biology Reports* **40**(3): 2369–2388.
DOI: <https://doi.org/10.1007/s11033-012-2318-0>
- Michelmore R.W. & Meyers B.C. (1998). Clusters of resistance genes in plants evolve by divergent selection and a birth-and-death process. *Genome Research* **8**(11): 1113–1130.
DOI: <https://doi.org/10.1101/gr.8.11.1113>
- Nagato Y. (1998). Report of the committee on gene symbolization, nomenclature and linkage groups. *Rice Genetics Newsletter* **15**: 13–73.
- Nalley L., Tsiboe F., Durand-Morat A., Shew A. & Thoma G. (2016). Economic and environmental impact of rice blast pathogen (*Magnaporthe oryzae*) alleviation in the United States. *PloS One* **11**(12): e0167295.
DOI: <https://doi.org/10.1371/journal.pone.0167295>
- Narayanan N.N., Baisakh N., Vera Cruz C.M., Gnanamanickam S.S., Datta K.B. & Datta S.K. (2002). Molecular breeding for the development of blast and bacterial blight resistance in rice cv. IR50. *Crop Science* **42**(6): 2072–2079.
DOI: <https://doi.org/10.2135/cropsci2002.2072>
- Narusaka M., Shirasu K., Noutoshi Y., Kubo Y., Shiraishi T., Iwabuchi M. & Narusaka Y. (2009). RRS1 and RPS4 provide a dual Resistance-gene system against fungal and bacterial pathogens. *The Plant Journal* **60**(2): 218–226.
DOI: <https://doi.org/10.1111/j.1365-3113.2009.03949.x>
- Ordon F. & Kühne T. (2014). Response to viral pathogens. In: *Biotechnological Approaches to Barley Improvement*, pp. 181–196. Springer, Berlin, Heidelberg, Germany.
DOI: https://doi.org/10.1007/978-3-662-44406-1_10
- Poland J.A., Balint-Kurti P.J., Wisser R.J., Pratt R.C. & Nelson R.J. (2009). Shades of gray: the world of quantitative disease resistance. *Trends in Plant Science* **14**(1): 21–29.
DOI: <https://doi.org/10.1016/j.tplants.2008.10.006>
- Qing-Hua P.A.N., Zhen-Di H.U., Takatoshi T. & Ling W. (2003). Fine mapping of the blast resistance gene Pi15, linked to Pii. *Journal of Integrative Plant Biology* **45**(7): 871–877.
- Ramalingam J., Cruz C., Kukreja K., Chittoor J., Wu J., Lee S., Baraoidan M., George M. L., Cohen M., Hulbert S., Leach J. & Leung H. (2003). Candidate defense genes from rice, barley, and maize and their association with qualitative and quantitative resistance in rice. *Molecular Plant-Microbe Interactions* **16**: 14–24.
DOI: <https://doi.org/10.1094/MPMI.2003.16.1.14>
- Reddy I.B.L., Reddy D.S., Narasu M.L. & Sivaramakrishnan S. (2011). Characterization of disease resistance gene homologues isolated from finger millet (*Eleusine coracana* L. Gaertn). *Molecular Breeding* **27**(3): 315–328.
DOI: <https://doi.org/10.1007/s11032-010-9433-1>
- Rocherieux J., Glory P., Giboulot A., Boury S., Barbeyron G., Thomas G. & Manzanares-Dauleux M.J. (2004). Isolate-specific and broad-spectrum QTLs are involved in the control of clubroot in *Brassica oleracea*. *Theoretical and Applied Genetics* **108**(8): 1555–1563.
DOI: <https://doi.org/10.1007/s00122-003-1580-x>
- Said J.I., Lin Z., Zhang X., Song M. & Zhang J. (2013). A comprehensive meta QTL analysis for fiber quality, yield, yield related and morphological traits, drought tolerance, and disease resistance in tetraploid cotton. *BMC Genomics* **14**(1): 776.
DOI: <https://doi.org/10.1186/1471-2164-14-776>
- Sallaud C., Lorieux M., Roumen E., Tharreau D., Berruyer R., Svestasrani P., Garsmeur O., Ghesquière A. & Notteghem J.-L. (2003). Identification of five new blast resistance genes in the highly blast-resistant rice variety IR64 using a QTL mapping strategy. *TAG. Theoretical and Applied Genetics. Theoretische Und Angewandte Genetik* **106**: 794–803.
DOI: <https://doi.org/10.1007/s00122-002-1088-9>
- Salvador-Guirao R., Baldrich P., Tomiyama S., Hsing Y.I., Okada K. & San Segundo B. (2019). OsDCL1a activation impairs phytoalexin biosynthesis and compromises disease resistance in rice. *Annals Of Botany* **123**(1): 79–93.

- DOI: <https://doi.org/10.1093/aob/mcy141>
- Sekhwal M.K., Li P., Lam I., Wang X., Cloutier S. & You F.M. (2015). Disease resistance gene analogs (RGAs) in plants. *International Journal of Molecular Sciences* **16**(8): 19248–19290.
- DOI: <https://doi.org/10.3390/ijms160819248>
- Semagn K., Beyene Y., Warburton M.L., Tarekegne A., Mugo S., Meisel B., Schabiague P. & Prasanna B.M. (2013). Meta-analyses of QTL for grain yield and anthesis silking interval in 18 maize populations evaluated under water-stressed and well-watered environments. *BMC Genomics* **14**(1): 313.
- DOI: <https://doi.org/10.1186/1471-2164-14-313>
- Sharma T.R., Madhav M.S., Singh B.K., Shanker P., Jana T.K., Dalal V., Pandit A., Singh A., Gaikwad K., Upreti H.C. & Singh N.K. (2005). High-resolution mapping, cloning and molecular characterization of the Pi-k(h) gene of rice, which confers resistance to Magnaporthe grisea. *Molecular Genetics and Genomics* **274**(6): 569–578.
- DOI: <https://doi.org/10.1007/s00438-005-0035-2>
- Sharma T.R., Rai A.K., Gupta S.K., Vijayan J., Devanna B.N. & Ray S. (2012). Rice blast management through host-plant resistance: retrospect and prospects. *Agricultural Research* **1**(1): 37–52.
- DOI: <https://doi.org/10.1007/s40003-011-0003-5>
- Sreenivasaprasad S. (2004). *Rice Sheath Blight Complex Caused by Rhizoctonia Species: Pathogen Epidemiology and Management Strategies*, pp. 101. Final technical report of project ID: R 7778 (ZA 0406). University of Warwick, UK.
- St. Clair D. A. (2010). Quantitative disease resistance and quantitative resistance loci in breeding. *Annual Review of Phytopathology* **48**: 247–268.
- DOI: <https://doi.org/10.1146/annurev-phyto-080508-081904>
- Stiekema W.J., van der Vossen A.G., van der Voort J.R., Bakker J. & Lankhorst R.K. (1999). Molecular isolation of two cyst nematode resistance genes: the *HsIP ro-1* gene of beet and the GPA2 gene of potato. In: *Genetics and Breeding for Crop Quality and Resistance*, pp. 185–193. Springer, Dordrecht, Germany.
- DOI: https://doi.org/10.1007/978-94-011-4475-9_21
- Su J., Wang W., Han J., Chen S., Wang C., Zeng, L., Feng A., Yang J. Zhou B. & Zhu X. (2015). Functional divergence of duplicated genes results in a novel blast resistance gene *Pi50* at the *Pi2/9* locus. *Theoretical And Applied Genetics* **128**(11): 2213–2225.
- DOI: <https://doi.org/10.1007/s00122-015-2579-9>
- Tabien R., Li Z., Paterson A., Marchetti M., Stansel J. & Pinson S. (2002). Mapping QTLs for field resistance to the rice blast pathogen and evaluating their individual and combined utility in improved varieties. *Theoretical And Applied Genetics* **105**(2–3): 313–324.
- DOI: <https://doi.org/10.1007/s00122-002-0940-2>
- Tabien R.E., Li Z., Paterson A.H., Marchetti M.A., Stansel J.W., Pinson S.R.M. & Park W.D. (2000). Mapping of four major rice blast resistance genes from 'Lemont' and 'Teqing' and evaluation of their combinatorial effect for field resistance. *Theoretical and Applied Genetics* **101**(8): 1215–1225.
- DOI: <https://doi.org/10.1007/s001220051600>
- Tabien R.E., Pinson S.R.M., Marchetti M.A., Li Z., Park W.D., Paterson A.H. & Stansel J.W. (1996). Blast resistance genes from Teqing and Lemont. In: *Rice Genetics III, Part 2*, pp. 451–455. World Scientific, Singapore.
- DOI: https://doi.org/10.1142/9789812814289_0046
- Talukder Z.I., McDonald A.J.S. & Price A.H. (2005). Loci controlling partial resistance to rice blast do not show marked QTL x environment interaction when plant nitrogen status alters disease severity. *The New Phytologist* **168**(2): 455–464.
- DOI: <https://doi.org/10.1111/j.1469-8137.2005.01507.x>
- Tanksley S.D. (1993). Mapping polygenes. *Annual Review of Genetics* **27**(1): 205–233.
- DOI: <https://doi.org/10.1146/annurev.ge.27.120193.001225>
- Tanweer F.A., Rafii M.Y., Sijam K., Rahim H.A., Ahmed F. & Latif M.A. (2015). Current advance methods for the identification of blast resistance genes in rice. *Comptes Rendus Biologies* **338**(5): 321–334.
- DOI: <https://doi.org/10.1016/j.crvi.2015.03.001>
- Toriyama K. (1972). Breeding for resistance to major rice diseases in Japan. In: *Rice Breeding* (ed. IRRI), pp. 253–281. International Rice Research Institute, Manila, Philippines.
- Veyrieras J.B., Goffinet B. & Charcosset A. (2007). MetaQTL: a package of new computational methods for the meta-analysis of QTL mapping experiments. *BMC Bioinformatics* **8**(1): 49.
- DOI: <https://doi.org/10.1186/1471-2105-8-49>
- Wamishe Y.A., Mulaw T., Rojas C.M., Jia Y. & Gebremariam T. (2018). Field germplasm evaluation, and development of diagnostic methods for bacterial panicle blight disease of rice in Arkansas. *Research Series: Arkansas Agricultural Experiment Station* **651**: 122–130.
- Wang G.-L. & Valent B. (2009). *Advances in Genetics, Genomics and Control of Rice Blast Disease*. Springer Nature, Switzerland.
- DOI: <https://doi.org/10.1007/978-1-4020-9500-9>
- Wang G.L., Mackill D.J., Bonman J.M., McCouch S.R., Champoux M.C. & Nelson R.J. (1994). RFLP mapping of genes conferring complete and partial resistance to blast in a durably resistant rice cultivar. *Genetics* **136**(4): 1421–1434.
- DOI: <https://doi.org/10.1093/genetics/136.4.1421>
- Wang L., Xu X., Lin F. & Pan Q. (2009). Characterization of rice blast resistance genes in the pik cluster and fine mapping of the Pik-p locus. *Phytopathology* **99**: 900–905.
- DOI: <https://doi.org/10.1094/PHYTO-99-8-0900>
- Wang X., Lee S., Wang J., Ma J., Bianco T. & Jia Y. (2014). Current advances on genetic resistance to rice blast disease. In: *Rice-Germplasm, Genetics and Improvement*, pp. 195–217. IntechOpen.
- DOI: <https://doi.org/10.5772/56824>
- Wiesner-Hanks T. & Nelson R. (2016). Multiple disease resistance in plants. *Annual Review of Phytopathology* **54**: 229–252.
- DOI: <https://doi.org/10.1146/annurev-phyto-080615-100037>

- Xiao N. *et al.* (12 authors) (2017). Improving of rice blast resistances in japonica by pyramiding major R genes. *Frontiers in Plant Science* **7**: 1918.
DOI: <https://doi.org/10.3389/fpls.2016.01918>
- Yadava S.K., Arumugam N., Mukhopadhyay A., Sodhi Y.S., Gupta V., Pental D. & Pradhan A.K. (2012). QTL mapping of yield-associated traits in *Brassica juncea*: meta-analysis and epistatic interactions using two different crosses between east European and Indian gene pool lines. *Theoretical And Applied Genetics* **125**(7): 1553–1564.
DOI: <https://doi.org/10.1007/s00122-012-1934-3>
- Yang S., Feng Z., Zhang X., Jiang K., Jin X., Hang Y. & Tian D. (2006). Genome-wide investigation on the genetic variations of rice disease resistance genes. *Plant Molecular Biology* **62**(1–2): 181–193.
DOI: <https://doi.org/10.1007/s11103-006-9012-3>
- Yu Z., Mackill D., Bonman J. & Tanksley S. (1991). Tagging genes for blast resistance in rice via linkage to RFLP markers. *TAG. Theoretical and Applied Genetics. Theoretische Und Angewandte Genetik* **81**: 471–476.
DOI: <https://doi.org/10.1007/BF00219436>
- Zarbaifi S.S. & Ham J.H. (2019). An overview of rice QTLs associated with disease resistance to three major rice diseases: blast, sheath blight, and bacterial panicle blight. *Agronomy* **9**(4): 177.
DOI: <https://doi.org/10.3390/agronomy9040177>
- Zenbayashi K., Ashizawa T., Tani T. & Koizumi S. (2002). Mapping of the QTL (quantitative trait locus) conferring partial resistance to leaf blast in rice cultivar Chubu 32. *TAG. Theoretical and Applied Genetics*. **104**(4): 547–552.
DOI: <https://doi.org/10.1007/s00122-001-0779-y>
- Zhang X. *et al.* (13 authors) (2015). A genome-wide survey reveals abundant rice blast R genes in resistant cultivars. *The Plant Journal* **84**(1): 20–28.
DOI: <https://doi.org/10.1111/tpj.12955>
- Zhong Z. *et al.* (27 authors) (2016). Directional selection from host plants is a major force driving host specificity in *Magnaporthe* species. *Scientific Reports* **6**: 25591.
DOI: <https://doi.org/10.1038/srep25591>
- Zou J., Pan X.-B., Chen Z., Xu J.Y., Lu J., Zhai W. & Zhu L. (2000). Mapping quantitative trait loci controlling sheath blight resistance in two rice cultivars (*Oryza sativa* L.). *TAG Theoretical and Applied Genetics* **101**: 569–573.
DOI: <https://doi.org/10.1007/s001220051517>

RESEARCH ARTICLE

Marine Atmosphere

Tropical cyclones in the Arabian Sea and the Bay of Bengal: comparison of environmental factors

G Pathirana^{1*} and K Priyadarshani²

¹ Department of Oceanography and Marine Geology, Faculty of Fisheries and Marine Science and Technology, University of Ruhuna, Wellamadama, Mathara.

² Department of Limnology and Water Technology, Faculty of Fisheries and Marine Sciences and Technology, University of Ruhuna, Wellamadama, Mathara.


Submitted: 24 February 2021; Revised: 12 July 2021; Accepted: 27 August 2021

Abstract: The Northern Indian Ocean is vulnerable to tropical cyclone (TC) related hazards that adversely affect people, infrastructure, and economies in the region. Considering the region's importance, supportive environmental factors for TC (> 17 knots) activity in the Arabian Sea (AS) and the Bay of Bengal (BoB) have been examined utilizing ocean-atmosphere datasets (1891–2016). The reasons for more TCs during 2011 and 2015 and less during 2013 in the AS than the BoB have been discussed. A decreasing (increasing) trend in the TC frequency is observed in the BoB (AS), which correlates negatively (positively) with sea surface temperature (SST). Though the TC frequency is larger in the BoB, the AS has experienced higher TC frequency on five occasions (1902, 2001, 2004, 2011 and 2015) during the 1891–2016 period. The observed trend in the Indian Ocean Dipole (IOD) index emphasizes a positive impact on the TC genesis in the AS. Results revealed that warmer SSTs supported by the co-occurrence of El Niño/Southern Oscillation (ENSO) and IOD events associated with a relatively deep 26 °C isothermal layer (D26) enhanced the TC formation in the AS during 2011 and 2015. The TC genesis is suppressed under the neutral conditions of ENSO and IOD (i.e., 2013) in the AS, and that brings the relative importance of the SST cooling associated with a deeper mixed-layer and shallow D26. Further, the observed differences in parameters between the regions are larger during the primary TC peak season (October - December). Although a recent increment of TCs is noted in the AS (compared to the BoB), the specific roles of the influencing factors on TC activities over the AS remain debatable.

Keywords: Arabian Sea, Bay of Bengal, ENSO, IOD, tropical cyclones.

INTRODUCTION

Tropical cyclones (TCs) are one of the disastrous natural hazards which cause numerous ecological and economical losses to the environment and society under favourable conditions. As TCs can cause catastrophic losses, related studies have practical importance in minimizing such possible damages. Nearly 7 % of TCs in the world are considered to occur in the Northern Indian Ocean (NIO) (WMO, 2008), which holds unique characteristics compared to the other two major Oceans. The Arabian Sea (AS) and the Bay of Bengal (BoB) enhance the complexity of the NIO region. Mohanty *et al.* (2012) demonstrated that the BoB contributes ~75 % of TCs while AS constitutes the remaining 25 % in the NIO. Due to the region's importance, many recent studies have been carried out to understand the TC activity in the NIO (Evan & Camargo, 2010; Girishkumar & Ravichandran, 2012; Mahala *et al.*, 2015). By utilizing data over 122 years (1877–1998), Singh *et al.* (2001) have suggested that the TC activities in the BoB indicate an increasing trend during November and May, while such a trend is absent in the AS. Further, Webster *et al.* (2005) have highlighted that the warming in the NIO is influencing the increased TCs activity in the region. Studies have shown that the TC frequency is high during the primary (October - December) and the secondary (April - June) TC peak seasons in the NIO and albeit their short-term time scales and extreme conditions. Several studies have

* Corresponding author (upgpathirana@fish.ruh.ac.lk;  <https://orcid.org/0000-0002-4670-579X>)



This article is published under the Creative Commons CC-BY-ND License (<http://creativecommons.org/licenses/by-nd/4.0/>). This license permits use, distribution and reproduction, commercial and non-commercial, provided that the original work is properly cited and is not changed in anyway.

discussed the importance of upper-ocean variability during the formation and intensification of TCs in the NIO (Lin *et al.*, 2009; Wang & Han, 2014).

TC genesis is influenced by the warmer ($> 28^{\circ}\text{C}$) sea surface temperature (SST), higher relative humidity (RH), weaker tropospheric wind shear, and thermodynamically unstable atmosphere (Henderson *et al.*, 1998; McPhaden *et al.*, 2009). Also, Sarma *et al.* (1990) have pointed out that the cyclone heat potential and the depth of the 26°C isothermal layer (D26) are two major influencing factors for the TC activities in the region. Further, the two major modes of climate variability, the El Niño-Southern Oscillation (ENSO) (McPhaden, 2002) and the Indian Ocean Dipole (IOD) (Saji *et al.*, 1999), are thought to influence the TC activity in the NIO (Girishkumar & Ravichandran, 2012; Mahala *et al.*, 2015). The impact of different phases of ENSO (La Niña, El Niño, and neutral ENSO) and IOD (*pIOD*: positive IOD, *nIOD*: negative IOD, and neutral IOD) on the TC activity in the BoB have been discussed in Mahala *et al.* (2015). Further, the same study reveals that the maximum frequency of TCs in the BoB is observed during La Niña years, *nIOD* years, and during the co-occurrence of La Niña with *nIOD*. Yuan and Cao (2013) have shown that the TC activity in the NIO is notably influenced by the IOD mode and PIOD events associated with warmer (cooler) SST anomalies strengthen (weaken) the convection over the western (eastern) NIO. However, less importance of higher SSTs to the hurricane frequency in the North Atlantic Ocean has been discussed in Donnelly and Woodruff (2007) and has suggested that the noted variability in the intense hurricane frequency was probably modulated by the atmospheric dynamics associated with ENSO and West African monsoon. Further, the possible impact of

anthropogenic warming on TC activity in the AS has been argued in Murakami *et al.* (2017). It shows that the continued anthropogenic forcing will further amplify the risk of TCs in the AS. However, the interactive influence from these phenomena to the formation and intensification of TCs in the NIO is still debatable. Thus, predicting the TC activity in the NIO has been a challenging problem due to the dynamics in the region.

In this study, TC activity in the NIO during 1891–2016 is examined by utilizing ocean-atmosphere datasets. Further, using the most recent observations from January 2010 to December 2016 as a case study, it has been discussed why did the AS only favoured the TCs during 2011 and 2015 (i.e., did not favour during 2013), compared to that observed in the BoB. Understanding the TC activity and related influencing factors between the AS and the BoB will enhance the accuracy of the model predictions in the region.

MATERIALS AND METHODS

The annual frequency of depressions and tropical cyclones (D/TCs) over the AS and the BoB during 1891–2016 was obtained from the Regional Specialized Meteorological Centre (RSMC), Indian Meteorological Department (IMD). The D/TCs with maximum wind speed higher than 17 knots had been considered, (Depressions: 17–33 knots, Cyclonic Storms: 34–47 knots, severe cyclonic storms: ≥ 48 knots). Based on the past D/TCs events, the region in the BoB ($5^{\circ}\text{N} - 20^{\circ}\text{N}$, $82^{\circ}\text{E} - 96^{\circ}\text{E}$) and AS ($5^{\circ}\text{N} - 20^{\circ}\text{N}$, $58^{\circ}\text{E} - 72^{\circ}\text{E}$) were selected to comparatively examine the atmospheric and oceanic conditions (Figure 1). Monthly mean data from extended reconstructed monthly sea surface temperature

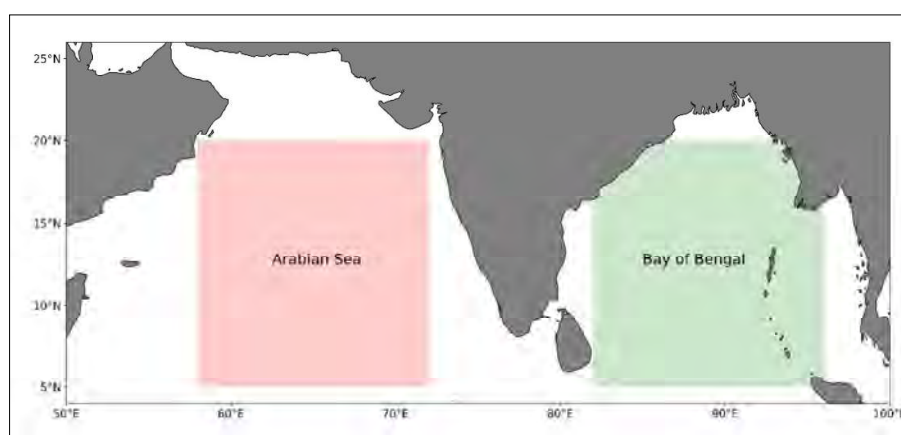


Figure 1: The study area: selected region ($5^{\circ}\text{N} - 20^{\circ}\text{N}$, $58^{\circ}\text{E} - 72^{\circ}\text{E}$) in the Arabian sea (shaded in red) and selected region ($5^{\circ}\text{N} - 20^{\circ}\text{N}$, $82^{\circ}\text{E} - 96^{\circ}\text{E}$) in the Bay of Bengal (shaded in green)

version 5 (ERSSTV5) was used to examine the SST variability during 1891–2016 (Huang *et al.*, 2017). Monthly mean zonal and meridional winds at 200 hPa and 850 hPa levels were extracted (Kalnay *et al.*, 1996) to examine the variability of the wind shear during 1891–2016 in the NIO.

ENSO intensity was calculated based on Niño 3.4 index, which is an area average of SST anomalies over 5° N - 5° S and 170° W - 120° W (Kim *et al.*, 2014) for the period of 1891–2016. For the same period IOD index was calculated, as the difference between SST anomalies in two regions of the tropical Indian Ocean (West: 10° S - 10° N, 50° E - 70° E, and East: 10° S - 0° S, 90° E - 110° E) (Saji *et al.*, 1999).

Three recent years were selected as a case study (i.e., 2011, 2013, and 2015) to comparatively examine the environmental factors which influence the TC frequency in the AS and the BoB. Further, daily SST data from Optimum Interpolation Sea Surface Temperature (OISST) (Huang *et al.*, 2021), daily wind data [from the Advanced Scatterometer (ASCAT)], daily air temperature (T_{air}), sea level pressure (SLP), and relative humidity (RH) data [from National Centre for Environmental Prediction (NCEP2)] were used to study the sea surface and atmospheric conditions in the region. Radiative (shortwave and longwave radiation) and turbulent (latent and sensible heat fluxes) air-sea

heat flux data were obtained from the TropFlux (Praveen Kumar *et al.*, 2012). The daily data were smoothed using a 30 d running mean filter. Further, the mixed-layer depth (MLD), barrier layer thickness (BLT), 26 °C isothermal layer depth (D26), and 20 °C isothermal layer depth (D20) were computed using Argo data. The MLD has been estimated as the depth where the density change is equivalent to 0.2 °C temperature criterion starting from a reference depth of 10 m (de Boyer Montegut *et al.*, 2004). The BLT has been computed as the difference between the top of thermocline depth and the MLD (Sprintall & Tomczak, 1992). All the datasets were area-averaged to facilitate the analysis.

RESULTS AND DISCUSSION

Long term variability of the TC frequency in the NIO

Earlier studies have pointed out the dominance of the D/TCs activity in the BoB (compared to the AS) by considering the observed ocean-atmosphere conditions between the regions. Similarly, analysis of this study indicates that the total observed D/TC frequency (> 17 knots) since 1891 in the BoB has been around ~20/year (Figure 2a) while it has been around ~3/year in the AS (Figure 2b). However, the observed D/TCs frequency tends to decrease after the 1960s in the BoB while increasing in the AS after the 1990s. However, it is noted that the observed D/TCs frequency in the AS was higher than the BoB on five

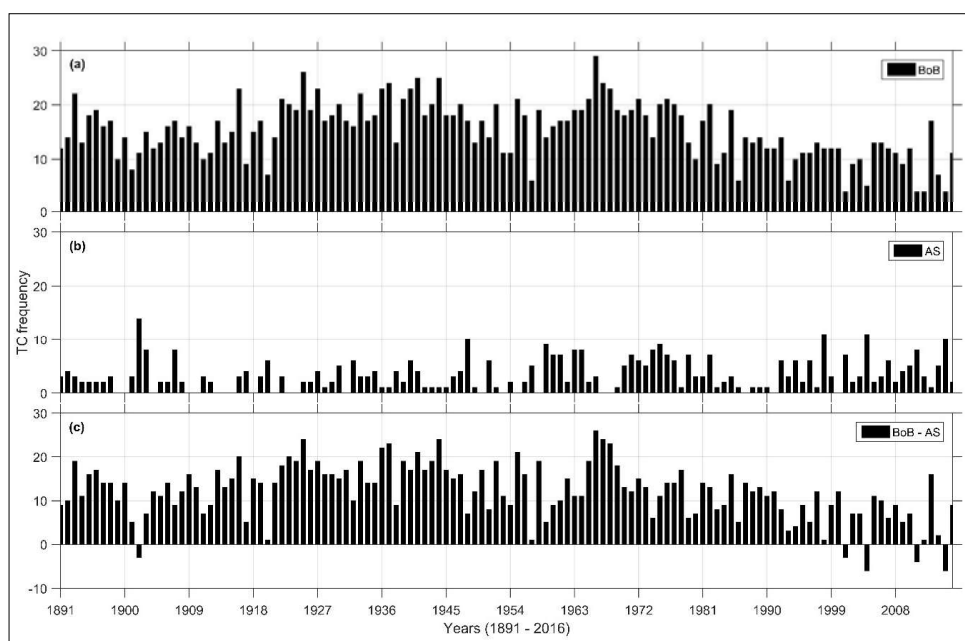


Figure 2: The observed tropical cyclone (TC) frequency during 1891 – 2016: (a) in the Bay of Bengal (BoB), (b) in the Arabian sea (AS), and (c) the differences in the TC frequency (BoB - AS). Only the TCs with a maximum wind speed larger than 17 knots have been considered in the study.

occasions (i.e., 1902, 2001, 2004, 2011, and 2015) (Figure 2c). Notably, four of these cases occurred after 2000. It emphasizes the importance of D/TCs activity in the AS and the role of the influencing factors. Murakami *et al.* (2017)

argued that anthropogenic forcing has likely increased the extremely severe TCs in the AS since the pre-industrial era. However, that study does not discuss how and why the TC activity in the AS is increasing.

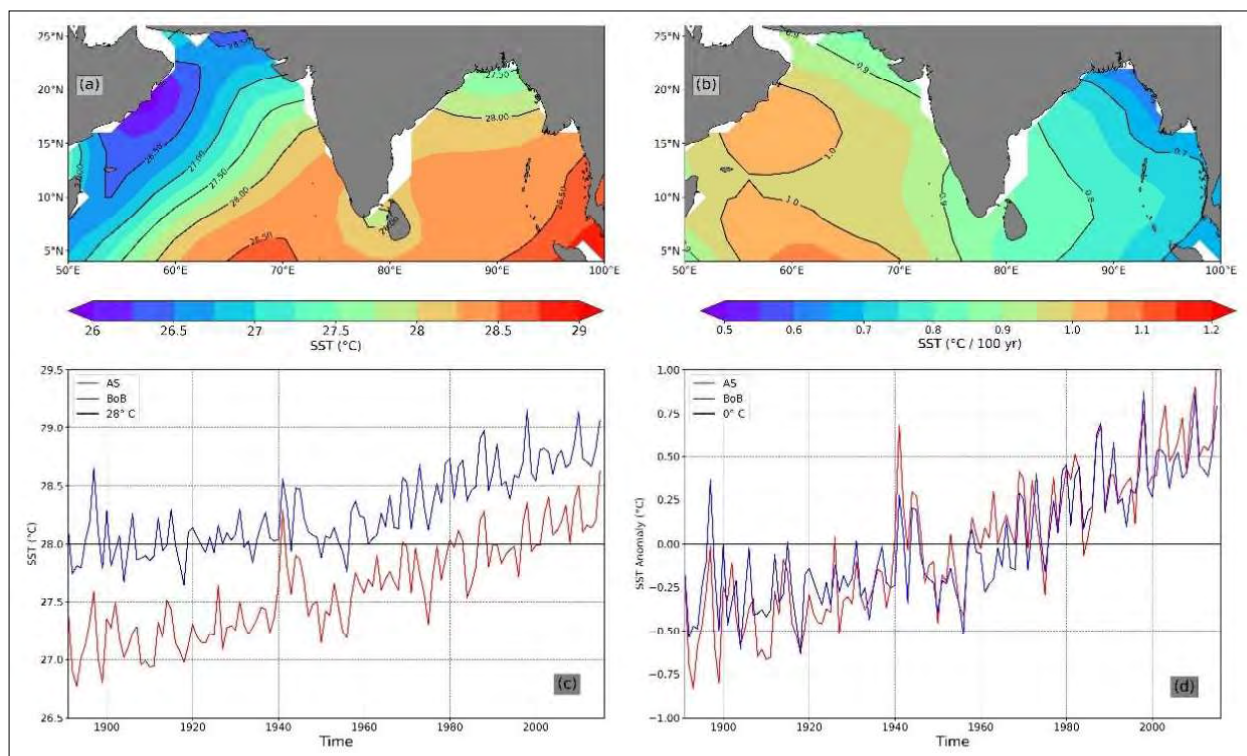


Figure 3: Observed (a) Sea surface temperature (SST) climatology (1891 – 2016), (b) SST linear trend (1891 – 2016), (c) area-averaged SST time series [$\sigma = \pm 0.41$ and ± 0.34 , Arabian sea (AS) and Bay of Bengal (BoB) respectively], and (d) SST anomaly calculated removing the SST climatology of each region.

Warmer SSTs and weaker vertical wind shear are two important factors that influence the TC activity in the NIO. Climatology indicates that the AS has been relatively cool compared to the BoB (Figure 3a) over the study period, and it has been warming (~ 1 °C/Century) faster than the BoB (Figure 3b). Average SST in the BoB region remains around the threshold for TC activity (i.e., 28 °C) during the pre-industrial period and gradually started to warm after the 1950s, while the AS started to exceed the SST threshold in the late 1990s (Figure 3c). Timeseries of SST anomalies calculated with respect to the climatology of each region emphasize that both regions have been warming since the 1890s (Figure 3d). Further, a positive correlation between the mean SST and the D/TC frequency in the AS ($r = 0.2$) is evident in the results, while the relation is negative for the BoB ($r = -0.5$). Although the mean SST in both regions is increasing, the noted difference in the relation between mean SST and the D/TC frequency highlights other

factors that may influence the TC activities in the region. The vertical wind shear variability between 200 hPa and 850 hPa levels over the regions has been examined, and a weakening of zonal wind shear is identified (Figures 4a and 4c). The variability of meridional wind shear is trivial in the BoB and is likely to increase in the AS (Figures 4b and 4d). Considering the magnitude of the vertical wind shear, the zonal wind shear is likely to dominate over the meridional wind shear in the region. The observed weakening of zonal wind shear is relatively large in the AS than in the BoB and may play a supportive role for the region's TC activities.

ENSO and IOD are considered as two major modes of climate variability in the Indian Ocean on interannual time scales (Saji *et al.*, 1999; McPhaden, 2002; Meyers *et al.*, 2007). The impact of ENSO and IOD on TC activity has been discussed in many of the previous studies (e.g., Girishkumar & Ravichandran, 2012; Mahala *et al.*,

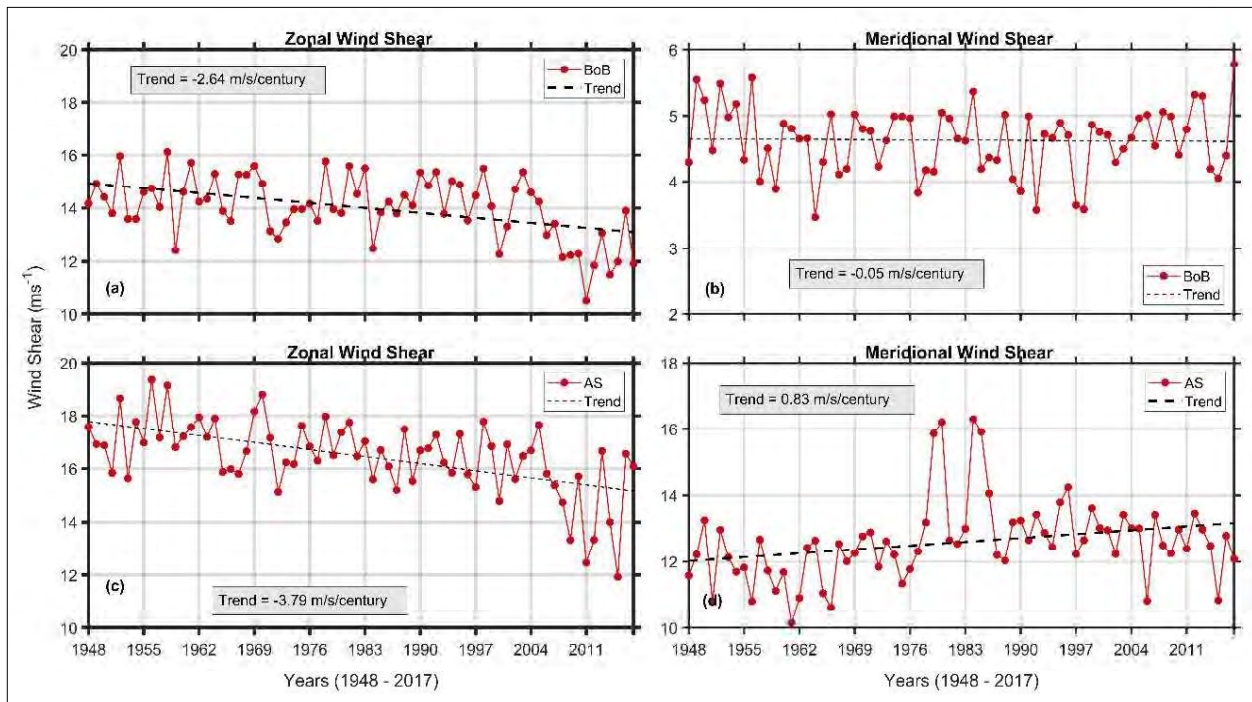


Figure 4: The estimated vertical wind shear over the Arabian sea (AS) and Bay of Bengal (BoB) from 1948 – 2016. (a) Zonal wind shear in the BoB, (b) meridional wind shear in the BoB, (c) zonal wind shear in the AS, and (d) meridional wind shear in the AS. The dashed black line in each figure illustrates the calculated trend m/s per century.

2015). Based on 117 years of data, Mahala *et al.* (2015) pointed out that the maximum frequency of TCs in the BoB is evident during La Niña years, *nIOD* years, and La Niña with *nIOD*. Further, they have suggested the possibility of more severe cyclones during La Niña + *pIOD* years, and the TC formation region can be shifted based on the type of IOD in the BoB. It is evident in the results that during the co-occurrence of *pIOD* with either La Niña (2011) or El Niño event (2015), the frequency of D/TCs is higher in the AS than that in the BoB. Girishkumar and Ravichandran (2012) pointed out that the *nIOD* year is favourable for extreme TC activity in the BoB and argued that the SST and vertical wind shear might not be the reason for the observed differences in the TC activity during ENSO events (either La Niña or El Niño) in the BoB.

The variability of the ENSO and IOD indexes are presented in Figure 5. Although the ENSO index indicates a weaker trend (~ 0), it points out the occurrence of strong El Niño events (Niño 3.4 index > 2.0 °C) after the 1950s than strong La Niña events (Figure 5a). The TC activity is found to be suppressed during El

Niño years mainly due to the increased vertical wind shear (Murakami *et al.*, 2017), and many studies have pointed out the positive impact from La Niña years on TC formation and intensification (Mohanty *et al.*, 2012; Mahala *et al.*, 2015). ENSO index correlates positively with AS SST ($r = 0.29$) and with BoB SST ($r = 0.17$). Though these correlations are not strong, still they suggest that the impact of ENSO on SST is likely higher in the AS than the BoB. In agreement with the observed warming trend in the western Indian Ocean (Figure 3b), the IOD index also indicates a positive trend, which may favour more *pIOD* events in the future (Figure 5b). The *pIOD* is thought to increase the convection activity in the AS, which favours the formation of D/TCs. Thus, the positive trend of IOD favours the D/TCs genesis in the AS compared to that in the BoB. Further, observed higher TC frequency in the AS after 2000 brings the relative importance of the variability of SST warming and weakening of vertical wind shear associated with ENSO and IOD. A comparative examination of ENSO and IOD influences in the two regions was undertaken by selecting three years after 2010. The results of that comparative study are discussed below.

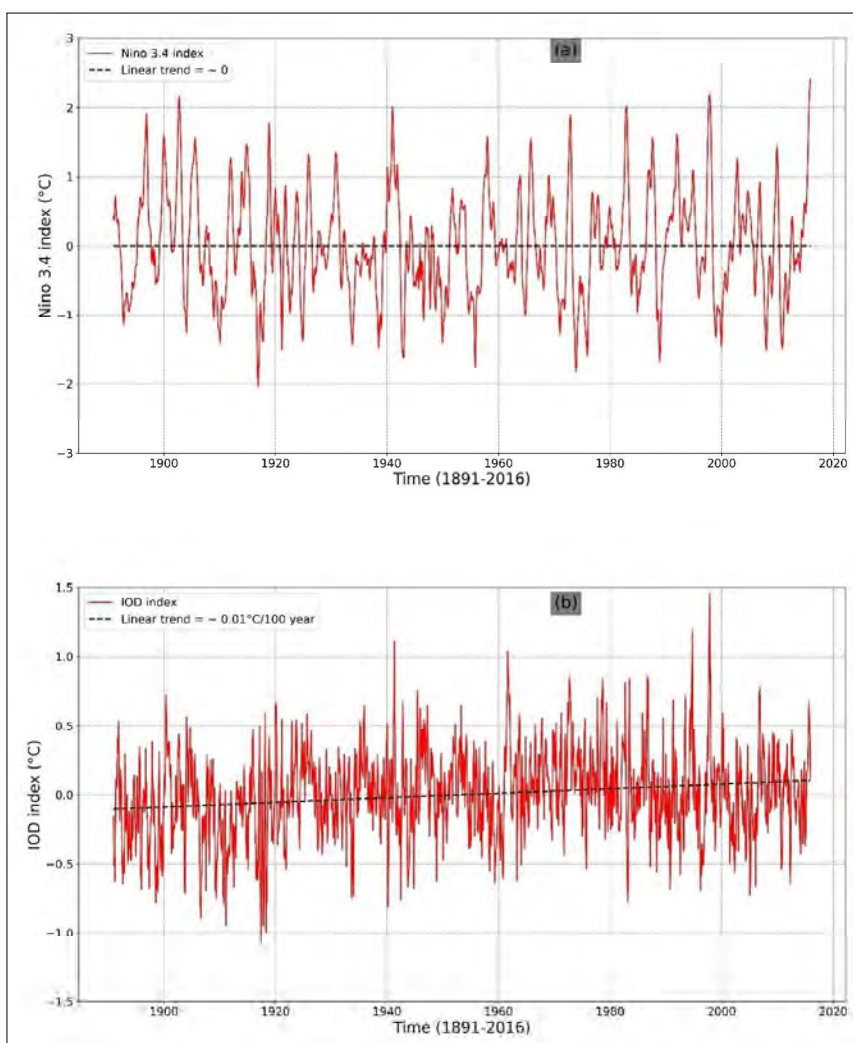


Figure 5: (a) The Niño 3.4 index variability during 1891 – 2016, and (b) Indian ocean dipole (IOD) index variability during 1891 – 2016. The dashed black line in each figure represents the observed trend (per century) during the specific time periods.

Variability of TC frequency during 2010 – 2016 in the NIO

Observed depressions and TCs in the AS and the BoB during 2010 – 2016

Both atmospheric and oceanic conditions influence the formation of D/TCs. Hence understanding their relative importance is important for a complex region like NIO. A total of 59 cases [depressions (Ds): 35, cyclonic storms (CS): 15, severe cyclonic storms (SCS): 9] in the BoB and 34 cases (Ds: 19, CS: 10, SCS: 5) in the AS from January 2010 to December 2016 have been selected (Figure 6a). During 2011 and 2015, the observed frequency of D/TCs

was higher in the AS than in the BoB. The formation of D/TCs is (almost) suppressed in the AS (1 case). The maximum number of D/TCs in the BoB (17 cases) was observed in 2013 (Figure 6a). The observed differences highlight the importance of the interactive role of the ocean atmosphere. Many studies have pointed out the relative importance of low-level vorticity, weak vertical wind shear, warmer SSTs associated with ENSO and IOD for the formation and intensification of D/TCs in the NIO (e.g., Mahala *et al.*, 2014). To understand the influence of the upper ocean, the impact of ENSO and IOD during the study period was examined, and the results are presented in Figure 6b.

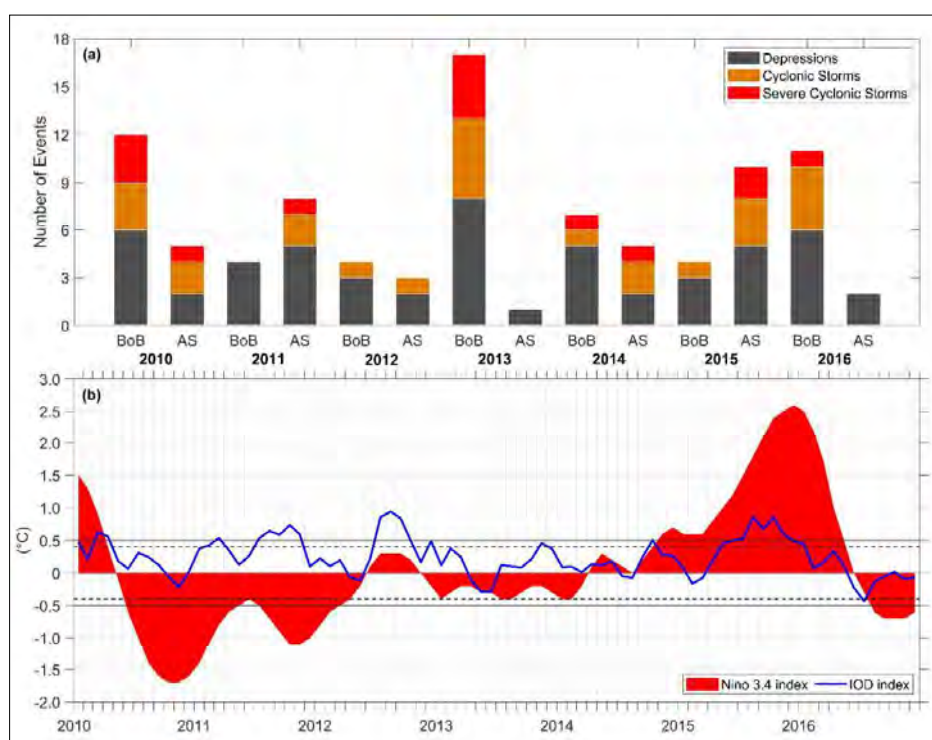


Figure 6: (a) The number of tropical cyclones observed during 2010 – 2016 in the Arabian sea (AS) and Bay of Bengal (BoB), and (b) variability of Niño 3.4 index and Indian ocean dipole (IOD) during 2010 – 2016. The following threshold values are considered in the present study. The solid black lines represent the threshold for Niño 3.4 index ($\pm 0.5^\circ \text{C}$): El Niño ($> +0.5^\circ \text{C}$), and La Niña ($< -0.5^\circ \text{C}$). The black dashed lines represent the threshold for IOD index ($\pm 0.4^\circ \text{C}$): $pIOD$ ($> +0.4^\circ \text{C}$), and $nIOD$ ($< -0.4^\circ \text{C}$).

The occurrence of the La Niña event (June 2010 – March 2012), neutral ENSO (April 2012 – October 2014), and El Niño event (November 2014 – May 2016) during the study period is evident from Niño 3.4 index data. The IOD data illustrates the presence of three $pIOD$ years (2011, 2012, and 2015) during the study period (Figure 6b). During the absence of ENSO and IOD (2013: hereafter neutral year), the number of D/TCs is highest (minimum) in the BoB (AS). Based on the observed differences in the number of D/TCs between the AS and the BoB, the years 2011 (La Niña + $pIOD$), 2013 (neutral year), and 2015 (El Niño + $pIOD$) has been selected as a case study to examine the influence from atmospheric and oceanic conditions comparatively.

Importance of surface conditioning in the AS and the BoB during 2010 – 2016

The annual mean of the surface parameters (i.e., SST, T_{air} , wind speed, RH, and SLP) have been estimated for the two

regions, and the results are presented in Table 1a. SST of the AS reached its minimum during 2013 and maintained a warmer surface during 2011 and 2015. However, the BoB was warmer than the AS during the selected years. This difference of SST between the two regions is largest during 2013 (0.65°C) compared to that in 2011 (0.56°C) and 2015 (0.43°C) (Table 1a). The seasonal cycle of T_{air} follows a similar pattern to the observed seasonal cycle of SST, thus indicating cooling in the AS and the BoB during 2013 than the years 2011/2015 (Table 1a). Winds over the AS are higher than that of BoB during the selected years, and that may be due to the strengthening of low-level jet streams (Findlater jet) over the AS and western India during summer (Findlater, 1969). Also, the estimated zonal vertical wind shear is larger in the AS compared to the BoB during the selected years, and it is maximum during 2013 in the AS (Table 1a). The mean RH is almost similar in both regions, and the mean SLP is relatively high over the AS compared to which is observed in the BoB. Thus, the noted favourable

conditions associated with relatively high SSTs, T_{air} , RH, relatively low SLP, and wind shear suggest higher D/TCs in the BoB than in the AS. Nevertheless, differences

observed in the formation of D/TCs during 2011, 2013, and 2015 highlight the interactive influence of other factors on D/TCs genesis in the two regions.

Table 1a: Mean surface conditions were observed in the Arabian sea (AS) ($5^{\circ}\text{N} - 20^{\circ}\text{N}$, $58^{\circ}\text{E} - 72^{\circ}\text{E}$) and the Bay of Bengal (BoB) ($5^{\circ}\text{N} - 20^{\circ}\text{N}$, $82^{\circ}\text{E} - 96^{\circ}\text{E}$) during the selected years.

Parameter	2011		2013		2015		Std.	
	AS	BoB	AS	BoB	AS	BoB	AS	BoB
SST ($^{\circ}\text{C}$)	27.99	28.55	27.90	28.55	28.47	28.90	1.07	0.84
T_{air} ($^{\circ}\text{C}$)	26.81	27.51	26.67	27.33	26.87	27.47	1.27	1.25
WSPD (ms^{-1})	6.26	6.20	6.28	6.09	6.44	6.21	2.43	2.12
Z Wind shear (ms^{-1})	15.7	12.3	13.3	11.8	14.0	11.5	1.4	1.2
RH (%)	74.3	75.3	75.3	75.8	74.4	75.8	4.61	4.29
SLP (mb)	1010	1008.8	1010.6	1009.4	1011	1009.4	2.20	2.3

Table 1b: Mean air-sea heat fluxes were observed in the Arabian sea (AS) ($5^{\circ}\text{N} - 20^{\circ}\text{N}$, $58^{\circ}\text{E} - 72^{\circ}\text{E}$) and the Bay of Bengal (BoB) ($5^{\circ}\text{N} - 20^{\circ}\text{N}$, $82^{\circ}\text{E} - 96^{\circ}\text{E}$) during the selected years.

Parameter (Wm^{-2})	2011		2013		2015		Std.	
	AS	BoB	AS	BoB	AS	BoB	AS	BoB
Q_{SW}	216.3	190.0	214.7	186.0	215.8	195.5	35.2	39.7
Q_{LW}	-56.6	-47.8	-55.5	-47.4	-55.7	-47.7	16.0	16.0
Q_{L}	-121.7	-108.7	-124.1	-113.5	-121.4	-111.7	32.3	26.0
Q_{S}	-8.0	-8.5	-7.9	-8.8	-8.1	-8.4	3.7	3.8
Q_{NET}	33.53	28.0	30.0	18.7	34.0	30.3	57.3	53.9

Variation of air-sea heat fluxes in the AS and the BoB during 2010 – 2016

The variability of air-sea heat fluxes is examined utilizing data from TropFlux to understand their relative importance on D/TCs genesis during the study period. The annual mean air-sea heat fluxes [i.e., shortwave radiation (Q_{SW}), longwave radiation (Q_{LW}), latent heat flux (Q_{L}), sensible heat flux (Q_{S}), and net surface heat flux (Q_{NET})] in the AS and the BoB during 2011, 2013, and 2015 are presented in Table 1b. Inconsistent with earlier studies, the bimodal pattern of the air-sea heat fluxes is evident in both regions. Average heat gain through Q_{SW} is higher in the AS than BoB, while the mean heat loss due to Q_{LW} is also higher in the AS (Table 1b). Thus, the radiative fluxes dominate the AS compared to the BoB with relatively high values during the study period. Q_{L} dominates over Q_{LW} in both regions and indicates a higher heat loss controlling the heat gain through Q_{SW} . Heat loss through Q_{S} is almost similar in both regions and

remains around -8 Wm^{-2} . Further, the average heat loss due to turbulent heat fluxes are relatively high in 2013 compared to 2011/2015 in both regions and provides evidence for strong wind mixing during 2013 (Table 1b). The impact of the radiative and turbulent heat fluxes is summarized in Q_{NET} . The annual mean Q_{NET} is positive in both regions and indicates potential warming during the study period. More heat energy is stored in the AS than in the BoB. This difference is more considerable during 2011/2015 than in 2013 (Table 1b). The difference in the mean Q_{NET} between the regions is maximum (11.3 Wm^{-2}) during 2013, while it is minimum ($\sim 3.7 \text{ Wm}^{-2}$) during 2011. Though the mean Q_{NET} indicates higher warming in the AS during the selected years (i.e., 2011, 2013, and 2015), warmer SSTs are not evident (compared to the BoB). Relatively higher SSTs are evident in the BoB during the selected years, and the differences observed between the regions highlight the importance of upper ocean variability, which can influence the SST cooling/warming.

Table 1c: Mean upper-ocean variability observed in the Arabian sea (AS) (5° N - 20° N, 58° E - 72° E) and the Bay of Bengal (BoB) (5° N - 20° N, 82° E - 96° E) during the selected years.

Parameter (m)	2011		2013		2015		Std.	
	AS	BoB	AS	BoB	AS	BoB	AS	BoB
MLD	55.1	37.9	54.3	36.5	49.3	38.2	17.4	6.2
BLT	3.2	15.8	4.5	16.6	4.0	14.9	4.1	7.2
D20	129.0	126.5	137.2	122.6	137.5	122.3	11.5	6.9
D26	73.5	78.9	73.5	75.4	73.3	75.4	10.4	7.0

Upper-ocean variability in the AS and the BoB during 2010 – 2016

Monthly average gridded Argo data is used to examine the variability of MLD, BLT, D20, and D26 during the study period. Table 1c shows the annual mean of the above parameters in the two regions during 2011, 2013, and 2015. Average MLD remains ≥ 50 m in the AS, while it is less than 40 m in the BoB during 2011, 2013, and 2015 (Table 1c). The deepening of the MLD in the AS indicates the influence of wind mixing during weaker stratification (compared to the BoB). A barrier layer between the bottom of the mixed-layer and the top of the thermocline restricts the mixing of water between the mixed-layer and the thermocline (Vialard & Delecluse, 1998b). A barrier layer is evident, and the mean BLT remains higher in the BoB, where it is relatively low in the AS (Table 1c). The barrier layer in the AS almost disappeared during summer when MLD reaches its maximum due to wind mixing. Thus, a relatively low MLD with a thicker barrier layer indicates that the BoB does not favour strong mixing in the upper-waters and tends to maintain warmer SSTs during summer than that in the AS.

Henderson *et al.* (1998) suggested the importance of a deeper thermocline, which is favourable for the formation of D/TCs. D20 was selected as the representative layer for the thermocline to examine its variability in the AS and the BoB. Like the variability observed in MLD and BLT, a deeper D20 is observed in the AS (compared to the BoB) during the study period. D26 is another important factor determining the formation and intensification of D/TCs (Sarma *et al.*, 1990). The heat content of the water column above the D26 is defined as the cyclone heat potential, which provides evidence for the energetically active zones in the ocean that are favourable for the formation of D/TCs. The average D26 remains shallow in the AS during 2011, 2013, and 2015. Though differences in the parameters are observed between the two regions during the selected years, the annual mean conditions do not provide any clear evidence for why D/TC frequency is larger during 2011/2015 in the AS compared to 2013.

Therefore, the variability of the environmental factors during the primary and secondary TC peak seasons between the regions is examined.

Comparison of the environmental factors during the Primary and Secondary TC peak seasons

Seasons have been categorized following Girishkumar and Ravichandran (2012) as primary TC peak season (PTCS) (October – December) and secondary TC peak season (STCS) (April – June). McPhaden *et al.* (2009) suggested that these months are favourable for D/TCs activity due to the existence of warmer SSTs, thermodynamically unstable atmosphere, and weak tropospheric wind shear in the BoB. Studying the TCs genesis over the AS for 1979 – 2008, Evan and Camargo (2010) also show the importance of the primary and secondary peak seasons on the formation of D/TCs.

The SST variability during the primary and secondary TC peak seasons are presented in Figure 7. It indicates that the co-occurrence of ENSO and IOD influenced both regions during PTCS and STCS. The warmest SSTs are noted during the co-occurrence of El Niño + *pIOD* (2015) in the NIO compared to the La Niña + *pIOD* event (2011). In comparison with 2011/2015, cooler SSTs during the neutral year (2013) are identified. Though both the regions maintain an average SST, it is higher than 29 °C during the STCS and less than 28 °C during the PTCS. The presence of warmer SSTs during the STCS is supported by the spring mini-warm pool that exists in the BoB (Pathirana & Priyadarshani, 2020). As the warmer temperatures in upper-waters positively influence the TC genesis, SST variability observed during 2010 – 2016 brings its relative importance to TC genesis in the region. Though the BoB favours the formation of D/TCs during either La Nina or El Nino events in compared to Neutral years due to relatively higher SSTs, the TC genesis in the BoB is lower than that observed in the AS during 2011 and 2015. Hence the co-occurrence of an ENSO+IOD event may have influenced the formation of D/TCs in the region. Thus, the results suggest the importance of

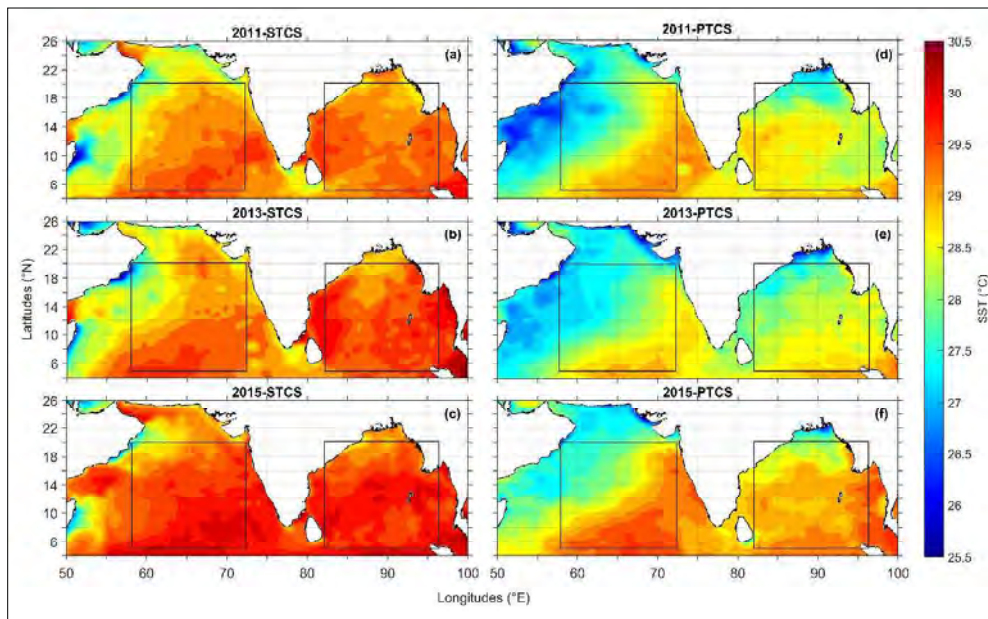


Figure 7: The variation of mean Sea surface temperature (SST) in the NIO during the primary tropical cyclone (TC) peak season (April-June) (a) 2011, (b) 2013, and (c) 2015, and the variation of mean SST during the secondary TC peak season (October-December) (d) 2011, (e) 2013, and (f) 2015. The boxes represent the selected region between 5° N - 20° N, 58° E - 72° E in the Arabian sea (AS) and the selected region between 5° N - 20° N, 82° E - 96° E in the Bay of Bengal (BoB).

Table 2: Variability in the mean conditions during the primary and secondary tropical cyclone (TC) peak seasons in the Arabian sea (AS) and the Bay of Bengal (BoB).

	2011				2013				2015			
	Primary		Secondary		Primary		Secondary		Primary		Secondary	
	AS	BoB	AS	BoB	AS	BoB	AS	BoB	AS	BoB	AS	BoB
SST	28.29	28.47	29.19	29.35	28.08	28.35	29.14	29.56	28.73	28.99	29.63	29.72
T _{air}	26.73	26.92	28.27	28.84	26.55	26.95	28.28	28.83	26.28	26.88	28.77	29.03
WSPD	5.3	5.4	5.5	6.6	5.3	5.9	5.3	5.4	4.9	5.9	6.5	6.0
RH	73.5	74.4	73.8	75.8	75	75	75.1	75.9	71.9	74.7	74.3	75.2
SLP	1010.8	1010.3	1009.1	1007.2	1011.4	1010.6	1009.2	1007.6	1012	1010	1009.6	1008
Q _{SW}	188.5	181.9	246.6	216.4	203.9	165.6	233.2	200.5	183	176.7	238.3	209.8
Q _{LW}	-55.4	-51.3	-52.3	-43.6	-58	-45.8	-49.7	-41.7	-49.8	-48	-50.5	-42
Q _L	-120.8	-114	-131.2	-113.3	-138.7	-122.4	-126	-112.6	-119.2	-111.1	-119.5	-114.6
Q _S	-8.1	-8.2	-8.8	-6.7	-8.2	-9.9	-7.8	-7.7	-8.5	-9	-7.7	-8.2
Q _{NET}	0.1	8.3	64.4	57.4	-4.4	-11.7	60	44.1	-1.6	10.5	69.9	51.1
MLD	49.1	32.6	37.4	32.3	43.6	32.0	41.4	35.6	43.0	32.5	32.3	34.8
BLT	3.1	17.7	4.8	7.8	-0.4	19.2	5.4	8.6	1.6	17.5	3.6	7.4
D20	123	117.4	135.6	131.1	123.1	115	141.6	126.3	127.7	114	141.2	128.4
D26	71.4	69.6	76.6	85.6	61.3	68.3	81.1	81.9	67.4	69.1	74.9	82.2

the interaction within other influencing factors, which determines the effect of SST on TC genesis in the region. Seasonal changes in the analyzed atmosphere-ocean conditions during 2011, 2013, and 2015 are presented in Table 2. The differences between the observed parameters during the STCS are relatively lower than those observed in the PTCS. The lowest SSTs are observed during the PTCS of 2013 in the AS and the BoB. The relative weakening of Q_{LW}, Q_L, and Q_S has the potential to enhance the seasonal warming in the NIO (Pathirana *et al.*, 2020). The Q_{NET} indicates a cooling tendency in both regions during the PTCS of 2013. However, they also indicate a warming tendency during 2011 and 2015. During all the seasons, MLD in the AS remains deeper than the BoB, with an average difference of ~ 15 m. The barrier layer that influences the SST by restricting the mixing in the upper ocean remains relatively low in the AS during all the seasons. The lowest BLT (-0.4 ± 5.4 m) is recorded during the PTCS of 2013. Like the observed MLD and BLT, the D20 is also deeper in the AS (compared to the BoB). Further, the depth of the D26 is deeper during the PTCS of 2011/2015 in the AS, while it is shallower during 2013.

Thus, the relative importance of the cooler SSTs, cooler T_{air}, higher heat loss through air-sea heat fluxes are observed in the AS during 2013 and points out that AS did not favour the formation of TCs (compared to the BoB) in 2013. Also, the observed deeper mixed-layer, relatively thinner barrier layer associated with shoaling D26 does not facilitate the TC genesis in the AS during 2013. During the absence of forcing from ENSO and IOD, the SST in the AS indicates a cooling tendency supported by wind mixing and upwelling of cold thermocline waters. Warmer SSTs and relatively strong stratification in the BoB enhance the conditions and favour the TC genesis. The atmospheric and oceanic conditions in the AS enhanced under the influence of ENSO and IOD. Thus, based on the variability of atmosphere-ocean conditions with the impact of ENSO and IOD, the study demonstrates the variability of D/TCs genesis in the AS and the BoB. However, this study is focused on the relative importance of the ocean surface and subsurface conditions and their influence on the D/TCs genesis in the NIO. The interactive roles from the low-level relative vorticity and D/TC genesis locations are not examined, and therefore, more studies are required to understand the dynamics in the region.

CONCLUSION

Environmental factors for TC (>17 knots) activity in the AS and the BoB have been examined utilizing atmosphere-ocean data sets (1891 – 2016). Further, utilizing recent observations (2010 – 2016), reasons for why AS favors TCs during 2011/2015 (and not during 2013) are also discussed (compared to the BoB). Based on long term data, the study shows that the TC frequency in the AS (BoB) is relatively increasing (decreasing). Results revealed a warming trend with increasing SSTs in both regions. The observed increment in the SST anomaly indicates the impact is higher in the AS than the BoB. Zonal wind shear is weakening, and the declining trend is higher in the AS than in the BoB. The Niño 3.4 index emphasizes a decreasing trend with time, while it correlates well with the AS's SST compared to BoB. IOD is positively increasing and provides evidence for warming in the western Indian Ocean. Thus, it is evident in the study that the SST, wind shear, ENSO, and IOD positively impact the TC genesis in the AS. However, the noted variability in the atmosphere-ocean conditioning during the selected years (2011, 2013, and 2015) indicates that the conditions relatively favor the TC genesis in the BoB compared to that in the AS. Further, the differences in the conditions between the regions are more significant during PTCS than in STCS. Relatively cooler SSTs associated with negative Q_{NET}, deeper mixed-layer, absence of barrier-layer, shallower D26, and the increasing wind shear may have suppressed the TC genesis in the AS during the 2013, Neutral year (compared to the BoB). Though the ocean surface and subsurface conditions were not favorable for the TC genesis during 2011 and 2015, the co-occurrence of ENSO and IOD may have supported the TC genesis in the AS. Based on the occurrence of extremely severe cyclonic storms (ESCS) in the PTCS during 2014 and 2015, Murakami *et al.* (2017) argued that anthropogenic global warming had increased the probability of ESCS over the AS. Though the D/TCs are frequent phenomena in the BoB, the noted increment in the AS during recent years underlines the importance of understanding the influencing factors and their interactive roles. However, the specific roles of the influencing factors on the TC activity over the AS are still debatable and therefore, more studies are required to enhance the understanding of TC activities in the NIO.

Acknowledgement

The authors thank the members of the Department of Oceanography and Marine Geology, Faculty of Fisheries and Marine Sciences & Technology, University of Ruhuna, Sri Lanka, for their encouragement and providing facilities to conduct this study.

REFERENCES

- De Boyer Montegut C., Madec G., Fischer A.S., Lazar A. & Iudicone D. (2004). Mixed layer depth over the global ocean: an examination of profile data and a profile-based climatology. *Journal of Geophysical Research* **109**: C12003
DOI: <https://doi.org/10.1029/2004JC002378>
- Donnelly J.P. & Woodruff J.D. (2007). Intense hurricane activity over the past 5,000 years controlled by El Niño and the West African monsoon. *Nature* **447**: 465–468.
DOI: <https://doi.org/10.1038/nature05834>
- Evan A.T. & Camargo S.J. (2010). A Climatology of Arabian sea cyclonic storms. *Journal of Climate* **24**: 140–158.
DOI: <https://doi.org/10.1175/2010JCLI3611.1>
- Findlater J. (1969). A major low-level air current near the Indian Ocean during the northern summer. *Royal Meteorological Society* **95**(404): 362–380.
DOI: <https://doi.org/10.1002/qj.49709540409>
- Girishkumar M.S. & Ravichandran M. (2012). The influences of ENSO on tropical cyclone activity in the Bay of Bengal during October–December. *Journal of Geophysical Research* **117**: C02033.
DOI: <https://doi.org/10.1029/2011JC007417>
- Henderson A. *et al.* (1998). Tropical cyclones and global climate change: A post-IPCC assessment. *American Meteorological Society* **79**: 19–38.
DOI: [https://doi.org/10.1175/1520-0477\(1998\)079<0019:TCAGCC>2.0.CO;2](https://doi.org/10.1175/1520-0477(1998)079<0019:TCAGCC>2.0.CO;2)
- Lin I.I. *et al.* (2009). Warm ocean anomaly, air-sea fluxes, and the rapid intensification of tropical cyclone Nargis (2008). *Geophysical Research Letters* **36**: L03817.
DOI: <https://doi.org/10.1029/2008GL035815>
- Kim S.T., Cai W., Jin F.-F., Santoso A., Wu L., Guilyardi E. & An S. (2014). Response of El Niño sea surface temperature variability to greenhouse warming. *Nature*
DOI: <https://doi.org/10.1038/nclimate2326>
- Mahala B.K., Nayak B.K. & Mohanty P.K. (2015). Impacts of ENSO and IOD on tropical cyclone activity in the Bay of Bengal. *Natural Hazards* **75**: 1105–1125.
DOI: <https://doi.org/10.1007/s11069-014-1360-8>
- Murakami H., Vechchi G.A. & Underwood S. (2017). Increasing frequency of extremely severe cyclonic storms over the Arabian Sea. *Nature Climate Change*,
DOI: <https://doi.org/10.1038/s41558-017-0008-6>
- McPhaden M.J. (2002). El Niño and La Niña: causes and global consequences. *Encyclopedia of Global Environmental Change* In: ed. T. Munn pp. 353–370. John Wiley Chichester, UK.
- McPhaden M.J. *et al.* (2009). Ocean-atmosphere interactions during cyclone Nargis. *Eos Trans. AGU*, **90**(7): 53–54.
DOI: <https://doi.org/10.1029/2009EO070001>
- Meyers G., McIntosh P., Pigot L. & Pook M. (2007). The years of El Niño, La Niña and interactions with the tropical Indian Ocean. *Journal of Climate* **20**: 2872–2880.
DOI: <https://doi.org/10.1175/JCLI4152.1>
- Mohanty U.C., Osuri K.K., Pattanayak S. & Sinha P. (2012). An observational perspective on tropical cyclone activity over Indian seas in a warming environment. *Natural Hazards* **63**: 1319–1335.
DOI: <https://doi.org/10.1007/s11069-011-9810-z>
- Pathirana G., Priyadarshani K., Dongxiao W., Chen G. & Priyadarshana T. (2020). Effect of spring mini-warm pool on the tropical cyclones in the Bay of Bengal: Case studies. *Journal of Nanjing University of Information Technology (Natural Science Edition)* **12**(4): 460–471.
- Pathirana G. & Priyadarshani K. (2020). A mini-warm pool during spring in the Bay of Bengal. *Journal of the National Science Foundation of Sri Lanka* **48**(4): 345–355.
DOI: <http://dx.doi.org/10.4038/jnsfsr.v48i4.9256>
- Praveen Kumar B. *et al.* (2012). TropFlux: air-sea fluxes for the global tropical oceans—description and evaluation. *Climate Dynamics* **38**(7–8): 1521–1543.
DOI: <https://doi.org/10.1007/s00382-011-1115-0>
- Saji N.H., Goswami B.N., Vinayachandran P.N. & Yamagata T. (1999). A dipole mode in the tropical Indian Ocean. *Nature* **401**: 360–363.
DOI: <https://doi.org/10.1038/43854>
- Sarma Y. Murty V. & Rao D. (1990). Distribution of cyclone heat potential in the Bay of Bengal. *Indian Journal of Marine Sciences* 102–106.
- Singh O.P., Khan T.M.A. & Rahman M.S. (2001). Has the frequency of intense tropical cyclones increased in the north Indian Ocean? *Current Science* **80**: 575–580.
- Sprattall J. & Tomczak M. (1992). Evidence of the barrier layer in the surface layer of the tropics. *Journal of Geophysical Research* **97**(C5): 7305–7316.
DOI: <https://doi.org/10.1029/92JC00407>
- Vialard J. & Delecluse P. (1998b). An OGCM study for the TOGA decade. Part II. Barrier-layer formation and variability. *Journal of Physical Oceanography* **28**: 1089–1105.
DOI: [https://doi.org/10.1175/1520-0485\(1998\)028<1089:AOSFTT>2.0.CO;2](https://doi.org/10.1175/1520-0485(1998)028<1089:AOSFTT>2.0.CO;2)
- Wang J.W. & Han W. (2014). The Bay of Bengal upper-ocean response to tropical cyclone forcing during 1999. *Journal of Geophysical Research* **119**: 98–120.
DOI: <https://doi.org/10.1002/2013JC008965>
- Webster P.J., Holland G.J., Curry J.A. & Chang H.R. (2005). Changes in tropical cyclone number, duration, and intensity in a warming environment. *Science* **309**: 1844–1846.
DOI: <https://doi.org/10.1126/science.1116448>
- WMO (2008). WMO Technical Report 2008. Available at <https://library.wmo.int/>, accessed 12 October 2020.
- Yuan J.P. & Cao J. (2013). North Indian Ocean tropical cyclone activities influenced by the Indian Ocean Dipole mode. *Journal of Science China Earth Sciences* **56**(5): 855–865.
DOI: <https://doi.org/10.1007/s11430-012-4559-0>

RESEARCH ARTICLE

Medical Physics

Determination of safe zone of the mandible for implant and bone harvesting (using CBCT) of mandible in a group of Sri Lankan subjects

RMAU Dharmapala^{1,2}, DM Satharasinghe¹, SPI Silva² and J Jeyasugiththan^{1*}

¹ Department of Nuclear Science, Faculty of Science, University of Colombo, Colombo 03.

² Dental Imaging Unit, National Dental Teaching Hospital, Colombo.


Submitted: 01 April 2021; Revised: 08 August 2021; Accepted: 27 August 2021

Abstract: Bone grafting procedures are required for patients with insufficient bone volumes for dental implants. The incisive mandibular nerve is more prone to iatrogenic injury during bone graft harvesting. This study aimed at examining the relative position of the mandibular canal (MC), gender Variation and to observe a safe zone for the implant and bone harvesting. Cone beam computed tomography (CBCT) scans of 200 patients (males 56 %) with age ranging from 16 to 70 years (mean age, 34.1 ± 14.5 years) were selected from the database of the Dental Imaging Unit of the National Dental Teaching Hospital of Sri Lanka. The MC length, mental foramen (MF) diameter, and location and the safe zone distance for bone graft harvesting were recorded for each hemi-mandible. The mean length of left and right MC of males were 6.99 ± 0.21 cm and 6.98 ± 0.22 cm, respectively while for females the mean length was equal for both sides (6.88 cm). The mean MF horizontal length of males was 0.32 ± 0.03 cm on the left and right sides while for females it was 0.31 ± 0.03 cm on either side. The vertical length of MF was 0.25 cm for both left and right (for both genders). The mean safe zone distance of the left and right mandibles for males were 0.27 ± 0.07 cm and 0.30 ± 0.06 cm, respectively while for females the values were 0.26 ± 0.06 cm and 0.27 ± 0.06 cm, respectively. The most frequent position of the MF among males was below the second premolar on each side of the mandible. The MF of females were frequently located below and between the first and second premolar on each side of the mandible. MC and other measurements showed a high sexual dimorphism. Therefore, gender variation in MC length, diameter and location of MF should be considered during surgical interventions such as implant and bone harvesting.

Keywords: CBCT, cone beam computed, tomography, mandibular canal, mental foramen.

INTRODUCTION

The mandible or inferior maxillary bone is the largest, strongest, and lowest bone in the human face (Breeland *et al.*, 2020). It acts as the lower jaw and consists of the body and ramus. Ramus divides into a coronoid process and head, which articulates with the mandibular fossa (Lev & Artzi, 2020). The inferior alveolar nerve (IAN), which is a branch of the mandibular nerve transmits through the mandibular canal (MC) towards the mental foramen (MF) (Drake *et al.*, 2014; Jena *et al.*, 2021). The IAN gives off the mental nerve at the MF, which supplies to the skin of the lower lip and the mucus membranes. Due to the high density of neurovascular structures, dental implantation in the mandibular region is risky with several complications (Kämmerer & Al-Nawas, 2020). The most common and severe complication is the neurosensory disturbance of the IAN (incidence of approximately 7 % of surgeries) (Goodacre *et al.*, 2003). The surgical procedures performed close to the mental foramen of the mandible present a minor risk of injury to the neurovascular structures. Therefore, the mental foramen is identified as a safe zone for surgical procedures such as bone graft removal, mentoplasty surgery, and fixation of fractures by placing plates (Mraiwa *et al.*, 2003). Knowledge of anatomical structures located in this region is important in pre-operative planning for dental surgeries (Imada *et al.*, 2014). The position and the dimension of the MC are critical as the IAN, which

* Corresponding author (jeyasugiththan@nuclear.cmb.ac.lk  <https://orcid.org/0000-0003-2896-3768>)



This article is published under the Creative Commons CC-BY-ND License (<http://creativecommons.org/licenses/by-nd/4.0/>). This license permits use, distribution and reproduction, commercial and non-commercial, provided that the original work is properly cited and is not changed in anyway.

travels through it, is susceptible to injury during surgical interventions of the mandible. Also, the relative position of the MC, mental and mandibular foramina in adults are age-dependent and show sexual dimorphism (Angel *et al.*, 2011). Moreover, anatomical variations such as deviated MC trajectory, bifid MC and anterior loops of the mental nerve are common in the mandibular region (Guimaraes *et al.*, 2014; Okumus & Dumlu, 2019).

Therefore, the variation in the anatomical position of the MC must always be taken into account to avoid iatrogenic inferior alveolar nerve damage. Dental radiological imaging plays an essential role in understanding the variations of these structures, such as intraoral periapical (IOPA) X-ray images, occlusal images, orthopantomogram (OPG) and cone-beam computed tomography (CBCT) (Shah, 2014). A cadaveric study had proven that the reproducibility and accuracy of the mandibular canal CBCT measurements were superior and even comparable to that of digital calliper measurements (Kamburoglu *et al.*, 2009). In addition, high image quality and the comparatively lower radiation dose in CBCT has made it a convenient mode of assessing three-dimensional (3D) craniofacial structures in dental practice (Liang *et al.*, 2009). According to the author's knowledge, an evaluation of the mandibular region's vital anatomical structures, including the safe zone for bone grafting, has not been conducted in Sri Lankan subjects. Therefore, the present study focuses

on several parameters of the anatomical structures within the mandible (length of MC and diameter of MF), including the safe zone for surgical interventions exclusively for the Sri Lankan population using CBCT. While acknowledging that only a few CBCT units are available in Sri Lanka, the findings of this study would become a helpful guide in centres where CBCT is not available to take accurate measurements.

MATERIALS AND METHODS

This cross-sectional study was carried out in the Dental Imaging Department of the National Dental Teaching Hospital, Sri Lanka. Among 355 patients who were presented to the department between December 2018 to January 2020, a sample of 200 patients (16–70 years) was included for the final evaluation after excluding those having mandibular fractures, deformities, pathological conditions, and previous manipulation which could alter the position of the IAN MC canal. All the scans were acquired using field of view (FOV): 15×9 cm, tube potential: 90 kVp, tube current: 10 mA and exposure time: 11.3 s. Mandibular canal length, the diameter of the anterior loop of mental foramen and distance from the root endpoint to the opening of the inferior border of MC (safe distance) were measured for each patient. In addition, the frequent location of the mental foramen was recorded and graded according to the criteria given in Table 1.

Table 1: Assigned grade according to the location of the mental foramen

Location of the mental foramen	Grade
Below the canine	1
Below and between the canine and the first premolar	2
Below the first premolar	3
Below and between the first and second premolar	4
Below the second premolar	5
Below and between the second premolar and the first molar	6

The linear measurements were performed on the axial section of the mandible with 0.5 mm slice thickness. Point 1 was selected in the first trans-axial view immediately after the origin of MF, where the loop of mandibular canal is formed. This was selected as point 1 and interludes of 10 mm were selected for subsequent measurements along the MC (respectively, points 2, 3, 4). This point-by-point connections resulted in a 2D view of the mandible, where the mandibular canal was seen beginning to end (Figure 1).

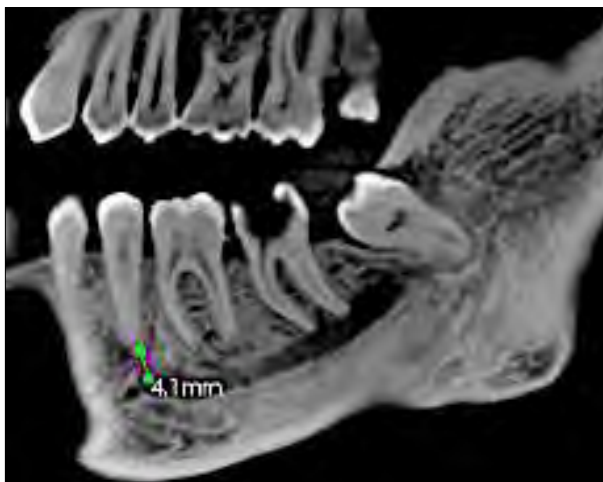
The measurements were obtained using the virtual ruler option available with Carestream (CS) imaging software version 7.0.2.8 (CS Health, Inc, 150, Verona Street, Rochester, NY 14608, USA). Each measurement was recorded in cm and repeated for both left and right sides of the mandible. Descriptive and non-parametric statistics were used to analyze the data which did not follow a normal distribution with 95 % confidence interval. Spearman's correlation was run to measure the correlation between recorded linear dimensions and age.



(a)



(b)



(c)

Figure 1: Illustration of (a) mandibular canal as seen in CBCT para-sagittal section of the mandible. The green path indicates the mandibular canal (b) mental foramen as seen in CBCT para-sagittal section of the mandible. The green line connecting the two dots indicates the mental foramen diameter and (c) safe zone for bone grafting as seen in CBCT para-sagittal section of the mandible. The green line indicates the safe length

RESULTS AND DISCUSSION

Table 2 illustrates the descriptive statistics of the study sample and the distribution of MC length, dimension of the MF, and safe zone length. The values are given for both sides of the mandible (left and right) for males, females and both genders (overall). The mean lengths of left and right MC of males were 6.99 ± 0.21 cm and 6.98 ± 0.22 cm, respectively, while for females the mean length was equal for both sides (6.88 cm). The mean vertical length of males' left and right MF were 0.25 ± 0.33 cm and 0.25 ± 0.02 cm, respectively. The vertical length of left and right MF of females was similar to that of males. The mean horizontal length of MF of males were similar for both sides (0.32 ± 0.03 cm), while for females, it showed a similar trend but lower mean length for both sides (0.31 ± 0.03 cm). The mean safe zone distance of the left and right mandible for males was 0.27 ± 0.07 cm and 0.30 ± 0.06 cm, respectively while for females, the values were 0.26 ± 0.06 cm and 0.27 ± 0.06 cm, respectively. The association between age and measured parameters were assessed and found that only a weak correlation exists between age and MC length for females (Figure 2).

MC length

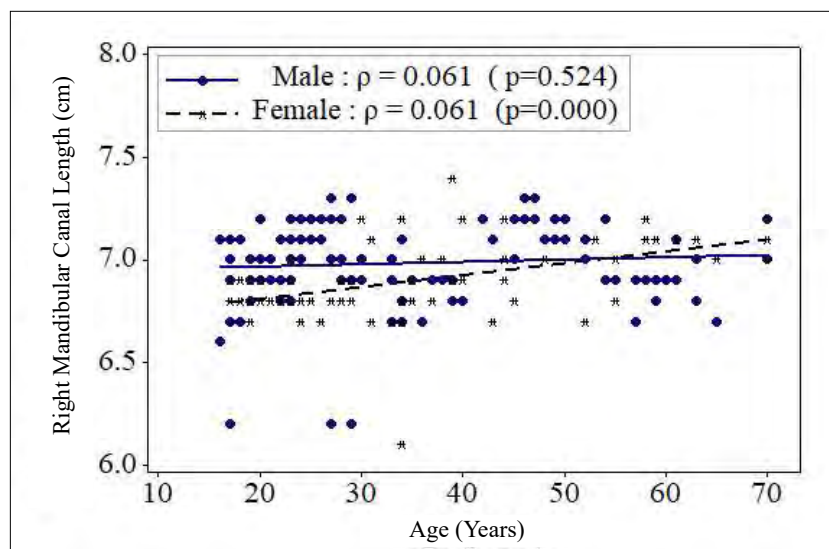
A gender-Variation in the mean length of MC was observed in the study sample (Table 2). However, the mean MC length was nearly similar for both sides of the mandible irrespective of gender. Figure 3 compares the mean MC lengths of India (Komal *et al.*, 2020), Turkey (Direk *et al.*, 2018) and Chile (Gonzalo *et al.*, 2017) with the findings of the present study. The mean MC values of left and right mandibles for the Indian population (6.57 and 6.60 cm, respectively) as suggested by Mraiwa *et al.* (2003) was lower compared to our results (6.95 and 6.94 cm, respectively, for left and right sides). However, remarkably, the values suggested by the Chile study (7.1 and 7.08 cm for left and right sides, respectively) were comparable with the MC lengths of the present study. These individual differences may be due to the morphological variation seen among different ethnicities. A weak correlation was noted for MC length against age for females (Spearman's $\rho = 0.528$ and 0.413) for left and right sides, respectively (Figure 2).

MF Dimensions

The size, shape, location, and direction of the opening of the MF can vary depending on the ethnicities and gender. Neiva *et al.* (2004) had found that the mean diameter of MF was 0.36 ± 08 cm (range 0.2 – 0.55 cm). The above measurements were done on 22 Caucasian cadaveric skulls. Also, Apinhasmit *et al.* (2006) had examined

Table 2: Descriptive statistics of the study sample and results summary

Gender		Male	Female	Overall
Sample size (n)		112	88	200
Mean age (\pm SD) in years		35.3 \pm 15.3	32.5 \pm 13.2	34.1 \pm 14.5
	(range)	(16 – 70)	(17 – 70)	(16 – 70)
Mean length (\pm SD) of mandibular canal (cm)	Left	6.99 \pm 0.21	6.88 \pm 0.16	6.95 \pm 0.20
	(range)	(6.30 – 7.90)	(6.50 – 7.30)	(6.30 – 7.90)
	Right	6.98 \pm 0.22	6.88 \pm 0.17	6.94 \pm 0.20
	(range)	(6.20 – 7.80)	(6.70 – 7.40)	(6.10 – 7.80)
Mean (\pm SD) vertical length of mental foramen (cm)	Left	0.25 \pm 0.03	0.25 \pm 0.27	0.25 \pm 0.02
	(range)	(0.21 – 0.36)	(0.22 – 0.34)	(0.21 – 0.36)
	Right	0.25 \pm 0.02	0.25 \pm 0.02	0.25 \pm 0.02
	(range)	(0.21 – 0.34)	(0.22 – 0.34)	(0.21–0.34)
Mean (\pm SD) horizontal length of mental foramen (cm)	Left	0.32 \pm 0.03	0.31 \pm 0.03	0.32 \pm 0.03
	(range)	(0.26 – 0.41)	(0.27 – 0.41)	(0.20 – 0.40)
	Right	0.32 \pm 0.03	0.31 \pm 0.03	0.31 \pm 0.03
	(range)	(0.27 – 0.41)	(0.27 – 41)	(0.27 – 0.41)
Mean (\pm SD) of safe zone distance (cm)	Left	0.27 \pm 0.07	0.26 \pm 0.06	0.27 \pm 0.07
	(range)	(0.20 – 0.40)	(0.20 – 0.40)	(0.20 – 0.40)
	Right	0.30 \pm 0.06	0.27 \pm 0.06	0.29 \pm 0.07
	(range)	(0.20 – 0.40)	(0.20 – 0.40)	(0.20 – 0.40)



(a)

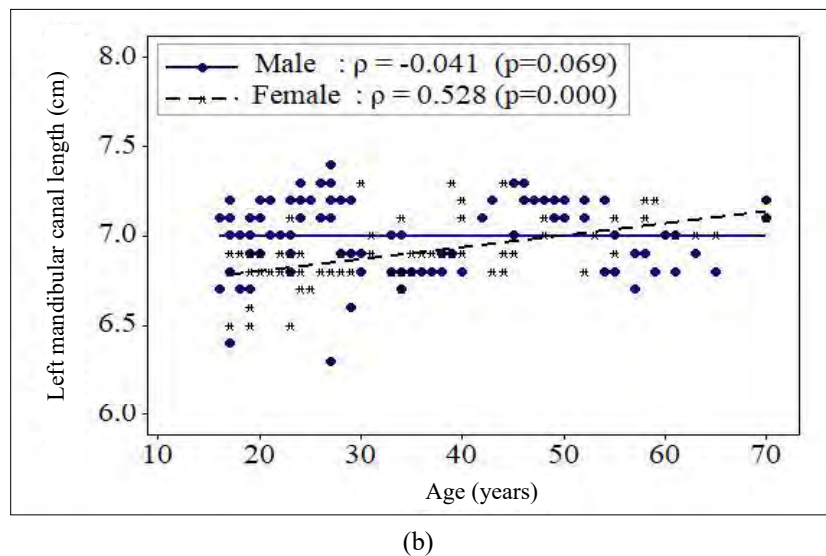


Figure 1: Correlations plots of (a) left mandibular canal length (cm) against age (years) and (b) right mandibular canal length (cm) against age (years). Spearman's correlation coefficient (ρ), level of significance (p)

106 Thai adult skulls and found that the mean MF width was 0.28 ± 0.07 cm. In addition to these cadaveric studies, many authors have determined the MF size using radiographic imaging techniques such as OPG and CBCT. Sheikhi *et al.* (2015) had assessed 180 CBCTs and found that the mean MF diameter for the Iran cohort was 0.36 cm. The resultant mean MF diameters (horizontal length) for Sri Lankan males were 0.32 ± 0.03 cm for both sides, while for females, it was 0.31 ± 0.03 cm on either side. In addition to the horizontal dimension, the

vertical length of MF was assessed to determine the shape of MF. It was found that the overall vertical length of MF was 0.25 ± 0.02 cm for both left and right, and it is the same for both genders. This suggests that the shape of the MF is oval for both genders.

MF location

Except for these size variations, MF also varies in location and direction of the opening (Neiva *et al.*,

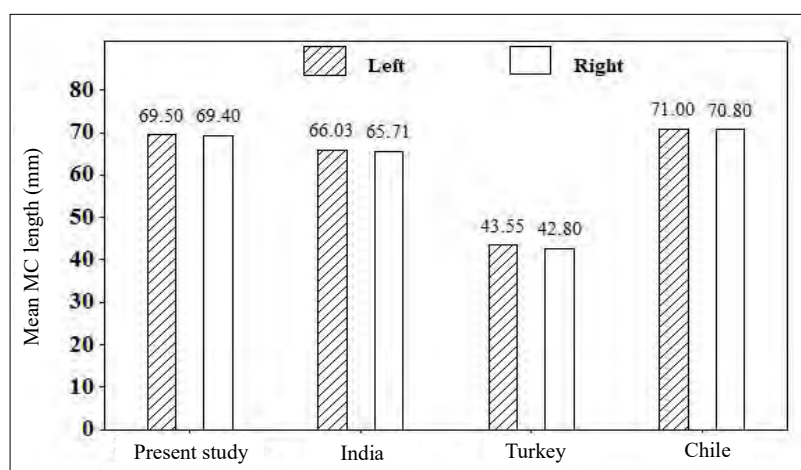


Figure 3: Comparison of present study data (mandibular canal mean length) with similar studies found in literature. India, Turkey and Chile

2004; Apinhasmit *et al.*, 2006). Due to variations in the location, injuries to MF are common during achieving anaesthesia or surgery. Therefore, precise identification of the MF location is clinically essential to avoid chances of iatrogenic injuries (Juodzbalys *et al.*, 2010). According to Srivastava *et al.* (2017) the frequent position of MF was below the second premolar in the Indian population. However, in the present study findings, the location of MF is observed to be different between genders (Figure 4). The MF is frequently located below the second premolar in males, while it is below and between the first and second premolar for females.

Safe zone dimensions

Moreover, to prevent IAN damage during bone graft harvesting, a safe zone had been recommended by Al-Ani *et al.* (2013). The most preferred site is between the root apex to the open of mental foramen. The present study results indicate that the safe zone distance for

males are 0.27 ± 0.07 cm and 0.30 ± 0.06 cm on left and right sides, respectively. For females, the measured lengths on the left and right sides were 0.26 ± 0.06 cm and 0.27 ± 0.06 cm, respectively. Yang *et al.* (2017) suggests that the area of 4 mm anterior and 8 mm inferior to the mental foramen is adequate, and if operated by a safe hand. Also, Pommer *et al.* (2008) suggest that the bone should be harvested at 8 mm below the tooth apices with a maximum harvest depth of 4 mm. However, the present findings suggest that the safe zone is much narrower than what is suggested in the literature. Therefore, a different reference mark should be applied during such interventions. The present study evaluated the variations of a wide range of dimensions related to mandibular anatomy using CBCT. However, to gain insight into the Sri Lankan population, a more significant sample representative of the whole country should be evaluated. This was a significant limitation in our study and should be considered to ensure a definite conclusion in future studies.

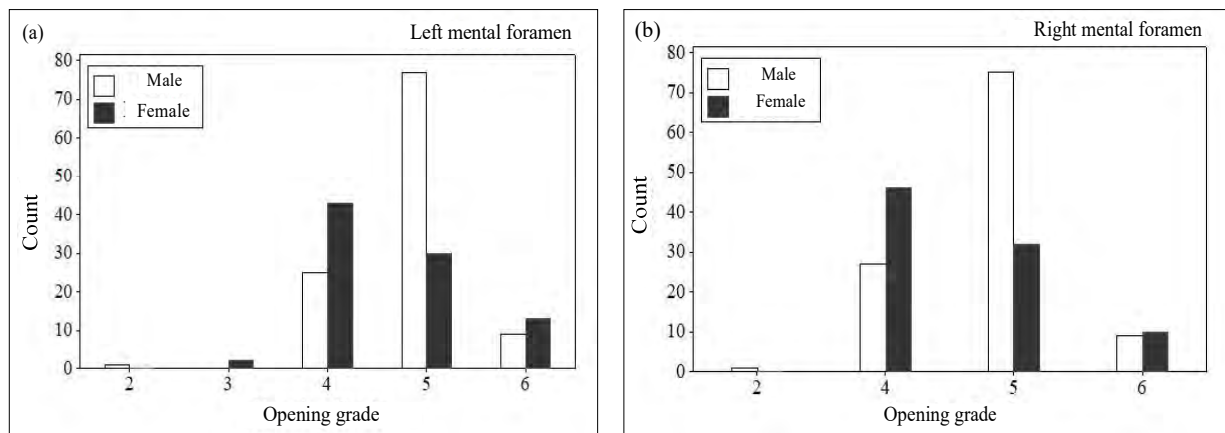


Figure 4: Gender wise variation in the opening grade of (a) left and (b) right mental foramen based on the grading given in Table 1

CONCLUSION

Mandibular canal length, safe zone distance and the horizontal length of mental foramen showed sexual dimorphism. Almost all the measurements were higher in males compared to females. Also, the frequent location of the MF varied between genders (MF located below the second premolar in males and between the first and second premolar in females). These variations in the resultant values may be attributed to morphological and ethnic diversity seen among the different populations. Therefore, gender-wise variation in MC length, diameter

and location of MF should be considered during surgical interventions such as implant and bone harvesting. This will positively influence the surgical results and reduce the potential of iatrogenic injuries. The large deviation in the length and the spatial pathway of intra-bony nerve canals suggest that the exposure of anterior loop and mandibular canal using CBCT is fundamental for preoperative evaluation in the mandibular region. Finally, the authors recommend studies with a larger population to determine the precise relative position of the mandibular canal and associated structures using CBCT.

Acknowledgments

Authors would like to thank for the support given by the staff members of the Dental Imaging Department of National Dental Teaching Hospital, Sri Lanka to conduct the study.

REFERENCES

- Al-Ani O., Nambiar P., Ha K.O. & Ngeow W.C. (2013). Safe zone for bone harvesting from the interforaminal region of the mandible. *Clinical Oral Implants Research* **24**: 115–121.
DOI: <https://doi.org/10.1111/j.1600-0501.2011.02393.x>
- Angel J.S., Mincer H.H., Chaudhry J. & Scarbecz M. (2011). Cone-beam computed tomography for analyzing variations in inferior alveolar canal location in adults in relation to age and sex. *Journal of Forensic Sciences* **56**(1): 216–219.
DOI: <https://doi.org/10.1111/j.1556-4029.2010.01508.x>
- Apinhasmit W., Chompoopong S., Methathrathip D., Sansuk R. & Phetphunphiphat W. (2006). Supraorbital notch/foramen, infraorbital foramen and mental foramen in Thais: anthropometric measurements and surgical relevance. *Journal of the Medical Association of Thailand* **89**(5): 675–82.
DOI: <https://doi.org/10.1053/joms.2003.50070>
- Breeland G., Aktar A. & Patel B.C. (2020). Anatomy, head and neck, mandible. Stat Pearls [Internet]. Available at <http://www.ncbi.nlm.nih.gov/pubmed/30335325>
- Direk F., Uysal I.I., Kivrak A.S., Unver Dogan N., Fazliogullari Z. & Karabulut A.K. (2018). Reevaluation of mandibular morphometry according to age, gender, and side. *Journal of Craniofacial Surgery* **29**(4): 1054–1059.
DOI: <https://doi.org/10.1097/SCS.00000000000004293>
- Drake R., Vogl A.W., Mitchell A.W.M., Drake R., Wayne V.O.G.L. & Adam W.M.M. (2015). *Gray's Anatomy for Students*, 3rd edition. Elsevier Churchill Livingstone, UK.
- Goodacre C.J., Bernal G., Rungharassaeng K. & Kan J.Y.K. (2003). Clinical complications with implants and implant prostheses. *Journal of Prosthetic Dentistry* **90**(2): 121–122.
DOI: [https://doi.org/10.1016/S0022-3913\(03\)00212-9](https://doi.org/10.1016/S0022-3913(03)00212-9)
- Guimaraes D., Pontes F.S., Pontes H.A. & Da Mata Rezende D.D. (2014). Anatomical variation of mandibular canal simulating a recurrence of odontogenic tumor. *Annals of Maxillofacial Surgery* **4**(1): 107.
DOI: <https://doi.org/10.4103/2231-0746.133088>
- Imada T.S.N., Ramos F.L.M.P.D.S., Stuchi C.B., Christiano D.O.S., Marques H.H. & Fischer R.B.I.R. (2014). Accessory mental foramina: prevalence, position and diameter assessed by cone beam computed tomography and digital panoramic radiographs. *Clinical Oral Implants Research* **25**(2): 1–6.
DOI: <https://doi.org/10.1111/clr.12066>
- Jena S., Panigrahi R., Pati A.R. & Hasan S. (2021). Prevalence, patterns and variations of anterior loop of inferior alveolar nerve|A CBCT based retrospective study. *Indian Journal of Otolaryngology and Head Neck Surgery* **2021**: 1–8.
DOI: <https://doi.org/10.1007/s12070-021-02691-w>
- Juodzbaly G., Wang H.L. & Sabalys G. (2010). Anatomy of mandibular vital structures. part II: Mandibular incisive canal, mental foramen and associated neurovascular bundles in relation with dental implantology. *Journal of Oral and Maxillofacial Research* **1**(1): 1–10.
DOI: <https://doi.org/10.5037/jomr.2010.1103>
- Kamburoğlu K., Kiliç C., Ozen T. & Yuksel S.P. (2009). Measurements of mandibular canal region obtained by cone-beam computed tomography: a cadaveric study. *Oral Surgery, Oral Medicine, Oral Pathology, Oral Radiology, and Endodontology* **107**(2): 34–42.
DOI: <https://doi.org/10.1016/j.tripleo.2008.10.012>
- Käämmerer P.W. & Al-Nawas B. (2020). Complications in oral implant placement. In: *Complications in Cranio-Maxillofacial and Oral Surgery*, pp. 133–150. Springer, Switzerland.
- Komal A., Bedi R.S., Wadhvani P., Aurora J.K. & Chauhan H. (2020). Study of normal anatomy of mandibular canal and its variations in indian population using CBCT. *Journal of Oral and Maxillofacial Surgery* **19**(1): 98–105.
DOI: <https://doi.org/10.1007/s12663-019-01224-x>
- Lev D. & Artzi Z. (2020). The anatomy of the maxilla and the mandible: related structures and inserted muscles. In: *Bone Augmentation by Anatomical Region: Techniques and Decision-Making*, pp. 1–16. Wiley Online.
- Liang X., Jacobs R., Hassan B., Li L., Pauwels R., Corpas L., Souza P.C., Martens W., Shah-bazian M. & Ivo A.A.L. (2010). A comparative evaluation of cone beam computed tomography (CBCT) and multi-slice CT (MSCT) part I. on subjective image quality. *European Journal of Radiology* **75**(2): 265–269.
DOI: <https://doi.org/10.1016/j.ejrad.2009.03.042>
- Mraiwa N., Jacobs R., Van Steenberghe D. & Quirynen M. (2003). Clinical assessment and surgical implications of anatomic challenges in the anterior mandible. *Clinical Implant Dentistry and Related Research* **5**(4): 219–225.
DOI: <https://doi.org/10.1111/j.1708-8208.2003.tb00204.x>
- Mu noz G., Dias F.J., Weber B., Betancourt P. & Borie E. (2017). Anatomic relationships of mandibular canal: a cone beam CT study. *International Journal of Morphology* **35**(4): 1243–1248.
DOI: <https://doi.org/10.4067/S0717-95022017000401243>
- Neiva R.F., Gapski R. & Wang H.L. (2004). Morphometric analysis of implant related anatomy in caucasian skulls. *Journal of Periodontology* **75**(8): 1061–1067.
DOI: <https://doi.org/10.1902/jop.2004.75.8.1061>
- Okumuş O. & Dumlu A. (2019). Prevalence of bifid mandibular canal according to gender, type and side. *Journal of Dental Sciences* **14**(2): 126–133.
DOI: <https://doi.org/10.1016/j.jds.2019.03.009>
- Pommer B., Tepper G., Gahleitner A., Zechner W. & Watzek G. (2008). New safety margins for chin bone harvesting based on the course of the mandibular incisive canal in CT. *Clinical Oral Implants Research* **19**(12): 1312–1316.
DOI: <https://doi.org/10.1111/j.1600-0501.2008.01590.x>
- Shah N. (2014). Recent advances in imaging technologies in dentistry. *World Journal of Radiology* **6**(10): 794.

- DOI: <https://doi.org/10.4329/wjr.v6.i10.794>
 Srivastava S., Patil R.K., Tripathi A., Khanna V. & Sharna P. (2017). Evaluation of mental foramen in U. P. population- a CBCT study. *Journal of Otolaryngology-ENT Research* **8**(4): 8–11.
 DOI: <https://doi.org/10.15406/joentr.2017.08.00253>
 Sheikhi M., Karbasi Kheir M. & Hekmatian E. (2015). Cone-beam computed tomography evaluation of mental foramen variations: a preliminary study. *Radiology Research and Practice* **2015**: 1–5.
 DOI: <https://doi.org/10.1155/2015/124635>
 Yang X.W., Zhang F.F., Li Y.H., Wei B. & Gong Y. (2017). Characteristics of intrabony nerve canals in mandibular interforaminal region by using cone-beam computed tomography and a recommendation of safe zone for implant and bone harvesting. *Clinical Implant Dentistry and Related Research* **19**(3): 530–538.
 DOI: <https://doi.org/10.1111/cid.12474>

RESEARCH ARTICLE

Traffic Engineering

Increasing the effectiveness of T-junctions with an innovative geometrical and phasing arrangement

NK Jayasooriya^{1*}, HLK Perera² and JMSJ Bandara²

¹ Department of Interdisciplinary Studies, Faculty of Engineering, University of Sri Jayewardenepura, Gangodawila, Nugegoda.

² Department of Civil Engineering, Faculty of Engineering, University of Moratuwa, Katubedda, Moratuwa.

Submitted: 07 September 2020; Revised: 23 September 2021; Accepted: 28 September 2021

Abstract: Improper usage of control mechanisms at intersections would lead to significant delays resulting in road user frustration. The traditional methods of traffic islands or traffic signals would no longer be effective due to the high traffic movements at intersections, heterogeneity of such traffic, and uneven pedestrian movements. To minimize unnecessary delays and improve multi-user satisfaction, there is a need to use advanced traffic management systems but at an increased cost. This research aims to develop an innovative yet cost-effective arrangement to use the existing traffic signals (modified) with a geometric alteration to reduce delays at T-junctions while catering to the high pedestrian demands effectively. The arrangement proposed in this study is twofold. First, the right turns from the minor road is forced to turn left and subsequently, a U-turn is arranged. Secondly, a signal phasing arrangement to manage the revised turning movements effectively and efficiently is introduced. The proposed arrangement was first designed using theoretical means identifying the proper scenarios, and later it was verified using an existing T-junction (case study) with real traffic and geometric data. For verification, VISSIM traffic simulation software was used after proper calibration to simulate local traffic conditions. Sensitivity analysis was also carried out to test for other possible scenarios. The results of the case study confirm that the proposed design for T-junction can reduce the delays at intersections by around 20 %, increasing the efficiency of the intersection.

Keywords: Delay reduction, junction capacity improvement, innovative signal phasing, traffic management, traffic signal design, VISSIM.

INTRODUCTION

Traffic congestion has been a widespread issue in a majority of urban centres at present. Lack of proper management and control of intersections have resulted in various problems creating unnecessary delays and wasting valuable time of road users (Liu & Chang, 2011). Among those, T-junctions of major-minor road intersections at town centres are prone to much delays due to improper usage of traffic control (Yu *et al.*, 2012). The traditional geometric design, signal phasing, and green times given at some signalized intersections need revision to increase the efficiency of the intersection. At present most of the T-Junctions in Sri Lanka are uncontrolled or operated with traffic signals with three or more signal phases. Sometimes, manual control is imposed by the police for controlling the traffic signals during peak hours. One of the main reasons for such deficiencies is that the existing design and phasing arrangement does not possess the optimum condition (Liu & Chang, 2011). Not having regular updates for signal timing is another reason. Besides the optimization of signal design at such intersections, capacity increases at an intersection by means of adding extra lanes [(for the critical lane(s), mostly the right turns)] found to be a very common strategy in the urban environment (El Esawey & Sayed, 2013). However, the issue broadens due to the limited space availability when it comes to widening of

* Corresponding author (nadika@sjp.ac.lk  <https://orcid.org/0000-0003-4341-2198>)



This article is published under the Creative Commons CC-BY-ND License (<http://creativecommons.org/licenses/by-nd/4.0/>). This license permits use, distribution and reproduction, commercial and non-commercial, provided that the original work is properly cited and is not changed in anyway.

intersections at town centres, where space is restricted for road widening.

One of the main challenges faced by traffic engineers when controlling the traffic at T-junctions is the right turns to and from the main road, which creates additional delays to other movements and pedestrian flows (Zhang & Zhang, 1988). To accommodate right turns to and from the major road, two separate signal phases (or time intervals in manual control) should be provided. This restricts the through movement on the main road in the opposing direction to the right turn. In addition, the through movement on the main road needs to be restricted to accommodate pedestrians to cross the main road. These effectively increase the cycle time and hence result in an increase in delays. Restricting right turns may not be a viable solution due to the fact that major disturbance to the public transport those who are making right turns, extra distance imposed on heavy vehicles (this create many other secondary problems) and of course affecting the user desire.

Therefore, this research aims to provide an innovative geometric design and supportive signal phasing arrangement to increase the efficiency of the T-junctions. In order to understand the existing knowledge on innovative intersection designs, especially with signals and phasing layouts, relevant past studies and various secondary data sources are referred to and briefly explained below.

Traffic congestion has been identified as a major issue in most countries (Li *et al.*, 2011), which cannot be eliminated but can be managed through proper implementation of traffic control measures. As a result, various methodologies have been developed and implemented in the past, considering both geometric design (capacity increase) as well as signal design. One of the older methods developed was to use semi-graphical methods to optimize green splits in isolated intersections (Gazis, 1964; Muller, 1970). Increasing the throughput in every approach (Yu *et al.*, 2012) has been the centre of attraction by introducing intersection treatments like lane additions, restrictions of turning movements and grade separations (Yu *et al.*, 2012). These traditional treatments may increase the capacity of the intersection and relieve the traffic congestion but at a high cost. The traffic at downstream intersections may get deteriorated due to the increase of upstream arrivals (Yu *et al.*, 2012). The situation can get worsened with the extended queues at downstream intersections, negatively affecting the upstream intersections also, despite the treatments at upstream intersections (Yu *et al.*, 2012). The above phenomena are heavily observed in urban areas of almost all the countries, irrespective of the developed or

developing countries, and the situation can get worsened with the high traffic volumes, longer cycle lengths and close proximity of intersections (Yu *et al.*, 2012).

In order to solve the congestion issues at intersections, various techniques are proposed, including the conventional and unconventional arterial intersection designs (El Esawey & Sayed, 2013). The literature identifies basic conventional intersection designs and different types of unconventional intersection designs.

Conventional intersection designs can partially or fully prohibit the right turns, especially from minor roads. El Esawey and Sayed (2013) mentioned that the prohibited right could be replaced by a left turn followed by a median “U” Turn. However, the conventional designs alone would require sufficient space at the intersections. Most of the conventional designs have failed at high congestion levels when the geometric designs are not compatible with the traffic signal phasing and timings (Yang *et al.*, 2012). Therefore, providing geometrical differences only can create additional conflicting scenarios at the junctions as well as at the median “U” Turn openings.

In order to reduce the conflicting movements at the intersections, unconventional intersection designs are proposed (Olarde & Kaisar, 2011). Unconventional intersection designs can also be of various types, but the most common ones would be right turn displaced or bypassed lanes and diverging lanes (Olarde & Kaisar, 2011). The main highlight of the unconventional intersection designs is that the minor road traffic volumes are not allowed to cross the intersections (through movements and right turns) (El Esawey & Sayed, 2013). Only the major road through movements are allowed (but right turns for major roads are also prohibited) (El Esawey & Sayed, 2013).

Most unconventional geometrical arrangements would be beneficial when a majority of the light vehicles are present (Hanowski *et al.*, 2007). However, when the heavy vehicles, buses and commercial vehicles are at a considerable component in the traffic mix, the unconventional intersection designs require additional space at the intersection to cater for the higher turning radius of these types of vehicles (Hanowski *et al.*, 2007). As per Hanowski *et al.* (2007), unconventional arrangements can generally fail when land acquisition at the intersection is not possible. This would further increase the congestion levels away from the Junction at median U-turn openings due to the slow turning manoeuvring speeds of the heavy vehicles, including buses (Hanowski *et al.*, 2007).

In addition to this, continuous flow intersections (Intersection clusters where both major directions are coordinated) are also introduced and has become quite popular in the early years of 2000, and could only be used for newly planned cities (Park & Rakha, 2010; Sun *et al.*, 2015). The main reason behind that was the requirement of sufficient lands at and near intersections, which is highly impossible in established cities where the acquisition of the land at the intersection is fairly difficult. Most of the time, the congestion would take place due to the non-availability of sufficient space at the intersections. Therefore, techniques like continuous flow intersections are highly discouraged for already congested intersections.

Therefore, it is really important to come up with solutions that are not only geometric based but also tied up with an appropriate traffic signal phasing arrangement.

Xuan *et al.* (2011) suggested providing mid-block openings with pre-right turns bays, which is controlled by a pre-signal as a mechanism of elimination right turns just at the intersection. Similarly, the authors also carried out a study looking at how effectively an advanced centre median opening can accommodate U-turns, eliminating U-turns at the intersection. The delay reduction due to this arrangement was found to be around 10 % (Jayasooriya *et al.*, 2016).

Making use of unutilized right turn areas have also been researched to make them utilized in allowing vehicles to wait at the spaces provided (Yang *et al.*, 2012). Xi *et al.* (2013) has also analyzed the concepts of right turn waiting areas to be utilized for the improvement of the efficiency of the intersections.

However, all these geometric solutions will require sufficient space just at the intersection in order to obtain the maximum benefit. However, most of the intersections which are over-saturated currently do not have the possibility to acquire more space just at the intersection. Wu and Yang (2013) has developed a model to solve the above issues using RFID detector data for the estimation of the real-time queue. This model addresses the issues with the traditional input-output based method, and the model has been validated using real-time practical scenarios (Wu & Yang, 2013). Further to these, several important models such as 'RHODES real-time traffic-adaptive signal control system' (Mirchandani & Head, 2001), RT-TRACS Real-time adaptive Control System

(Gartner *et al.*, 2001) are also developed which use real-time traffic flow data as input data to solve a particular traffic problem. Another modern way of controlling the real-time signals is to use multi-modal high-resolution data (Muralidharan *et al.*, 2016) in the management of intersections.

However, these advanced methods also require plenty of additional space and significant technological advancements, which are not possible or affordable for most congested intersections, especially in developing countries.

MATERIALS AND METHODS

In most congested intersections, it is not possible to provide any of the solutions discussed above due to the limited space available. Therefore, it is required to come up with innovative mechanisms such as a limited number of signal phases to increase the efficiency of the intersection management.

However, prohibiting the right turns, which cause the major issues at an intersection, will not be a wise decision from the perspective of road users when considering the convenience. The new system should be able to cater to all the demands at the intersection and should be able to reduce the overall delays. The research methodology focuses on developing different scenarios to capture the effects due to different arrangements. Therefore, the following methodology is proposed.

Step 1: convert right turns from minor roads at an intersection to left turns, followed by a U-turn at a given specific location

Step 2: re-design the signal phasing with two phases accommodating additional left and U-turns with pedestrians allowed to cross the main road only from the right-hand side of the minor road

Converting all right turns to left turns would certainly reduce the delay at an intersection, but the additional U-turns may add delay to users. However, there will be a delay reduction due to the reduced number of phases, but again additional green times given to make left and U-turns may increase the delay. Therefore, this proposed solution need a thorough investigation before application. Thus, we propose the following mechanism to test the viability of this proposed solution.

Development of the scenarios

In order to establish the theoretical background, the existing situation is compared with the following three main scenarios (Figures 1-3)

Scenario 1: Signalized intersection with no separate right-turn lanes (one lane for each leg)

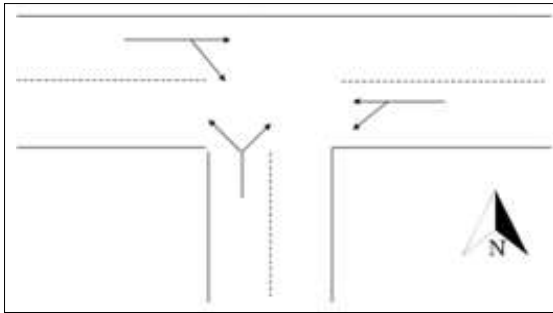


Figure 1: Lane arrangement for Scenario 1

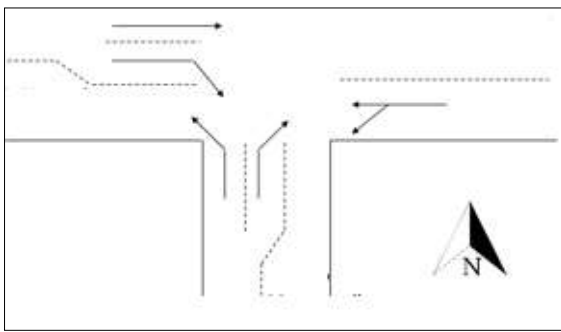


Figure 2: Lane arrangement for Scenario 2

Scenario 1 focuses on a situation where the traffic signals are introduced to an intersection, with a single lane is used in all directions, without any separate turning lanes.

Scenario 2: Signalized intersection with separate right-turn lanes

Scenario 2 focuses on providing separate turning lanes for major road right turns and minor road right turns.

Scenario 3: New Phasing arrangement for the proposed development

Scenario 3 focuses on eliminating the right turns from a minor road and replacing them with a left turn followed up by a U-turn at the centre median. A separate loon is to be provided when the space available for 'U'turn manoeuvring is not sufficient, especially when large vehicles are present.

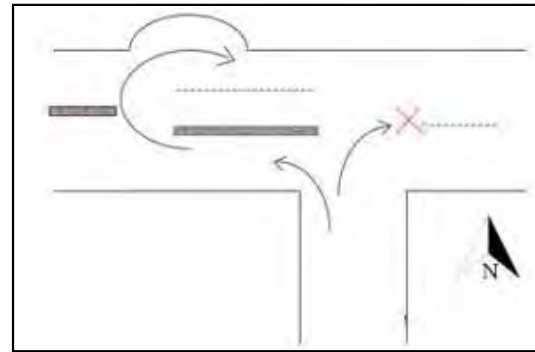


Figure 3: Lane arrangement for Scenario 3

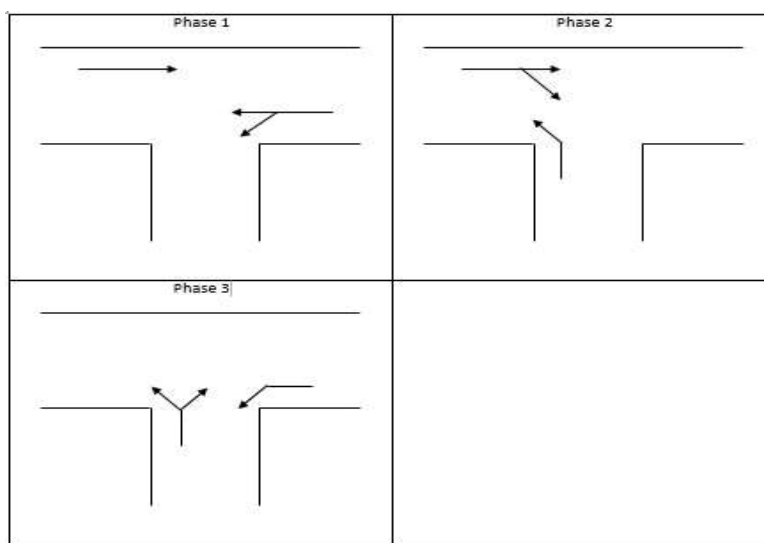


Figure 4: Basic three-phase arrangement at a signalized "T" Junction

Phasing arrangement for the scenarios

The basic arrangement of the three-phase systems at a signalized intersection is shown in Figure 4. This phasing arrangement is used in Scenario 1 and Scenario 2, where the difference is the availability of separate right turns lanes.

The arrangement of the new phasing system is proposed to be used in Scenario 3. The main intention is to eliminate the impact created by right turns from a minor road at an intersection. However, as discussed previously, complete prohibition of right turns will not solve the problems,

and thus it is required to provide an alternative for the restricted right turns while reducing the impact.

For this purpose, a left turn followed up by a 'U' turn at a separate opening of the centre median is proposed (Figure 3).

The main highlight of this arrangement is the elimination of the right turns from minor roads, and the provision of a left turn followed up by a 'U' turn at the centre median of the main road.

The respective phasing arrangement for the new system is shown in Figure 5.

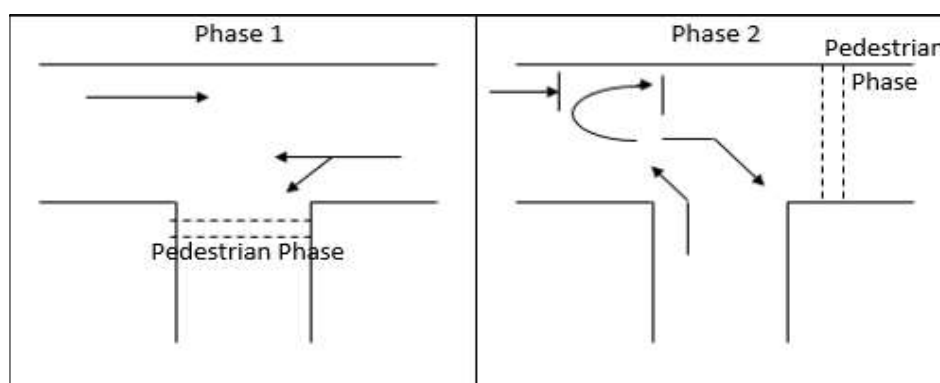


Figure 5: New phasing arrangement

The phasing for right turns from the minor road is prohibited at junctions, which is the main consideration of this phasing arrangement when compared to the base scenario. The traffic would be handled by a basic two-phase arrangement. Pedestrians would be facilitated along a minor road in phase 1 and the main road in phase 2 (Figure 5). However, depending on the volume of pedestrians, the timing for the pedestrians can be adjusted, and the lead/lag green phase for pedestrians can also be provided within the given phase timings. Since phase 1 caters for the major road with high vehicular volumes, the timings provided for phase 1 would generally be high when compared to phase 2. Therefore, pedestrians would have sufficient time for identification of the gaps with respect to the left-turning vehicles. On the other hand, there will not be an issue for the pedestrians in phase 2 since there is no conflicting vehicle traffic.

Phase 1 of the new phasing system would be similar to Phase 1 of the traditional base scenario, which would

allow only the through and left turns on the main road for both directions. The right turns from the west direction will get themselves stored on the right turning lane.

Phase 2 would facilitate the main road right turns to the minor road along with the left turns from the minor road. The through movement from the main road would be stopped upstream of the U-turn opening, allowing the vehicles wanting to turn right from a minor road, to get themselves stored at the space, created due to advance stopping of through traffic after taking the U-turns at the centre median in the same phase. After a certain time, Phase 1 would re-start as usual, and the new system would continue throughout.

Since there can be situations when the roads are narrow, and the proper turning radius is not available. In such situations, when the turning radius at the centre median opening is not sufficient, a loon should be provided along with the U-turn opening (Figure 6) so that

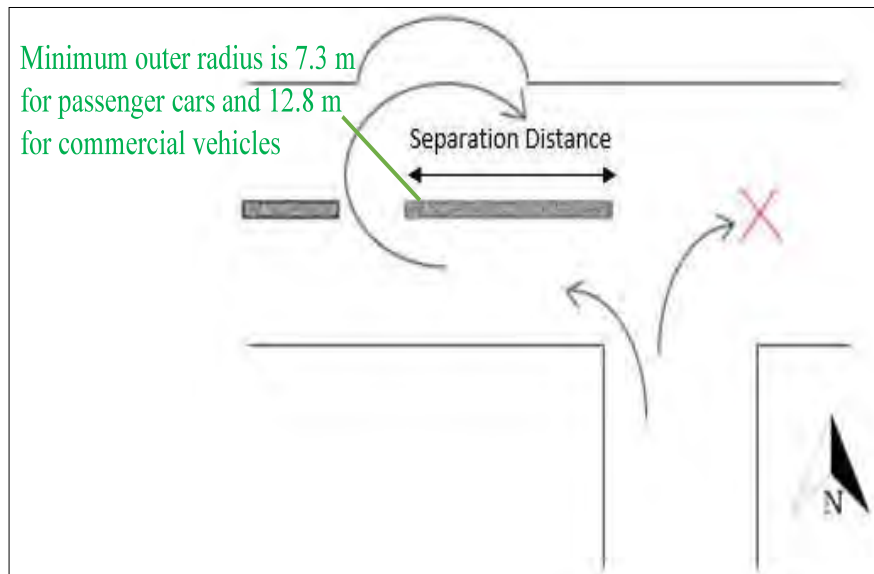


Figure 6: Separate opening with the loons provided

the minimum outer turning radius of 7.3 m for passenger cars and 12.8 m for commercial vehicles are satisfied (CCDP, 2018), so that turning vehicles can make their turns smoothly.

This new phasing and geometrical arrangement would reduce the three-phase signal arrangement to synchronized two phases and would thus reduce the delays at the intersection.

Simulation-based analysis

For verification purposes, VISSIM traffic microsimulation software was used. Since the simulation software has to be calibrated for the local condition, which experiences heterogeneous traffic, non-lane behaviour, different vehicle mix, the calibration parameters provided by the authors' previous work (Jayasooriya *et al.*, 2018) were used. The calibration has been done considering the queue length and travel time as calibration parameters.

For analysis purposes, a case study was conducted. The calibrated software was first utilized to model the existing situation and then to model the three scenarios developed in Section 3A. The micro traffic simulations

using VISSIM software was performed for a total time period of one and half hours. The first half an hour has been utilized as the warm-up period, and the following one hour was used for obtaining indicators for evaluation. Since the objective is to increase the efficiency of the intersection by minimizing the delays, the mean delay per vehicle was considered as the key performance indicator of the Junction.

Case study

Kochchikade-Madampalle Junction was selected as a case study. This intersection has three approaches, as shown in Figure 7 and Figure 8.

Currently, the intersection is uncontrolled, and it is proposed to introduce traffic signals to control the intersection. The current existing pedestrian crossing can be moved to the east side of the Junction across the main road when modelling the other scenarios. The existing pedestrian crossing is expected to be moved further east after the Junction, as per the bus stop locations proposed. Moving the pedestrian crossing to the east side of the Junction would also facilitate the smooth functioning of the traffic signal system and the proposed schemes.

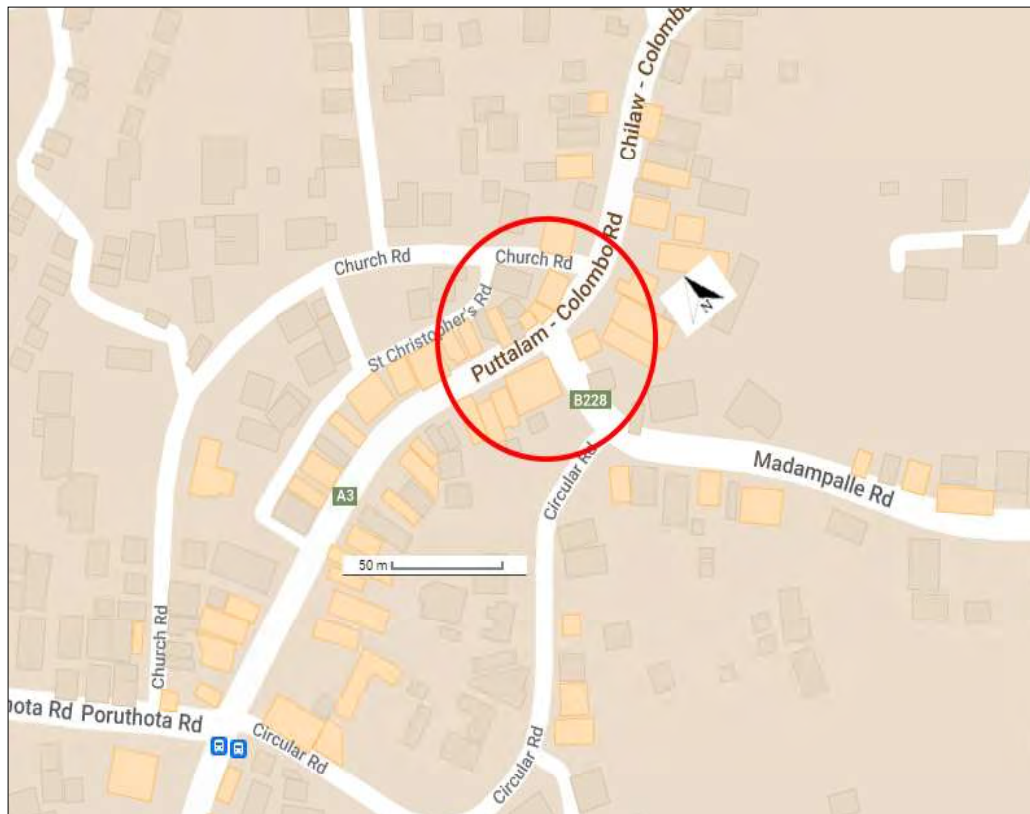


Figure 7: Kochchikade-Madampalle Junction



Figure 8: Kochchikade-Madampalle Junction Geometry

A traffic survey was carried out to obtain the existing traffic condition at the intersection on a usual day. Traffic flow volumes observed in the morning peak hour from 7 am to 8 am are depicted in Figure 9.

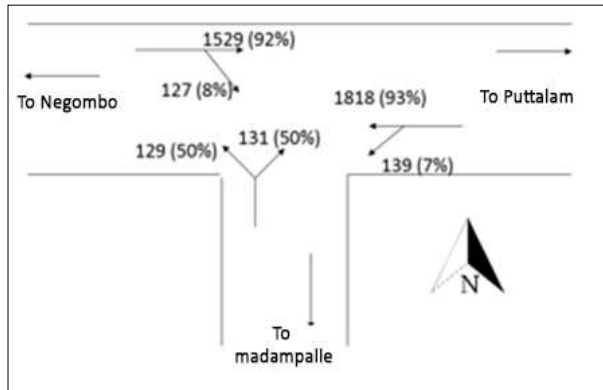


Figure 9: Existing traffic volumes observed at the morning peak hour (in PCU)

In order to have a good understanding of the present condition, the calibrated VISSIM microsimulation software was used to model the existing condition of the Junction. The existing scenario, based on the traffic flows mentioned in Figure 10, generates a mean vehicle delay of 78 s/veh.

Scenario 1: Signalized intersection with no separate right-turn lanes

As for Scenario 1, a basic three-phase arrangement is proposed using Webster's Method (1958) with the following phasing and timings (Table 1), as per the guidelines developed by authors' previous work carried out on limiting the cycle time to a maximum of 90 to 120 seconds (Jayasooriya & Bandara, 2019).

The phasing arrangement of Figure 4 is used for Scenario 1 with the following timings (Table 1). The calculated timings of phase 3 have to be increased to facilitate pedestrian movements.

Table 1: Timings used for Scenario 1

Phase	Timing
Phase 1	32 s
Phase 2	42 s
Phase 3	16 s
Total cycle time	90 s

The simulation using VISSIM traffic microsimulation software for a period of one hour has generated the mean vehicle delay of 72 s/veh for Scenario 1.

Scenario 2: Signalized intersection with separate right-turn lanes

With the introduction of right-turn lanes for the main road and the by road, the following phasing arrangement and timings were observed.

The phasing arrangement of Figure 4 is used for Scenario 2 also with the following timings (Table 2)

Table 2: Timings used for Scenario 2

Phase	Timing
Phase 1	58 s
Phase 2	16 s
Phase 3	16 s
Total cycle time	90 s

In both situations, the cycle times calculated were very high due to the heavy flows encountered at the intersection. As per the location-specific details and traffic level and also for proper comparison purposes, cycle time is kept as the 90 s as per the guidelines proposed in the previous work of the authors (Jayasooriya & Bandara, 2019).

VISSIM traffic microsimulation of Scenario 2 has estimated the mean vehicle delay as 42. Compared to Scenario 1, the mean vehicle delay estimated in Scenario 2 was found to be significantly reduced, which was simply due to the provision of separate right turning lanes.

Scenario 3: New Phasing System with the modified geometrical arrangement

As for the new phasing arrangement, the simulation was conducted keeping the same base case scenario but with a modified phasing arrangement and geometrical modification depicted in Figure 10. The number of phases is reduced to two phases, and subsequently, the total cycle time was reduced to the 70 s.

For easy understanding, phase 1 is structured into two sub-phases, as shown in Figure 11.

The signal timings obtained for Scenario 3 are as follows (Table 3)

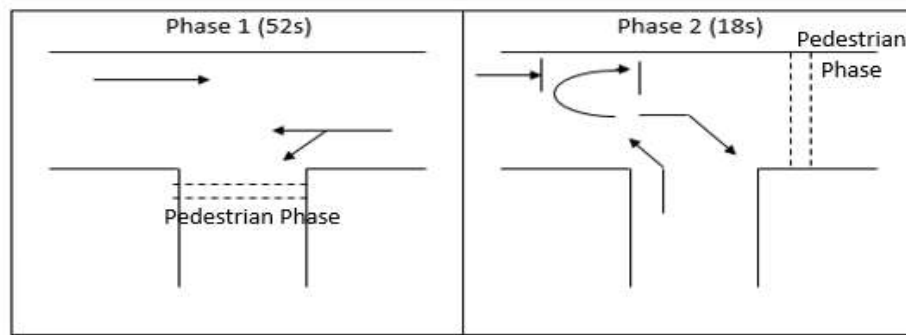


Figure 10: Phasing and timing for Scenario 3

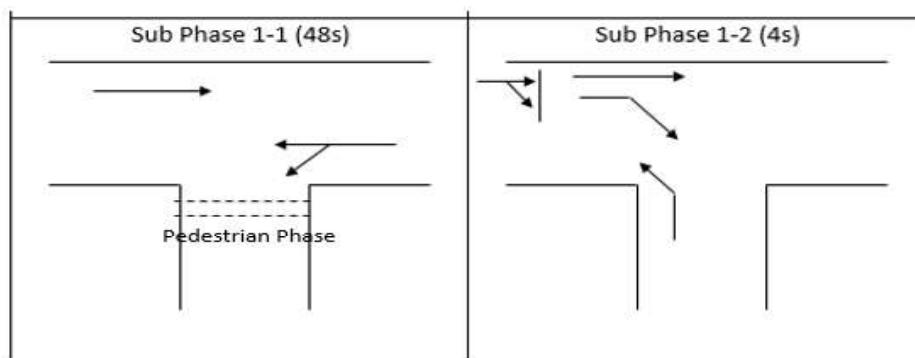


Figure 11: Sub phases of phase 1

Table 3: Signal timings for Scenario 3

Phase	Timing
Phase 1	52 s
Phase 2	18 s
Total cycle time	70 s

In this arrangement, the pedestrian phases are also provided across Madampalle Road in Phase 1 and also across Main Road towards Puttalam side in Phase 2 (Figure 5 and Figure 10).

Out of the two pedestrian phases provided, the critical phase for pedestrians' movement would be phase 2 (Figure 5 and Figure 10) due to two reasons. One is that the pedestrian demand will usually be high across the main road, and the second reason is that the

provided timing to cater for main road pedestrians will be comparatively low, which is only 18 s, opposed to 52 s across the minor road. However, since there is no conflicting movement from vehicles for pedestrians, the delays for vehicles due to pedestrians will not occur. Therefore, only the adequacy of timing for pedestrians to safely cross the road is checked as indicated in Table 4, subject to the following assumptions.

- The average walking speed of a pedestrian is 1.2 m/s
- The total width of the road for crossing is 11 m
- Cycle time is the 70 s (Table 3)
- Start-up delay (ϵ) for pedestrians to enter the crossing is taken as 7 seconds for critical situations.

As per the analysis using the pedestrian data for the considered time period, the provided timing of 18 seconds is found to be satisfactory (required timing is only 16 seconds).

Table 4: Pedestrian flow and analysis

Time	Pedestrian demand (per hour)			Total ped. per hour	No. of cycles per hour	Ped. per cycle	Required time to cross (s)	Total time required	Total time provided
	North to South	South to North	Total						
7.00 – 7.15	32	8	40	174	51	3.38	9.2	16.2	18.0
7.15 – 7.30	32	10	42						
7.30 – 7.45	34	11	45						
7.45 – 8.00	20	18	38						

However, when it comes to Phase 1, the situation would be different, where the pedestrians will have to cross in between the vehicles. Therefore, as per the data collected for the pedestrians, the disturbances that could occur for vehicles due to the provided pedestrian crossing has to be incorporated in the analysis in the considered simulation for Phase 1 (It is not required to consider the adequacy of timing for pedestrians for this phase, since the timing provided for phase 1 would be 52 seconds, which is more than adequate for pedestrians to cross).

Satisfying the requirements, the simulations were performed for the new phasing system, and the estimated mean vehicle delay was found as 34. When compared with the two previous scenarios, through the introduction of the new phasing arrangement, the delay per vehicle has been reduced from 42 s/veh to 34 s/veh, which is a 19 % reduction of delay times.

To make sure that the analysis is applicable for all the scenarios with respect to pedestrian changes, the number of pedestrians catering in phase 1 was doubled, and the simulation was performed again. As per the analysis, the total vehicle delay was increased by only 1 s/veh, where the total delay was observed as 35 s/veh, which is still a 17 % reduction when compared with the previous scenarios.

Sensitivity analysis: changing minor road turning movements

In the case study considered, the right turn and left turn percentage from the minor road is observed as 50 % each. However, this may not be the case when various other T junctions are considered, and therefore, a few more highly likely situations (scenarios) were created (as described below) so that the concept is applicable elsewhere also. The scenarios are analyzed using the VISSIM microsimulation model, and results from the VISSIM model is presented in Table 5.

Scenario 3.1. Right turns from minor road 70 % and left turns from minor road 30 %

Scenario 3.2. Right turns from minor road 60 % and left turns from minor road 40 %

Scenario 3.3. Right turns from minor road 40 % and left turns from minor road 60 %

Scenario 3.4. Right turns from minor road 30 % and left turns from minor road 70 %

Table 5: Results of Scenario 3.1 & Scenario 3.2

Considered scenario	Mean vehicle delay (seconds/vehicle)
Scenario 3.1 (70 % right and 30 % left)	41 s
Scenario 3.2 (60 % right and 40 % left)	37 s
Scenario 3.3 (40 % right and 60 % left)	31 s
Scenario 3.4 (30 % right and 70 % left)	30 s

The Values obtained through the sensitivity analysis in all the scenarios are anyway lower than the values obtained through Scenario 1 (72 s/veh) and Scenario 2 (42 s/veh). However, as expected, the mean vehicle delays are increasing with the presence of right turns from the minor road is increasing.

Sensitivity analysis: changing major road right turning movements

Another sensitivity analysis is conducted, changing the major road right turning movements to capture the possible variations of the off-peak peak scenarios and also to check the validity of the proposed method in varying traffic demands.

Taking the current scenario as the base scenario (8% right-turning vehicles), four more additional scenarios were considered, changing the main road right-turning percentages to 5 %, 10 %, 15 % and 20 %. The same simulation analysis is conducted (keeping other parameters the same), and the mean vehicle delays

Table 6: Results for Scenarios - changing major road right turning movements

Scenario	Main road right turning percentage	Delay (seconds/veh)	Maximum queue length (m)	Proposed maximum separation distance to U-turn opening (m)
Scenario 4 (Current)	8 %	34 s	12.35	13 m
4.1	5 %	32 s	7.43	8 m
4.2	10 %	36 s	14.87	15 m
4.3	15 %	39 s	22.30	23 m
4.4	20 %	41 s	29.73	30 m

per vehicle is obtained. Further to this, the maximum queue length that is generated due to the right turning movements of the main road is obtained from the simulations. The results are indicated in Table 6.

It is proposed to provide the storage space equivalent to the expected maximum queue length for more efficient management of the entire system. This is considered as the maximum separation distance. Increasing the

separation distance more than the required amounts can create unnecessary delays due to the proposed arrangements due to high all-red times and additional time required to cross the intersection.

RESULTS AND DISCUSSION

The summary of the results obtained through the scenarios conducted above is mentioned in Table 6.

Table 6: Summary of the results for scenarios

Scenario	Mean vehicle delay (seconds/vehicle)	Storage space required (separation distance to the centre median opening)
Exiting Situation	78 s/veh	Not Applicable
Scenario 1	72 s/veh	
Scenario 2	42 s/veh	
Scenario 3	34 s/veh	
Scenario 3.1	41 s/veh	
Scenario 3.2	37 s/veh	
Scenario 3.3	31 s/veh	
Scenario 3.4	30 s/veh	
Scenario 4	34 s/veh	13 m
Scenario 4.1	32 s/veh	8 m
Scenario 4.2	36 s/veh	15 m
Scenario 4.3	39 s/veh	23 m
Scenario 4.4	41 s/veh	30 m

As per the results obtained for the existing situation, delays at the intersection is very high, which is around 78 s/veh, whereas the accepted delay per vehicle at an intersection according to Highway Capacity Manual is 35 s/veh. However, when compared with the existing situation, Scenario 1 reduces delay by only 6 seconds/vehicle. The main reason is that even in the existing situation and Scenario 1, no proper geometrical improvement has been introduced to the intersection. This clearly indicates that the said benefits of traffic signals cannot be harnessed if no proper geometrical improvements can be carried out.

This is further verified when considering Scenario 2, where the delays are considerably reduced to 42 s/veh with the introduction of right turn bays for the intersection. However, the introduction of right turn bays comes at a cost. If the land use surrounding the intersection does not permit such an improvement, the option is not viable. Therefore, the decision should consider the existing land uses, such as buildings adjacent to the major and minor roads.

In Scenario 3, the mean vehicle delay is further reduced to 34 s/veh due to the proposed innovative phasing arrangement as well as the geometric changes introduced. The additional savings obtained through the proposed phasing arrangement, when compared with the existing situation, is considerable. When analyzing the above results, the delay saving applicable per vehicle is around 44 s/veh (The difference between the existing scenario (78 s/veh) and the proposed scenario (34 s/veh). The daily traffic at this intersection is estimated to be 53,000 vehicles based on the traffic flow counts available. When considering average occupancy of around 2.5 persons/vehicle, the expected savings can be around Rs.130 million over a year (USD 0.65 million) if the value of travel time is considered as Rs. 220 /hour/person (Jayasooriya *et al.*, 2019). This is a considerable amount of saving. However, this improvement also needs some land to be acquired (to provide a loon), not at the Junction, but a little away from it (as per the guidelines provided). Therefore, one-time expenditure needs to be set off against the opportunity cost savings.

In addition to this, the sensitivity analysis conducted by varying the main road right-turning percentage also provides a good indication of the success and applicability of the proposed method. It also provides a clear indication of the separation distance that should be provided for the centre median opening for the “U”, which can be considered as the storage space.

The overall results clearly indicate that the new phasing arrangement would reduce the delays at intersections even when the turning movements are varied. When the minor road right-turning percentage is higher than left turns, the situation becomes more critical than when left turns are higher, justifying that right turns from the minor road is the critical movement

However, in order to have a successful operation of the proposed phasing arrangement, it is important to have a sufficient turning radius for the vehicles making U-turns at the centre medians. Especially when buses and heavy vehicles are turning right at the intersection and replacing that movement with a left turn and U-turn at the centre median has to be carefully looked into. This can create additional issues when the required turning radius is not available.

When the turning radius is not available for the U-turns, it is required to provide loons to facilitate the vehicle manoeuvring. However, the additional land required to provide a loon will be very minimal compared to land required for a lane addition at the intersection, and also, the land for a loon is taken away from the intersection, which further reduces the negative impact.

CONCLUSION

In order to manage the increasing traffic congestion and delays at intersections, given the limitations of space available as well as land acquisition, it is required to introduce a novel solution when the situation cannot be easily controlled by conventional phasing arrangements or simply applying many other traffic management options.

As a result, this research was focused on replacing the minor road right turns at three-leg signalized junctions, with a left turn followed up by “U” turn at the centre median opening. When the required turning radius is not available, a loon area is provided to facilitate smooth manoeuvring.

First, the research approach focussed on the development of theoretical background and new phasing arrangement. Secondly, it was verified using a traffic simulation conducted at a 3-leg junction at Kochchikade using calibrated VISSIM simulation software.

The results show a comparison among the existing situation and a conventional three-phase signalized system with the new phasing arrangement proposed,

which reduces the three phases to two phases. The proposed system has reduced the delays at an intersection by 44 s/veh, which is a delay reduction of around 56 % when compared with the existing non signalized situation.

The sensitivity analysis conducted at the intersection varying the turning movements from the by road and also from the main road also showed that the new phasing arrangement would be desirable for most of the traffic flow conditions, but high benefits can be obtained when the right turning percentages are less.

Limitations and further research areas

In terms of further research areas, the researchers can focus on other types of arrangements of the same concept, such as replacing the major road right turns with a through turn followed up by a U-turn downstream. Further, the same concept can also be applied at the four-leg junctions to reduce the conventional four-phase system to either a three-phase or two-phase system, which will, in return, reduce the vehicle delays.

Acknowledgement

The authors would like to appreciate the financial support provided by the National Research Council (NRC) of Sri Lanka.

REFERENCES

- CCDP (2018). *City of Colombo Development Plan*. Urban Development Authority, Sri Lanka.
- El Esawey M. & Sayed T. (2013). Analysis of unconventional arterial intersection designs (UAIDs): state-of-the-art methodologies and future research directions. *Transportmetrica A: Transport Science* **9**: 860–895. DOI: <https://doi.org/10.1080/18128602.2012.672344>
- Gartner N.H., Pooran F.J. & Andrews C.M. (2001). Implementation of the OPAC adaptive control strategy in a traffic signal network, in: ITSC 2001. *Proceedings of 2001 IEEE Intelligent Transportation Systems*. 25–29 August. ITSC, Oakland, USA, pp. 195–200. DOI: <https://doi.org/10.1109/ITSC.2001.948655>
- Gazis D.C. (1964). Optimum control of a system of oversaturated intersections. *Operations Research* **12**: 815–831. DOI: <https://doi.org/10.1287/opre.12.6.815>
- Hanowski R.J., Hickman J.S., Wierwille W.W. & Keisler A. (2007). A descriptive analysis of light vehicle–heavy vehicle interactions using in situ driving data. *Accident Analysis and Prevention* **39**: 169–179. DOI: <https://doi.org/10.1016/j.aap.2006.06.016>
- Jayasooriya Nadika, H.L.K. Perera & J.M.S.J. Bandara (2016). Assessing the suitability of providing separate openings for turns at signalized intersections. *Annual Sessions of IESL 2016*, October 2016. The Institute of Engineers, Colombo, Sri Lanka.
- Jayasooriya N. & Bandara S. (2018). Calibrating and validating VISSIM microscopic simulation software for the context of Sri Lanka. *Proceedings of 2018 Moratuwa Engineering Research Conference (MERCon)*. 30 May–1 June 2018. Moratuwa, Sri Lanka, pp. 494–499. DOI: <https://doi.org/10.1109/MERCon.2018.8421918>
- Jayasooriya N. & Bandara S. (2019). Improving the efficiency of an intersection through traffic signal phasing arrangement when no separate right turn lanes available. *Proceedings of 2019 Moratuwa Engineering Research Conference (MERCon)*. 3–5 July 2019. Moratuwa, Sri Lanka, pp. 521–526. DOI: <https://doi.org/10.1109/MERCon.2019.8818769>
- Jayasooriya N.K., Perera H.L.K., Pasindu H.R. & Bandara J.M.S.J. (2019). Developing a reliable estimate for value of time for transportation projects. *Advances in Transportation Studies* **48**.
- Liu Y. & Chang G.-L. (2011). An arterial signal optimization model for intersections experiencing queue spillback and lane blockage. *Transportation Research Part C: Emerging Technologies* **19**: 130–144. DOI: <https://doi.org/10.1016/j.trc.2010.04.005>
- Li Y., Guo X., Yang J., Liu Y. & He S. (2011). Mechanism analysis and implementation framework for traffic signal control of over-saturated intersection group. *Journal of Transportation Systems Engineering and Information Technology* **11**: 28–34. DOI: [https://doi.org/10.1016/S1570-6672\(10\)60130-4](https://doi.org/10.1016/S1570-6672(10)60130-4)
- Mirchandani P. & Head L. (2001). A real-time traffic signal control system: architecture, algorithms, and analysis. *Transportation Research Part C: Emerging Technologies* **9**: 415–432. DOI: [https://doi.org/10.1016/S0968-090X\(00\)00047-4](https://doi.org/10.1016/S0968-090X(00)00047-4)
- Mueller E.A. (1970). Aspects of the history of traffic signals. *IEEE Transactions on Vehicular Technology* **19**: 6–17. DOI: <https://doi.org/10.1109/T-VT.1970.23426>
- Muralidharan A., Coogan S., Flores C. & Varaiya P. (2016). Management of intersections with multi-modal high-resolution data. *Transportation Research Part C: Emerging Technologies* **68**: 101–112. DOI: <https://doi.org/10.1016/j.trc.2016.02.017>
- Olarte C.L. & Kaiser E.I. (2011). Operational performance comparison between three unconventional intersection designs: left-turn bypass, diverging flow and displaced left-turn. *Proceedings of 9th Latin American and Caribbean Conference*. 3–5 August. Medellin, Colombia.
- Park S. & Rakha H. (2010). Continuous flow intersections: a safety and environmental perspective. *Proceedings of the 13th International IEEE Conference on Intelligent Transportation Systems*, pp. 85–90.
- Sun W., Wu X., Wang Y. & Yu, G. (2015). A continuous-flow-intersection-lite design and traffic control for oversaturated bottleneck intersections. *Transportation Research Part C: Emerging Technologies* **56**: 18–33. DOI: <https://doi.org/10.1016/j.trc.2015.03.011>

- Webster F.V. (1958). *Traffic Signal Settings*. Department of Scientific and Industrial Research, London, UK.
- Wu A., Qi L. & Yang X. (2013). Mechanism analysis and optimization of signalized intersection coordinated control under oversaturated status. *procedia - social and behavioral sciences, intelligent and integrated sustainable multimodal transportation systems. Proceedings from the 13th COTA International Conference of Transportation Professionals (CICTP2013)* **96**: 1433–1442.
DOI: <https://doi.org/10.1016/j.sbspro.2013.08.163>
- Xi X., Zhao Cheng H., WenBo S., ZhanQiu C., JunFeng G. (2013). Traffic impact analysis of urban intersections with comprehensive waiting area on urban intersection based on PARAMICS. *Procedia - Social and Behavioral Sciences* **96**: 1910–1920.
DOI: <https://doi.org/10.1016/j.sbspro.2013.08.216>
- Xuan Y., Daganzo C.F. & Cassidy M.J. (2011). Increasing the capacity of signalized intersections with separate left-turn phases. *Transportation Research Part B: Methodological* **45**: 769–781.
DOI: <https://doi.org/10.1016/j.trb.2011.02.009>
- Xuan Y., Gayah V.V., Cassidy M.J. & Daganzo C.F. (2012). Presignal used to increase bus- and car-carrying capacity at intersections: theory and experiment. *Transportation Research Record* **2315**: 191–196.
DOI: <https://doi.org/10.3141/2315-20>
- Yang Z., Liu P., Chen Y. & Yu H. (2012). Can left-turn waiting areas improve the capacity of left-turn lanes at signalized intersections. *Journal of Transport Engineering* **139**(11).
- Yu X., Suljoadikusumo & G. Prevedouros P. (2012). Analysis of downstream queues on upstream capacity expansion of urban signalized intersection. *Journal of Transportation Systems Engineering and Information Technology* **12**: 98–108.
DOI: [https://doi.org/10.1016/S1570-6672\(11\)60206-7](https://doi.org/10.1016/S1570-6672(11)60206-7)
- Zhang X.Y. & Zhang S.S. (1988). Conflicts and delay studies at unsignalized intersections In: *Intersections Without Traffic Signals* (ed.W.Brilon), pp. 236–247. Springer, Berlin, Germany.

RESEARCH ARTICLE

Phenology

Vegetative and reproductive phenology of *Cinnamomum verum* J. Presl grown in intermediate climatic zone of Sri Lanka

K.A.S. Hansika^{1*}, K.A.S. Kodikara¹, A.A. Wijeweera², G. Senanayake³ and L.P. Jayatissa¹

¹Department of Botany, Faculty of Science, University of Ruhuna, Matara.

²National Cinnamon Research and Training Center, Palolpitiya, Thihagoda.

³Department of Agricultural Biology, Faculty of Agriculture, University of Ruhuna, Mapalana, Kamburupitiya.

Submitted: 20 October 2020 ; Revised: 06 October 2021; Accepted: 24 September 21

Abstract: Efficient harvesting of cinnamon while maximizing the yield is highly dependent on its phenology. Many important studies on Ceylon cinnamon have been undertaken, though in-depth studies on vegetative and reproductive phenology of *Cinnamomum verum* are limited. Therefore, this study investigated the vegetative and reproductive phenology of *C. verum*, giving particular emphasis on the major phenological phases such as leaf flushing, flowering, and fruiting. The investigation was carried out from January 2018 to March 2019 to cover a complete annual phenological cycle at the Thihagoda site, in the intermediate climatic zone of Sri Lanka. The results indicate that the leaf emergence of *C. verum* in Sri Lanka takes place in flushes which appeared to be controlled by two factors, the seasonality and the rainfall after a dry period. The seasonal flushing took place in the four months period from February to May. The leaf longevity of *C. verum* in Sri Lanka is longer than 15 months. The leaf fall was not continuous and limited to a five -month period from March to July with a peak in March. The flowering in *C. verum* took place during October and November, however only 18.6 ± 5.6 % of flower buds matured to flowers. Moreover, 94.1 ± 8.5 % of flowers developed into young fruits. The timing of these phenological traits is important to manage the cinnamon productivity as it is recognized that the peeling ability of *C. verum* depends on the cambial activity which is controlled by source-sink relationships in assimilate partitioning in *C. verum*.

Keywords: Annual cycle, *Cinnamomum verum*, peelability, phenology.

INTRODUCTION

Cinnamon or true cinnamon, *i.e.*, *Cinnamomum verum* is one of the important economic crops in Sri Lanka. It provides export earnings of nearly 31,000 million rupees annually (Department of Export Agriculture, 2018). Accordingly, cinnamon is at the top among the minor export crops of Sri Lanka, in terms of export earnings. Among the cinnamon cultivating countries, Sri Lanka is the world's largest true cinnamon producer and it is mainly used as a spice or food additive (Pushpitha, 2006). In addition to the condiment and flavoring value, cinnamon is being used as a herbal medicine due to its antioxidant, anti-inflammatory, and anti-diabetic properties (Wiert, 2002; Rao & Gan, 2014). Moreover it provides various chemicals such as cinnamaldehydes, alkaloids, eugenol, proanthocyanidin, flavonoid, and terpenoid for pharmaceutical and perfume industries (Wiert, 2002). *C. verum* belongs to family Lauraceae and the genus *Cinnamomum* consists of about 250 species of evergreen trees and shrubs, distributed in Asia and Australia (Rani *et al.*, 2017). There are eight *Cinnamomum* species recorded in Sri Lanka (*i.e.*, *C. dubium* Nees, *C. citriodorum* Thw., *C. capparum coronde* Blume, *C. litseaefolium* Thw., *C. ovalifolium* Weight, *C. rivulorum* Kostermans, *C. sinharajaense* Kostermans and *C. verum* J. Presl) and all of them

* Corresponding author (hshashini.w@gmail.com  <https://orcid.org/0000-0002-3187-7804>)



This article is published under the Creative Commons CC-BY-ND License (<http://creativecommons.org/licenses/by-nd/4.0/>). This license permits use, distribution and reproduction, commercial and non-commercial, provided that the original work is properly cited and is not changed in anyway.

grow naturally in the wild. However, *C. verum* is the only species domesticated and cultivated commercially in Sri Lanka. Cinnamon produced from *C. verum* is exported to the world market as true cinnamon (or Ceylon cinnamon). *C. verum* is cultivated in about 30,000 ha in Sri Lanka and it is mainly distributed in part of the wet zone including Galle, Kalutara, Kandy, Matale, Rathnapura, Nuwara Eliya, Kegalle and in the intermediate zone including Matara, Badulla, and Monaragala (Figure 1). There is another cinnamon species, i.e., *Cinnamomum cassia* Blume (Cassia cinnamon), grown commercially in China, Indonesia, and Vietnam (Thomas & Kuruvilla, 2012); they produce more than 82.5% of the world supply of cinnamon (Ravindran *et al.*, 2004). However, Ceylon cinnamon is considered superior to Cassia cinnamon and the superiority is mainly due to the better taste and lower content of the toxic compound, Coumarin (Ravindran *et al.*, 2004). Mainly, five important items are produced from the cinnamon plant namely, quills, featherings, chips, bark oil and leaf oil in Sri Lanka. Quills are the major product of export, which accounts for 90% among the other cinnamon products (Pushpitha, 2006). As the leading producer, Sri Lanka provides around 90% of the true cinnamon supply in the world, while the Seychelles, India and Madagascar produce the rest (Ravindran *et al.*, 2004).

Some studies on *C. verum* covering taxonomic features (Abeyasinghe & Scharaschkin, 2019), genetic relationship among the species and varieties (Abeyasinghe *et al.*, 2014), eco-physiological aspects and chemical composition with special attention to essential oils (Wijesinghe *et al.*, 2004; Saumyasiri *et al.*, 2006), soil fertility and plant nutrition management (Samaraweera *et al.*, 2013), insect pest management and plant protection (Jayasinghe *et al.*, 2006), agronomy (Abeykoon, 1998), crop improvement and varietal development (Wijesinghe & Pathirana, 1998), cinnamon characterization, phylogenetics and special variations in the quality of products (Wijesinghe *et al.*, 2008) etc. have been carried out in Sri Lanka during the past. However, there are no publications on the phenology of *C. verum* in Sri Lanka even though knowledge on vegetative and reproductive phenology is important in managing the productivity of cinnamon cultivations. Particularly, cinnamon cultivators in Sri Lanka face a problem in harvesting their crops (or getting the bark extracted) as the peelability (i.e., easiness of removing the bark from the stem) varies from time to time. This variation interrupts harvesting of *C. verum* throughout the year and the peelability variation seems to be governed by many factors such as edaphic and/or climatic factors. Publications on reproductive

or vegetative phenology of cinnamon in relation to peelability variations are scanty. Thus, it is important to conduct phenological research for cinnamon to boost the cinnamon industry in Sri Lanka.

Phenology is the timing of plant and animal life cycle activities parallel to the seasonality (Leith, 1974). Phenological studies involve observation, recording, and interpretation of the timing of life history events of plants (Fenner, 1998) and such studies are important to understand the species interactions and community functions. Furthermore, phenological models can be used to assess the impact of climate change on the functioning and productivity of different ecosystems (Kramer *et al.*, 2000). Phenological events of the plants which are, regulated both by biotic and abiotic factors are important to avoid competition for pollination by either attracting or dispersing pollinators.

Understanding of such behavior of the communities is useful in developing a proper management strategy. Information on phenology is essentially useful in predicting the interactions of plants and animals to the changing environment (Bhat *et al.*, 2001). Furthermore plant phenology plays a major role in the pest-plant relationship. Host plant selection and host shifts of certain plants depend on the plant phenology (How *et al.*, 1993). For the timing of management practices in certain crops (Ansquer *et al.*, 2009) and to assess the effect of climate change on plants (Post & Stenseth, 1999), the study of phenology is of great importance. Also phenological studies allow efficient crop management and harvesting, thereby maximizing the yield.

Therefore, this study aimed to explore the vegetative and reproductive phenological variations of *C. verum* in Sri Lanka. Accordingly, the following research questions were addressed: a) What are the patterns/trends of vegetative and reproductive phenology of *C. verum*? b) What factor/s may govern the phenology of *C. verum*?

MATERIALS AND METHODS

Study area

Out of the total extent of *Cinnamomum verum* planted in Sri Lanka, only 10 % is distributed in the dry zone. Even though the percentage coverage in the wet zone (62 %) is the highest (Punyawardene, 2008), the distinction between dry and wet seasons is not much pronounced in the wet zone as the rainfall is distributed throughout the year. On the other hand, some phenological variations

should be measured at very short intervals, with all the measurements taken by the same person to reduce the personal errors. Thus, the intermediate zone was selected to conduct phenological observations and cinnamon plantations in the premises of the Cinnamon Research Institute at Thihagoda ($6^{\circ} 03' \text{ N}$, $80^{\circ} 56' \text{ E}$) were selected for the study (Figure 1). Meteorological data (rainfall and air temperature) from Matara were obtained as it is the meteorological station closest to the study site. The total annual rainfall of Thihagoda area was 1239.9 mm and the mean annual temperature was $26.9 \pm 0.35^{\circ}\text{C}$ during the study period. The studies were carried out from January 2018 to March 2019.

Study design

The total coverage of the cinnamon plantation under the Cinnamon Research Institute is about 16 ha and the plantation has been established covering a set of small hillocks and flat lands (between hillocks). The elevation of the area is 22.3 m.a.s.l. Therefore, plants for the phenological study were selected to represent the three geomorphological settings; valleys between hillocks, slopes of hillocks, and tops of hillocks. Accordingly, altogether 12 plants, each with a diameter larger than 2.5 cm, were selected randomly to include four plants for each of the geomorphological settings. Cinnamon

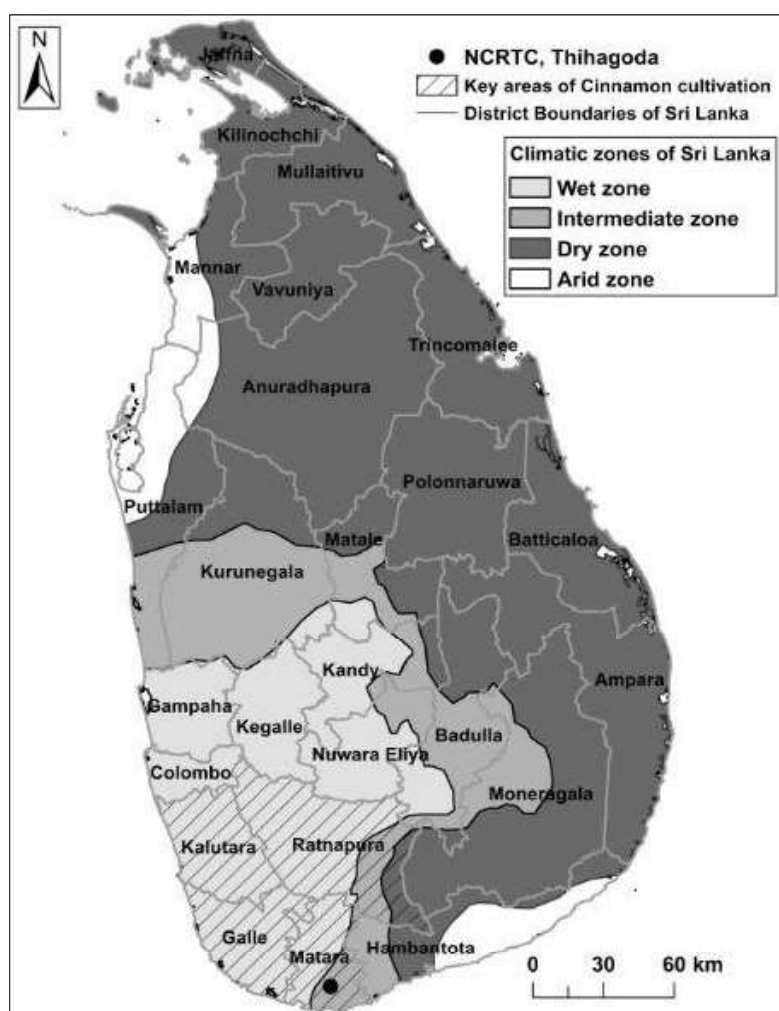


Figure 1: The map of Sri Lanka showing the major climatic zones, the cinnamon cultivated areas of the country and the study site at the premises of Cinnamon Research Institute (Source: Punyawardene, 2008)

plants with a Diameter ≥ 2.5 cm were used for the phenological measurement as the individuals of the same size are selected for harvesting in the cinnamon industry.

Phenological observations

The phenological observations were taken on the following pheno-phases such as, (1) leaf emergence/initiation and maturation, (2) initiation of floral buds and flowering, (3) fruiting, and (4) leaf and fruit shedding, for a period of 15 months starting from January of 2018. Three branches at three different heights of each plant (in total, 36 branches) in all locations were marked and used for the phenological observations.

These selected shoots were tagged by using numbered plastic strips which were looped around the stem of 'study branches' keeping five leaves and a bud above the tag (hereafter the term 'study branch' is used in this research to designate such twigs with five leaves, and their progressive growth including new leaves and new branches produced).

Vegetative phenology

Those study branches were used to monitor the emergence of new leaves, their growth and leaf fall. Five leaves above the tag in the study branches were numbered consecutively on the adaxial surface with a xylene free permanent marker. Those study branches were checked once a week for the emergence of new leaves. Any young leaves above the numbered leaves on these shoots were treated as newly emerged leaves and were labeled in the same way giving consecutive numbers. The total number of leaves in each shoot was counted at each visit over the monitoring period. The emergence of any lateral shoot, producing new branches above the tag was considered together in counting of the leaves in each branch. Loss of a senescent leaf from the selected branches was considered as a leaf fall.

The growth rates of leaves were measured at three different times/seasons, *i.e.*, budding period, developing stage, and mature stage, during the study period by starting from a newly emerged leaf bud. The maximum length of the leaf blade, of the selected leaves were recorded from the day of the first observation until its fall. Growth measurements were taken daily at the young stage, but the measuring frequency gradually decreased up to once a week with the maturity of the leaves.

Reproductive phenology

Emergence of new flower buds, and their development until blooming, fruit set, and their development until the fruit drop were studied. Newly emerged flower buds in study branches were monitored during the study period continuously for their progress. The increase in the size of flower buds were measured once a week or more frequently until the flowers were open. The same shoots used to monitor the progress of flower buds were carefully observed from the open flower to the fruit set, and then until the ripened fruits were shed. The sizes of the fruits were measured once a week or more frequently as necessary, in order to record the exact timing of fruit drop. The total number of flower buds, flowers, and fruits on the study branches were counted once a week. The above measurements were started initially with a higher number of replicates, as a precautionary measure to compensate for any damage caused by the pests, including monkeys. Replicates damaged by pests were discarded and a minimum of three undamaged replicates were used in the data analyses.

Statistical analysis

Leaf length and fruit length were considered continuous variables while number of leaves per branch, number of flower buds per branch, number of flowers per branch,

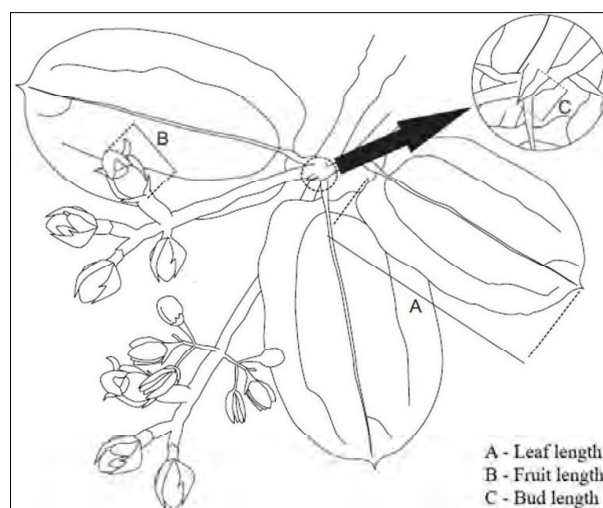


Figure 2: The measurements of leaf length, fruit length and bud length measured in the phenological study.

and number of fruits per branch were treated as count data. Descriptive analysis was performed to calculate the mean, variance and standard error. Prior to all the analyses, Shapiro-Wilk's and Levene's tests were used to examine the data for normality and homogeneity of variance, respectively. The Pearson correlation test was performed to check the correlation between rainfall and the variable, number of leaves (leaf- emergence). Generalized Linear Model (GLM) with Poisson distribution was carried out to check the significance difference of the number of flower buds and number of fruits in the dry season and rainy season. One-way ANOVA was performed to check the significance of leaf length and fruit length in

the aforementioned two seasons. All the analyses were conducted by using the R-3.2.2 statistical programme.

RESULTS AND DISCUSSION

Climatic conditions of the study site

The mean (SE) monthly rainfall of the study area was 94.04 ± 20.69 mm and the rainfall in the months of February, March, April, July, August, September, November, and December were lower than that of the mean value, while it was higher than the monthly mean rainfall in the other months, *i.e.*, January, May, June, and October (Figure 3).

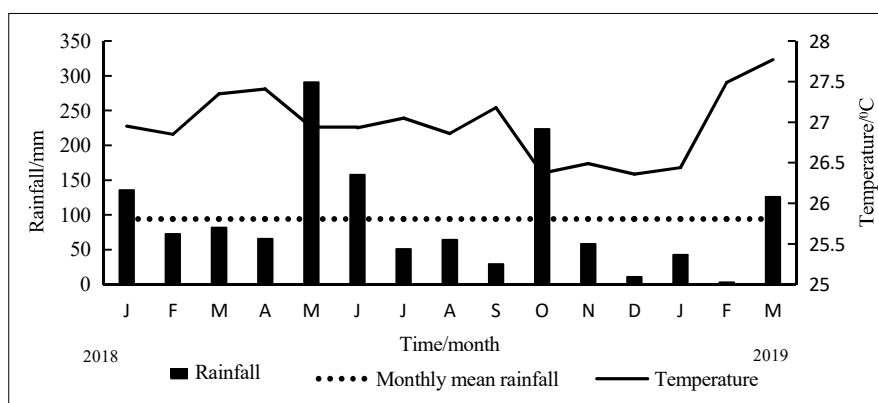


Figure 3: Variation of the mean monthly rainfall and temperature of the study area (2018-2019), 12.5 km from the study site (Source: Meteorological Station, Matara)

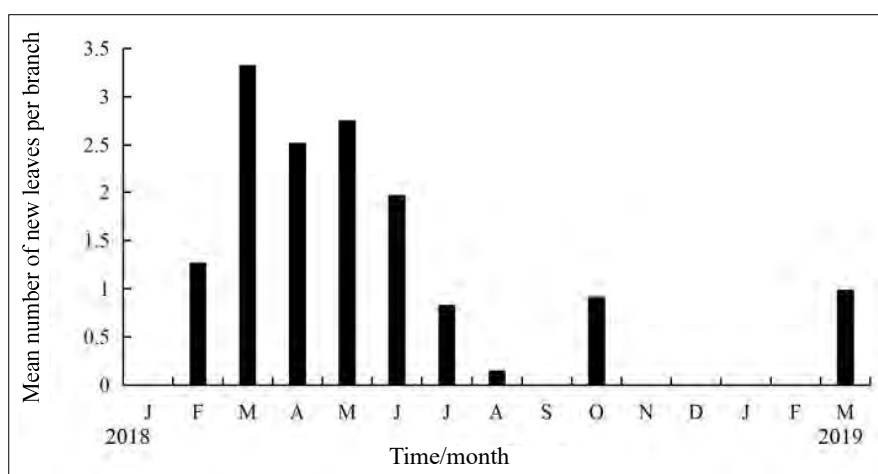


Figure 4: Variations in the mean number of new leaves per branch of *Cinnamomum verum* over 15 month-period (January 2018 to March 2019)

Vegetative phenology

Emergence of new leaves and leaf growth

The leaf emergence of *C. verum* showed a multimodal pattern in which leaf emergence was apparent during the months of February to June (Figure 4). However, the leaf emergence scenario displayed mixed- multimodal pattern. The highest and second highest values of leaf emergence were observed in March and May of 2018, respectively. Hence the four-month period (February to May) can be considered as the period of leaf flushing. Considerably higher leaf emergences were observed in February, July, and October 2018 and March 2019.

The leaf emergence in all the other months was zero or negligible.

A leaf started from a leaf bud/primordium and it was observed that a leaf primordium took mean duration of 29.0 ± 8.5 days to become an opened leaf. Leaves were opened and then grew slowly increasing their size, reaching to their maximum mean (\pm SD) length of 63.7 ± 4.0 mm, in a mean duration of 57 ± 16 days. Afterwards, the leaf remained a long period without further increase in size. None of the leaves that emerged at the beginning of the study showed any sign of senescence, indicating that the life span of a leaf of *C. verum* is longer than 15 months (Figure 5).

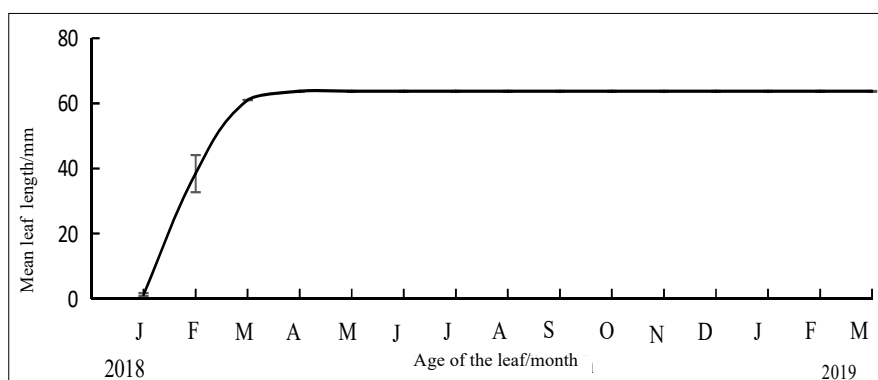


Figure 5: The leaf development of *Cinnamomum verum* in mean leaf length (mm) over 15 months study period (January 2018 to March 2019). Error bars represent standard error of the mean.

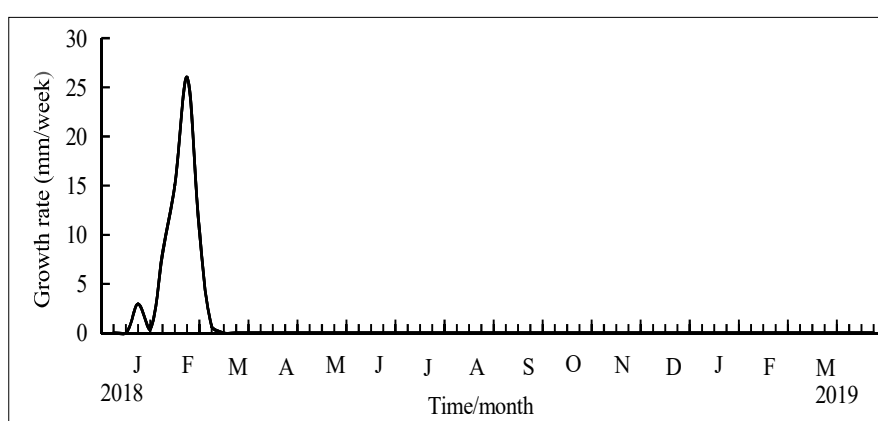


Figure 6: Mean growth rate of the leaf of *Cinnamomum verum* during the study period

The emergence of new leaves of *C. verum* is not all-year round and a sporadic nature in leafing was observed, in addition to the peak in the four-month period from March to June. The above sporadic increases of the leaf emergence were compatible with the high rainfall, but not fully compatible with the peak of leafing from March to June (Figure 3). However, based on the data collected in this study, the mean rate of leaf emergence in *C. verum* was 1.14 ± 0.29 new leaves/branch/month. According to the Pearson correlation, rainfall showed a significant correlation with leaf emergence $r = 0.656$; $df = 13$, $p = 0.00867$) and it explained 65 % of the total correlation.

The mean growth rate of leaves of *C. verum* had two peaks. The first small peak was observed during the first 2 weeks due to the growth of leaf primordia, and the second large peak was observed during the next 5 weeks period due to the growth of the opened leaf (Figure 6).

In an evergreen perennial plant, the emergence of leaves can take place either continuously throughout the year (Munne-Bosch, 2007) or as flushes, *i.e.*, a higher number of leaves produced within few days or few weeks and no leaf emergence during the next few months. The leaf emergence of *C. verum* in Sri Lanka takes place, not on a regular or continuous basis, but in flushes, as evidenced in this study.

Young leaves are reddish in color at the leaf initiation and then turn to dark green at the end, being greenish yellow at the transition of young leaves to mature leaves. The time period between two flushes and the intensity

of the flush appeared to be controlled by two factors: the inherent seasonality and the rainfall after a dry period. In this study, it was revealed that the emergence of leaves started in February, reached to a peak in March and remained at the peak until May and then gradually decreased during the next two months. In addition to this main leaf flush during a six months period, there were two isolated leafing events in October and March of the following year and these two events overlapped with high rainfall.

However, rainfall is very low during the first half of the main leaf flush, *i.e.*, during the three months period from February to April, indicating that the leaf flush during this period is not triggered by the rainfall, but some other factor(s). Therefore, we suggest that this scenario could be linked with an inherent factor such as evolutionary adaptation to the ‘spring,’ that is, from February to April in the northern hemisphere. However, further studies are required to confirm it. The two isolated leaf flushes in October 2018 and March 2019, as well as the second half of the main leaf flush from May to June, 2018, overlapped with rainfall after dry spells. Hence, it can be surmised that the high rainfall after a dry spell also trigger the leaf emergence in *C. verum* in Sri Lanka. Singh and Kushwaha (2005b) have also reported that when there is a severe drought, the plant tends to survive with a long growth constraining dry period, and produces a flush of new leaves in the following rainy season. The availability of enough water for the favorable growth of leaves ensures the emergence of a new flush in the rainy season (Monasterio & Sarmiento, 1976; Falkenmark *et al.*, 1989).

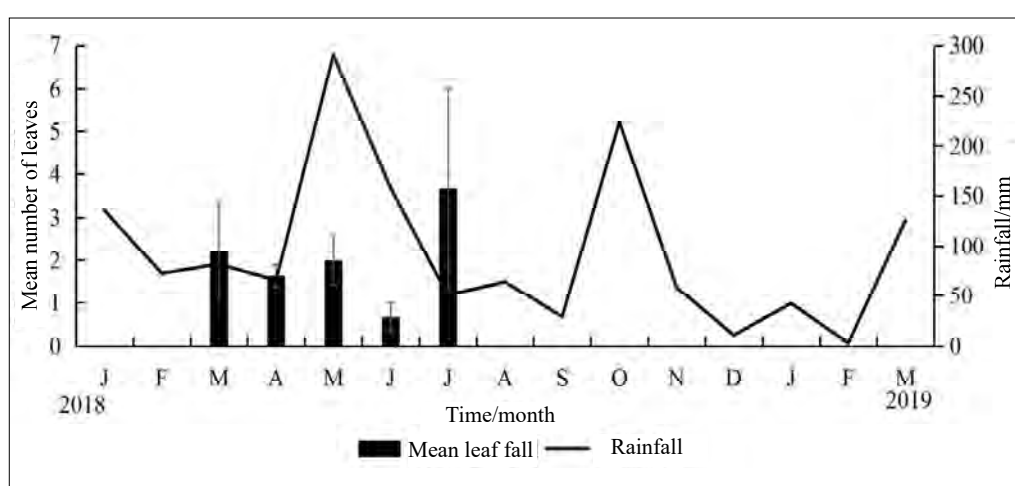


Figure 7: Variations in the mean number of leaf fall of *Cinnamomum verum* over a 15 month-period (January 2018 to March 2019). Error bars represent standard error of the mean.

During the study period, few leaves were fallen in the 5-month period from March to July and at least sporadic leaf fall was not observed during the rest of the 10-month period (Figure 7). The monthly average leaf fall was 0.85 ± 0.71 leaves/branch/month.

None of the newly emerged leaves during the study period of 15 months were fallen and at least had not reached senescence, indicating that the leaf longevity of *C. verum* in Sri Lanka is longer than 15 months. Further studies are required to find out the exact leaf longevity of *C. verum* in Sri Lanka. A longer life span of leaves in any plant further indicates a few other features; the number of leaves produced by such a plant within a specified period is comparatively less and their photosynthetic rate is also low, but it does not decrease rapidly through time (Kikuzawa, 1995). However, the life span of leaves of *C. verum*, may not be very long, because, out of the five leaves which were already there in 'study branches' when the study was commenced, 2.04 ± 1.08 leaves dropped during the study period. Moreover the leaf fall of *C. verum* was not continuous and limited to five-month period from March to July. This indicates that the leaf fall has one major peak of March to July.

Reproductive phenology

Flowering

Floral bud initiation in *C. verum* plants started in the month of September and showed a peak, in October (Figure 8). More precisely it was a single peak and the occurrence of flower buds was limited to a five weeks period, from the 3rd week of September to the 3rd week of October. Flower buds appeared in a panicle and the mean length of a panicle was 167.3 ± 9.5 mm. The mean number of flower buds per panicle was 33.5 ± 10.5 . Flower production commenced in early October and showed a peak at the 3rd week of October, in particular, a single peak at the 41st week. A flower bud took an average of 14 ± 4 days to become an open flower; however only 18.6 ± 5.6 % of the flower buds became open flowers and rest of the flower buds dropped. The flower production of *C. verum* was significantly lower than the bud production ($P < 0.05$). The peak of open flowers was observed in the 3rd week of October showing two week difference between the peaks of flower buds and open flowers. A flower of *C. verum* remained open approximately for 12 hours in the morning.

In this study the flowering in *C. verum* took place during October and November and it is compatible with

other reports in Sri Lanka (Ravindran *et al.*, 2004; Azad *et al.*, 2018). Even though some studies report off season flowering in March and April (Azad *et al.*, 2018), in this study we observed only one flowering event for the whole study period. The time period from the initiation of the flower bud to the open flower is about 14 ± 4 days. However, flowers of all the cinnamon trees do not bloom at the same time. Azad *et al.*, (2018) reported that cinnamon flowers exhibit protogynous dichogamy with two flower types as "Type A" and "Type B" in separate individual plants of which, flowerings during morning and flowerings during evening, respectively creating a temporal barrier for self-pollination. However, most of the flower buds produced within this period has dropped, leaving a smaller percentage of pollinated flowers to be converted to young fruits. This study indicates that only about 18.6 ± 5.6 % of flower buds become flowers. The rest of the flower buds dropped. Such a high percentage of dropping flower buds could be due to higher rainfall in the same season. There are many reports to confirm that high rainfall during flowering season could reduce the number of fruits produced (Davies, 1976). However, almost all the remaining flowers were able to produce young fruits, indicating that pollination has not been a limiting factor. It is reported that cinnamon flowers get pollinated mainly by wind (Ravindran *et al.*, 2004). In this study, only about 25 ± 3 % of the young fruits survived to become mature fruits and it took about six months for a young fruit to mature. This observation is compatible with the study carried out in Sri Lanka (Amador, 2019); GLM results showed that the number of flower buds (initiation of flowering) and the number of fruits (fruit production) were significantly higher in the rainy season as compared to the dry season [$p = 0.0012$; null-deviance: 15.77 (df = 18); $p = 0.0341$; null-deviance: 27.21 (df = 16) respectively]

Fruiting

Smaller fruits of *C. verum* were first observed during mid-October (Figure 9). Fruit production peaked at the end of October, showing a unimodal response (Figure 8). It was observed that only 94.1 ± 8.5 % of flowers developed into young fruits. The mean number of fruits per branch was 7.5 ± 3.6 . However, few or no new fruits were produced after the month of October. In other words, the number of fruits did not show any further increase after 2nd week from the start of the fruit initiation. All fruitlets did not develop to a mature fruit as a considerable number of fruitlets dropped, and out of the young fruits, only 25 ± 3 % got developed into mature fruits. Therefore, the number of fruits was reduced during

the 20 week period from January to March, 2019. The maximum fruit length recorded was 17.0 ± 0.3 mm and it was observed in February, 2019. One-way ANOVA results showed that leaf length and fruit length have significantly increased during the rainy season ($F = 32.2_{1,9}$; $p = 0.0025$; $F = 28.4_{1,8}$; $p = 0.0267$). When the timing of the above flowering, fruiting, and fruit shed are considered, the six month period from September to March can be considered as the reproductive phase of *C. verum* growing in the study area.

The phenological knowledge of a crop plant or 'the knowledge in the timing of recurring vegetative and reproductive events, their interactions to biotic and abiotic forces, and their interrelation of those aspects with other species' (Leith, 1974) can provide important information useful in development of that particular crop. Even though *C. verum* is the most important minor export crop in Sri Lanka, to the best of our knowledge, there is no phenological study conducted on *C. verum* in Sri Lanka. However, there are a few studies which

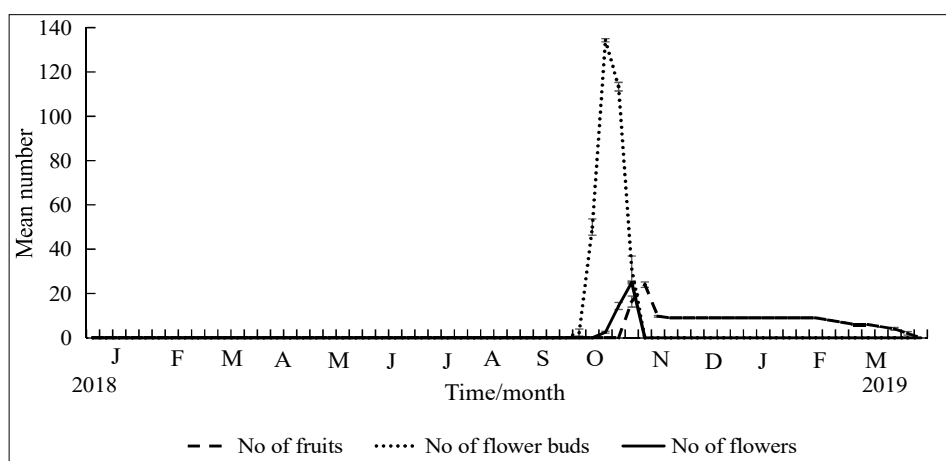


Figure 8: Variations in the mean number of flower buds, mean number of flowers and mean number of fruits of *Cinnamomum verum* per study branch during the 15 month study period (January 2018 to March 2019). Error bars represent standard error of the mean.

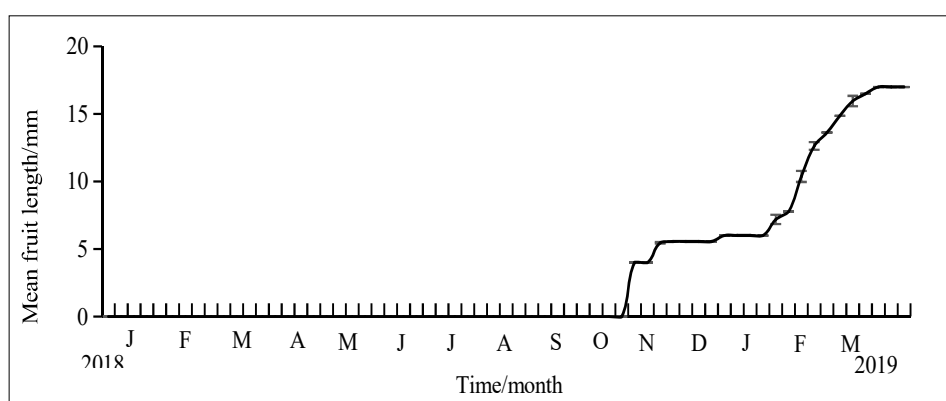


Figure 9: Variations in the mean fruit length (mm) of *Cinnamomum verum* per study branch during the 15 month study period (January 2018 to March 2019). Error bars represent standard error of the mean

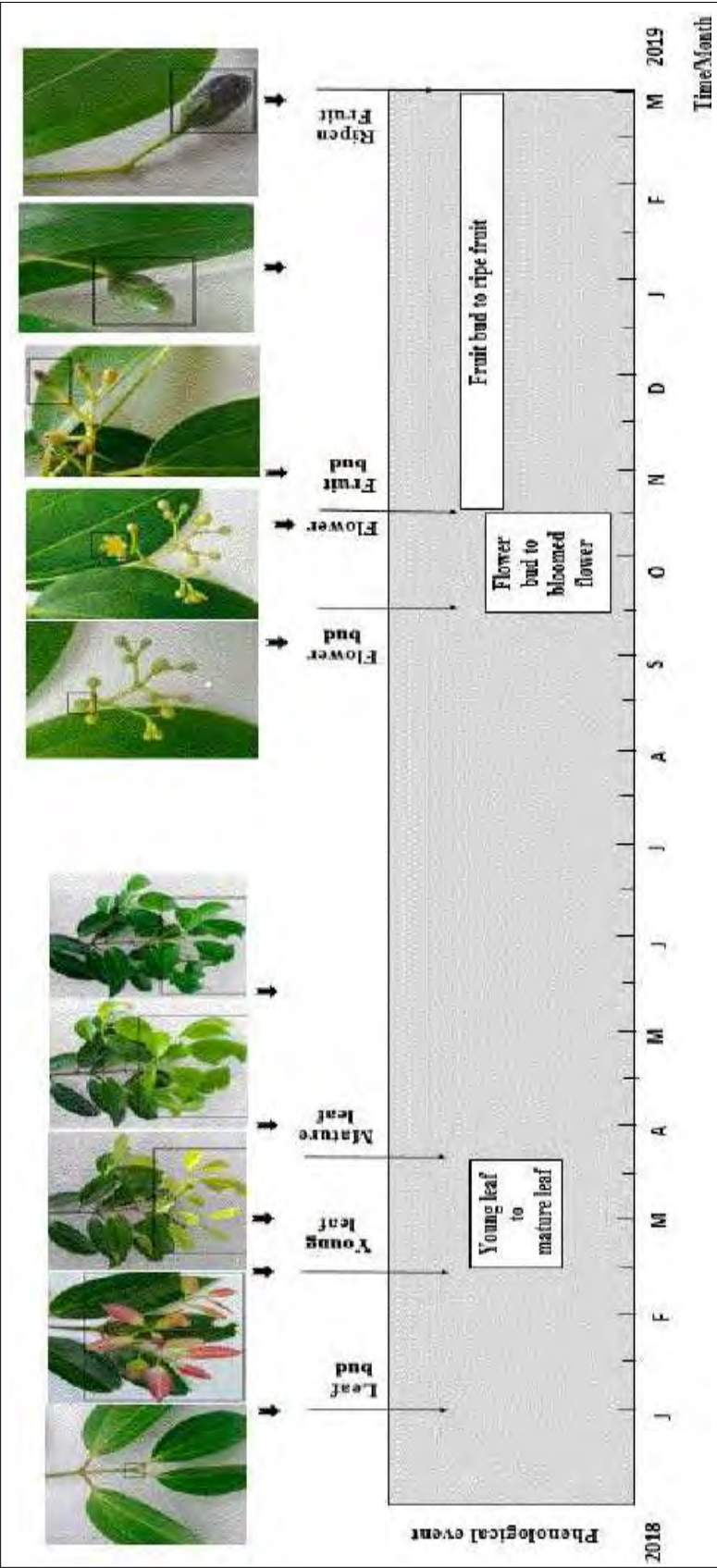


Figure 10: The graphical illustration of vegetative and reproductive phenological events of *Cinnamomum verum* over time. It shows the period of leaf bud formation, then leaf flush development, followed by development of flower buds, flowers, fruits and fruit ripening. Time period taken for each event is indicated by the box in the grey colour area and the image for each event is also given as a visual interpretation

have touched some aspects of the phenology of the same or other species of *Cinnamomum* conducted in other countries (Kasai *et al.*, 2002 ; Singh & Kushwaha, 2005a ; Shivaprasad *et al.*, 2015; Yulistyarini, 2020). Nevertheless, even such information may not be valid for *C. verum* growing in Sri Lanka as these details might represent completely different agro-ecological systems in other countries. As evidence, *C. verum* in Mahé Island, Seychelles, is considered as an aggressive alien invasive species (Fleischmann, 1999), the timing of the vegetative growth of which could be different from the non-aggressive and slow growth of *C. verum* in Sri Lanka.

The above behavior of phenological traits could vary depending on the variations in the agro-climatic region and soil factors etc. (Arntz *et al.*, 1998). However, the behavior of phenological traits of *C. verum* is very important for the cinnamon industry in Sri Lanka, because we assume that the peeling ability of cinnamon positively correlates with the cambium activity. The higher cambial activity may enhance the peeling ability of cinnamon in two ways: firstly increasing the thickness of the cambial region with delicate cells between xylem tissue on the inner side and the phloem tissue. Secondly, an active cambium increases the thickness of the phloem tissue increasing the ability to get it peeled off, with minimum damage. Cambial activity may be greatly affected by variations in assimilate partitioning that could be decided by phenological traits. It is recognized that source-sink relationships in assimilate partitioning change with the developmental stage (Evans, 1991). Accordingly, it can be assumed that allocation of assimilates for the cambial activity may get reduced during the leaf flush, flowering, and fruiting in *C. verum*, reducing the ability to peel. The knowledge of phenology or the timing of recurring vegetative and reproductive events of *C. verum* revealed in this study are of utmost importance to proper timing and management of harvesting of cinnamon in Sri Lanka. Also this will lead to studies on how to manage the seasonal and environmental effect on peelability so that it could be useful to maximize the harvestable yield of *C. verum* in Sri Lanka.

CONCLUSION

Leaf emergence of *C. verum* in Sri Lanka displayed a mixed-multimodal pattern and one that takes place in flushes which appeared to be controlled by two factors, the inherent seasonality and the rainfall after a dry period. The seasonal flushing took place in the four months period from February to May. A leaf primordium took

a mean number of 29.0 ± 8.5 days to become an opened leaf and leaves unfolded and then grew slowly increasing their size, reaching their maximum size in 57 ± 16 days. As evidenced from this study the leaf longevity of *C. verum* in Sri Lanka is longer than 15 months. The leaf fall was not continuous, and limited to a five-month period from March to July, with a peak in March.

Flowering in *C. verum* took place during October and November, however only $18.6 \pm 5.6\%$ of flower buds matured to flowers. Moreover, a mean number of $94.1 \pm 8.5\%$ of flowers developed into young fruits. The average number of fruits per branch was 7.5 ± 3.6 . Fruit production peaked at the end of October, showing a unimodal response. When timing of flowering fruiting and fruit shed are considered, the six month period from September to March can be considered as the reproductive phase of *C. verum* growing in the study area.

Conflict of interest statement

There is no conflict of interest.

Acknowledgement

The authors would like to thank the Staff of the Cinnamon Research Center, Palolpitiya, Thihagoda, Matara for their kind support and Mrs. S.K. Madarasinghe, Ph.D student, University of Ruhuna for map preparation.

REFERENCES

- Abeykoon A.M.D. (1998). Improved agronomic practices of cinnamon. In: Revitalization of cinnamon industry in Sri Lanka; constraints and remedies. *Proceedings of a workshop conducted by SLAAS section B in collaboration with Faculty of Agriculture University of Ruhuna and Department of Export Agriculture*. (eds. R.Senaratne and G.A. Dayatilake), Matara, Sri Lanka, 28-1998. Faculty of Agriculture, University of Ruhuna, Mapalana, Kamburupitiya, Sri Lanka, pp. 47-54
- Abeyasinghe P., Samarajeewa N.Li.G. & Wijesinghe K. (2014). Preliminary investigation for the identification of Sri Lankan *Cinnamomum* species using randomly amplified polymorphic DNA (RAPD) and sequence related amplified polymorphic (SRAP) markers. *Journal of the National Science Foundation of Sri Lanka* **42**(03): 201–208. DOI: <http://doi.org/10.4038/jnsfsr.v42i3.7393>
- Abeyasinghe P.D. & Scharaschkin T. (2019). Taxonomic value of petiole anatomy in the genus *Cinnamomum* (Lauraceae) found in Sri Lanka. *Ruhuna Journal of Science* **10**(1): 1–17. DOI: <http://doi.org/10.4038/rjs.v10i1.47>

- Amador C.K., De Silva A. & Madushani K.P. (2019). Capturing wealth from upstream human resources in Ceylon cinnamon industry. *Proceedings of the 8th International Conference on Management and Economics*, pp. 463 – 476.
- Ansquer P., Al Haj Khaled R., Cruz P., Theau J.P., Therond O. & Duru M. (2009). Characterizing and predicting plant phenology in species-rich grasslands. *Grass and Forage Science* **64**(01): 57–70.
DOI: <https://doi.org/10.1111/j.1365-2494.2008.00670.x>
- Arntz A., DeLucia E. & Jordan N. (1998). Contribution of photosynthetic rate to growth and reproduction in *Amaranthus hybridus*. *Oecologia* **117**: 323–330.
DOI: <https://doi.org/10.1007/s004420050665>
- Azad R., Kumara K.L.W., Senanayake G., Ranawaka R.A.A.K., Pushpakumara D.K.N. & Geekiyanage S. (2018). Flower morphological diversity of cinnamon (*Cinnamomum verum* Presl) in Matara District, Sri Lanka. *Open Agriculture* **3**(01): 236–244.
DOI: <https://doi.org/10.1515/opag-2018-0025>
- Bhat D.M., Murali K.S. & Ravindranath N.H. (2001). Formation and recovery of secondary forests in India: a particular reference to Western Ghats in South India. *Journal of Tropical Forest Science* **13**(04): 601 – 620.
- Davies S.J.J.F. (1976). Studies of the flowering season and fruit production of some arid zone shrubs and trees in Western Australia. *The Journal of Ecology* **64**(02): 665 – 687.
- Department of Export Agriculture (2018). *Annual Performance Report*. Ministry of Primary Industries and Social Empowerment, Sri Lanka.
- Evans A.S. (1991). Whole-plant responses of *Brassica campestris* (Cruciferae) to altered sink-source relations. *American Journal of Botany* **78**(03): 394 – 400.
- Falkenmark M., Lundqvist J. & Widstrand C. (1989). Maro-scale water scarcity requires micro-scale approaches. *Natural Resources Forum* **13**(04): 258 – 267.
DOI: <https://doi.org/10.1111/j.1477-8947.1989.tb00348.x>
- Fenner M. (1998). The phenology of growth and reproduction in plants. *Perspectives in Plant Ecology, Evolution and Systematics* **1**(01): 78 – 91.
DOI: <https://doi.org/10.1078/1433-8319-00053>
- Fleischmann K. (1999). Relations between the invasive *Cinnamomum verum* and the endemic *Phoenicophorium borsigianum* on Mané island, Seychelles. *Applied Vegetation Science* **2**(01): 37 – 46.
DOI: <https://doi.org/10.2307/1478879>
- How S.T., Abrahamson W.G. & Craig T.P. (1993). Role of host plant phenology in host use by *Eurosta solidaginis* (Diptera: Tephritidae) on *Solidago* (Compositae). *Environmental Entomology* **22**(02): 388 – 396.
DOI: <https://doi.org/10.1093/ee/22.2.388>
- Jayasinghe G.G., Gunaratne W., Darshanee H., Griepink F.C., Louwaars N.P. & Stol W. (2006). *Environmentally Sound Insect Control in Cinnamon: A Feasibility Study on the use of Insect Pheromones to Replace Large-scale use of Insecticides*. Report 119. Plant Research International B.V., Wageningen, Netherlands.
- Kasai A., Yano S., Nishida T., Kadono F. & Takafuji A. (2002). Spatial distribution pattern of domatia and seasonal occurrence of the eriophyid mite in relation to the foliation phenology of *Cinnamomum camphora*. *Japanese Journal of Applied Entomology and Zoology* **46**(03): 159–162.
- Kikuzawa K. (1995). The basis for variation in leaf longevity of plants. *Vegetatio* **121**:89–100.
DOI: <https://doi.org/10.1007/BF00044675>
- Kramer K., Leinonen I. & Loustau D. (2000). The importance of phenology for the evaluation of impact of climate change on growth of boreal, temperate and Mediterranean forests ecosystems: An overview. *International Journal of Biometeorology* **44**: 67–75. DOI: <https://doi.org/10.1007/s004840000066>
- Leith H. (1974). Phenology and seasonality modeling. pp. 444. Chapman and Hall, London, UK.
- Monasterio M. & Sarmiento G. (1976). Phenological strategies of plant species in the tropical savanna and the semi-deciduous forest of the Venezuelan Llanos. *Journal of Biogeography* **3**(04): 325 – 355.
- Munne-Bosch S. (2007). Aging in perennials. *Critical Reviews in Plant Sciences* **26**(03): 123 – 138.
DOI: <https://doi.org/10.1080/07352680701402487>
- Post E. & Stenseth N.C. (1999). Climatic variability, plant phenology, and northern ungulates. *Ecology* **80**(04): 1322–1339.
DOI: [https://doi.org/10.1890/0012-9658\(1999\)080\[1322:CVPPAN\]2.0.CO;2](https://doi.org/10.1890/0012-9658(1999)080[1322:CVPPAN]2.0.CO;2)
- Punyawardene B.V.R. (2008). *Shri-lankawe Warshapathanaya ha Krushi-parisarika Kalapa. (Rainfall and Agro-ecological Zones in Sri Lanka)*. Department of Agriculture, Sri Lanka.
- Pushpitha N.P.G. (2006). The design and construction of appropriate cinnamon processing device. *M. Phil thesis*, University of Ruhuna, Sri Lanka.
- Rani A., Pande C., Tewari G. & Patni K. (2017). A Review on aroma profile of cinnamomum species in north and North East India. *World Journal of Pharmaceutical Research* **6**(11): 1–22.
DOI: <https://doi.org/10.20959/wjpr201711-9501>
- Rao P.V. & Gan S.H. (2014). Cinnamon: a multifaceted medicinal plant. *Evidence-Based Complementary and Alternative Medicine* **2014**:1–12.
DOI: <https://doi.org/10.1155/2014/642942>
- Ravindran P.N., Babu K.N. & Shylaja M. (2004). *Cinnamon and Cassia: The genus Cinnamomum*, pp. 80 – 120. CRC Press.
- Samaraweera D.N., Malkanthi M.D., Ekanayake J.S. & Wijayasinghe W.A.D.A.N. (2013). Comparison of soil fertility status of some selected cinnamon (*Cinnamomum zeylanicum* Blume) growing soils in Matara district. *Proceedings of the Symposium of Miner Export Crops* (ed. B. Marambe), 12 – 13 September. Peradeniya, Sri Lanka, pp. 29.
- Saumyasiri M.M.K.G., Yakandawala D.M.D., Samaraweera P. & Wijesinghe K.G.G. (2006). Phylogenetic relationship of

- Cinnamomum* species in Sri Lanka. *Proceedings of the 11th Peradeniya University Research Sessions*, 30 November, pp. 134.
- Shivaprasad D., Prasannakumar C.N., Somashekar R.K. & Nagaraja B.C. (2015). Reproductive biology of *Cinnamomum sulphuratum* Nees. from wet evergreen forest of Western Ghats in Karnataka. *Proceedings of the International Academy of Ecology and Environmental Sciences*, 5, pp. 7–15.
- Singh K.P. & Kushwaha C.P. (2005a). Diversity of Flowering and fruiting phenology of trees in a tropical deciduous forest in India. *Annals of Botany* 97(02): 265–276.
DOI: <https://doi.org/10.1093/aob/mcj028>
- Singh K.P. & Kushwaha C.P. (2005b). Emerging paradigms of tree phenology in dry tropics. *Current Science* 89(06): 964 – 975.
- Thomas J. & Kuruvilla K.M. (2012). *Handbook of Herbs and Spices*, 2nd edition, volume 1 Woodhead Publishing Limited, UK. pp. 182–196,
DOI: <https://doi.org/10.1533/9780857095671.182>
- Wiat C. (2002). *Medicinal Plants of Southeast Asia*. Pelanduk Publications, Petaling Jaya, Selangor, Malaysia.
- Wijesinghe K.G.G. & Pathirana R. (1998). Germplasm screening and varietal development of cinnamon (*Cinnamomum verum* Presl) In: Revitalization of cinnamon industry in Sri Lanka; constraints and remedies. *Proceedings of a workshop conducted by SLAAS section B in collaboration with Faculty of Agriculture University of Ruhuna & Department of Export Agriculture*. (eds. R. Senaratne and G.A. Dayatilake), Matara, Sri Lanka. Faculty of Agriculture, University of Ruhuna, Mapalana, Kamburupitiya, Sri Lanka, pp. 15–16.
- Wijesinghe K.G.G., Samaraweera D.N., Jayasinghe D. & Gunaratna G.G. (2004). Development of cinnamon (*Cinnamomum verum* Presl) selection for higher yields with better quality characteristics. *CARP Competitive Contract Research Grants Programme* (eds. H.P.M. Gunasena, M.P. Dhanapala & T.U. Tillekawardana), pp 3–10. Sri Lanka Council for Agricultural Research Policy, Wijerama Mawatha, Colombo 07.
- Wijesinghe K.G.G., Weerasuriya S.N. & Kumari H.R.S.N. (2008). Growth performances of selected cinnamon cultivars at different locations in Matara, Galle, Kalutara and Rathnapura districts. *Proceedings of the 64th Annual Sessions of the Sri Lanka Association for the Advancement of Science*, part I, pp. 36.
- Yulistyarini T. (2020). Reproductive activity patterns of four species of *Cinnamomum* in Purwodadi Botanic Garden. *IOP Conference Series: Earth and Environmental Science* 456(1): 012055.

RESEARCH ARTICLE

Biomedical Engineering

Novel nebulizer design with adaptive flow regulation

U Dampage* and M Ariyasinghe

Faculty of Engineering, General Sir John Kotelawala Defence University (KDU), Rathmalana.

Submitted: 25 November 2020; Revised: 15 September 2021; Accepted: 21 September 2021

Abstract: Pharmaceutical therapy for certain respiratory diseases involves delivering aerosolized drugs directly to the respiratory tract through inhalation with nebulizers. This research is focused on designing an automated jet nebulizer that possesses the capability of dynamic flow regulation. The proposed nebulizer is composed of two modes, namely, the Compressed Air mode and the Oxygen Therapy mode. The automated triggering from one mode to another will be dependent upon the percentage of oxygen saturation of the patient, monitored from the SpO₂ sensor. The compressed airflow will be delivered to the patient according to his or her volumetric breathing rate, derived with the aid of a temperature sensor-based algorithm. The compressor circuitry is incorporated with a PID control unit, which is a novel feature that acts as feedback as well as a safety mechanism in ensuring that the patient receives compressed air as per the flow rate decided by the system. At the end of the drug delivery, if the liquid level sensor detects the absence of medication within the nebulizer chamber, the nebulization process will be terminated. The results obtained from simulations showed that the PID unit functioned smoothly, with less overshoot and response time. Thus, the dynamic regulation of the motor speed with respect to the volumetric breathing rates was accomplished. A laminar flow was obtained from the outlet of the compressor towards the nebulizer tubing, and a turbulent flow was obtained within the chamber, as expected. No excessive turbulent flows or rotational flow patterns were detected.

Keywords: Inhalation therapy, jet nebulizer, proportional integral derivative controller.

INTRODUCTION

A considerable percentage of people suffer from respiratory diseases such as asthma and chronic obstructive pulmonary disease (COPD). As per WHO statistics, 235 million people are affected with asthma and 64 million people are affected with COPD, while millions of others suffer from other unidentified chronic respiratory diseases (Hubbard, 2006). Jet nebulizers which atomize medication are widely used in aerosolized inhalation therapy for such respiratory diseases.

The nebulizer is a device which functions by converting drugs which are in liquid form into a wet mist, more specifically, aerosols of a size that can be inhaled by the lower respiratory tract, with the aid of a driven compressed gas flow (Hess, 2000 ; Ari, 2014).

Despite the introduction of lightweight and portable devices like metered-dose inhalers and dry powder inhalers, the popularity of nebulizers has not diminished due to their simplicity and their ability to be frequently used in inhalation therapy for infants, small children, and the elderly (Clay, 1987 ; Rau & Hess, 2009). They are considered advantageous because they have the ability to aerosolize several drug solutions and drug mixtures, and can be useful in treating debilitated or distressed

* Corresponding author (dampage@kdu.ac.lk;  <https://orcid.org/0000-0003-0121-8218>)



This article is published under the Creative Commons CC-BY-ND License (<http://creativecommons.org/licenses/by-nd/4.0/>). This license permits use, distribution and reproduction, commercial and non-commercial, provided that the original work is properly cited and is not changed in anyway.

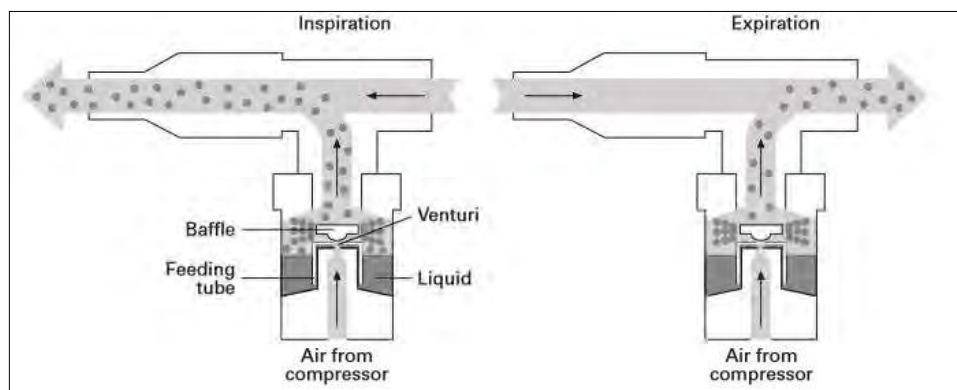


Figure 1: Conventional nebulizer design (O'Callaghan & Barry, 1997)

patients (Rau & Hess, 2009). However, most of the conventional nebulizers (Figure 1) fall short of desired preferences. One of the issues with the current nebulizers is the inadequate amount of aerosolized drugs delivered to the patient. According to several research reports (O'Callaghan & Barry, 1997; Chatburn & McPeck, 2007; Volsko & Chatburn, 2014), conventional nebulizers are considered highly inefficient due to the high wastage of aerosol.

The efficacy and the quality of the aerosol generated by a jet nebulizer are a product of the design of the device and the drug formulation (Bisgaard *et al.*, 2014). It was mentioned that the driving gas flow rate, the ratio of liquid to gas flow, and the characteristics of the compressor have an impact on the size of the droplets produced by a nebulizer (Barry, 1997; Hess, 2000; O'Callaghan & Kendrick *et al.*, 2014; Mittal *et al.*, 2014). In addition to that, controlling the relative humidity within the airflow between the nebulization source and patient can be achieved by simply controlling the flow rates in the system (Haddrell *et al.*, 2014). Furthermore, patient factors such as breathing rate also have an effect on drug delivery. In the case of a continuously operating compressor, a high fraction of the aerosol is lost to the atmosphere through the vent, if the patient doesn't inhale fast enough (Le Brun *et al.*, 2014). Specifically, 50 % of the volume of aerosol generated is wasted during exhalation (O'Callaghan & Barry, 1997). Some consequences of neglecting the importance of delivering the prescribed dosage of the inhaled medication and, applying proper administration techniques using aerosol generators include adverse reactions, bronchospasm, and exposure to high drug concentrations. (Rau & Hess, 2009).

Yardimci (2014) has developed a micro controller based on a jet nebulizer, in which the compressor is controlled using the fuzzy logic system for domiciliary use. However, the inhalation profile, which is an important factor, hasn't been considered when regulating the compressor. Ivanova and Glazova (2015) have conducted research on enhancing the performance of the ultrasonic nebulizer, through the incorporation of an indicator that registers time, duration of an asthma attack, and dosage. The study has been limited to children who are suffering from bronchial asthma.

One of the reasons behind the inability of conventional devices to deliver the entire dosage, as mentioned in the literature, is the fact that the driving gas flow is unidirectional and constant in contrast to the breathing pattern, which is bidirectional and variable. In order to address these issues, the proposed research is specifically focused on the regulation of the dynamic flow of the compressor in sync with the inhalation profile of the patient. The proposed design employed the use of a digital temperature sensor for monitoring the respiration rate during nebulization. How the temperature sensors could be incorporated in detecting respiration rate was studied with the help of the conceptual model described by Gupta and Qudsi (2013). For the purpose of regulating the compressed air flow, the proposed research takes the approach of employing an Arduino-based proportional integral derivative (PID) control system. PID control is one of the most widely used dynamic control techniques in industrial applications (Paz, 2013). It involves the use of a feedback controller, which changes the output based on the sensed or observed result, as shown in Figure 2.

The process variable of a given setpoint is measured by the sensor, which in turn is compared to the setpoint (desired output), in order to determine the error. The error signal is used to determine the controller output, which is delivered to the actuator. The difference between the

process variable and the setpoint is the error (Knospe, 2013). Here the integral time (T_i) and derivative time (T_d) refers to the time constants which are required to acquire the manipulated variable using the integral action and derivative action respectively.

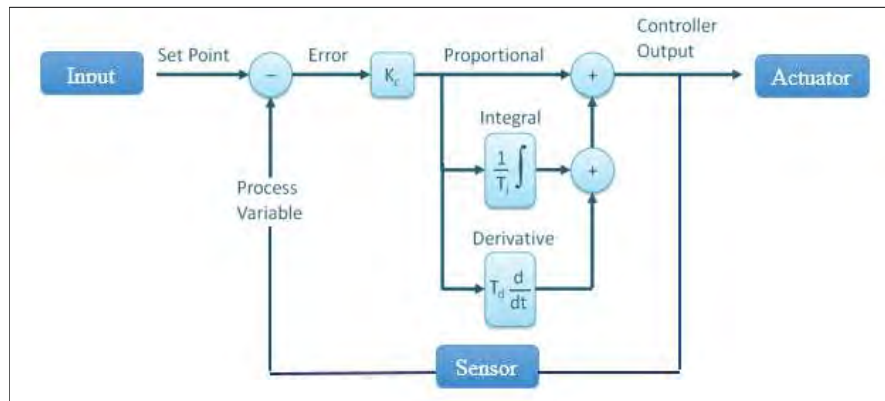


Figure 2: The schematic of a PID controller (Paz, 2013)

The present error is taken into account by the proportional term. The integral response takes all the errors, which are present in the system, from the starting point to a particular point of time in the process. The derivative response is proportional to the rate of change in process variable (Theopaga & Rizal, 2014).

MATERIALS AND METHODS

The approach and information gathering

After conducting market analysis on existing products, and a literature survey, the research problem was identified. Furthermore, information regarding nebulization was gathered during a visit to the National Hospital for Respiratory Diseases, located at Welisara.

The conceptual design and hardware components

The conceptual design (Figure 3) was done in such a way that there are two modes of operation, the compressed air Mode and oxygen therapy mode. The oxygen therapy mode is triggered, depending on the percentage of oxygen saturation of the patient being nebulized (94 % is the threshold). The temperature sensor monitors the temperature difference which occurs during inhalation and exhalation. Hence, the breathing count will be determined, which will be converted to a volumetric

breathing rate. The SpO_2 circuit monitors the percentage of oxygen saturation of the arterial blood. An initial set flow rate will be given to the diaphragm pump through the controlling unit of the nebulizer. The airflow sensor monitors whether the diaphragm pump is operating at that given flow rate. The airflow sensor readings will be taken up by the controlling unit. If there is some error present between the desired flow rate and the sensed flow rate, it will be altered by the PID function through the variation of the voltage fed to the motor controller through pulse width modulation. This process continues only if the oxygen saturation percentage is within the required range. If the oxygen saturation percentage of the arterial blood of the patient decreases below the specified limit, the oxygen therapy mode is triggered. Triggering of the oxygen therapy mode will cause oxygen therapy to be delivered via the opening and closing of the specific solenoid valves which will be done through the controlling unit. The non-contact liquid level sensor monitors the level of the medication in liquid form. Once it detects that no liquid is present within the nebulizer chamber, the process of nebulization will be terminated.

The sensing elements used for nebulizer design include one wire DS18B20 temperature sensor for monitoring the temperature of inhaled air and exhaled air. It has the capability of reading temperatures to a resolution of 0.0625. In addition to that, the YF-S201

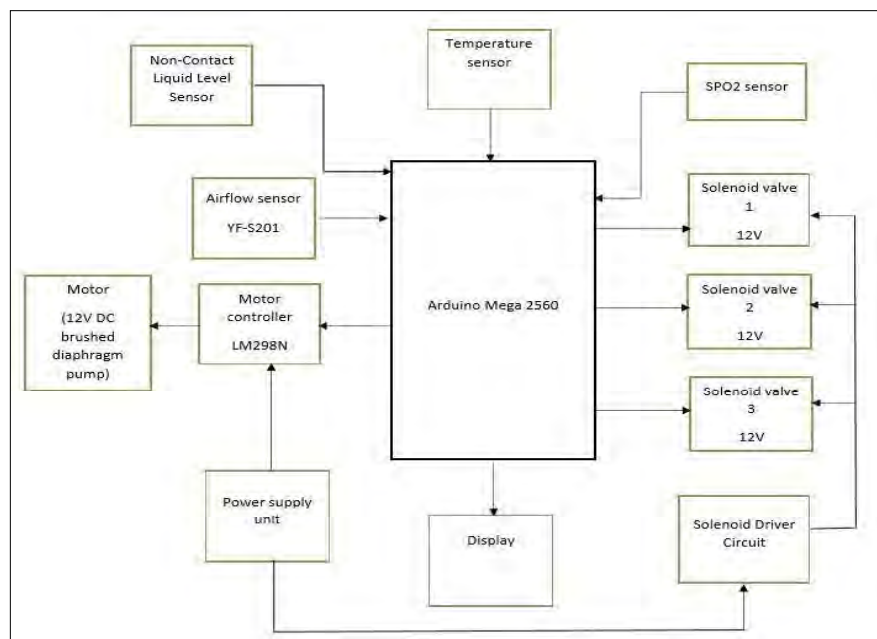


Figure 3: Conceptual design of the proposed nebulizer

airflow sensor was used for monitoring the compressed air flow rate. It consists of an integrated magnetic hall sensor which outputs an electrical pulse with every revolution. A non-contact liquid level sensor was used to achieve non-contact liquid level detection. The actuators used for the proposed nebulizer include a micro diaphragm pump (Figure 4), and an L298N motor controller. The micro diaphragm pump is composed of a DC brushed motor.

The rotational movement of the motor is converted into oscillating movement by an eccentric. It is connected through a connecting rod to the diaphragm, which moves up and down its central point. The elastic diaphragm in conjunction with an inlet and outlet valve generates a pumping action. The particular pump can be mounted in any position and can deliver a flow rate of up to 11 L/min.



Figure 4: DC micro diaphragm pump

The Arduino Mega 2560 microcontroller reads the signals obtained from the relevant sensors, makes logical decisions such as comparing the sensed signals with the desired signals, and finally transmits the necessary PWM signals to the actuators.

Designing the 3D model of the nebulizer

The dimensions were determined by referring to the service manuals of conventional nebulizers and altering those dimensions according to the requirements of the proposed equipment. The 3D model of the design was created with the aid of the SOLIDWORKS software, as depicted in Figure 5.



Figure 5: 3D model of the proposed nebulizer

The 3D model of the interior of the nebulizer was designed using SOLIDWORKS software as presented in Figure 6. The dimensions of every single component were studied thoroughly prior to designing it. Medical standards and guidelines were followed while doing so. Here the volume of the pump is equal to 88 mm x 65 mm x 40.5 mm. The inlet and outlet diameters are 3.4 mm and 6.5 mm, respectively. The airflow sensor is connected to the outlet of the pump and the tubing is connected to the outlet of the airflow sensor. The nebulizer tubing is connected to the nebulizer chamber and the mask is attached to the nebulizer chamber. The mask, nebulizer

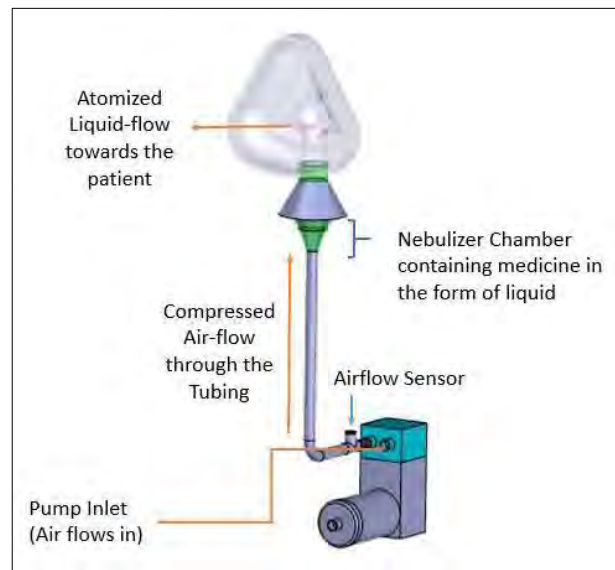


Figure 6: SOLIDWORKS model of the pump assembly

chamber, and nebulizer tubing were drawn as per the dimensions of the pre-existing nebulizers.

Analysis of the safety requirements and circuitry designing

Each subsystem of the overall system is a part of an integrated safety system. The system software can manage routine error handling and communicate the state of the system to the user. For example, the airflow sensor in combination with the PID function integrated within the controlling unit ensures that the patient does not receive an airflow of higher flow rate than the desired flow rate. In addition to that, the device is of unobtrusive and non-invasive type.

The circuit was designed using the “schematic capture” feature of the Proteus Design Suite. The power supply converts 230V AC to a 12V DC and 5V DC. The 12V DC supply is for powering up the motor controller and the three solenoid driver circuits, and the 5V DC supply is for powering up the display unit. The 12V and 5V requirements were fulfilled by the use of a 12V regulator (7812) and a 5V regulator (7805), respectively. The required components were selected from the Proteus library whilst referring to their datasheets. The components were placed in the workspace, and were routed to the Arduino as necessary.

Monitoring of the volumetric breathing rate and dynamic flow regulation of the compressor

The temperature is read through the analog input. It is then matched with the immediately previous value, to see if the value reaches a maximum or minimum. If the value of the temperature increases and suddenly decreases, or vice versa, a peak is reached. The peak could be either positive or negative.

On either of these peaks, a count is set as a value, so that the order can be checked to measure the time gap between two adjacent crests and a trough. Then this particular time difference is used to derive the breathing rate of the patient.

As the controller gets the flow rate set by the user, simultaneously the airflow sensor starts monitoring the airflow produced by the diaphragm pump. The flow rate entered by the user and the current flow rate are compared and the difference is calculated as an error. In accordance with that, the PWM signal given to the L298N IC for driving the motor through Arduino Mega 2560 is varied. The two pins are used as output for the motor driving, and the enable pin in the motor driver is supplied by the PWM signals from the Arduino. By supplying a high signal level to the enable (ENA) pin on the L298N, the motor driver provides the 12V supply to the motor, so by varying the signal to the enable pin, the motor speed will be varied. As shown in the above circuit diagram, ENA is connected to pin 11 of the Arduino, which serves as one of the output pins for its PWM function. The difference is counted as an error and from there onwards, PID calculation starts in the program. During the next step, the values of proportional, integral, and derivative errors are determined.

Performance evaluation of the nebulizer

Assessing the nebulizer motor performance

The motor function is a vital factor for the performance of the proposed nebulizer. Therefore, the motor control circuit was simulated using Matlab & Simulink (R2016b) software.

Since the PID control was to be applied for the DC brushed motor integrated within the micro diaphragm pump, the transfer function of the motor was chosen accordingly.

$$G(s) = \frac{\omega_n^2}{s^2 + 2\zeta\omega_n s + \omega_n^2} \quad \dots(1)$$

The above general equation (1) describes the behaviour of a typical second-order function with no zeros. Here ζ and ω_n are the damping ratio and the natural frequency respectively. The PID controller block was created within the controller subsystem and the output of the PID controller was connected to the input of the pump motor. The PID controller block output is a weighted sum and the weights are the proportional, integral, and derivative gain parameters. Then the inputs from the temperature sensor were added to the motor controlling circuitry. The MATLAB function contains the program for how the pump speed has to be varied according to the volumetric breathing rates of the patient. The pump speed has to be varied among 10, 8, and 6 L/min with the change of the volumetric breathing rate of the patient.

The PID controller was tuned automatically with the aid of the Control System Toolbox™. The goals of the motor controlling circuit were to achieve a settling time of less than 5 s and to get a zero steady-state error to the step reference input.

Circuitry simulation and experimental analysis

The circuitry simulation was run on Proteus 8.0 software. By way of checking the Arduino program for errors, and specifically, to check the functioning of the breath rate monitoring coding, an experimental setup was built using the hardware components mentioned under 'conceptual design and hardware components' section. However, due to the unavailability of the diaphragm pump, in place of it, a normal DC motor was used. The DC motor was checked for the RPM values corresponding to the flow rates of the pump.

CFD simulation of the compressed airflow

In order to incorporate design considerations into a prototype device consistent with project goals, an iterative design process was implemented. For this purpose, computational fluid dynamics simulation was performed on the conceptual device solid model. SOLIDWORKS Flow Simulation and ANSYS Fluent software were utilized.

The values given in Table 1 were entered under the properties option of the two software programs.

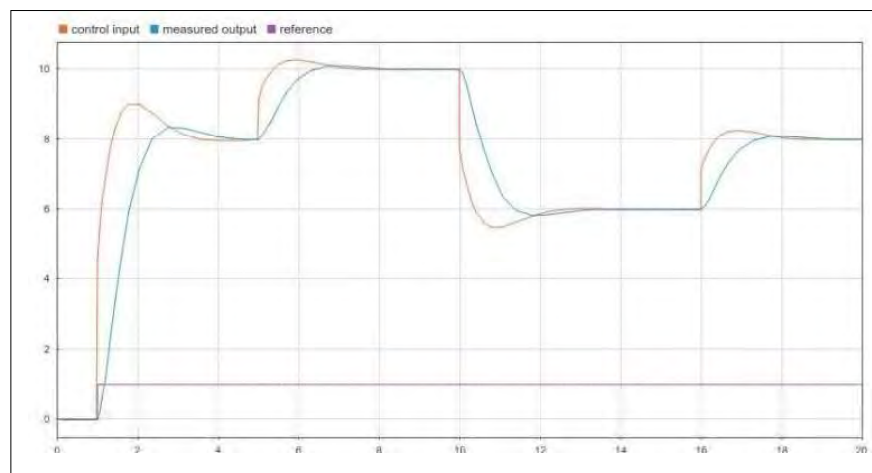
Table 1: Parameter characterization

Parameter	Value
Velocity	1.02 m/s, 1.36 m/s, 1.7 m/s
Flow rate	6 L/min, 8 L/min, 10 L/min
Pressure	101, 325 Pa
Fluid Type	Normal Air

RESULTS AND DISCUSSION

PID controller simulation on Matlab and Simulink

Since PID tuning is an iterative process, obtaining gain values using automated tuning of the linearized model and testing the entire Simulink model via simulation were carried out a few times till the desired results were obtained. After performing a series of simulations and

**Figure 7:** Closed loop system response (Flow rate vs time)

comparing them using Simulink, the most appropriate system response was chosen. Thus, Figure 7 denotes the response of the entire closed-loop system. It fulfills the design requirements. With the change of the volumetric breathing rates, the flow rates of the pump change smoothly without any unrealistic spikes, in a settling time of 2.63 seconds. There is only a slight difference between the control input and the measured output.

Circuitry simulation and experimental analysis

Due to the complexity of the circuitry, it was hard to simulate the entire circuit on Proteus software. Therefore, two errors were encountered: '[SPICE] transient GMIN stepping at time = 2.19633e-006' and 'Simulation is not running in real-time due to excessive CPU load.' However, when the power supply-motor controller circuit was simulated separately, correct voltage values were displayed on the DC voltmeters. The terminal voltage of the motor were shown as 12V. Thus, there were no errors in the power supply nor with the motor controller circuitry.

All the components that were used in the experimental setup functioned according to the uploaded program. The DC motor speed was regulated as per the rpm values specified in the Arduino program. The respiratory monitoring coding functioned successfully. The DS18B35 temperature sensor was able to detect the small fluctuations of temperature between inhalation and exhalation. This particular experiment suggested that there were no shortcomings in the coding.

CFD simulations carried out on SOLIDWORKS

SOLIDWORKS flow simulation

The simulation was turbulent and laminar, and time-independent with air as the fluid. Therefore, the airflow through the pump assembly was modelled and assessed using the flow trajectories generated as a result. At the pump, a turbulent flow was to be seen, as presented in Figure 8.

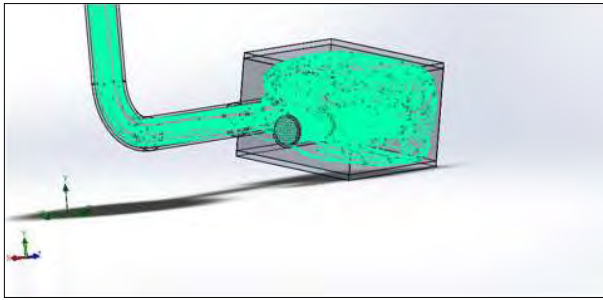


Figure 8: Flow trajectories within the pump

The flow generated from the outlet of the pump towards the nebulizer tubing shows the characteristics of laminar flow as depicted in Figure 9. The flow was steady. In addition to that, the flow of air through the nebulizer tubing was also examined and found to be uniform and laminar without any excessive turbulent flow or rotational flow pattern. The presence of rotational flow pattern is considered unacceptable because it imposes a restriction at recruiting drug particles and dispersing them through the mask, and dispositioning them within the airways.

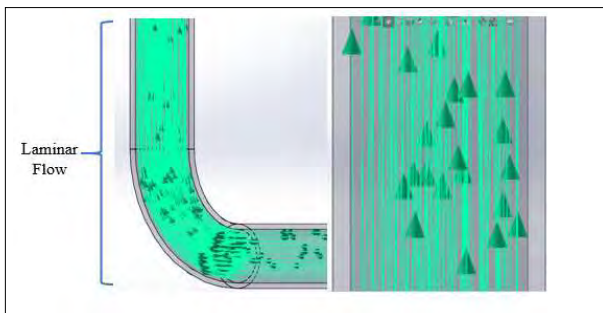


Figure 9: Flow trajectories within the nebulizer tubing

Within the nebulizer chamber, pressurized atomization air is discharged from an orifice and directed against baffles, which causes the air to flow with swirling turbulence over the orifice. The turbulent swirling flow of the atomization air is what causes the droplets to decrease in size. The flow path of the aerosol through the nebulizer chamber towards the mask shows a rapid change of direction to facilitate condensation of any large droplets in the aerosol, as presented in Figure 10 below.

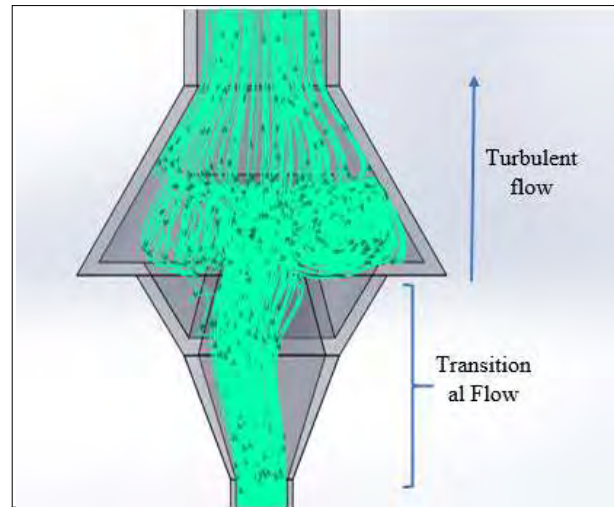


Figure 10: Flow trajectories within the nebulizer chamber

CONCLUSION

Due to the pervasive nature of respiratory diseases and the manner in which they are treated, the market for aerosol drug delivery devices is high. Despite the large market, insufficient drug delivery is a common issue associated with some of the conventional nebulizers. This particular issue is addressed by the current research. The reason for optimizing the control unit of the nebulizer was because the dynamic flow of compressed air is unidirectional and constant, whereas the breathing pattern of a patient is bidirectional. In the first phase of the research, the development of the temperature sensor-based algorithm for volumetric breathing rate detection, and implementation of the compressor control circuitry (PID) were completed successfully. All the objectives were met. The simulation results obtained from Simulink validated the performance of the PID control unit. In addition to that, the results gained from the physical simulations carried out on SOLIDWORKS and ANSYS Fluent 16, were satisfactory. No substantial amount of turbulent flow or rotational flows were detected within the device.

However, according to section VIII of us Food and drug Administration (FDA)1993, regulations 1993, *in vitro* testing is required prior to completing the product development. For this purpose, techniques like laser

scattering or cascade impactor need to be incorporated to determine, the size of the respirable droplet produced by the nebulizer and the amount of drug deposition (FDA, 1993). In addition to that, the device has to be tested for the available drug types.

REFERENCES

- Ari A. (2014). Jet, ultrasonic, and mesh nebulizers: an evaluation of nebulizers for better clinical outcomes. *Eurasian Journal of Pulmonology* **16**(1): 1–7.
<https://doi.org/10.5152/ejp.2014.00087>
- Clay M.M. (1987). Wastage of drug from nebulizers : a review. *Journal of the Royal Society of Medicine* **80**(1):38–9.
- O'Callaghan C. & Barry P.W. (1997). The science of nebulized drug delivery. *Thorax* **52**(2): S31.
<https://doi.org/10.1136/thx.52.2008.s31>
- Chatburn R.L. & McPeck M. (2007). A new system for understanding nebulizer performance. *Respiratory Care* **52**(8): 1037–50.
- FDA. (1993). *Reviewer guidance for nebulizers, metered dose inhalers, spacers, and actuators*. U.S. Department of Health and Human Services, Rockville, USA.
- Gupta M. & Qudsi H. (2013). Low-cost, thermistor based respiration monitor. Proceedings of the IEEE Annual Northeast Bioengineering Conference, NEBEC. 5-7 April. Syracuse, NY, USA, pp 287–288.
<https://doi.org/10.1109/NEBEC.2013.111>
- Haddrell A.E., Davies J.F., Miles R.E.H, Reid J.P., Dailey L.A. & Murnane D. (2014). Dynamics of aerosol size during inhalation: Hygroscopic growth of commercial nebulizer formulations. *International Journal of Pharmaceutics* **463**(1): 50–61
<https://doi.org/10.1016/j.ijpharm.2013.12.048>.
- Hess D.R. (2000). Nebulizers: principles and performance. *Respiratory Care* **45**(6): 609–622.
- Hubbard R. (2006). The burden of lung disease. *Thorax* **61**(7): 557–558.
<https://doi.org/10.1136/thx.2006.066050>
- Ivanova M.D. & Glazova A.Y. (2015). Nebulizer improvement for children suffering from bronchial asthma. *Proceedings of 2015 IEEE NW Russia Young Researchers in Electrical and Electronic Engineering Conference (EIConRusNW)*: 2-4 February. St. Petersburg, Russia, pp 329–331.
<https://doi.org/10.1109/EIConRusNW.2015.7102291>
- Knospe C. (2006). PID control. *IEEE Control Systems Magazine* **26**(1): 216–251.
<http://dx.doi.org/10.1109/MCS.2006.1580151>
- Kendrick A.H., Smith E.C. & Wilson R.S. (1997). Selecting and using nebulizer equipment. *Thorax* **52**(2): S92.
<https://doi.org/10.1136/thx.52.2008.s92>
- Le Brun P.P., de Boer A.H., Frijlink H.W. & Heijerman H.G.M. (2000). A review of the technical aspects of drug nebulization. *Pharmacy World and Science*, **22**(3): 75–81.
<https://doi.org/10.1023/a:1008786600530>
- Mittal G., Kumar N., Rawat H., Chopra M.K. & Bhatnagar A. (2010). A radiometric study of factors affecting drug output of jet nebulizers. *Indian Journal of Pharmaceutical Sciences* **72**(1): 31–8.
<https://doi.org/10.4103/0250-474X.62234>
- Paz R. A. (2001). *The Design of the PID Controller*. Klipsch School of Electrical and Computer Engineering, New Mexico, USA.
- Rau J.L. & Hess D. (2009). *A guide to Aerosol Delivery Devices for Respiratory Therapists*. American Association for Respiratory Care, MacArthur Boulevard, USA.
- Theopaga A.K., Rizal A. & Susanto E. (2014). Design and implementation of PID control based baby incubator. *Journal of Theoretical and Applied Information Technology* **70**(1): 19–24.
- Volsko T.A. (2014). *Equipment for Respiratory Care*. Jones & Bartlett Publishers, Burlington, USA.
- Yardimci A. (2011). Micro controller based jet nebulizer design with ANFIS compressor control for domiciliary use. *Proceedings of 2011 International Symposium on Innovations in Intelligent Systems and Applications*. 15-18 June, Istanbul, Turkey, pp 428–431.
<https://doi.org/10.1109/INISTA.2011.5946106>

RESEARCH ARTICLE

Environmental Chemistry

Characterization of landfill leachate at the Karadiyana open dumpsite, Sri Lanka, and assessment of water pollution in its vicinity

PA Koliyabandara, AT Cooray*, S Liyanage and C Siriwardhana

Department of Chemistry, Faculty of Applied Science, University of Sri Jayewardenepura, Gangodawila, Nugegoda.

Submitted: 23 December 2020; Revised: 24 May 2021; Accepted: 24 September 2021

Abstract: Contamination of ground and surface waters by landfill leachate is a prime environmental concern. The present research assesses chemical composition of leachate generated in the Karadiyana open dumpsite in Sri Lanka and the groundwater pollution caused by the landfill. The leachate pollution index (LPI) of Karadiyana is 34.00, suggesting that it has the potential to contaminate the environment. The nitrate, ammonia, and total phosphate concentrations in leachate varied in the range of 20.70 to 167.80, 376.55 to 580.33 and 10.00 to 84.00 mg/L respectively. Four major groups, namely, tryptophan- and tyrosine-like protein fractions, and fulvic and humic fractions were identified in leachate using fluorescence data. The bio chemical oxygen demand (BOD) to chemical oxygen demand (COD) ratio of leachate in the present study varied between 0.39 and 0.49 which categorizes leachate into intermediate age with medium biodegradability. This observation was further verified by the average pH and COD values of leachate; 6.81 ± 0.08 and 2221 ± 45 mg/L, respectively. Only one out of ten dug wells located in a radius of about a kilometer from Karadiyana dumpsite can be classified as good water for drinking purposes though eight of ten are used for drinking at the moment. All ten dug wells exceeded the WHO recommended nitrate level.

Keywords: Groundwater pollution, Karadiyana open dumpsite, landfill leachate, leachate pollution index, metal pollution index

INTRODUCTION

Municipal landfills are a common feature in many Sri Lankan cities and it has been estimated that there

are more than 260 small and large scale landfills in Sri Lanka (Jayaweera *et al.*, 2019; Koliyabandara *et al.*, 2020). All of the landfills except the ones Dompe and Aruwakkalu can be categorized as unregulated open dumpsites (Jayaweera *et al.*, 2019; Koliyabandara *et al.*, 2020). In addition, most of them have been built without proper environmental impact assessments (EIA) and as a result, dumpsites including Karadiyana, Muthurajawela, Gohagoda, and Ginthota are located very close to sensitive ecological habitats such as major river systems and wetlands in Sri Lanka. According to United States criteria for municipal solid waste (MSW) landfill siting and design, landfills should not be built on wetlands and flood plains, and a proper leachate collection and removal system should be installed to protect groundwater and underlying soil (Letcher & Vallero, 2019). Landfill leachate has been identified as one of the major sources of pollutants to ground and surface waters (Mor *et al.*, 2006). Landfill leachate is the liquid leaching out of landfills due to the infiltration of rainwater through solid waste piles in dumpsites. The leaching liquids are carrying all the water-soluble and suspended fractions of waste and waste degradation by-products. In addition, liquids squeezing out of waste in landfills with a high-water content is also known as leachate. Leachate generation may not be significant in very dry climates (Letcher & Vallero, 2019). Landfills in wet climates and those receiving waste containing a high water content produce a significant amount of leachate (Letcher and Vallero, 2019). The chemical composition

* Corresponding author (atcooray@sjp.ac.lk;  <https://orcid.org/0000-0002-4876-4224>)



This article is published under the Creative Commons CC-BY-ND License (<http://creativecommons.org/licenses/by-nd/4.0/>). This license permits use, distribution and reproduction, commercial and non-commercial, provided that the original work is properly cited and is not changed in anyway.

of leachate consists of a variety of components including particulate and dissolved organic matter, heavy metals, and inorganic compounds, due to the mixed nature of the waste in many landfills (de Godoy Leme & Miguel, 2018).

The risk of pollution of surface water and groundwater sources closer to dumpsites, such as dug and tube wells, rivers, and streams, which are used by humans for drinking or sanitary purposes, is most severe in open dump sites because of the lack of engineered liners and leachate collection systems (El-Salam & Abu-Zuid, 2015). The type and depth of the water table, the direction of groundwater flows, and the concentration of pollutants determine the severity of ground and surface water pollution (Aderemi *et al.*, 2011). Many toxic metals make stable water-soluble complexes with dissolved organic matter, which allows them to transport through the water channels easily. This is a prime issue in Asian countries as most of the landfills do not have liners to prevent contamination of groundwater and underlying soil (Rafizul *et al.*, 2012).

Due to lack of infrastructure and funds, poor landfill and waste management practices, and the negligence of enforcing environment protection laws in Sri Lanka, the country has faced a few landfills related disasters with loss of life and property. The collapse of the Meethotamulla open dumpsite on the 14th April 2017, with a loss of 32 people, was one of them (Jayaweera *et al.*, 2019). The discharge of the organic matter rich Gohagoda landfill leachate into the Mahaweli river, which is the major source of drinking water for the Kandy city, has been reported (Kumarathilaka *et al.*, 2016). In addition, harmful volatile organic compounds (VOCs), including benzene and toluene, have been detected in the Gohagoda landfill leachate (Kumarathilaka *et al.*, 2016). The chemical composition of leachate in Kataragama, Negombo, Matale and Hambantota landfills has been investigated previously and it has been found that many leachate samples contained high amounts of organic matter, nutrients, and heavy metals (Sewwandi *et al.*, 2013). The contamination of surface water bodies and sediments by Karadiyana dumpsite leachate has also been reported (Koliyabandara *et al.*, 2020; Mandakini *et al.*, 2016).

The characterization of landfill leachate is essential to investigate the risk of environmental pollution and to design leachate treatment facilities. Characterization of volatile and semi-volatile compounds in landfill leachate has been carried out specifically by GC-MS analysis. The

volatile and semi-volatile compounds in leachate related to cosmetics, medicine, pharmaceuticals, and plastics has been identified by the GC-MS data (Badoil & Benanou, 2009). In a particular study, GC-MS data revealed that a higher number of phosphorus-based compounds were present in leachate from a ten-year old landfill than in leachate from fresh landfill waste (Badoil & Benanou, 2009). In addition, GC-MS analysis has identified chlorinated aromatic xenobiotic organic matter (XOM), and many XOMs were found in the surface waters around dumpsites, indicating that they could be used as landfill leachate tracers (Banar *et al.*, 2009). Previous studies have shown the presence of XOMs, including benzene, methylbenzoic acids, aliphatic carboxylic acids, hydrocarbons, phenylpropionic acid, methyl phenols, aromatic carboxylic acids, and ethylphenols, in landfill leachate (Saadi *et al.*, 2006; Shouliang *et al.*, 2008).

Molecular fingerprinting using fluorescence excitation emission matrixes (EEM)s have been used in many sample matrixes, such as coloured wastewater, sewage effluents and polluted rivers (Ito *et al.*, 2016; Yamashita & Tanoue, 2003). Wastewater characterization with rapid fluorescence analysis has become a reliable and effective method (Stedmon *et al.*, 2003). Fluorescence has been used to fingerprint leachate in previous studies (Baker & Curry, 2004). It has been found that landfill leachate fluorescence properties are all characterized by intense fluorescence at excitation wavelengths (λ_{ex}) 220 to 230 nm, and emission wavelengths (λ_{em}) 340 to 370 nm, which was suggested to be derived from fluorescent components of the XOM fraction such as naphthalene (the "XOM peak"). A second fluorescence center, at λ_{ex} = 320 to 360 nm, and λ_{em} = 400 to 470 nm, is derived from a higher molecular weight fulvic-like fraction, and a third center at λ_{ex} = 270 to 280 nm and λ_{em} = 340 to 360 nm to tryptophan-like fluorescence.

Development of indexes such as leachate pollution index (LPI), water quality index (WQI), metal pollution index (MPI) and heavy metal pollution index (HPI/HMPI) to assess the pollution potential of landfill leachate provide essential information about the extent of pollution caused by dump sites (Giriappanavar & Patil, 2013; Umar *et al.*, 2010). The leachate pollution index is based on several pollution parameters which express the total leachate contamination potential of a landfill. Values exceeding 7.5 for LPI are an indication of an increased potential for environmental pollution (Umar *et al.*, 2010). Calculation of LPI can be useful in recognizing an appropriate landfill design, in forecasting the effect of leachate on the groundwater quality, identification

of hazard potential of leachate and developing proper mechanisms for the treatment of leachate (Sharma *et al.*, 2008). The water quality index (WQI) is also a useful technique in assessing water quality. Water quality parameters are converted to an overall index with the use of mathematical tools (Logeshkumaran *et al.*, 2015). One of the most commonly used WQI's was developed by the Canadian Council of Ministers of the Environment (CCME). It is known for its ease of use in summarizing a wide array of data (Giriappanavar & Patil, 2013).

It is essential to assess the contamination potential of landfill leachate to mitigate the risks associated with it. The main objective of the current study is to characterize leachate from the Karadiyana open dumpsite for the purpose of determining its potential to pollute water sources in its vicinity. In addition, the extent of ground water pollution of nearby dug wells generally used for drinking, washing, and sanitary purposes has also been assessed to evaluate their suitability for domestic use.

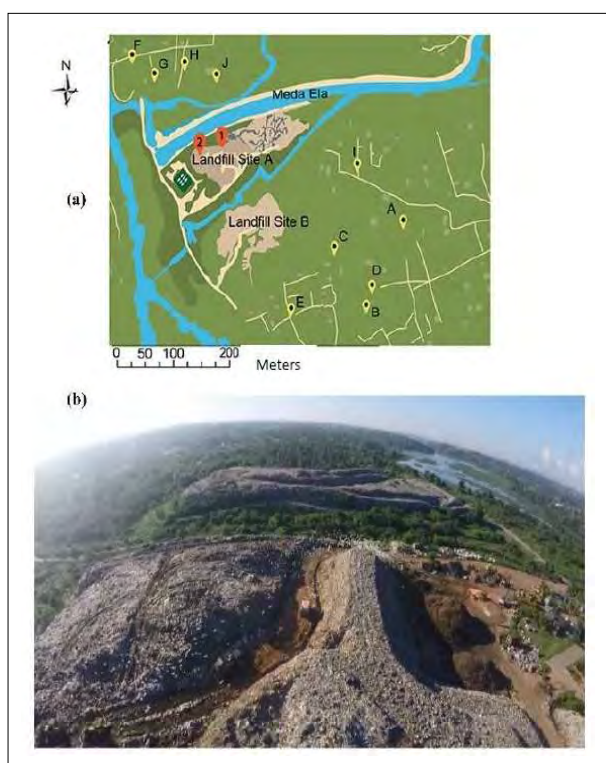


Figure 1: (a) Karadiyana solid waste dumpsite with leachate collection points 1, and 2, and groundwater collection points (dug wells) from A to J. (b) Birds eye view of the Karadiyana Dumpsite.

MATERIALS AND METHODS

Study area

The Karadiyana Waste Management Facility (6°48'58.32"N, 79°54'9.90"E), located in Kesbewa, Western Province of Sri Lanka, has a total area of about 0.10 km² with two waste dumping sites; site A that covers approximately 0.048 km² and site B that covers approximately 0.052 km² (Figure 1). The two waste dumping sites are separated by a canal. Site A was the active site receiving waste from local authorities and other public institutions during the study period (2016-2018). Karadiyana is the final waste disposal site for daily collected mixed and separated waste at a loading rate of approximately 575 T/day. It has been in operation for nearly 20 years as an unregulated open dumpsite receiving mixed waste. Because of its location close to a highly residential area, and to an ecologically sensitive Weras Ganga - Bolgoda Lake wetland system, arrangements are now in progress to convert the open dumpsite site into a semi-controlled landfill site.

Leachate and groundwater sample collection and analysis

Leachate samples were collected from two large leachate pools at locations 1 and 2 from site A as shown in Figure 1, during the period October 2016 to June 2018, in six sampling trips. Site A was the active site during the study period while leachate generation from site B was negligible. Lack of access roads to Site B due to its specific location in marshy land was also a reason to collect leachate only from site A. Groundwater samples were collected from 10 dug wells (~10 m deep) located in a radius of 0.5 to 1 km from the dumpsite and their approximate locations are shown in Figure 1. The exact geographical locations of dug wells are not stated in the manuscript due to an agreement with the well owners. All water and leachate samples were collected into acid washed pre-cleaned polypropylene bottles with zero head space to avoid aeration of the samples. Some water quality parameters were analyzed in the laboratory after transporting them in an ice box at 0 to 5 °C, and other parameters were analyzed in the field as described in the following section. All the water and leachate samples were collected, preserved, and tested according to standard methods (Eaton *et al.*, 2005).

The leachate and water samples were filtered (~0.45µm filter pore size) before analysis. Tests were triplicated to maintain accuracy and precision. Water

quality parameters namely biochemical oxygen demand (BOD), chemical oxygen demand (COD), ammonia, nitrate, nitrite, and the metals Cu, Fe, Zn, and Mn were determined. The determination of BOD₅ was done by the Winkler method, and the COD was done by the Cr₂O₇²⁻ oxidation method. Nitrate, nitrite, and ammonia analysis were done in the field using a YSI photometer and Palintest reagents. Leachate and surface water samples were digested with a sulphuric - nitric acid mixture prior to measuring total phosphates using YSI Model 9500 photometer and Palintest reagents. The total metal concentrations of copper (Cu), manganese (Mn), zinc (Zn), and iron (Fe) were determined because of their availability in landfill leachates. The leachate, and water samples were digested using high purity nitric acid before metals analysis using a Thermo Scientific iCE 3000 series atomic absorption spectrophotometer in flame and graphite furnace modes. Groundwater samples from dug wells were analyzed for anions using a Metrohm 930 IC flex ion chromatograph. YSI EXO2 water quality SONDE was used to estimate the pH and EC onsite.

Leachate characterization using fluorescence data

Leachate samples were brought to the laboratory and tested within 24 h. Samples were first filtered using Whatman microfiber filter papers previously heated to 450 °C to remove any organic matter. Fluorescence excitation-emission matrixes (EEMs) were produced using a Thermo Scientific luminescence spectrophotometer as described previously (Baker & Lamont-Black, 2001). A scan was carried out with excitation wavelengths from 200 to 370 nm and the emission were recorded from 250 to 500 nm and the samples were diluted when necessary. Absorption correction was not applied to the fluorescence spectra. The excitation and emission data were used to prepare excitation-emission matrixes (EMMs) which are then used to identify the major functional groups of fluorescent compounds in the leachate based on the position of the excitation and emission band peaks.

Leachate characterization using gas chromatography-mass spectrometry (GC-MS)

The volatile and semi-volatile organic fractions of landfill leachate was determined by GC - MS analysis (Agilent 7890A GC coupled to 5975C MS with Triple-Axis Detector) with HP5-MS capillary column (30 m, 0.25 mm, 0.25 µm). First, 200 mL of leachate samples were filtered through a 0.45 µm membrane, and then extracted with 30 mL CH₂Cl₂ (HPLC grade) at pH

values in the order of 7.0, 2.0 and 12.0. During the extraction process, the extract mixture was demulsified by centrifuging at 4000 rpm for 10 min. All the extract was mixed together, dehydrated with anhydrous Na₂SO₄, and then condensed to 1 mL with a rotary evaporator. The oven temperature of the GC was initially set at 65 °C and maintained for 2 min, then programmed to 220 °C at a rate of 9 °C min⁻¹ and maintained for 20 min. The injector was operated in a spitless mode, and the temperature was 300 °C. The MS was run at a voltage of 1050 V, electron ionization with electron energy of 70 eV, and an ion source temperature of 200 °C (Lei & Aoyama, 2010).

Calculation of leachate pollution index (LPI) and water quality index (WQI), metal pollution index (MPI)

The LPI of the Karadiyana dumpsite leachate was calculated with the sum of cumulative pollution ratings of all variables according to the following equation (Kumar & Alappat, 2005).

$$LPI = \sum_{i=1}^n w_i p_i / \sum_{i=1}^n w_i \quad \dots(1)$$

In equation (1), w_i is the weight factor for the i^{th} pollutant variable, p_i is the sub-index score of the i^{th} pollutant variable, and n is the number of known concentrations of leachate contaminant variables. Averaged sub-index curves are used to calculate the sub-index values as stated previously (Kumar & Alappat, 2005). The importance level of each parameter is considered when calculating the weights of individual parameters.

The WQI developed by CCME was used for analyzing ten dug well water samples using equation 2 where three elements known as F1 (scope), F2 (frequency) and F3 (amplitude) are calculated (CCME, 2001). Water quality parameters were given weights according to their importance, and the suitability of water for purposes like drinking, recreation, irrigation, and livestock was assessed accordingly.

$$CCME\ WQI = 100 - \sqrt{(F1^2 + F2^2 + F3^2)} / 1.732 \quad \dots(2)$$

In the equation F1 represents the number of variables that do not meet the water quality standards as a percentage. F2 represents the number of individual tests that do not meet the water quality standards as a percentage. F3 states the amount by which failed test values do not meet their guideline values.

The metal pollution index (MPI) was used to measure the overall metal content at the various sampling sites by using equation 3 (Usero *et al.*, 2005).

$$MPI = \frac{\sum_{i=1}^n w_i Q_i}{\sum_{i=1}^n w_i} \quad \dots(3)$$

Where w_i is the weightage of each parameter which is taken by inversely proportionate value of its standard value. Q_i is the sub index of i^{th} parameter. It can be calculated by the equation below.

$$Q_i = \sum \frac{(Mi(-)Ii)}{(Si(-)Ii)} \quad \dots(4)$$

Here M_i is the mean concentration value of a parameter, S_i is the standard permissible value and I_i is the highest desirable value of each parameter.

RESULTS AND DISCUSSION

Characterization of Karadiyana landfill leachate

The physicochemical characteristics of Karadiyana leachate were determined on two large leachate pools that were present during the entire study period as some of the other leachate pools were dried out in the dry season. In addition, some leachate pools were unreachable due to their location within the dumpsite and lack of access roads. The two sampled leachate pools had formed by merging several small leachate-flows in a depression of about 2 m in diameter with a depth of about 1 m. These pools were very close to the Meda-Ela canal, and it was observed that the pools overflow directly into the canal. The average values of leachate characteristics,

Table 1: The average values of the physicochemical characteristics of the Karadiyana open dump leachate with standards of tolerance limits for the discharge of effluent to inland surface waters by the Central Environmental Authority (CEA) of Sri Lanka (CEA, 2008)

Date	pH	EC $\mu\text{S}/\text{cm}$	NO_3^- mg/L	NH_3 mg/L	Total PO_4^{3-} mg/L	Cu mg/L	Fe mg/L	Zn mg/L	Mn mg/L	COD mg/L	BOD_5 mg/L	BOD/COD
Location 01												
10/2016	6.76	7,417.0	167.8	505.0	42.0	0.69	10.80	0.23	0.40	1,933	931	0.48
01/2017	6.80	6,598.0	153.2	451.9	31.0	0.44	9.66	0.35	0.38	1,800	723	0.40
06/2017	6.91	4,800.0	147.4	412.0	28.0	0.69	10.80	0.48	0.40	2,705	1,048	0.39
10/2017	6.70	4,300.0	145.9	527.2	31.0	0.40	8.70	1.20	0.41	1,908	938	0.49
02/2018	6.91	3,600.0	104.6	416.4	38.0	0.41	11.20	1.65	0.61	2,682	1,107	0.41
06/2018	6.78	1,100.0	21.9	376.6	33.0	0.70	10.50	0.30	0.58	2,300	968	0.42
Min.	6.70	1,100.0	21.9	376.6	28.0	0.40	8.70	0.23	0.38	1,800	723	0.39
Max	6.91	7,417.0	167.8	527.2	42.0	0.70	11.20	1.65	0.61	2,705	1,107	0.49
Avg.	6.81	4,636.0	123.5	448.2	33.8	0.55	10.28	0.70	0.46	2,221	953	0.43
Stdev.	0.08	2,249.4	54.0	58.2	5.12	0.15	0.93	0.58	0.10	403	132	0.04
Location 02												
10/2016	7.83	6,800.0	145.9	580.3	84.00	0.13	11.20	1.24	0.60	1,406	820	0.58
01/2017	7.50	5,600.0	155.6	509.5	72.00	0.01	7.50	2.10	0.47	1,380	648	0.47
06/2017	6.89	4,700.0	167.8	513.9	60.00	0.13	11.20	1.24	0.32	2,800	1,220	0.44
10/2017	6.70	3,800.0	145.9	434.1	45.00	0.07	10.20	2.20	0.38	2,400	1,280	0.53
02/2018	6.89	3,210.0	68.1	500.6	18.00	0.04	9.30	1.70	0.42	2,933	1,365	0.47
06/2018	6.80	2,900.0	20.7	487.3	10.00	0.11	10.80	1.30	0.45	2,703	1,630	0.60
Min.	6.70	2,900.0	20.7	434.1	10.00	0.01	7.50	1.24	0.32	1,380	648	0.44
Max.	7.83	6,800.0	167.8	580.3	84.00	0.13	11.20	2.20	0.60	2,933	1,630	0.60
Avg.	7.10	4,501.7	117.3	504.3	48.17	0.08	10.03	1.63	0.44	2,270	1,160	0.52
Stdev.	0.45	1,500.3	59.0	47.2	29.56	0.05	1.43	0.44	0.09	702	363	0.07
CEA	6.5-8.5	N/A	50	N/A	5	3	3	2	N/A	250	30	N/A

N/A Not available

Biochemical oxygen demand (BOD), chemical oxygen demand (COD)

determined using leachates collected during field trips between October 2016 and June 2018, are shown in Table 1.

According to the results, it is evident that the raw leachate does not meet the tolerance limits especially for ammonia, phosphate, BOD and COD levels for the discharge of effluent to inland surface waters specified by the Central Environmental Authority of Sri Lanka. The raw leachate from Karadiyana dump site must not directly flow into any surface or groundwater without treatment, as the contamination of Meda-Ela canal would lead to detrimental effects on the environment as a whole. The experimental data collected in this study shows that the pH of Karadiyana leachate ranged from 6.7 to 7.8, which is suitable for methanogenic bacteria. Literature states that generally, leachate shows pH values between 4.5 to 9.0 and the pH of leachate increases with the decrease of concentration of partially ionized free volatile fatty acids (Tatsi & Zouboulis, 2002). The pH of leachate greater than 7.5 marks the landfill as old while pH lower than 6.5 states that it has newer leachate (Robinson, 2007). The pH values of the landfill leachate increase with the aging of the landfill due to the biological decomposition of organic nitrogen into ammonium-N (Chen, 1996). Leachate samples with a slightly high pH ranging between 7.0 to 8.0 indicate the short acidic phase and early methanogenic phase (Tränkler *et al.*, 2005). On

the other hand, landfill leachate in Malaysia has shown an average value of pH around 6.7, which indicates that the leachate is recent, and the waste degradation is at the final stage of its acidic phase (Bahaa-Eldin *et al.*, 2008).

Nitrate, ammonia, and total phosphate in leachate varied in the range of 20.7 to 167.8, 376.0 to 580.0 and 10.0 to 84.0 mg/L respectively during the study period. Both new and old leachate is characterized by ammonia nitrogen, and hydrolysis and fermentation of the nitrogenous fraction of biodegradable waste cause older leachate to have a significant amount of ammonia nitrogen (Kulikowska & Klimiuk, 2008). Studies carried out in a Nigerian open dumpsite has recorded an average nitrate concentration of 55.82 ± 12.31 mg/L (Ibezute & Erhunmwunse, 2018). In comparison to several studies carried out worldwide, Karadiyana leachate shows values into the upper ranges exceeding 100 mg/L. Ammonia levels present in open dumpsite leachate recorded in other studies have ranged from 500 to 1500 mg/L (Tatsi & Zouboulis, 2002). In this study the average ammonia concentration was recorded as 448.2 mg/L. A major open dumpsite in Sri Lanka, Gohagoda has recorded values ranging between 6.0 to 4095.0 mg/L for ammonia nitrogen (Wijesekara *et al.*, 2014). Old leachate was determined to have nitrate values below 100 mg/L and ammonia is considered as a principal pollutant in old leachate because of the deamination of amino acids

Table 2: Pearson correlation matrix of parameters of leachate with rainfall variation

Location 1						
	Rainfall (mm)	NO ₃ ⁻ (mg/L)	NH ₃ mg/L	PO ₄ ³⁻ (mg/L)	COD (mg/L)	BOD (mg/L)
Rainfall (mm)	1.00					
NO ₃ ⁻ (mg/L)	0.32	1.00				
NH ₃ mg/L	0.80	0.73	1.00			
PO ₄ ³⁻ (mg/L)	0.06	0.06	0.24	1.00		
COD (mg/L)	-0.52	-0.34	-0.69	-0.12	1.00	
BOD (mg/L)	-0.08	-0.29	-0.33	0.17	0.85	1.00
Location 2						
Rainfall (mm)	1.00					
NO ₃ ⁻ (mg/L)	0.33	1.00				
NH ₃ (mg/L)	-0.26	0.19	1.00			
PO ₄ ³⁻ (mg/L)	0.26	0.87	0.57	1.00		
COD (mg/L)	-0.19	-0.50	-0.51	-0.80	1.00	
BOD (mg/L)	-0.01	-0.73	-0.53	-0.90	0.89	1.00

during destruction of original organic compounds. The phosphate levels present in leachate samples are comparable to those in studies carried out under the same environmental conditions and similar age of generation (Robinson, 2007; Wijesekara *et al.*, 2014).

According to the literature, a low BOD/COD (<0.5) ratio results due to the presence of higher amounts of humic and fulvic like compounds and low concentrations of volatile fatty acids (Kjeldsen *et al.*, 2002). A BOD/COD ratio greater than 0.5 suggests that the leachate originates from fresh (new) organic waste in a landfill. If the ratio decreases, approaching 0.1, studies have found out that it originates from an old and stable landfill (Kjeldsen *et al.*, 2002). The present study reveals that the leachate has BOD/COD values in the range of 0.39 to 0.60. It indicates that Karadiyana leachate is in its intermediate phase. As the site receives fresh MSW daily, generation of new leachate is possible. Showing values lower than 0.5, indicates that the Karadiyana landfill leachate has a relatively higher amount of humic and fulvic like compounds. The decay of organic matter into amino acids can affect the values of BOD, COD, and the ratio of BOD/COD. Values recorded for BOD/COD ratio for Sri Lankan dumpsites in Gohagoda, Matale and Kataragama are 0.08, 0.02 and 0.04 respectively, highlighting the presence of mature landfill leachate (Sewwandi *et al.*, 2013; Wijesekara *et al.*, 2014).

The temporal distribution of leachate varies along with rainfall as it facilitates mobility or dilution of

pollutants (Tränkler *et al.*, 2005). Correlation analysis for the parameters of leachate along with the rainfall variation is shown in Table 2. Rainfall shows strong positive correlation (0.8) with NH_3 in location 1. Nitrate and rainfall show positive correlation in both locations (location 1- 0.32, location 2- 0.33). It was also observed that the correlation coefficients between certain parameters are significantly different in the two locations. These include correlations between nitrate and phosphate, phosphate and BOD, and ammonia and rainfall. The exact reason for these differences is difficult to comprehend and it could be due many factors. It appears that the two leachate pools have slightly different chemical compositions. Leachate in Location 1 has more nitrate, and Cu than Location 2. On the other hand, Location 2 has more Zn, biodegradable carbon (ex-BOD) and phosphate than Location 1. The BOD/COD ratios of the locations are also different from each other. It is possible that these differences play an important role in the overall chemical and biological degradation processes taking place in leachate. As a result, correlation coefficients between certain parameters could be significantly different in the two locations.

Leachate pollution index

The sub-index values were calculated from averaged sub-index curves reported previously (Kumar & Alappat, 2005). An LPI value higher than 7.5 specifies that leachate can cause harm for both the environment and human health (Esakku *et al.*, 2007). The leachate pollution index

Table 3: Leachate pollution index (LPI) calculation for Karadiyana leachate

Parameter	Pollutant concentration	Sub-index value p_i	$W_i = \text{weight/total weight}$	Cumulative pollution rating ($\sum w_i p_i$)
pH	7.10	5	0.03	0.17
Ammonia (mg/L)	504.3	45	0.30	13.50
Nitrate (ppm)	117.3	5	0.03	0.17
Cu (mg/L)	0.08	5	0.03	0.14
Fe (mg/L)	10.03	5	0.03	0.14
Zn (mg/L)	1.63	5	0.03	0.14
Mn (mg/L)	0.44	5	0.03	0.14
COD (mg/L)	2,270.33	45	0.30	13.50
BOD (mg/L)	1,160.50	30	0.20	6.00
Total		150	1	34.00

of the Karadiyana open dumpsite was calculated as 34.00 (Table 3). Elevated levels of ammonia and COD make a major contribution to the cumulative pollution rating, indicating the effect of inorganic and organic pollution in the Karadiyana dumpsite. Open dumps located in similar environmental conditions (wet zone) in Sri Lanka have recorded LPI value of 31.31 for Bandaragama and 42.50 for Kolonnawa (Sewwandi *et al.*, 2013).

Characterization of dissolved organic matter (DOM) in leachate using fluorescence and GC-MS techniques

DOM in Karadiyana leachate was identified using fluorescence spectroscopic methods. Four major groups were identified, namely, tryptophan and tyrosine like protein fractions, and fulvic and humic fractions shown in Figure 2. Similar characterization has been carried out in previous research (Koliyabandara *et al.*, 2019). The presence of volatile fatty acids is identical in new leachate and in intermediate-age leachate. These are aliphatic mono-carboxylic acids with 2 to 6 or even 7 carbon atoms. These acids are generated due to the presence of massive loads of biodegradable waste (Stegmann *et al.*, 2005). Anaerobic fermentation is the process by which such acids are generated.

The GC-MS studies of Karadiyana leachate provide evidence for the presence of dodecyl acrylate, known to be an environmental hazard, phenol, 4-hydroxypyridine-

1-oxide, phthalic acid, nonadecane, eicosane, and hexadecane. Previous studies have shown the presence of benzene, methylbenzoic acids, aliphatic carboxylic acids, hydrocarbons, aliphatic compounds, phenylpropionic acid, methylphenols, aromatic carboxylic acids and ethylphenols in landfill leachate (He *et al.*, 2006; Saadi *et al.*, 2006). The concentrated leachates have shown the presence of ethylbenzene, chlorobenzene, and the esters of phthalic acid including dibutyl phthalate, dimethyl phthalate, and di-n-octyl phthalate. In all leachates, aliphatic carboxylic acids, and aromatic carboxylic acids such as benzoic acid, methylbenzoic acid, phenylacetic acid, and phenylpropionic acid have been detected. These acids are predominant components of the leachates (Zhang *et al.*, 2013). Researchers have identified toluene and ethyl methylbenzene in addition to esters of fatty acids, and aliphatic and aromatic alcohols (Trzcinski & Stuckey, 2010). The presence of toluene, trichlorethylene, benzene, toluene, and xylenes in leachate have also been identified in previous studies (DeWalle & Chian, 1981).

Assessment of the effects of leachate on groundwater quality

The average values of water quality parameters of dug wells located around the site are presented in Table 4 and Table 5. Most of the residents around the site still use dug-well water for washing and drinking purposes due to ease of access. Most of the water quality parameters

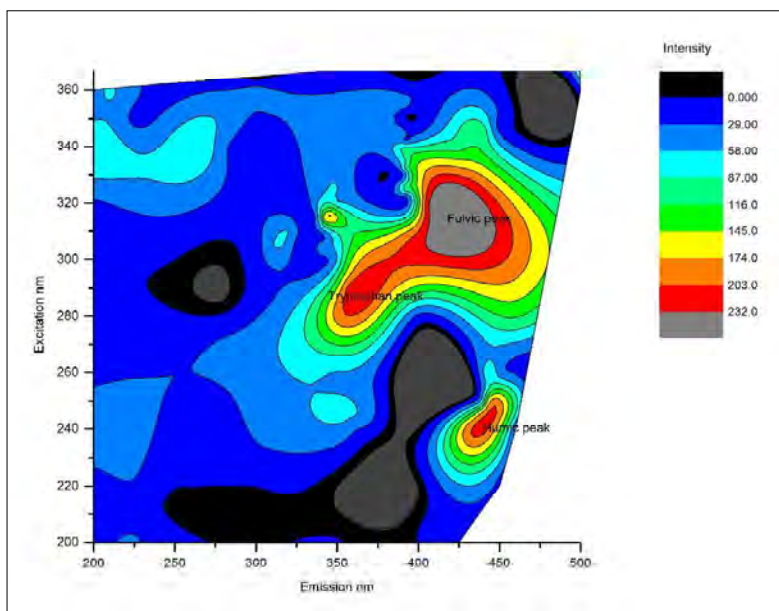


Figure 2: Fluorescence excitation-emission matrix for Karadiyana leachate DOMs.

of dug well water showed values below WHO drinking water standards (WHO, 2011) other than for nitrate and ammonia. Serious health issues can occur if nitrate levels in drinking water exceed 50 mg L^{-1} . All the dug-well water samples showed nitrate values above this limit, which indicates the possibility of mixing of leachate from the Karadiyana dump site. Unusually high nitrate levels have been observed in dug well E which is situated closer to the dump site. Contamination from leachate plumes and/or mixing with septic waste might have caused such higher concentrations. Dissolved nitrogen, which is present in the form of nitrates, is known to be one of the most common contaminants present in groundwater (Chaudhary *et al.*, 2010). Nitrate becomes hazardous when it is reduced to nitrite in the intestine. Hemoglobin is converted to methemoglobin

by nitrite which blocks oxygen transfer. The resulting condition is known as methemoglobinemia, which is even called blue baby syndrome (Kross, 2002). Elevated ammonia levels could be toxic in the environment and ammonification causes the production of ammonia and ammonium compounds by the degradation of nitrogen. It is known as an endogenously produced toxin (Wang *et al.*, 2007). Ammonia can cause a diverse range of diseases, including metabolic disorders, neurological malfunctions, coma, and even death (Ye *et al.*, 1997). Dug wells A, B, C, D, E, I and F, G, H, J can be considered as two separate groups according to their specific location. Considering ammonia and nitrate values of these samples the p value suggests that at 0.05 level there is a significant difference between these sample groups ($\text{NO}_3^- - 5.51 \times 10^{-6}$, $\text{NH}_3 - 9.36 \times 10^{-5}$).

Table 4: Water quality of dug wells around the dump site (n = 50, data is shown as average \pm stdev)

Location	Use for drinking	pH	Conductivity ($\mu\text{S}/\text{cm}$)	TDS (mg/L)	DO (mg/L)	BOD (mg/L)	NO_3^- (mg/L)	NH_3 (mg/L)	F ⁻ (mg/L)	Cl ⁻ (mg/L)	Br ⁻ (mg/L)
A	✓	7.51 ± 0.08	434.6 ± 5.4	258.4 ± 5.9	3.66 ± 0.08	24.7 ± 1.3	118.29 ± 5.93	0.43 ± 0.04	0.05 ± 0.01	38.25 ± 0.85	0.10 ± 0.01
B	✓	6.42 ± 0.24	254.8 ± 2.3	152.8 ± 1.9	4.85 ± 0.15	12.2 ± 0.8	34.78 ± 1.46	0.74 ± 0.07	0.03 ± 0.01	25.35 ± 0.79	0.05 ± 0.00
C	✓	6.65 ± 0.11	135.8 ± 2.1	85.0 ± 2.6	5.03 ± 0.19	9.8 ± 1.1	31.66 ± 1.16	0.87 ± 0.03	0.07 ± 0.01	27.37 ± 0.53	0.13 ± 0.04
D	✓	7.51 ± 0.17	529.2 ± 6.2	316.2 ± 1.9	5.15 ± 0.15	8.5 ± 0.4	63.42 ± 0.97	0.64 ± 0.04	0.01 ± 0.002	28.14 ± 0.26	0.31 ± 0.03
E	X	8.70 ± 0.04	648.7 ± 2.4	402.0 ± 5.4	4.35 ± 0.17	12.6 ± 0.4	406.62 ± 1.71	2.04 ± 0.04	0.01 ± 0.001	27.66 ± 0.15	0.34 ± 0.02
F	✓	6.74 ± 0.02	117.5 ± 1.0	71.8 ± 1.3	4.77 ± 0.13	63.8 ± 2.5	20.37 ± 1.39	0.14 ± 0.01	0.08 ± 0.002	29.28 ± 0.24	0.15 ± 0.04
G	X	6.88 ± 0.04	197.1 ± 1.0	118.0 ± 0.9	5.40 ± 0.05	83.6 ± 0.4	46.10 ± 0.66	0.27 ± 0.04	0.36 ± 0.33	10.78 ± 0.08	0.18 ± 0.01
H	✓	6.40 ± 0.05	261.6 ± 1.6	161.0 ± 4.5	4.68 ± 0.09	31.4 ± 1.3	73.64 ± 0.73	0.70 ± 0.04	0.05 ± 0.01	44.05 ± 1.00	0.12 ± 0.01
I	✓	6.37 ± 0.11	175.7 ± 0.7	105.1 ± 0.9	4.80 ± 0.04	22.8 ± 0.6	54.58 ± 1.45	0.35 ± 0.02	0.05 ± 0.01	83.04 ± 0.53	0.21 ± 0.01
J	✓	6.43 ± 0.04	260.6 ± 1.7	160.0 ± 4.2	4.67 ± 0.05	9.3 ± 0.2	323.06 ± 1.07	0.89 ± 0.04	0.04 ± 0.01	34.23 ± 0.80	0.07 ± 0.01
WHO 2011		6.5 - 8.5	N/A	500	N/A	N/A	50.0	N/A	1.5	250	1

The concentrations of selected heavy metals in dug wells are shown in Table 4. The presence of the metals, Fe, Zn, Cd, Cr, and Pb in the water samples exceeded the permissible levels set by WHO for drinking water (WHO, 2011). Elevated Cr levels in dug wells D and G might have been caused by vehicle tinkering and painting workshops observed in the vicinity of these wells. Only Mn and Cu showed values below the permissible maximum. Studies carried out for the evaluation of groundwater in Kelantan, Malaysia closer to an open dumping area has recorded values in the range of 0.80 to 47.40 mg/L for Fe, 0.20 to 3.0 mg/L for Cu, 1.10 to 109.70 mg/L for Zn, 0.10 to 1.20 mg/L for Cr and 0.20 to 40.00 mg/L for Mn (Ab Razak *et al.*, 2015).

Metal pollution index

The metal pollution index (MPI) is a method for ranking the quality of water. The index is the single resultant effect of every heavy metal on water quality and is designed to determine the water quality's effect on human health. If the index is greater than 100, the water is deemed hazardous to human health (Zhang *et al.*, 2009). At a

value of 100, the threshold of human health relative to water pollution has been reached. If the index is below 100, there is no significant heavy metal pollution, and there is much less of a cause of concern for consumers of the water. Well water in location E has an MPI of 120.34 and could be categorized as polluted water according to the MPI. It should be noted that, even though the MPI values in other locations were less than 100, the water could not be categorized as less polluted water due to the presence of toxic heavy metals Cr, Cd and Pb at elevated concentrations.

Water quality index

The water quality index according to CCME parameters, which are considered to be relevant to potability and health, should be prioritized when assessing drinking water quality. Potability related parameters are given as pH, EC, and chloride while health-related parameters are indicated as fluoride, nitrate, Fe, Mn, Zn, Cd, Cr, Cu, and Ni. Table 6 lists the CCME water quality index classification for dug wells around the site.

Table 5: Average metal concentrations of dug well water (n=100)

Location	Cu (mg/L)	Zn (mg/L)	Mn (mg/L)	Cd (mg/L)	Cr (mg/L)	Pb (mg/L)
A	0.051 ± 0.003	0.356 ± 0.004	0.079 ± 0.003	0.078 ± 0.005	0.662 ± 0.011	0.266 ± 0.005
B	0.030 ± 0.002	0.201 ± 0.013	0.049 ± 0.002	0.049 ± 0.003	0.419 ± 0.003	0.146 ± 0.003
C	0.109 ± 0.011	0.118 ± 0.003	0.030 ± 0.002	0.059 ± 0.003	0.051 ± 0.002	1.772 ± 0.055
D	0.064 ± 0.073	0.183 ± 0.019	0.037 ± 0.009	0.036 ± 0.013	31.70 ± 8.512	0.132 ± 0.011
E	0.329 ± 0.054	0.639 ± 0.087	0.350 ± 0.088	0.207 ± 0.014	0.104 ± 0.012	2.117 ± 0.050
F	0.114 ± 0.056	0.714 ± 0.666	0.027 ± 0.005	0.018 ± 0.006	0.017 ± 0.005	1.073 ± 0.095
G	0.239 ± 0.002	0.170 ± 0.001	0.030 ± 0.001	0.012 ± 0.001	42.30 ± 0.092	6.750 ± 0.115
H	0.218 ± 0.099	0.797 ± 0.451	0.218 ± 0.083	0.136 ± 0.043	0.043 ± 0.012	2.488 ± 0.156
I	0.094 ± 0.018	0.245 ± 0.055	0.090 ± 0.001	0.056 ± 0.005	0.030 ± 0.000	1.655 ± 0.020
J	0.123 ± 0.019	0.185 ± 0.029	0.095 ± 0.014	0.072 ± 0.004	0.037 ± 0.005	2.082 ± 0.162
WHO 2011	2.00	0.05	0.40	0.003	0.05	0.010

One out of ten dug wells can be classified as having good water under the category of drinking water, while five out of ten dug wells fall into the marginal water category. Regardless of the information obtained from water quality and metal pollution indexes, special care needs to be taken before using well water for domestic use because of the presence of toxic chemical compounds in the water.

Tracing landfill leachate

The use of tracers for the identification of pollution routes have been tested in studies carried out worldwide specially for the detection of groundwater contamination and surface water monitoring activities (Baker & Lamont-Black, 2001). Especially, in tracing leachate pollution occurring from open dumpsites, constituents

such as ammonia, bromide, and fluoride have been used in achieving the target, and ammonia may also be deemed a beneficial tracer of landfill leachate in surface waters, with average concentrations of leachate

mentioned (50 – 2,200 mg/L) (Christensen *et al.*, 2001). Fluorescence tracing of leachate has shown reliable results and it is a time saving and cost effective method (Baker & Lamont-Black, 2001). Looking at the

Table 6: WQI and classification of water quality of dug wells around the Karadiyana site

Location	Usage - drinking	Overall	Drinking	Aquatic	Recreation	Irrigation	Livestock
A	√	63 Marginal	50 Marginal	100 Excellent	100 Excellent	100 Excellent	57 Marginal
B	√	76 Fair	67 Fair	79 Fair	100 Excellent	100 Excellent	71 Fair
C	√	86 Good	78 Fair	100 Excellent	100 Excellent	100 Excellent	72 Fair
D	√	68 Fair	56 Marginal	100 Excellent	100 Excellent	100 Excellent	65 Fair
E	x	40 Fair	29 Poor	100 Excellent	100 Excellent	100 Excellent	44 Poor
F	√	82 Good	82 Good	100 Excellent	100 Excellent	100 Excellent	100 Excellent
G	x	84 Good	73 Fair	100 Excellent	100 Excellent	100 Excellent	69 Fair
H	√	68 Fair	55 Marginal	73 Fair	100 Excellent	100 Excellent	63 Marginal
I	√	72 Fair	60 Marginal	75 Fair	100 Excellent	100 Excellent	67 Fair
J	√	70 Fair	57 Marginal	75 Fair	100 Excellent	100 Excellent	63 Marginal

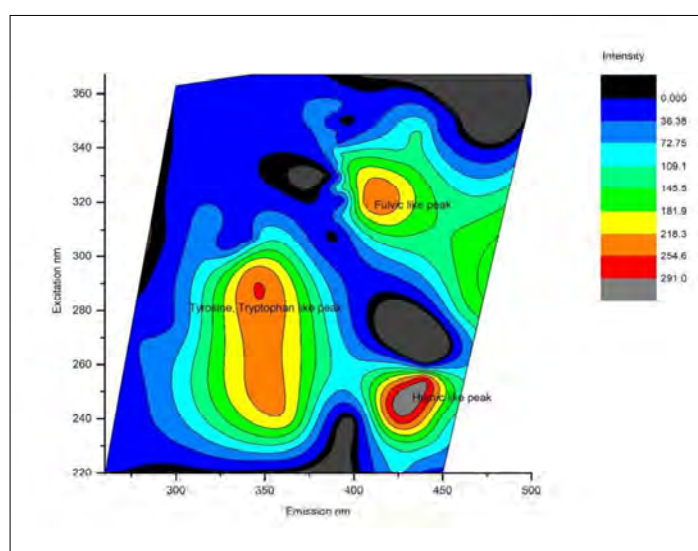


Figure 3: Fluorescence excitation-emission matrix for Karadiyana leachate DOMs from Location E.

fluorescence peaks present in dug well water samples; λ_{em} 320-340 nm and λ_{ex} 270-280 nm, it shows a large amount of unsaturated (aromatic) carbon bonding per organic carbon as well as much more complex organic structures, and these are assigned to the omnipresent tyrosine and tryptophan substances. Fluorescence studies help to identify and assume the possible contamination by leachate. Dug well E, which was recorded as having poor water quality, was characterized by the presence of humic fractions (240/440 nm), fulvic nature (310 – 340/420 – 440 nm), and tryptophan and tyrosine amino acids (240 – 300/350), as shown in Figure 3.

CONCLUSIONS

In this study, characterization of leachate generated by the Karadiyana open dumpsite and the contamination of water sources in the vicinity of the dumpsite were assessed. A leachate pollution index of 34.00 in the Karadiyana dumpsite suggests that the leachate is highly polluted, and appropriate treatment and a pollution mitigation process is essential before discharging into the neighboring water sources and environment. The fluorescence spectra of leachate showed the occurrence of tryptophan, tyrosine like substances, and humic substances. These compounds are present in intermediate (5 to 10 years) and old/stabilized (more than 10 years) leachate. A BOD/COD ratio of leachate in present study varies between 0.39 and 0.49 which categorizes leachate as intermediate in age, where biodegradability is medium according to the classification, further proven by an average pH of 6.81 ± 0.08 and an average COD of 2221 ± 45 . The MPI of dug wells showed that one out ten was categorized into the polluted category. The surface and dug well samples around the dumpsite were generally neutral, showing pH values in the range of 6.5 to 8.5. Some of the dug wells, which are used by residents for drinking purposes, have nitrate levels above the WHO recommended levels, which could lead to detrimental health effects. Location-specific water quality parameter variation is present, and the use of mitigation methods can be carried out on the flow direction of leachate. Based on the CCME-WQI classification, dug well water is not the best option to be used for drinking purposes because only one out of ten dug wells was classified as producing good water.

Data availability

Supplementary data is available upon request from the corresponding author.

Conflict of interest

The authors declare that there is no conflict of interest regarding the publication of this paper.

Acknowledgment

This research project was funded by the University of Sri Jayewardenepura under the research grant ASP/01/RE/SCI/2018/23

REFERENCES

- Ab Razak N.H., Praveena S.M., Aris A.Z. & Hashim Z. (2015). Drinking water studies: A review on heavy metal, application of biomarker and health risk assessment (a special focus in Malaysia). *Journal of Epidemiology and Global Health* **5**(4): 297–310.
DOI: <https://doi.org/10.1016/j.jegh.2015.04.003>
- Aderemi A.O., Oriaku A.V., Adewumi G.A. & Otitoloju A.A. (2011). Assessment of groundwater contamination by leachate near a municipal solid waste landfill. *African Journal of Environmental Science and Technology* **5**(11): 933–940.
- Badoil L. & Benanou D. (2009). Characterization of volatile and semivolatile compounds in waste landfill leachates using stir bar sorptive extraction–GC/MS. *Analytical and Bioanalytical Chemistry* **393**(3): 1043–1054.
DOI: <https://doi.org/10.1007/s00216-008-2512-z>
- Bahaa-Eldin E., Yusoff I., Rahim S.A., Wan Zuhairi W. & Abdul Ghani M. (2008). Heavy metal contamination of soil beneath a waste disposal site at Dengkil, Selangor, Malaysia. *Soil and Sediment Contamination* **17**(5): 449–466. DOI: <https://doi.org/10.1080/15320380802304342>
- Baker A. & Curry M. (2004). Fluorescence of leachates from three contrasting landfills. *Water Research* **38**(10): 2605–2613.
DOI: <https://doi.org/10.1016/j.watres.2004.02.027>
- Baker A. & Lamont-Black J. (2001). Fluorescence of dissolved organic matter as a natural tracer of ground water. *Groundwater* **39**(5): 745–750.
- Banar M., Cokaygil Z. & Ozkan A. (2009). Life cycle assessment of solid waste management options for Eskisehir, Turkey. *Waste Management* **29**(1): 54–62.
DOI: <https://doi.org/10.1016/j.wasman.2007.12.006>
- CCME (2001). *Canadian Water Quality Guidelines for the Protection of Aquatic Life*. Canadian Council of Ministers of the Environment, Winnipeg, Canada.
- CEA (2008). *Sri Lanka National Environmental (Protection and Quality) Regulations*, Central Environmental Authority, Colombo.
Available at: http://www.cea.lk/web/images/pdf/Waste_Water_Discharge_standards.pdf
- Chaudhary V., Kumar M., Sharma M. & Yadav B. (2010).

- Fluoride, boron and nitrate toxicity in ground water of northwest Rajasthan, India. *Environmental Monitoring and Assessment* **161**(1): 343–348.
DOI: <https://doi.org/10.1007/s10661-009-0750-y>
- Chen P.H. (1996). Assessment of leachates from sanitary landfills: Impact of age, rainfall, and treatment. *Environment International* **22**(2): 225–237.
- Christensen T.H., Kjeldsen P., Bjerg P.L., Jensen D.L., Christensen J.B., Baun A., Albrechtsen H.-J. & Heron G. (2001). Biogeochemistry of landfill leachate plumes. *Applied Geochemistry* **16**(7-8): 659–718.
DOI: [https://doi.org/10.1016/S0883-2927\(00\)00082-2](https://doi.org/10.1016/S0883-2927(00)00082-2)
- de Godoy Leme M.A. & Miguel M.G. (2018). Permeability and retention to water and leachate of a compacted soil used as liner. *Water, Air, and Soil Pollution* **229**(11): 1–19.
DOI: <https://doi.org/10.1007/s11270-018-4001-0>
- DeWalle F.B. & Chian E.S. (1981). Detection of trace organics in well water near a solid waste landfill. *Journal of American Water Works Association* **73**(4): 206–211.
- Eaton A., Clesceri L.S., Rice E.W., Greenberg A.E. & Franson M. (2005). APHA: standard methods for the examination of water and wastewater. *Centennial Edition., APHA, AWWA, WEF, Washington, DC.*
- El-Salam M.M.A. & Abu-Zuid G.I. (2015). Impact of landfill leachate on the groundwater quality: A case study in Egypt. *Journal of Advanced Research* **6**(4): 579–586.
- Esakku S., Karthikeyan O.P., Joseph K., Nagendran R., Palanivelu K., Pathirana K., Karunarathna A. & Basnayake B. (2007). Seasonal variations in leachate characteristics from municipal solid waste dumpsites in India and Srilanka. *Proceedings of the international conference on sustainable solid waste management* Anna University, Chennai, India, PP. 341–347.
- Giriappanavar B. & Patil R. (2013). Application of CCME WQI in assessing water quality of Fort Lake of Belgaum, Karnataka. *Indian Journal of Applied Research* **3**(4): 32–33.
- He P.-J., Xue J.-F., Shao L.-M., Li G.-J., & Lee D.-J. (2006). Dissolved organic matter (DOM) in recycled leachate of bioreactor landfill. *Water Research* **40**(7): 1465–1473.
DOI: <https://doi.org/10.1016/j.watres.2006.01.048>
- Ibezute A.C. & Erhunmwunse O. (2018). Assessment of Leachate Characteristics and Pollution Index of Ikhueni Dumpsite in Benin City, Edo State, Nigeria. *IOSR Journal of Environmental Science, Toxicology and Food Technology* **12**(6): 38 – 44.
- Ito T., Adachi Y., Yamanashi Y. & Shimada Y. (2016). Long-term natural remediation process in textile dye-polluted river sediment driven by bacterial community changes. *Water Research* **100**: 458–465.
DOI: <https://doi.org/10.1016/j.watres.2016.05.050>
- Jayaweera M. et al. (11 authors) (2019). Management of municipal solid waste open dumps immediately after the collapse: An integrated approach from Meethotamulla open dump, Sri Lanka. *Waste Management* **95**: 227–240.
DOI: <https://doi.org/10.1016/j.wasman.2019.06.019>
- Kjeldsen P., Barlaz M.A., Rooker A.P., Baun A., Ledin A. & Christensen T.H. (2002). Present and long-term composition of MSW landfill leachate: a review. *Critical Reviews in Environmental Science and Technology* **32**(4): 297–336.
DOI: <https://doi.org/10.1080/10643380290813462>
- Koliyabandara S., Asitha T.C., Sudantha L. & Siriwardana C. (2020). Assessment of the impact of an open dumpsite on the surface water quality deterioration in Karadiyana, Sri Lanka. *Environmental Nanotechnology, Monitoring and Management* **14**: 100371.
DOI: <https://doi.org/10.1016/j.enmm.2020.100371>
- Koliyabandara S., Cooray A., Liyanage S., & Siriwardana C. (2019). Characterisation of organic matter in karadiyana dumpsite leachate by fluorescence tracing and gas chromatography mass spectrometry (GCMS) studies. *Proceedings of the 6th International Conference on Multidisciplinary Approaches (iCMA)*, 3 December, Faculty of Graduate Studies, University of Sri Jayewardenepura.
- Kross B. (2002). Nitrate toxicity and drinking water standards—a review. *Journal Preventive Medicine* **10**(1): 3–10.
- Kulikowska D. & Klimiuk E. (2008). The effect of landfill age on municipal leachate composition. *Bioresource Technology* **99**(13): 5981–5985.
- Kumar D. & Alappat B. J. (2005). Analysis of leachate pollution index and formulation of sub-leachate pollution indices. *Waste Management and Research* **23**(3): 230–239.
DOI: <https://doi.org/10.1177/0734242X05054875>
- Kumarathilaka P., Jayawardhana Y., Basnayake B.F.A., Mowjood M.I.M., Nagamori M., Saito T., Kawamoto K. & Vithanage M. (2016). Characterizing volatile organic compounds in leachate from Gohagoda municipal solid waste dumpsite, Sri Lanka. *Groundwater for Sustainable Development* **2-3**: 1–6.
DOI: <https://doi.org/10.1016/j.gsd.2016.04.001>
- Lei L. & Aoyama I. (2010). Effect-directed investigation and interactive effect of organic toxicants in landfill leachates combining Microtox test with RP-HPLC fractionation and GC/MS analysis. *Ecotoxicology* **19**(7): 1268–1276.
- Logeshkumaran A., Magesh N., Godson P.S. & Chandrasekar N. (2015). Hydro-geochemistry and application of water quality index (WQI) for groundwater quality assessment, Anna Nagar, part of Chennai City, Tamil Nadu, India. *Applied Water Science* **5**(4): 335–343.
DOI: <https://doi.org/10.1007/s13201-014-0196-4>
- Mandakini L.L.U., Mannapperuma N., Bandara N.J.G.J., Silva, K.D.C.C.J. and Perera, M .T.C. (2016). Leachate characterization and assessment of surface water quality near Karadiyana solid waste dump site. *Proceedings of the Twenty first International Forestry and Environment Symposium*, Department of Forestry and Environmental Science, University of Sri Jayewardenepura, Sri Lanka. 231
- Mor S., Ravindra K., Dahiya R. & Chandra A. (2006). Leachate characterization and assessment of groundwater pollution near municipal solid waste landfill site. *Environmental Monitoring and Assessment* **118**(1): 435–456.
DOI: <https://doi.org/10.1007/s10661-006-1505-7>
- Rafizul I.M., Howlader M.K. & Alamgir M. (2012). Construction and evaluation of simulated pilot scale landfill lysimeter in

- Bangladesh. *Waste Management* **32**(11): 2068–2079.
DOI: <https://doi.org/10.1016/j.wasman.2012.02.008>
- Robinson H. (2007). The composition of leachates from very large landfills: an international review. *Communications in Waste and Resource Management* **8**(1): 19–32.
- Saadi I., Borisover M., Armon R. & Laor Y. (2006). Monitoring of effluent DOM biodegradation using fluorescence, UV and DOC measurements. *Chemosphere* **63**(3): 530–539.
DOI: <https://doi.org/10.1016/j.chemosphere.2005.07.075>
- Sewwandi B.G.N., Takahiro K., Kawamoto K., Hamamoto S., Asamoto S. and Sato, H. (2013). Evaluation of leachate contamination potential of municipal solid waste dumpsites in Sri Lanka using leachate pollution index. Proceedings of Fourteenth International Waste Management and Landfill Symposium. Sardinia, Italy 212–223.
- Sharma A., Meesa S., Pant S., Alappat B.J. & Kumar D. (2008). Formulation of a landfill pollution potential index to compare pollution potential of uncontrolled landfills. *Waste Management and Research* **26**(5): 474–483.
DOI: <https://doi.org/10.1177/0734242X07086515>
- Shouliang H., Beidou X., Haichan Y., Liansheng H., Shilei F. & Hongliang L. (2008). Characteristics of dissolved organic matter (DOM) in leachate with different landfill ages. *Journal of Environmental Sciences* **20**(4): 492–498.
- Stedmon C. A., Markager S. & Bro R. (2003). Tracing dissolved organic matter in aquatic environments using a new approach to fluorescence spectroscopy. *Marine Chemistry* **82**(3): 239–254.
DOI: [https://doi.org/10.1016/S0304-4203\(03\)00072-0](https://doi.org/10.1016/S0304-4203(03)00072-0)
- Stegmann R., Heyer K.U. and Cossu R., (2005). Leachate treatment. Proceedings of Tenth International Waste Management and Landfill Symposium. Sardinia, Italy.
- Tatsi A. & Zouboulis A. (2002). A field investigation of the quantity and quality of leachate from a municipal solid waste landfill in a Mediterranean climate (Thessaloniki, Greece). *Advances in Environmental Research* **6**(3): 207–219.
- Tränkler J., Visvanathan C., Kuruparan P. & Tubtimthai O. (2005). Influence of tropical seasonal variations on landfill leachate characteristics—Results from lysimeter studies. *Waste Management* **25**(10): 1013–1020.
- Trzcinski A.P. & Stuckey D.C. (2010). Treatment of municipal solid waste leachate using a submerged anaerobic membrane bioreactor at mesophilic and psychrophilic temperatures: analysis of recalcitrants in the permeate using GC-MS. *Water Research* **44**(3): 671–680.
- Umar M., Aziz H.A. & Yusoff M.S. (2010). Variability of parameters involved in leachate pollution index and determination of LPI from four landfills in Malaysia. *International Journal of Chemical Engineering*, **2010** Article ID 747953.
- Usero J., Morillo J. & Gracia I. (2005). Heavy metal concentrations in molluscs from the Atlantic coast of southern Spain. *Chemosphere* **59**(8): 1175–1181.
- Wang L.-S., Hu H.-Y. & Wang C. (2007). Effect of ammonia nitrogen and dissolved organic matter fractions on the genotoxicity of wastewater effluent during chlorine disinfection. *Environmental Science and Technology* **41**(1): 160–165.
DOI: <https://doi.org/10.1021/es0616635>
- WHO (2011). Guidelines for drinking-water quality. *WHO Chronicle* **38**(4): 104–108.
- Wijesekara S., Mayakaduwa S.S., Siriwardana A., de Silva N., Basnayake B., Kawamoto K. & Vithanage M. (2014). Fate and transport of pollutants through a municipal solid waste landfill leachate in Sri Lanka. *Environmental Earth Sciences* **72**(5): 1707–1719.
- Yamashita Y. & Tanoue E. (2003). Chemical characterization of protein-like fluorophores in DOM in relation to aromatic amino acids. *Marine Chemistry* **82**(3): 255–271.
DOI: [https://doi.org/10.1016/S0304-4203\(03\)00073-2](https://doi.org/10.1016/S0304-4203(03)00073-2)
- Ye X., Robinson M. B., Pabin C., Quinn T., Jawad A., Wilson J. M. & Batshaw M. L. (1997). Adenovirus-mediated in vivo gene transfer rapidly protects ornithine transcarbamylase-deficient mice from an ammonium challenge. *Pediatric Research* **41**(4): 527–534.
- Zhang Q.-Q., Tian B.-H., Zhang X., Ghulam A., Fang C.-R. & He R. (2013). Investigation on characteristics of leachate and concentrated leachate in three landfill leachate treatment plants. *Waste Management* **33**(11): 2277–2286.
DOI: <https://doi.org/10.1016/j.wasman.2013.07.021>
- Zhang W., Feng H., Chang J., Qu J., Xie H. & Yu L. (2009). Heavy metal contamination in surface sediments of Yangtze River intertidal zone: An assessment from different indexes. *Environmental Pollution* **157**(5): 1533–1543.
DOI: <https://doi.org/10.1016/j.envpol.2009.01.007>

RESEARCH ARTICLE

Environmental Engineering

Optimization of high solids batch anaerobic co-digestion of lignocellulosic biomass and cow dung under mesophilic temperature conditions

A.L. Wickramaarachchi^{1*}, P.G. Rathnasiri¹, M. Torrijos (Late)², Renaud Escudie² and M. Narayana¹

¹Dept. of Chemical and Process Engineering, University of Moratuwa, Moratuwa.

²INRAE, Univ Montpellier, LBE, 102 avenue des Etangs, Narbonne, France.

Submitted: 4 January 2021 ; Revised: 05 September 2021; Accepted: 24 September 2021


Abstract: Anaerobic digestion is applied to recover energy from rice straw (RS) which is a lignocellulosic agricultural residue produced in huge quantities in Asia and Africa. Because of the high solids content of this feedstock, high solids anaerobic co-digestion in batch mode must be further investigated. In this study, optimal operating conditions for the anaerobic co-digestion of RS with cow dung (CD) in batch mode, with and without leachate recirculation, were assessed under mesophilic temperature conditions. Preliminary experiments carried out in 2 L batch reactors confirmed that the concentration of RS in the mixture of substrates S_0 , in g VS_{RS}/kg of mixture is an important parameter. Only batch reactors with the lowest S_0 values (29 g VS_{RS}/kg) produced biogas and rest of the reactors followed a long lag phase. The use of digestate from a previous batch as an inoculum was investigated with S_0 values of 29 and 55 g VS_{RS}/kg . Use of the digestate with S_0 of 29 g VS_{RS}/kg improved both initial degradation kinetics and the methane yield measured after 60 days. However, at S_0 of 55 g VS_{RS}/kg , the degradation kinetics were affected and after two months, 32 % of the biodegradable organic matter could not be eliminated. When leachate recirculation was performed in 6L leach-bed reactors (LBRs) with S_0 between 30 and 65 g VS_{RS}/kg , the highest methane yield was recorded at the lowest S_0 value. It can be concluded that under batch mode, an RS concentration around 30 g VS_{RS}/kg may be recommended for industrial applications.

Key words: High solids anaerobic co-digestion, leachate recirculation, lignocellulosic biomass, mesophilic.

INTRODUCTION

Rice straw (RS) is a lignocellulosic agricultural residue that is widely produced, particularly in Asia and Africa. RS is a dry material with a very high total solids (TS) and volatile solids (VS) content (He *et al.*, 2008; Contreras *et al.*, 2012) with cellulose, hemicellulose and lignin as its main components (Liotta *et al.*, 2015; Hills & Roberts, 1981). Cellulose and hemicellulose are its principal biodegradable components but the complex lignocellulosic structure and relatively high lignin content (*i.e.*, 10-15 % dry weight) increase its resistance to anaerobic biodegradation (Mussoline *et al.*, 2011; Brown *et al.*, 2012). Methane generation potentials ranging from 92 to 280 L/kg of VS have been reported in the literature for RS (Mussoline *et al.*, 2011; Achinas *et al.*, 2016) with or without pretreatment under different inocula.

The high C:N ratio of rice straw indicates a potential risk of insufficient nitrogen for bacterial growth in the case of mono-digestion of RS. Thus an external source of nitrogen is essential for the effective digestion of RS. Optimal digestion conditions, such as pH (6.5 - 8.0), temperature (35 - 40 °C), and nutrients [C:N ratio of (25-35):1] are critically important for stable anaerobic

* Corresponding author (ayeshlakshithaw@gmail.com  <https://orcid.org/0000-0002-3289-1632>)



This article is published under the Creative Commons CC-BY-ND License (<http://creativecommons.org/licenses/by-nd/4.0/>). This license permits use, distribution and reproduction, commercial and non-commercial, provided that the original work is properly cited and is not changed in anyway.

conversion (Mussoline *et al.*, 2011). In addition to limited moisture and nitrogen content, lignocellulosic biomass such as RS also possesses low micronutrient content. Micronutrients such as Fe and Ni are critical for enzymatic activity and the micronutrient deficiency can lead to failure of the anaerobic digestion (AD) process. Thus, the anaerobic co-digestion (AcoD) of RS is essential to overcome the problems associated with its mono-digestion (Khalid *et al.*, 2011; Hagos *et al.*, 2016). Several researchers have listed the benefits ensuing from AcoD; these include enhanced process stability, increase of methane yield, dilution of inhibitory substances, nutrient balance, adjustment of the required solids content in digester feeding, the synergetic effects of microorganisms, and an increase in the organic loading rate (Shah *et al.*, 2015; Ge *et al.*, 2016; Neshat *et al.*, 2017; Guven *et al.*, 2018). For example, the high-solids anaerobic co-digestion (HS-AcoD) of food waste (FW) and straw (maize, sorgo, and wheat) at mesophilic temperatures showed a 39.5 % increase in the methane yield of FW and a 149.7 % increase from straw compared to their mono-digestion (Yong *et al.*, 2015). In a study conducted by Brown *et al.* (2013), the HS-AcoD of food waste and yard waste also gave a 20 % increase in volumetric methane production.

Both wet anaerobic digestion (*i.e.*, TS content < 10–12 %) and high-solids anaerobic digestion (HS-AD) with TS content \geq 10–12 % (Abbassi-Guendouz *et al.*, 2012) can be used in the AcoD of rice straw. However, HS-AD has attracted increasing attention in recent years, especially for the digestion of lignocellulosic biomass such as wheat or rice straw. This is due to less consumption of water, no or only slow-moving parts for mixing, a lower energy requirement for heating and mixing, and easy handling of the end product (Li *et al.*, 2011; Brown *et al.*, 2012). In addition, problems arising in wet AD such as the floating and stratification of fats and fibers do not occur in HS-AD (Chanakya *et al.*, 1999).

On the other hand, poor start-up performance, incomplete mixing, the accumulation of volatile fatty acids (VFAs), a relatively low methane yield, and potential instability are considered as significant disadvantages of HS-AD of lignocellulosic biomass (Jha *et al.*, 2011; Shi *et al.*, 2013; Yang & Li, 2014; Liotta *et al.*, 2015;). Low methane yield from HS-AD can be caused by the recalcitrance of lignocellulosic biomass and by mass transfer limitations within the digester content, leading to reduction in the rate of hydrolysis, which is the rate limiting step in HS-AD of lignocellulosic feedstock. Moisture content is a critical factor in facilitating mass transfer. In HS-AD, the high solids content implies high heterogeneity that leads to slow mass transfer between microbes and substrates, resulting in possible slow

methane production and low methane yield (Kalyuzhnyi *et al.*, 2000; Bollon *et al.*, 2013; Liotta *et al.*, 2015). A high TS content of 30–35 % may even hinder solid-liquid-gas transfer, leading to accumulation of carbon dioxide (CO₂) and hydrogen (H₂) that inhibit methanogens (Bollon *et al.*, 2011).

Both continuous and batch reactors can be operated under HS-AD conditions. Continuous processes dominate among HS-AD systems treating municipal solid waste (MSW) but they are not widely applied to the processing of lignocellulosic biomass, due to mixing techniques which are not suited to HS-AcoD of lignocellulosic biomass (Li *et al.*, 2011; Degueurce *et al.*, 2016). HS-AcoD of lignocellulosic biomass such as RS presents a number of advantages when running in batch mode: relative simplicity, minimum maintenance requirement, low energy consumption, minimum capital cost. However, operating conditions of such reactors, such as temperature, pH, buffering capacity, inoculation, and control of VFAs concentration still need to be optimized in order to maximize the biogas production during a shorter retention time.

Experimental strategies such as re-use of digestate and leachate recirculation have been applied in various studies for different types of waste, including food waste and spent animal bedding. Treated spent animal bedding in batch reactors with leachate recirculation, also known as leach-bed reactors (LBRs) showed that LBRs could achieve an average of 89 % \pm 11 % of the bio-chemical methane potential (BMP) after 60 days of operation (Chugh *et al.*, 1998; Michele *et al.*, 2015; Shah *et al.*, 2015; Riggio *et al.*, 2016, 2017). According to a study conducted by using food waste as the substrate, Gottardo *et al.* (2017) found that proper leachate recirculation could control the pH value of the reactor above 5, which is important at the initial phase of the anaerobic digestion process to control acidification. Wilson *et al.* (2016) conducted anaerobic co-digestion of food waste and yard waste (leaves and grass clippings) in LBRs by combining leachate recirculation with re-use of digestate (~10 % by mass). They observed the enhancement of methane due to improvement of hydrolysis. When evaluating all these studies, authors considered basically the TS content within the reactor for the HS-AD process. But VS concentration of the highly acid producing substrate at the initial stages of the HS-AcoD process is a key parameter, as most of the reactors fail during first few days of operation.

In this study, anaerobic digestion of RS using cow dung (CD) as a co-substrate was investigated in batch mode, both with and without leachate recirculation. The aim was to define the optimal conditions to be used for

HS-AcoD of RS and CD in batch mode for application on an industrial scale. In the first part, initial conditions were studied in order to define the optimal RS and CD ratio by mass for the initiation of HS-AcoD process and continual operation, more specifically the influence of initial RS concentration (S_0). Then the digestate was reused in successive batches, and finally, experiments were conducted in batches, with leachate recirculation, in LBRs.

MATERIALS AND METHODS

Substrates

Rice straw (RS) and cow dung (CD) were used as substrates in this study. These were collected from two different farms located in the South of France. Rice straw was ground into 30-40 mm pieces using a 3 kW Blick BB230 shredder.

Experimental setups and operation

Batch reactors without leachate recirculation

All batch experiments were carried out in 2 L glass bottles. The bottles were sealed after introducing the substrate mixtures and maintained at 35 °C without agitation. All batch experiments were duplicated. Each reactor was connected to a gas collection bag (Tedlar bag, Zefon International, Inc.) in order to collect and store the biogas produced. Biogas volume in gas collection bags was measured regularly using the water displacement method. For all the reactors, the parameters monitored were biogas volume and composition. At the end of the digestion period, TS and VS concentrations of the digestate and VFA concentrations were measured.

In a preliminary experimental set-up (see Appendix 1), different mixture ratios of RS and CD were evaluated to modify the initial TS contents from 15 to 36 % and the

initial VS concentration of RS (S_0) (g VS of rice straw per kg mixture (g VS_{RS}/kg)) from 29 to 232 g VS_{RS}/kg .

The effect of inoculation on the HS-AcoD of RS and CD was investigated by re-using the digestate from one batch to the next one. Three successive batch reactors named Batch 1, Batch 2 and Batch 3 were operated using different substrate quantities, and the compositions are as shown in Table 1. Batch 1 was operated without an external source of inoculum, and operating conditions of this reactor is similar to the reactor that produced methane in the preliminary experiment (see Appendix - 1). At the end of the digestion period, digestate recovered from the Batch1 reactors was used as an inoculum source for Batch 2 reactors; similarly, digestate recovered from Batch 2 reactors was used as the inoculum for Batch 3 reactors. In Batch 1 and Batch 2 reactors, initial TS content of the mixture was 15 % and 16 %, respectively. Initial VS concentration of RS (S_0) in the mixture was same (29 g VS_{RS}/kg) in these two reactors. In Batch 3 reactor, both TS content and S_0 were increased to 20 % and 55 g VS_{RS}/kg , respectively.

Leach-bed batch reactors

Four leach-bed batch reactors (LBRs) made of glass (14.5 cm internal diameter, 45 cm high) with a working volume of 6 L were used (Riggio *et al.*, 2017). In order to retain the leachate at the bottom of the each reactor, the solid and liquid fractions were kept apart by a mesh (1 mm holes) placed at 10 cm up from the bottom of the reactor. Leachate was re-circulated using a peristaltic pump. In order to equalize the pressure between the two compartments, the headspace and the volume below the mesh were connected by using a tube. Each reactor was connected to a water bath and temperature was kept at 35 °C by recirculating water through the jacket. Each reactor was also equipped with a Ritter gas flow meter (MGC-1 V3.1 Milligascounter) to automatically measure the biogas volumes, and a gas collection port

Table 1: Experimental conditions for successive batches

	Batch 1	Batch 2	Batch 3
RS (g)	25	25	50
CD (g)	650	350	480
Solid digestate (g)	-	300	190
Initial TS content of mixture (%)	15	16	20
S_0 (g VS_{RS}/kg)	29	29	55

was available in each reactor to collect biogas for subsequent composition analysis. A leachate collection port was connected to the leachate stock of each reactor in order to collect leachate for pH measurement and VFA analysis (Riggio *et al.*, 2017).

Inoculation and leachate preparation

Solid and liquid fractions of digestate were collected from a batch digester installed at a farm which uses lignocellulosic substrate and cow manure as the feedstock for the first LBR experiment. This digestate was used as the inoculum and for liquid recirculation. The TS and VS content of the solid fraction of the digestate were 17.0 % and 11.8 %, respectively. The TS and VS content of the liquid fraction of the digestate were, 4.5 % and 2.6 % respectively, and alkalinity, total VFA concentration, and pH were 17.9 g CaCO₃/L, 743 mg COD-VFA/L, and 8.5, respectively. The leachate used for recirculation within the LBRs was prepared by mixing the liquid fraction of the digestate with water at a ratio of 1:1 by Volume.

Operating conditions

Two sets of experiments were carried out using LBRs. In the first set, four 6 L leach-bed reactors were used. The first three reactors were run with different quantities of rice

straw in order to increase the initial VS concentration of rice straw (S_0). Rice straw, cow dung and solid digestate were mixed together to obtain initial S_0 concentrations in each reactor of 30, 36, and 47 g VS_{RS}/kg, and an initial TS content of around 12.5 %. Substrate-to-inoculum (S/I) ratios in a VS basis (rice straw VS mass / solid digestate VS mass) were 0.7, 1 and 2, respectively (Table 2). The fourth reactor was operated only with digestate and served as a control reactor.

After filling each reactor with the prepared mixture of substrate, a 7 kg weight was applied to the top of each substrate mixture for 10 min in order to reduce its bulk volume. Then the reactors were closed and, the leachate was re-circulated through the top of the reactors for 5 min using a peristaltic pump to saturate the bulk volume with water. No further leachate recirculation was carried out in the control reactor. For other three reactors, leachate recirculation was set automatically, once in every 12 h at a rate of 600 mL/min for 2 mins. After 55–60 ds, all the reactors were opened and the solid digestate and leachate samples were collected.

The solid digestate obtained from each reactor of the first set-up, except from the control reactor, were mixed together with RS and CD to prepare mixtures of substrate and inoculum for the second set of LBR experiments. For

Table 2 : Quantities of substrate, digestate and water added for first and second LBR experiments

Reactor	1 st LBR experiment (P-1)				2 nd LBR experiment (P-2)			
	1-(1)	1-(2)	1-(3)	1-(4) (Control)	2-(1)	2-(2)	2-(3)	2-(4) (Control)
RS (g)	132	156	205	0	205	250	300	0
CD (g)	450	600	778	0	771	900	1000	0
Solid digestate (g)	1262	1044	686	2500	779	950	1139	2865
Liquid digestate (g)	820	830	900	500	850	760	615	500
Water (g)	820	830	900	500	850	760	615	500
S_0 (g VS _{RS} /kg)	30	36	47	0	47	55	65	0
Global TS content (%)	12.3	12.5	12.7	12.8	13	14.7	16.9	10.8
S/I (VS mass rice straw/VS mass solid digestate)	0.7	1	2	-	2	2	2	-

the first three reactors, solid digestate recovered from first LBRs experiment, RS and CD were mixed together to obtain initial rice straw VS concentration (S_0) values of 47, 55, and 65 g VS_{RS}/kg , respectively. Initial TS content and S/I ratio (VS basis) were kept at 13–17 % and 2, respectively, for the three reactors (Table 2). The remaining digestate was used for the fourth reactor which was operated as the control reactor. Operations, monitoring and analysis were carried out in a manner similar to previous experimental setup.

Analytical methods and experimental protocols

The total solids (TS) and volatile solids (VS) content, as well as the alkalinity of the substrates and digestate were measured in accordance with the APHA standard methods (APHA, 2005). Triplicates of each substrate sample were taken in order to obtain average values of TS and VS percentages.

Biochemical methane potentials (BMPs) of rice straw and cow dung were evaluated using a protocol described by Riggo *et al.* (2017).

For all experiments, biogas composition was analyzed using gas chromatography (GC Perkin 580) in which argon gas was used as the carrier gas. For the LBRs, pH of the leachates collected at leachate collection ports were measured using a pH probe. VFAs were analyzed using gas chromatography (Perkin-Elmer Clarus 580 GC) with N_2 as the carrier gas.

RESULTS AND DISCUSSION

At the beginning, both rice straw (RS) and cow dung (CD) were characterized. TS and VS contents of RS were 92.8 % and 79.4 % respectively and 12.3 % and 10.6 % respectively for CD. BMP of RS and CD were 254 ± 11 and 173 ± 1 NmL/g VS. The BMP value of RS was almost 50 % higher compared to that of CD. This lower BMP value of CD indicates that the biodegradable volatile-solids fraction in the CD was lower than that in the RS. It can be determined that a certain fraction had already been digested via the digestive system of the cows.

Co-digestion of RS and CD in batch reactors

The main objective of conducting batch anaerobic digestion in preliminary experiments (Appendix 1) was to evaluate the inoculation efficiency of cow dung and understand the effect of the initial VS concentration (S_0) of rice straw for HS-AcoD process of lignocellulosic biomass.

Only the reactor operated with the lowest S_0 of 29 g VS_{RS}/kg produced biogas. High substrate concentrations and particularly high RS concentrations, led to digester failure by acidification. In addition, it was observed that the effectiveness of cow dung as a source of inoculum was rather poor as this reactor had a 15-day lag phase and quite low degradation rates. Three successive batches were treated under the operating conditions presented in Table 1. In order to evaluate the effect of inoculation, digestate from the 15 %TS reactor (Batch 1) was re-used as an inoculum for a Batch 2 reactor whose operating conditions remained very similar to Batch 1 (*i.e.*, TS content of 16 % and the same S_0 concentration of 29 g VS_{RS}/kg). For the Batch 3 reactor, digestate of the Batch 2 reactor was re-used as inoculum, but a higher TS content of 20 % and a higher S_0 concentration of 55 g VS_{RS}/kg were maintained in order to investigate the impact of higher S_0 concentrations.

Figure 1 (a) and 1 (b) present, respectively, the evolution of methane production and the methane yield over time for the three successive batches. Methane production in each reactor was corrected by deducting the contribution to methane production by the digestate alone. To normalize methane yield in each reactor it was calculated based on the quantity of volatile solids added from the substrates to each reactor. Therefore, VS added in the calculation consists only of VS from RS and CD.

In Batch 2 reactor, almost 50 % of the cow dung in the initial mixture was replaced by digestate from the first batch. The re-use of digestate as an inoculum enhanced the anaerobic digestion performance. The lag-phase period was drastically reduced, from 15 ds to almost 0 ds (Figure 1), and a 103 % increase in the methane yield was achieved.

From the individual BMP values of RS and CD, the expected cumulative methane volume and methane yield of the second batch were 11.1 L and 202.7 mL CH_4 / g VS, respectively, compared with the experimental values of 12.1 L and 221.8 mL CH_4 / g VS, respectively. The difference between the expected and actual values was less than 10 % for both parameters. This suggests that all the added biodegradable VS had been eliminated under the experimental conditions of the second batch.

In the Batch 3 reactor, both TS % and S_0 were increased compared to Batch 1 and Batch 2 reactors. However, compared to the Batch 2 reactor, only an 18 % increase in total methane production was observed after almost two months. As a consequence, the methane yield was much lower in the Batch 3 reactor compared to the Batch 2 reactor. The expected methane yield calculated

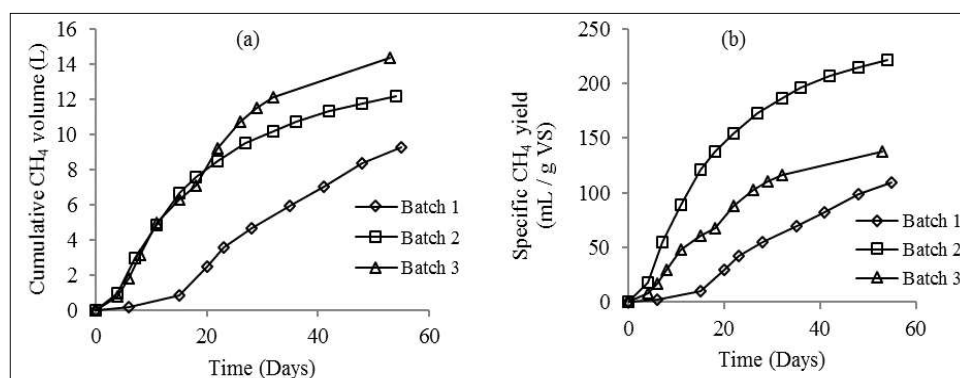


Figure 1: Evolution of cumulative CH_4 (a) and specific methane yield (b) over time of 2 L batch reactors, for the three successive batches

for the Batch 3 reactor was 203.6 mL CH_4 /g VS whereas the experimental value was 137.7 mL CH_4 /g VS which indicates that only 68 % of the biodegradable organic matter had actually been degraded. This lower methane production in the Batch 3 reactor can be explained by two factors: the higher TS concentration of the initial mixture and the higher initial RS concentration (S_0). In the first part it has been shown that the initial VS concentration of rice straw within the substrate mixture is a critical parameter and in the Batch 3 reactor this concentration was too high, i.e., 55 g VS_{RS} /kg. Furthermore, data from the literature suggests that an increase in the TS concentration of the digestate could lead also to a negative impact on the performance of anaerobic digestion.

Abbassi-Guendouz *et al.* (2012) investigated the effects of TS on AD by using cardboard as a substrate and found that the VS-based methane production rate decreased when the reactor TS increased from 10 % to 35 %. Similarly, Motte *et al.* (2013), using wheat straw as a substrate, also showed declining VS-based methane production rate as TS increased from 15 % to 25 %. Xu *et al.* (2014) also investigated the effect of TS content on the anaerobic digestion of rice straw and found that when TS % varied between 15 % to 20 %, methane production rate increased. When exceeding this threshold limit, it decreases. TS content is a key parameter that affects the mass transfer between gas-liquid-solid phases in HS-AcoD. This parameter affects the rate of substrate degradation and the accumulation of inhibitors such as VFAs (Abbassi-Guendouz *et al.*, 2012; Xu *et al.*, 2014; Liotta *et al.*, 2015). TS content has been assumed to affect the hydrolysis rate constant, the maximum microbial growth rate and diffusion constant as well (Xu *et al.*, 2014).

In conclusion, the results obtained from the batch experiments including preliminary experiments

suggested that not only the TS content, but the initial rice straw VS concentration (S_0) is also a critical parameter, which leads to acidification and failure of the reactors. Thus it is suggested that initial S_0 values should not exceed 30 g VS_{RS} /kg.

Co-digestion of RS and CD in leach bed reactors

Leachate re-circulation is a strategy that has been using in high-solids batch anaerobic digestion to control production of VFAs at start-up in reactors known as LBRs. From the physico-chemical point of view, leachate recirculation is used to increase the moisture content of the bulk of the substrate, thereby improving mass transfer and access to organic matter (Chanakya *et al.*, 1999; Jha *et al.*, 2011). Leachate recirculation leads to leaching out the VFAs produced, to diluting inhibitor compounds, and to increasing the buffer capacity of the medium. From a biological point of view, increasing moisture content improves the growth of microorganisms (Batstone *et al.*, 2002). This will result in higher biodegradation of lignocellulosic substrates. Furthermore, the re-use of digestate facilitates improvement of the start-up of the reactor because it was possible to recycle already acclimatized biomass to the substrate.

In this study, two sets of experiments were carried out to investigate the effect of leachate re-circulation and the initial RS concentration, on the high-solids anaerobic co-digestion of RS and CD in LBRs. In the first set of experiments, three conditions were tested with initial rice straw VS concentrations (S_0) at 30, 36 and 47 g VS_{RS} /kg (Table 2). In the second set of experiments, initial rice straw VS concentrations of 47, 55 and 65 g VS_{RS} /kg were tested (Table 2). The maximum reaction time for all conditions was fixed at 60 days. In these experiments, the quantities of RS and CD were increased but the proportion of RS and CD in terms of VS remained very close, with

rice straw VS representing on average 67.4 ± 1.3 % for the six mixtures used. As a result, the accumulated volume of methane produced from RS represented 75.2 ± 1.1 % of the expected total volume of methane produced and the average expected methane yield of the mixtures was 228 ± 1 mL CH₄/g VS. The only difference between the two sets of experiments was the digestate used for inoculation. In the first experiments, digestate was sampled from an industrial-scale LBR whereas, for the second experiment, digestate collected at the end of the first experiment was used.

Methane production

Figure 2 (a) and 2 (b) present the total volume of methane produced by the LBRs and the methane yield, respectively, as a function of the initial VS concentration of rice straw (S_0). The initial RS concentration was selected to plot these curves due to three reasons: (i) 75 % of methane volume is produced from RS; (ii) organic matter of RS has the highest degradation kinetics; and (iii) it was shown previously in batch mode that the initial VS concentration of rice straw (S_0) is a critical parameter in reactor acidification and failure.

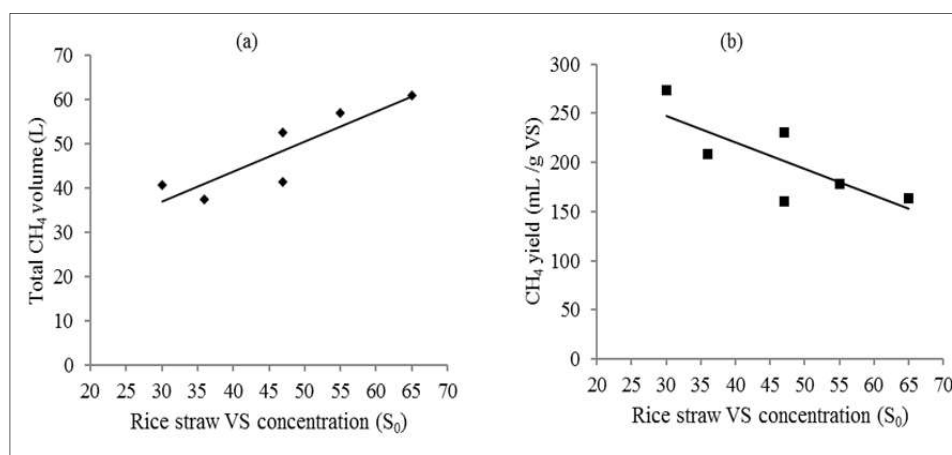


Figure 2: Evolution of the total volume of CH₄ produced (a) and of the specific methane yield (b) over the quantity of rice straw VS added for the experiments in LBRs

Figure 2 (a) shows that total methane production increased with increasing S_0 values. However, this increase was not proportional to the added quantity of VS. For example, if the two extreme values are compared, only an additional 50 % of CH₄ was produced when the initial RS quantity was doubled. As a consequence, the methane yield decreased when S_0 was increased. For the lowest quantities of substrate added, the methane yield observed in LBRs (240 ± 32 mL CH₄/g VS) was close to the BMP of the mixtures calculated from the BMP of RS and CD (228 ± 1 mL CH₄/g VS) whereas, for the highest substrate load, the methane yield was only 70 % of the expected value, indicating that during the two months period, all the organic matter added was not degraded.

VFAs concentration, pH and alkalinity

Total concentration of VFAs and pH were measured regularly in the liquid fraction, *i.e.*, leachate of each reactor. Figure 3 presents the variation of total VFA and

pH throughout the digestion period. VFAs production was high at the beginning of the batch experiments indicating that methanogenesis was slower than acidogenesis.

The maximum total concentration of VFAs in each reactor was reached after 5-6 days of operation, ranging between 6000 and 12000 mg COD-VFA/L (Figure 3 (a) and 3 (c)). At the same time, pH decreased as shown in Figure 3 (b) and 3 (d) but always remained above 6.6 due to the high alkalinity of the mixture of digestate and substrates (above 8.3 g CaCO₃/L).

VFA concentrations of the leachate dropped rapidly to almost 0 mg/L before day 20. Several authors have reported similar behaviors. Mussoline *et al.* (2012) have observed an initial peak of VFA in terms of acetic acid (3375 mg HAc/L) which occurred at the beginning of the experiment on dry AD of rice straw and piggery wastewater. In this study, at day 57, VFA concentration dropped below 200 mg HAc/L. Similar observations

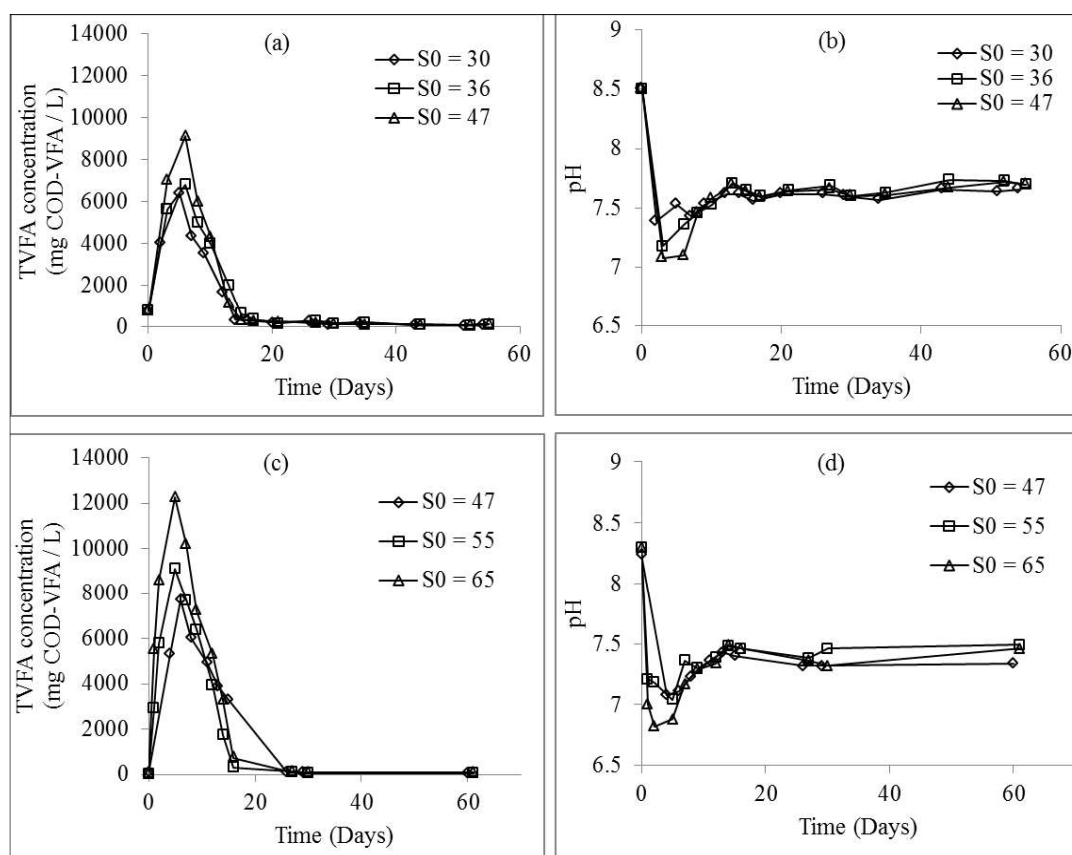


Figure 3: Total VFA and pH variation in the first (a and b) and second (c and d) LBR experiments, over time

could be found in the study on hybrid solid anaerobic digestion of the organic fraction of municipal solid waste conducted by Massaccesi *et al.* (2013). From these results, the stable operation of the reactors and the optimization of the leachate recirculation time period can be identified as highly important factors when these types of reactors are operated on a large scale.

Effect of leachate re-circulation

In order to evaluate the influence of leachate recirculation, results obtained without recirculation in pure batches, *i.e.*, 2 L bottles of successive batches and with recirculation in 6 L LBRs were compared at two initial RS concentrations of 30 and 55 g VS_{RS}/kg . In terms of methane yield, the performances observed in LBRs were slightly better than those in 2 L batch reactors without recirculation. In terms of specific methane yields, it was 273 mL CH_4/g VS in the LBR compared to 222 mL CH_4/g VS in the 2 L batch reactor (a 23 % increase) at 30 g VS_{RS}/kg ; and 179 mL CH_4/g VS in the LBR compared to 138 mL CH_4/g VS in the 2 L batch reactor (a 30 % increase) at 55 g VS_{RS}/kg . Specific methane production rates are shown in Figure 4. At S_0 of 30 g VS_{RS}/kg , specific methane production rates

were slightly higher in the LBR compared to the batch reactor at the beginning of the operation. However, after 1 month of operation, the slowly-biodegradable organic matter had similar rates of degradation. At S_0 of 55 g VS_{RS}/kg , rates were quite close except during the period 10 - 20 days, during which lower rates were reported for the batch without recirculation. This is due to some partial inhibition in that period resulting from VFA production and a drop in pH. After day 20, rates once again showed similar trends.

As already shown, both specific methane production rates and specific methane yields dropped with the increase of initial rice straw VS concentration. In conclusion, leachate recirculation slightly improved both performance and stability of the reactors, but operation in a pure batch still remained possible under the operating conditions applied.

Optimal operating conditions for LBRs

From the results obtained in the two sets of experiments with LBRs, it was possible to assess the optimal operating conditions of LBRs treating a mixture of RS

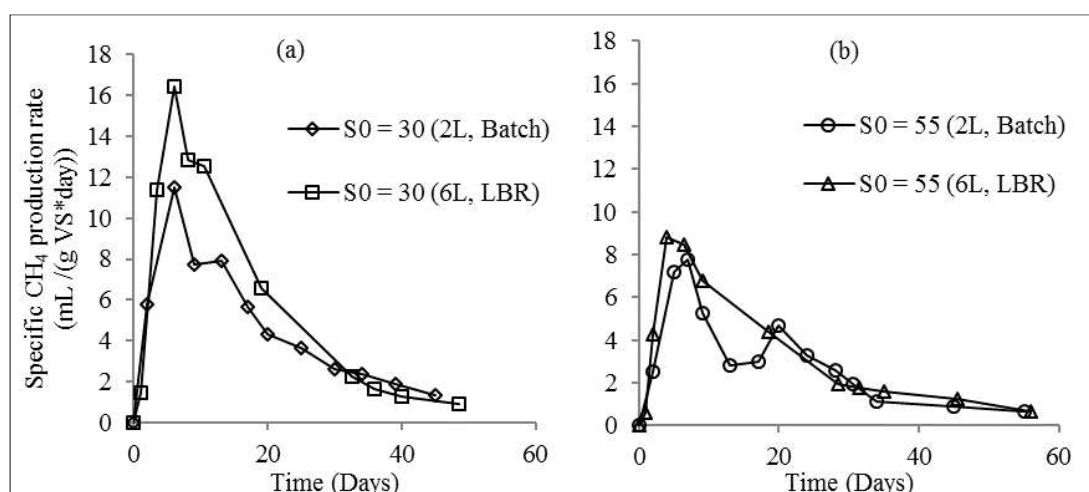


Figure 4: Specific methane production rates: comparison of 2 L batch reactors and 6 L LBRs that have S_0 (a) value of 30 and (b) 55 g VS_{RS}/kg

and CD. Figure 5 clearly demonstrates that the maximum total VFA concentration increased with the increase of initial rice straw concentration (S_0); however reactors were operated safely even at higher S_0 . This is due to the buffering capacity provided by the leachate and the washout of VFAs by leachate recirculation. However, use of higher initial RS concentrations might have led to potential inhibition at the beginning of the batch. It could be noted that the maximum total concentration of VFAs measured at the beginning of the batch with a S_0 of 65 g VS_{RS}/kg was 12,200 mg COD-VFA/L and the minimum pH was 6.82, which is close to the critical value for methanogenesis inhibition of 6.6 (Batstone *et al.*, 2002; Mussoline *et al.*, 2011)

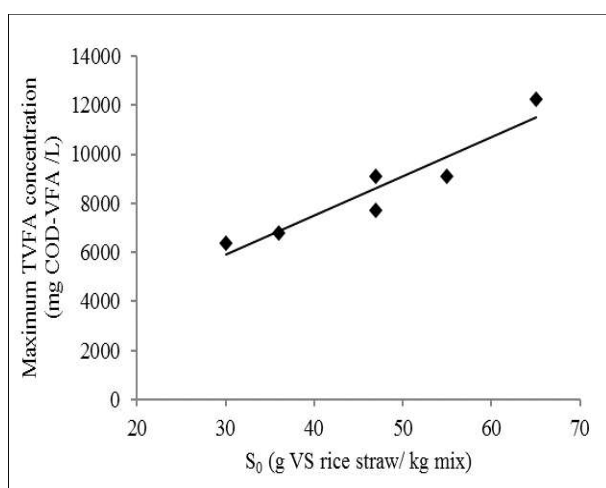


Figure 5: Maximum total volatile fatty acids concentration in LBRs with initial VS concentration of rice straw (S_0)

Furthermore, specific methane yield decreased as substrate loads increased (Fig. 2 (b)) and VS removal for the highest substrate load was only 70 % of the calculated value after two months of operation. As a result, in order to obtain optimal methane production in LBRs, along with the maximal VS reduction and operational safety, the recommended initial RS concentration S_0 in the mixture should be at a maximum of 30 g VS_{RS}/kg.

The results obtained in this study also suggest that leachate recirculation can be stopped after 15 days of operation as total VFA production at this time had drastically decreased and the accumulated VFA concentration was below 740 mg COD-VFA/L, even for the highest substrate load. André *et al.* (2015) also found that during the dry AD of cattle manure, leachate recirculation had no effect on methane production rates after 19 days of degradation.

CONCLUSIONS

In this study, the anaerobic co-digestion of mixtures of rice straw and cow dung was studied both in pure batch reactors and batch reactors with leachate recirculation. Preliminary experiments carried out with RS and CD alone at different initial concentrations showed a high risk of acidification at the higher substrate concentrations and low efficiency and effectiveness of cow dung as a source of inoculum. Therefore, two strategies were investigated: first, the re-use of digestate for inoculation in the pure batches and, second, leachate recirculation using leach-bed reactors (LBRs). When the digestate from a previous batch is used as an inoculum, the lag phase for

methane production in batch was reduced from 15 days to almost none and the specific methane production rates increased significantly. Furthermore, after 55 days of digestion, a 103 % increase of the cumulative volume of methane produced was achieved in 16 % TS batch reactors ($S_0 = 29$) operated with the digestate re-use strategy, compared to the reactor fed only with a mixture of rice straw and cow dung. In terms of methane yield, the performances observed in LBRs were slightly better than those in the batch reactors with a 23 % increase for the S_0 of 30 g VS_{RS}/kg and 30 % increase for the S_0 of 55 g VS_{RS}/kg. However, specific methane yields and specific methane production rates dropped with the increase of lignocellulosic substrate concentration within the reactors. For optimal methane production in batch and in LBRs, as well as for operational safety, initial RS concentration in the mixture S_0 should be at a maximum of 30 g VS rice straw/ kg mixture. Therefore, further investigations should be conducted to ascertain the threshold values (*i.e.*, TS content and S_0) for optimizing the HS-AcoD of lignocellulosic biomass.

Acknowledgement

Authors would like to acknowledge senate research grant University of Moratuwa Sri Lanka, French Embassy of Sri Lanka, INRAE-LBE Narbonne, France and Campus France for providing all necessary funding and facilities to undertake the research work.

REFERENCES

- Abbassi-Guendouz A., Brockmann D., Trably E., Dumas C., Delgenès J.P., Steyer J.P. & Escudé R. (2012). Total solids content drives high solid anaerobic digestion via mass transfer limitation. *Bioresource Technology* **111**: 55–61. DOI: <https://doi.org/10.1016/j.biortech.2012.01.174>
- Achinas S. & Euverink G.J.W. (2016). Theoretical analysis of biogas potential prediction from agricultural waste. *Resource-Efficient Technologies* **2**(3): 143–147. DOI: <https://doi.org/10.1016/j.reffit.2016.08.001>
- André L., Durante M., Pauss A., Lespinard O., Ribeiro T. & Lamy E. (2015). Quantifying physical structure changes and non-uniform water flow in cattle manure during dry anaerobic digestion process at lab scale : Implication for biogas production. *Bioresource Technology* **192**: 660–669. DOI: <https://doi.org/10.1016/j.biortech.2015.06.022>
- APHA (2005). *Standard Methods for the Examination of Water and Wastewater*, 21st. American Public Health Association, Washington, DC. USA.
- Batstone D.J., Keller J., Angelidaki I., Kalyuzhnyi S.G., Pavlostathis S., Rozzi A., Sanders W., Siegrist H. & Vavilin V. (2002). Anaerobic digestion model no. 1. *Water Science and Technology* **45**(10): 65–73. DOI: <https://www.researchgate.net/publication/11198259>
- Bollon J., Benbelkacem H. & Buffiere P. (2011). Development of a kinetic model for anaerobic dry digestion processes: Focus on acetate degradation and moisture content. *Biochemical Engineering Journal* **56**(3) : 212–218. DOI: <https://doi.org/10.1016/j.bej.2011.06.011>
- Bollon J., Benbelkacem H., Gourdon R. & Buffiere P. (2013). Measurement of diffusion coefficients in dry anaerobic digestion media. *Chemical Engineering Science Journal* **89**: 115–119. DOI: <https://doi.org/10.1016/j.ces.2012.11.036>
- Brown D., Shi J. & Li Y. (2012). Comparison of solid-state to liquid anaerobic digestion of lignocellulosic feedstocks for biogas production. *Bioresource Technology* **124**: 379–386. DOI: <https://doi.org/10.1016/j.biortech.2012.08.051>
- Chanakya H.N., Srikumar K.G., Anand V., Modak J. & Jagadish K.H. (1999) Fermentation properties of agro-residues , leaf biomass and urban market garbage in a solid phase biogas fermenter. *Biomass and Bioenergy* **16**: 417–429. DOI: [https://doi.org/10.1016/S0961-9534\(99\)00015-X](https://doi.org/10.1016/S0961-9534(99)00015-X)
- Chugh S., Clarke W., Pullammanappallil P. & Rudolph V. (1998). Effect of recirculated leachate volume on MSW degradation. *Waste Management and Research* **6**(16): 564–573. DOI: <https://doi.org/10.1177/0734242X9801600607>
- Contreras L.M., Schelle H., Sebrango C.R. & Pereda I. (2012). Methane potential and biodegradability of rice straw, rice husk and rice residues from the drying process. *Water Science and Technology* **65**(6): 1142–1149. DOI: <https://doi.org/10.2166/wst.2012.951>
- Degueurce A., Trémier A. & Peu P. (2016). Dynamic effect of leachate recirculation on batch mode solid state anaerobic digestion: influence of recirculated volume, leachate to substrate ratio and recirculation periodicity. *Bioresource Technology* **216**: 553–561. DOI: <https://doi.org/10.1016/j.biortech.2016.05.113>
- Ge Xu., Xu F & Li Y. (2016). Solid-state anaerobic digestion of lignocellulosic biomass: recent progress and perspectives. *Bioresource Technology* **205**: 239–249. DOI: <https://doi.org/10.1016/j.biortech.2016.01.050>
- Gottardo M., Micolucci F., Bolzonella D., Uellendahl H. & Pavan P. (2017). Pilot scale fermentation coupled with anaerobic digestion of food waste - effect of dynamic digestate recirculation. *Renewable Energy* **114**(B): 455–463. DOI: <https://doi.org/10.1016/j.renene.2017.07.047>
- Güven H., Sadik M., İren E., Keleş F., Öztürk I. & Altınbaş M. (2018). Co-digestion performance of organic fraction of municipal solid waste with leachate: preliminary studies. *Waste Management* **71**: 775–784. DOI: <https://doi.org/10.1016/j.wasman.2017.04.039>
- Hagos K., Zong J., Li D., Liu C. & Lu X. (2016). Anaerobic co-digestion process for biogas production: progress, challenges and perspectives. *Renewable and Sustainable Energy Reviews* **76**: 1485–1496. DOI: <https://doi.org/10.1016/j.rser.2016.11.184>
- He Y., Pang Y., Liu Y., Li X. & Wang K. (2008). Physicochemical characterization of rice straw pretreated with sodium hydroxide in the solid state for enhancing biogas production. *Energy and Fuels* **22**(4): 2775–2781. DOI: <https://doi.org/10.1021/ef8000967>

- Hills D.J. & Roberts D.W. (1981). Anaerobic digestion of dairy manure field crop residues. *Agricultural Wastes* **3**: 179–189.
DOI: [https://doi.org/10.1016/0141-4607\(81\)90026-3](https://doi.org/10.1016/0141-4607(81)90026-3)
- Jha A. K., Li J., Nies L. & Zhang Li. (2011). Research advances in dry anaerobic digestion process of solid organic wastes. *African Journal of Biotechnology* **10**(65): 14242–14253.
DOI: <https://doi.org/10.5897/AJB11.1277>
- Kalyuzhnyi S., Veeken A. & Hamelers B. (2000). Two-particle model of anaerobic solid state fermentation. *Water Science and Technology* **41**(3): 43–50.
DOI: <https://doi.org/10.2166/wst.2000.0054>
- Khalid A., Arshad M., Anjum M., Mahmood T. & Dawson L. (2011). The anaerobic digestion of solid organic waste. *Waste Management* **31**(8): 1737–1744.
DOI: <https://doi.org/10.1016/j.wasman.2011.03.021>
- Li Y., Park S.Y. & Zhu J. (2011). Solid-state anaerobic digestion for methane production from organic waste. *Renewable and Sustainable Energy Reviews* **15**(1): 821–826.
DOI: <https://doi.org/10.1016/j.rser.2010.07.042>
- Liotta F., Chatellier P., Esposito G., Fabbicino M., Frunzo L., Eric D.V.H., Piet N.L.L. & Pirozzi F. (2015). Modified anaerobic digestion model no.1 for dry and semi-dry anaerobic digestion of solid organic waste. *Environmental Technology* **36**(7): 870–880.
DOI: <https://doi.org/10.1080/09593330.2014.965226>
- Liotta F., Esposito G., Fabbicino M., Eric D.V.H., Piet N.L.L., Pirozzi F. & Pontoni L. (2015). Methane and VFA production in anaerobic digestion of rice straw under dry, semi-dry and wet conditions during start-up phase. *Environmental Management* **37**(5): 505–512.
DOI: <https://doi.org/10.1080/09593330.2015.1074288>
- Michele P., Giuliana D., Carlo M., Sergio S. & Fabrizio A. (2015). Optimization of solid state anaerobic digestion of the OFMSW by digestate recirculation: A new approach. *Waste Management* **35**: 111–118.
DOI: <https://doi.org/10.1016/j.wasman.2014.09.009>
- Motte J.C., Escudie R., Bernet N., Delgenes J.P., Steyer J.P. & Dumas C. (2013). Dynamic effect of total solid content, low substrate / inoculum ratio and particle size on solid-state anaerobic digestion. *Bioresource Technology* **144**: 141–148.
DOI: <https://doi.org/10.1016/j.biortech.2013.06.057>
- Mussoline W., Esposito G. & Giordano A. (2011). The anaerobic digestion of rice straw: a review. *Critical Reviews in Environmental Science and Technology* **43**(9): 895–915.
DOI: <https://doi.org/10.1080/10643389.2011.627018>
- Neshat S.A., Mohammadi M., Najafpour G.D. & Lahijani P. (2017). Anaerobic co-digestion of animal manures and lignocellulosic residues as a potent approach for sustainable biogas production. *Renewable and Sustainable Energy Reviews* **79**: 308–322.
DOI: <https://doi.org/10.1016/j.rser.2017.05.137>
- Riggio S., Torrijos M., Debord R., Esposito G., Eric D.V.H., Steyer J.P. & Escudie R. (2017). Mesophilic anaerobic digestion of several types of spent livestock bedding in a batch leach-bed reactor: substrate characterization and process performance. *Waste Management* **59**: 129–139.
DOI: <https://doi.org/10.1016/j.wasman.2016.10.027>
- Shah F.A., Mahmood Q., Rashid N., Pervez A., Raja I.A. & Shah M.M. (2015). Co-digestion, pretreatment and digester design for enhanced methanogenesis. *Renewable and Sustainable Energy Reviews* **42**: 627–642.
DOI: <https://doi.org/10.1016/j.rser.2014.10.053>
- Shi J., Wang Z., Stiverson J.A., Yu Z. & Li Y. (2013). Reactor performance and microbial community dynamics during solid-state anaerobic digestion of corn stover at mesophilic and thermophilic conditions. *Bioresource Technology* **136**: 574–581.
DOI: <https://doi.org/10.1016/j.biortech.2013.02.073>
- Wilson L.P., Sharvelle S.E. & De Long S.K. (2016). Enhanced anaerobic digestion performance via combined solids- and leachate-based hydrolysis reactor inoculation. *Bioresource Technology* **220**: 94–103
DOI: <https://doi.org/10.1016/j.biortech.2016.08.024>
- Xu F., Wang Z., Tang L. & Li Y. (2014). A mass diffusion-based interpretation of the effect of total solids content on solid-state anaerobic digestion of cellulosic biomass. *Bioresource Technology* **167**: 178–185.
DOI: <https://doi.org/10.1016/j.biortech.2014.05.114>
- Yang L. & Li Y. (2014). Anaerobic digestion of giant reed for methane production. *Bioresource Technology* **171**: 233–239.
DOI: <https://doi.org/10.1016/j.biortech.2014.08.051>
- Yong Z., Dong Y., Zhang X. & Tan T. (2015). Anaerobic co-digestion of food waste and straw for biogas production. *Renewable Energy* **78**: 527–530.
DOI: <https://doi.org/10.1016/j.renene.2015.01.033>

Appendix-1

Preliminary experimental setup

In this experimental setup, four different initial TS contents were used: 36, 29, 22 and 15%. To obtain the different TS percentages, two substrate mixing strategies were applied. In the first strategy (Mixing strategy-1), only rice straw (RS) and cow dung (CD) were mixed together to obtain the relevant TS% in the mixture. As a consequence, the quantity of CD was increased to reduce the initial TS content of mixture. The quantities of RS and CD added are presented in Table 1. In the second strategy (Mixing strategy-2), the quantities of RS and CD were identical in all the batch reactors (i.e. corresponding to the TS content of 36% of Mixing strategy-1) and water was added to fix the percentage of TS. The quantities of RS, CD and water added are presented in Table 1. The initial VS concentration of RS (S_0) in g VS of rice straw per kg mixture (g VS_{RS}/kg) was also calculated; it was between 29 and 232 g VS_{RS}/kg .

Table 1: Experimental conditions for the preliminary experimental setup

	Mixing strategy-1 (E-1)				Mixing strategy-2 (E-2)			
Initial TS content of mixture (%)	36	29	22	15	36	29	22	15
RS (g)	50	50	50	25	50	50	50	50
CD (g)	120	188	355	650	120	120	120	120
Water (g)	-	-	-	-	-	40	107	236
S_0 (g VS_{RS}/kg)	232	166	98	29	232	188	143	97

Figure 1 (a) shows the evolution of cumulative methane volumes produced over time for all the eight conditions tested. The only reactor which actively produced biogas was the 15% TS reactor which contained a mixture of 25 g RS and 650 g CD. Furthermore, the same reactor also showed a 15-day lag phase. None of the other reactors produced any significant volumes of biogas over the 80 days. In addition, Fig. 1 (b) shows that the final VFAs concentration in all these non-producing reactors was very high and rose with the increase of the initial TS percentage in both feeding strategies. This shows that strong acidification occurred in the reactors, except for the batches carried out at 15% TS and at the lower initial S_0 of 29 g VS_{RS}/kg .

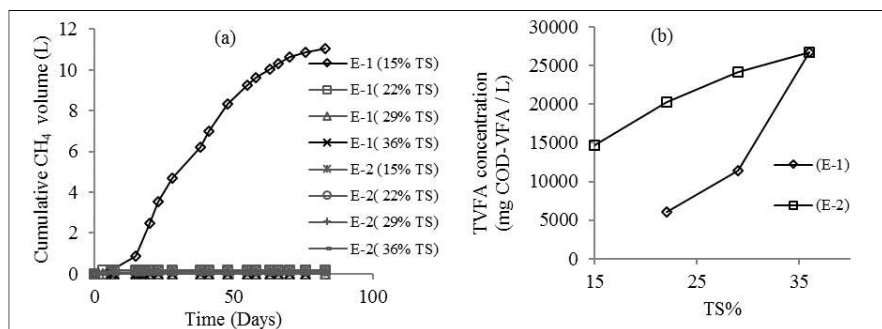


Figure 1: Cumulative methane volumes produced (a) over time and final total volatile fatty acids concentrations (b) in the preliminary experiment

RESEARCH ARTICLE

Bacterial Phylogenetics

Predominance of phylogenetic group B2 among commensal *Escherichia coli* in humans from Kandy District, Sri Lanka

BNLD Rangama^{1*}, CL Abayasekara² and DM Gordon³

¹ Postgraduate Institute of Science, University of Peradeniya, Peradeniya.

² Department of Botany, Faculty of Science, University of Peradeniya, Peradeniya.

³ Australian National University, Australia.

Submitted: 09 February 2021; Revised: 20 April 2021; Accepted: 25 June 2021

Abstract: *Escherichia coli* is a commensal bacterial gut inhabitant in vertebrates, while some strains are pathogens. Analysis of the genetic substructure within *E. coli* has identified nine phylogenetic groups within the species, as group A, B1, B2, C, D, E, F, G and cryptic clade I. These groups vary in attributes such as host characteristics, pathogenicity, antibiotic sensitivity patterns and virulence profiles. The current study was conducted to determine the distribution of phylogenetic groups, commonly encountered sequence types (ST), and group B2 subgroups (SG) of human faecal *E. coli* in a sample population in the Kandy District, Sri Lanka. A total of 158 faecal swabs, collected from healthy individuals, were cultured on MacConkey agar and presumptive *E. coli* isolates were confirmed by a negative reaction on Simmons citrate agar. *E. coli* isolates were characterized according to their phylogenetic group, SG, and ST distribution by a series of PCR protocols. Results revealed a predominance of group B2 (28 %), followed by B1 (23 %), A (17 %), D (14 %), C (5 %), F (4 %), and E (3 %). Within phylogroup B2, SG III was predominant while ST 73, 95, and 131 were detected at low frequencies. ST 69 accounted for 20 % of the group D isolates. Distribution of phylogroups was independent of host gender except group D, which was significantly over-represented by males. As B2 *E. coli* are strongly associated with extraintestinal infections and a high degree of virulence, characterization of these human faecal *E. coli* isolates for antibiotic susceptibility and virulence profiles would be of clinical importance.

Keywords: Commensal, *Escherichia coli*, PCR, phylogenetic groups, ST.

INTRODUCTION

Escherichia coli is a well-known member of the bacterial family Enterobacteriaceae. Its primary habitat is the lower gut of vertebrates, where it usually thrives as the predominant aerobic bacterium (Tenaillon *et al.*, 2010), whereas water, sediment, and soil can be considered as its secondary habitat (Savageau, 1983). *E. coli* plays a remarkable dual role as a widespread gut commensal and a versatile pathogen.

As a result of phylogenetic studies performed on *E. coli* since the late 20th century, a nine- group phylogeny with groups A, B1, B2, C, D, E, F, G and *Escherichia* clade I has been established (Milkman, 1973; Ochman & Selander, 1984; Walk *et al.*, 2009; Chaudhuri & Henderson, 2012; Clermont *et al.*, 2013; 2019). Within these phylogenetic groups, clonal complexes (CCs)/ sequence types (STs) are identified based on the genetic sequence similarity between *E. coli* strains that are related and share a common set of characteristics. Numerous studies have shown that the distribution of *E. coli* phylogenetic groups is non-random. For instance, in humans, groups A and B2 have been found to be the most common, while groups B1 and D are less prevalent. In animals, B1 strains are predominant followed by A, B2 and D (Chaudhuri & Henderson, 2012). Analysis of

* Corresponding author (lakshmie_ran@yahoo.com;  <https://orcid.org/0000-0001-5400-7564>)



This article is published under the Creative Commons CC-BY-ND License (<http://creativecommons.org/licenses/by-nd/4.0/>). This license permits use, distribution and reproduction, commercial and non-commercial, provided that the original work is properly cited and is not changed in anyway.

human commensal *E. coli* from different climate regions has shown that subjects in tropical areas exhibit a more diverse *E. coli* microbiota than those in temperate areas (Escobar-Páramo *et al.*, 2004).

Importantly, human extra-intestinal pathogenic *E. coli* (ExPEC) strains are more likely to belong in group B2, and to a lesser extent, group D, whereas strains belonging to groups A or B1 are less virulent (Boyd & Hartl, 1998; Picard *et al.*, 1999; Johnson *et al.*, 2001). Further, analyzing large collections of ExPEC has shown a predominance of Sequence Types (STs) 69, 73, 95, and 131 from groups D and B2, leading researchers to investigate the virulence profiles and antibiotic sensitivity patterns of these lineages (Adams-Sapper *et al.*, 2013; Banerjee *et al.*, 2013). Thus, for instance, being aware of the resistance of the infamous ST 131 of group B2 to antibiotics such as fluoroquinolones and third-generation cephalosporins, clinicians are enabled to plan appropriate therapy for such infections, when the phylogenetic identity of the pathogenic *E. coli* strain is known. Not only is the clinical community interested in phylotyping of *E. coli*, but also a growing number of aquatic microbiologists, the investigators involved in water quality or source of contamination studies (Walk *et al.*, 2007; Carlos *et al.*, 2010; Stoppe *et al.*, 2014), food microbiologists (Bergeron *et al.*, 2012), botanists (Méric *et al.*, 2013), and scientists in many other disciplines consider that *E. coli* phylotyping is essential in this molecular era of *E. coli* studies.

However, except for a study on avian pathogenic *E. coli* (APEC) strains originating from Sri Lanka by Dissanayake *et al.*, (2014), no attempts have been made to assess the phylogroup distribution of human *E. coli* isolates from Sri Lanka. Moreover, to the best of our knowledge, apart from the study on commensal *E. coli* of Pakistani infants by Nowrouzian *et al.*, (2009), South Asian human communities/societies have not been screened for the distribution of commensal *E. coli*, though phylogenetic studies on pathogenic *E. coli* have been reported (Chakraborty *et al.*, 2015; Singh *et al.*, 2017). This is a major drawback when considering the extent to which *E. coli* phylogenetic studies have developed beyond phylogroup determination and the amount of knowledge generated from studies arising from other regions of the world. Thus, the present study was launched to investigate the distribution of phylogenetic groups, commonly encountered sequence types (ST) and group B2 subgroups (SG) of *E. coli* isolates recovered from human faeces from a sample population residing in Kandy district, Sri Lanka.

MATERIALS AND METHODS

Sample collection

A total of 158 faecal swabs were collected from healthy volunteer Sri Lankan individuals that could be contacted by the investigators (convenience sampling). The subjects were included irrespective of their age or gender, provided that they had not received antibiotic therapy nor had a history of gastrointestinal disease during the previous month. A commercial collection and transport system for bacteria that consisted of a sterile cotton wool swab and a tube of Amies medium without charcoal (BBL™ CultureSwab™ Plus) was provided to each participant, and instructions were given on obtaining the swab sample. The faecal swab samples received were either taken immediately for bacterial culturing or stored in a laboratory refrigerator at 4 °C when immediate culturing was not possible.

Isolation of *E. coli* from faecal samples

Faecal swab samples received were cultured on MacConkey agar plates so as to obtain isolated bacterial colonies and incubated at 37 °C for 18 h. A selected presumptive *E. coli* colony (with a pink/red colour and a non-mucoid appearance) grown from each faecal sample was spot inoculated into a Simmons citrate agar plate and a Luria agar plate and incubated at 37 °C for 18 h. Cultures failing to produce a colour change (citrate negative) on Simmons citrate agar were presumed to be *E. coli*. Cultures on Luria agar were used for short term storage of *E. coli* colonies in a laboratory refrigerator at 4 °C.

Molecular analysis

DNA extraction from bacterial cells (from colonies grown on Luria agar) was performed using the DNAzol® genomic DNA isolation reagent (Molecular Research Center Inc., USA) according to the manufacturer's recommendations with modifications.

Approximately half of each *E. coli* colony on Luria agar was re-inoculated into 100 µL of sterile Luria broth in microfuge tubes and incubated for 18 hours with shaking at 36 °C. Then, 80 µL from each tube were discarded and the tubes with the remaining culture were centrifuged at maximum speed (15,000 r.p.m) for 1 min. After removing the supernatant, the pellet was re-suspended in 25 µL of 10X Sodium chloride-Tris-EDTA (STE) buffer by vortexing. Next, the suspensions

were mixed by inverting the tubes after each addition of 50 µL of DNAzol® followed by 45 µL of 95 % ethanol for 2 min and 1 min, respectively. The tubes were centrifuged for 3 min at maximum speed and the supernatant was discarded. The pellets were then mixed with 250 µL of 75 % ethanol by inverting the tubes 10 times. Tubes were centrifuged at maximum speed for 1 min, the supernatant

discarded and drained on paper towels. The pellets were dried at 50 °C for 45 min. Subsequently, 100 µL of a 0.03 M solution of sodium hydroxide in Tris-EDTA (TE) buffer were added to each tube and they were left in the oven at 65 °C for 5 min. After ensuring that the DNA had completely dissolved resulting in a clear solution, the tubes with DNA extracts were stored at -20 °C.

Table 1: Details of primers employed in the various PCR programmes of the current study

PCR programme	Amplification target	Primers	Primer sequences (5'-3')	PCR product (bp)	Reference
Clermont quadruplex	chuA	chuA.1b	ATGGTACCGGACGAACCAAC	288	Clermont <i>et al.</i> , 2013
		chuA.2	TGCCGCCAGTACCAAAGACA		
	yjaA	yjaA.1b	CAAACGTGAAGTGTCAGGAG	211	
		yjaA.2b	AATGCGTTCCTCAACCTGTG		
	TspE4.C2	TspE4C2.1b	CACTATTCGTAAGGTCATCC	152	
		TspE4C2.2b	AGTTTATCGCTGCGGGTCGC		
Group E	arpA	AceK.f	AACGCTATTCGCCAGCTTGC	400	Clermont <i>et al.</i> , 2013
		ArpA1.r	TCTCCCCATACCGTACGCTA		
	arpA	ArpAgpE.f	GATTCCATCTTGTCAAAATATGCC	301	
		ArpAgpE.r	GAAAAGAAAAAGAATTCCCAAGAG		
	trpA	trpAgpC.1	AGTTTATGCCCAGTGCGAG	219	
		trpAgpC.2	TCTGCGCCGGTCACGCC		
Group C	trpA	trpBA.f ^b	CGGCGATAAAGACATCTTCAC	489	Clermont <i>et al.</i> , 2013
		trpBA.r ^a	GCAACGCGCCTGGCGGAAG		
	1, ST73, CFT073 (AE014075) ^b	ST73_for	TGGTTTACCATTGTGTCGGA	490	
		ST73_rev	GGAAATCGTTGATGTGGCT		
	19, ST131, NA114 (CP002797) ^b	ST131_for	GACTGCATTTCGTCGCCATA	310	
		ST131_rev	CCGGCGGCATCATAATGAAA		
New primer pool	9, ST95, UTI89 (CP000243) ^b	ST95_for	ACTAATCAGGATGGCGAGAC	200	Doumith <i>et al.</i> , 2015
		ST95_rev	ATCACGCCCATTAATCCAGT		
	21, ST69, UMN026 (CU928163) ^b	ST69_for	ATCTGGAGGCAACAAGCATA	104	
		ST69_rev	AGAGAAAGGGCGTTCAGAAT		
	Group B2 sub-typing (Panel 1)	pabB II	pabBgpII.f	GAGTCACTGCCAGAAATTGCA	415
			pabBgpII.r	GGCGAAAGGCTTAAATTGCACT	
Group B2 sub-typing (Panel 1)	trpA III	trpAgpIII.f	GACGCGCTGGAATTAGGCTC	255	Clermont <i>et al.</i> , 2014
		trpAgpIII.r	ATCGGCAACCAGCACCGAAT		
	dinB VI	dinBgpVI.f	CAGCGTGAGATGCGCGAT	652	
		dinBgpVI.r	TCGTCAATGCCCTGACTACA		
	icd VII	icdgpVII.f	GCGGTATTCGCTCTCTGAAT	810	
		icdgpVII.r	CAATTAAATCAGCCGCTTCG		
Group B2 sub-typing (Panel 1)	aes IX	aesgpIX.f	CCTGGCCTGCAACGGGAG	160	Clermont <i>et al.</i> , 2014
		aesgpIX.r	TCTGGCTGCGGATAAAAGAG		
	chuA Internal control	chuAgene.1	CGATACGGTTCGATGCAAAAAG	1013	
		chuAgene.2	TTGGACAACATCAGGTCATC		

Continued -

Continued from page 139 -

PCR programme	Amplification target	Primers	Primer sequences (5'-3')	PCR product (bp)	Reference
Group B2 sub-typing (Panel 2)	putP I	putPgpI.f	GGTATCGCTTACTTTAACGG	373	Clermont <i>et al.</i> , 2014
		putPgpI.r	ACCACCGGACCAAACGCC		
	trpA IV	trpAgpIV.f	TGCCAGTGGAAGAGTCCGCT	261	
		trpAgpIV.r	CCGGGGCGGAAATACCAAAG		
	polB V	polBgpV.f	GCCGTTTCGCCGAAGATAAA	530	
		polBgpV.r	TAATGATCTTCAGCGCCTGT		
ST 131	aes X	aesgpX.f	GACCGTTGTGAATACTCTTCA	713	Johnson <i>et al.</i> , 2009
		aesgpX.r	TATAACAGGGCGGCACATTT		
	gyrB	gyrB47.f	CGCGATAAGCGCGAC	132	
		gyrB47.r	ACCGTCTTTTCGGTGGA		
	Svg	svg.1	TCCGGCTGATTACAAACCAAC		
		svg.2	CTGCACGAGGTTGTAGTCCTG		
ST 69	gyrB	gyrB27.f	GGTGCGTTTCTGGCCA		
		gyrB27.r	GACGCCGATACCATC		

a. The primers trpBA.f and trpBA.r are added in Group E and Group C specific PCR reactions as an internal control.

b. The number designated for the target region of the genome sequence, the sequence type (ST) and the accession number of the relevant *E. coli* genome in GenBank database as cited in the original article by Doumith *et al.* (2015).

Table 2: Concentrations of the primers and PCR conditions used in the current study

PCR programme	Primer	Concentration (μM)	PCR conditions	Electrophoresis conditions
Clermont quadruplex	chuA.1b	0.4	Denaturation for 5 min at 94 °C, 30 cycles of 30 s each at 94 °C, 55 °C and 72 °C and a final extension step of 7 min at 72 °C	1.5 % agarose gel, 100 V for 45 minutes
	chuA.2	0.4		
	yjaA.1b	0.4		
	yjaA.2b	0.4		
	TspE4C2.1b	0.5		
	TspE4C2.2b	0.5		
	AceK.f	0.6		
	ArpA1.r	0.6		
Group E	ArpAgpE.f	0.5	Denaturation for 5 min at 94 °C, 30 cycles of 5 s at 94 °C and 25 s at 57 °C and a final extension step of 5 min at 72 °C	1.5 % agarose gel, 100 V for 45 minutes
	ArpAgpE.r	0.5		
Group C	trpAgpC.1	0.5	Denaturation for 5 min at 94 °C, 30 cycles of 5 s at 94 °C and 25 s at 60 °C and a final extension step of 5 min at 72 °C	1.5 % agarose gel, 100 V for 45 minutes
	trpAgpC.2	0.5		
New primer pool	trpBA.f ^a	0.25	Denaturation for 3 min at 94 °C, 30 cycles of 30 s each at 94 °C, 60 °C and 72 °C and a final extension step of 5 min at 72 °C	1.5 % agarose gel, 90 V for 45 minutes
	trpBA.r ^a	0.25		
	ST73_for	0.4		
	ST73_rev	0.4		
	ST131_for	0.4		
	ST131_rev	0.4		
	ST95_for	0.4		
	ST95_rev	0.4		
	ST69_for	0.6		
	ST69_rev	0.6		

Continued -

Continued from page 140 -

PCR programme	Primer	Concentration (μM)	PCR conditions	Electrophoresis conditions
Group B2 sub-typing (Panel 1)	pabBgpII.f	0.4	Denaturation for 4 min at 94 °C, 30 cycles for 5 s at 94 °C and 20 s at 63 °C and a final extension step of 4 min at 72 °C.	2 % agarose gel, 85 V for 60 min
	pabBgpII.r	0.4		
	trpAgpIII.f	0.2		
	trpAgpIII.r	0.2		
	dinBgpVI.f	0.4		
	dinBgpVI.r	0.4		
	icdgpVII.f	0.5		
	icdgpVII.r	0.5		
	aesgpIX.f	0.6		
	aesgpIX.r	0.6		
	chuAgene.1	0.4		
	chuAgene.2	0.4		
Group B2 sub-typing (Panel 2)	putPgpl.f	0.4	Denaturation for 4 min at 94 °C, 30 cycles for 5 s at 94 °C and 20 s at 63 °C and a final extension step of 4 min at 72 °C	2 % agarose gel, 85 V for 60 min
	putPgpl.r	0.4		
	trpAgpIV.f	0.4		
	trpAgpIV.r	0.4		
	polBgpV.f	0.4		
	polBgpV.r	0.4		
	aesgpX.f	0.4		
	aesgpX.r	0.4		
ST 131	gyrB47.f	0.4	Denaturation for 10 min at 95 °C, 32 cycles for 30 s each at 94 °C and 65 °C and 30 s, and 2 min at 68 °C	2 % agarose gel, 100 V for 45 min
	gyrB47.r	0.4		
ST 95	svg.1	0.4	Denaturation for 15 min at 95 °C; 30 cycles of 30 s at 94 °C, 90 s at 55 °C, and 90 s at 72 °C and a final extension step of 10 min at 72 °C.	1.5 % agarose gel, 100 V for 45 min
	svg.2	0.4		
ST 69	gyrB27.f	0.4	Denaturation for 10 min at 95 °C, 32 cycles for 30 s each at 94 °C and 60 °C for 1 min at 72 °C and a final extension at 72 °C for 10 min.	1.5 % agarose gel, 100 V for 45 min
	gyrB27.r	0.4		

Polymerase chain reaction (PCR) and gel electrophoresis

All the PCRs (Table 1) were carried out in a TaKaRa PCR Thermal Cycler Dice™ TP600 (Takara Bio Inc, Japan) in 10 μL reaction volumes. The PCR mixture contained 5.0 μL of GoTaq® Green Master Mix, 2X (Promega Corporation, USA; a premix of DNA polymerase, 2X reaction buffer, 400 μM each of dNTPs and 3 mM magnesium chloride), 0.6 μL of DNA extract, relevant primers (concentrations mentioned in Table 2) and nuclease-free water. After each PCR, the products were subjected to horizontal gel electrophoresis (MultiSUB Choice, Cleaver Scientific Ltd.) under conditions mentioned in Table 2. The gels were stained with ethidium bromide (concentration approximately

0.5 μg/mL in the gel) and PCR product sizes were estimated using a molecular marker (HyperLadder™ 50 bp, Bioline). The gel images were captured and saved using a gel documentation system (Bio-Vision -3026).

The Clermont quadruplex PCR was conducted on all isolates to determine their 'quadruplex genotypes' as described in Clermont *et al.*, (2013) (Figure 1). Isolates designated 'group D or E' by the quadruplex PCR were then subjected to the group E PCR which differentiated isolates into group D or group E (Figure 2). Similarly, those designated 'group A or C' were differentiated by group C PCR into group A or group C. Next, the isolates designated as groups B2 and D were collectively subjected to new primer pool PCR to identify the major STs (ST 73, 95, 131, and 69) among them (Figure 3).

Group B2 isolates were then again analyzed for their subgroups with group B2 sub-typing PCR (Figure 4). Finally, the STs/subgroups assigned for group B2 ST 95 and 131 isolates and group D ST 69 isolates were confirmed by the corresponding ST PCRs.

Statistical analysis

To determine whether there was a significant association between the *E. coli* phylogenetic group and the gender of the host, Fisher's exact test was performed, as 43% of the cells in the contingency table had expected frequencies below five. The level of statistical significance was defined as 0.05. The statistical analysis was performed using IBM® SPSS® Statistics Version 22.

RESULTS AND DISCUSSION

Commensal populations of *E. coli* show a 'clonal population structure', despite the occurrence of genetic recombination; thus delineation of major phylogenetic

groups is possible (Selander & Levin, 1980; Tenaillon *et al.*, 2010). Also, it has been shown that for a given host, the predominant isolate (i.e., the faecal *E. coli* isolate that accounts for more than half of the total colonies isolated in a stool culture), and the resident strain, (i.e., the one which persists in a person's gut for a long period) are likely to be the same (Sears *et al.*, 1950, Caugant *et al.*, 1981). This knowledge forms the basis for assigning *E. coli* phylogenetic groups to individual hosts, by analyzing a single *E. coli* colony from a stool culture (that consists of many *E. coli* colonies).

Out of the 158 faecal swabs collected, 58 were from males and 84 were from females. The gender of the remaining 16 subjects was not provided. On MacConkey agar, 157 swabs yielded bacterial growth. Fourteen of the isolates selected were citrate positive and one isolate failed to produce bands from the phylotyping PCR, resulting in a subtotal of 142 *E. coli* isolates for phylogroup analysis. Representative gel images of the main PCR programmes are shown in Figures 1- 4.

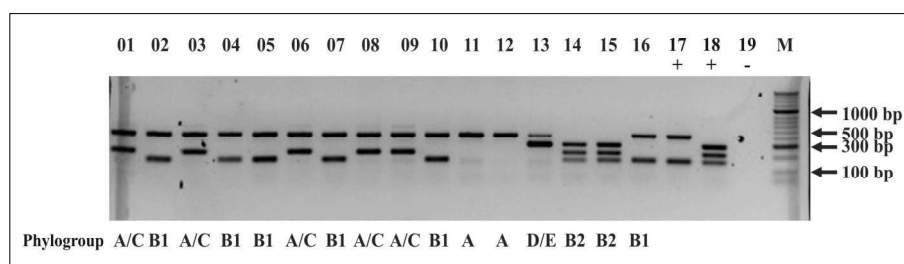


Figure 1: A gel profile of Clermont quadruplex PCR programme. Lanes 1-15, *E. coli* isolates analyzed in this study; lane 17, group B1 positive control; lane 18, group B2 positive control, lane 19, negative control; M- molecular weight marker

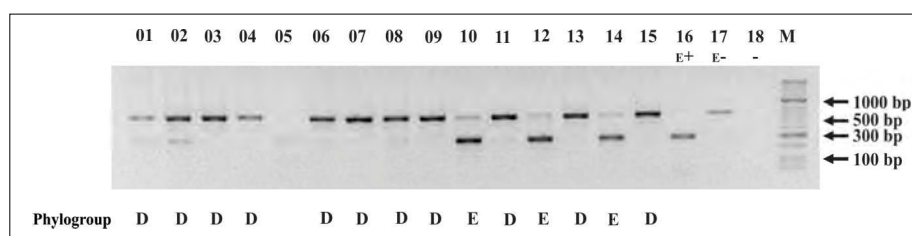


Figure 2: A gel profile of Clermont group E PCR programme. Lanes 1-15, *E. coli* isolates designated as group D or E by Clermont quadruplex PCR; lane 16, group C positive control; lane 17, group C negative control, lane 18, PCR negative control; M- molecular weight marker

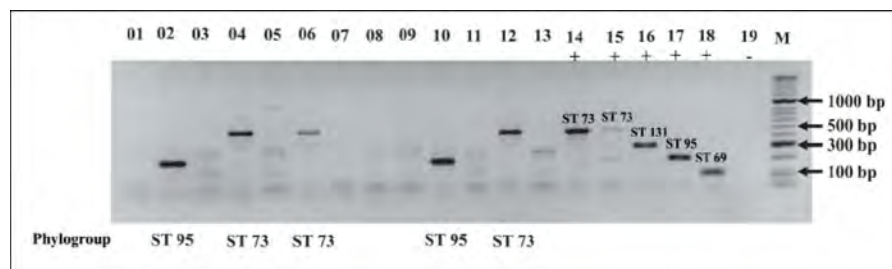


Figure 3: A gel profile of the new primer pool PCR programme. Lanes 1-13, *E. coli* isolates designated as group B2 by Clermont quadruplex PCR; lanes 14-18, positive controls (labeled in the image); lane 19, PCR negative control; M- molecular weight marker

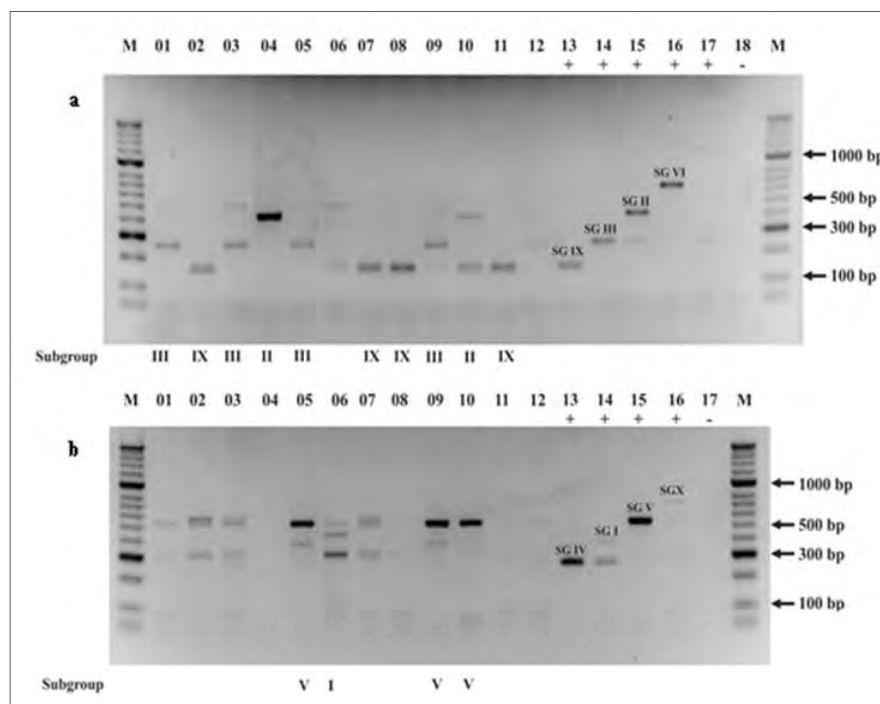


Figure 4: Gel profiles of the panel I/ panel II PCR programme. (a) Panel I. Lanes 1-12, *E. coli* isolates designated as group B2 by Clermont quadruplex PCR; lanes 13-17, positive controls of B2 subgroups (labeled in the image) ; Lane 18, PCR negative control; M- molecular weight marker (b) Panel II. Lanes 1-12, *E. coli* isolates analyzed in this study; lanes 13-16, positive controls of B2 subgroups (labeled in the image); Lane 17, PCR negative control; M- molecular weight marker

The distribution of phylogenetic groups within the study population

Phylogroups B2 and B1 were the most prevalent, followed by phylogroups A and D (Figure 5). Phylogroups C, F, and E each represented $\leq 5\%$ of the *E. coli* isolates. The

prevalence of *E. coli* phylogenetic groups in the current study population can be arranged as B2 (28 %) > B1 (23 %) > A (17 %) > D (14 %) > C (5 %) > F (4 %) > E (3 %). The dominance of phylogroups A, B1, B2, and D reflects the results of other studies examining *E. coli* phylogroup distribution in humans (Tenaillon *et al.*, 2010).

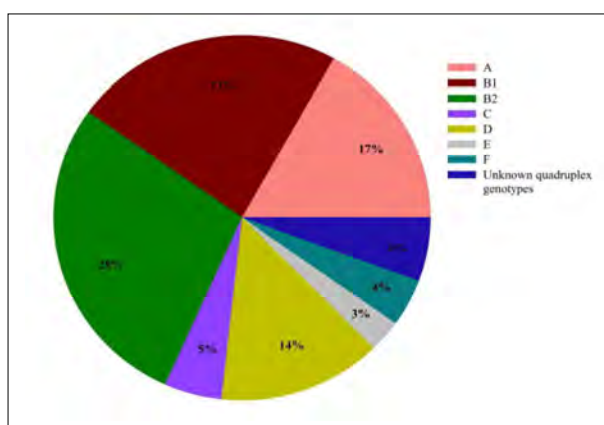


Figure 5: Distribution of the major *E. coli* phylogroups among faecal isolates of healthy individuals from Kandy District, Sri Lanka

Early studies examining the prevalence of *E. coli* phylogroups in samples collected from humans living in different countries, led to the view that phylogroup A strains dominated among isolates taken from people living in the tropics, while phylogroups B2 and D were more prevalent among isolates taken from people in temperate regions (Duriez *et al.*, 2001; Escobar-Páramo *et al.*, 2004). However, the more recent studies on phylogroup distribution of *E. coli* have established the view that the influence of the environment in terms of socioeconomic factors, (such as the diet and the level of hygiene) in a human population is more important than the climate in which the host lives. For instance, in a study that compared intestinal *E. coli* isolated from subjects who had recently migrated from temperate region (metropolitan France) to tropical region (French Guyana) with that of natives of the two regions, the prevalence of groups A and B2 isolates in the migrant group was intermediate compared to the two native groups, suggesting that the commensal gut flora of humans changes dynamically in response to new environmental conditions (Skurnik *et al.*, 2008; Bailey *et al.*, 2010; Tenaillon *et al.*, 2010).

In addition, the *E. coli* phylogroup distribution in human hosts has been thought to be influenced by differences in morphology, physiology, and diet of different sexes or ages (Gordon *et al.*, 2005). Massot *et al.*, (2016) reported that within a single 'locality', phylogroup distribution changes over time. It would have been of interest to look into the findings of Mushtaq *et al.*, (2011) and Mukherjee *et al.*, (2015) on studies carried out

in South Asia on *E. coli* phylogenetic groups. However, since these studies are of pathogenic isolates and not on commensal *E. coli* of human hosts, a comparative analysis on the South Asian region (where Sri Lanka is located) is not possible. In summary, the above reports and the evidence of more recent phylogroup distributions of *E. coli* show that there is a variation by locality, and this variation seems to be due to geographic variation of socio-economic factors rather than the climate.

Predominance of group B2 in the current study population is noteworthy, as isolates belonging to group B2 have been shown to be the most common cause of ExPEC disease such as urinary tract infections (Zhang *et al.*, 2002; Matsukawa *et al.*, 2019), neonatal bacterial meningitis (Bingen *et al.*, 1998; Johnson *et al.*, 2002), peritonitis and bacteremia (Hilali *et al.*, 2000; Bert *et al.*, 2010). From an evolutionary perspective, group B2 is believed to show an early genetic divergence within the species and its extra-intestinal virulence appears to be a 'coincidental by-product of commensalism' (Picard *et al.*, 1999). In a study considering only the antibiotic resistant commensal *E. coli* strains and their virulence genes isolated from Indian children, the proportion of antibiotic resistant (extended spectrum beta lactamase producing) commensal *E. coli* carrying a virulence factor associated with urinary tract infections in phylogenetic group B2 has been found to be significantly higher when compared to groups A and D (Chandran *et al.*, 2017). Diard *et al.*, 2010, stated that traits that enable extra-intestinal infection and long-term colonization of the intestine are more frequent among B2 strains than in other groups. Even though these traits make phylogenetic group B2 more likely to be the most prevalent group in a community, the fact that this phylogroup is not universally predominant indicates the involvement of other factors in shaping phylogroup prevalence. For example, Unno *et al.*, (2009) report the absence of group B2 isolates in humans and domesticated animals in a province in the Republic of Korea.

Effect of gender and age

The relative abundance of phylogroups differed between male and female hosts ($p < 0.05$) (Figure 6).

Phylogroups D and C isolates were more prevalent in males, while isolates belonging to phylogroups A, B2, E, and F were more common in female hosts. There was no statistically significant change in phylogroup abundance with respect to host age ($p > 0.1$) (Figure 7).

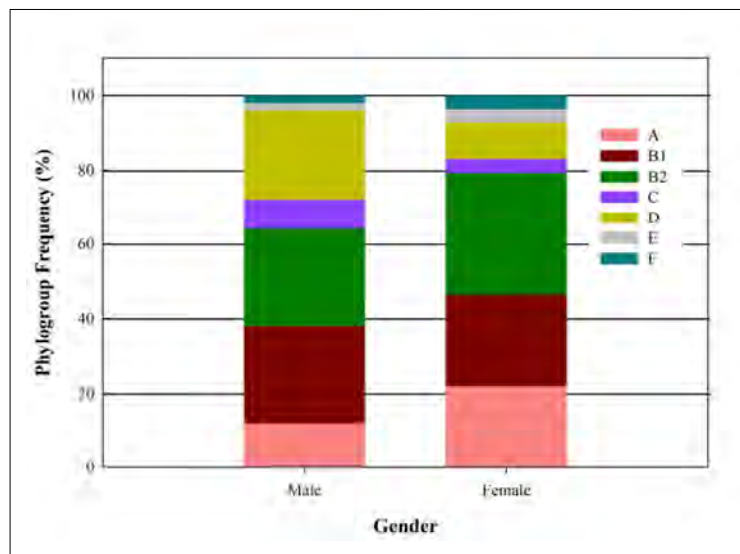


Figure 6: Relative abundance of major phylogenetic groups among male and female participants (n=118 whose gender was provided and phylogenetic group identified)

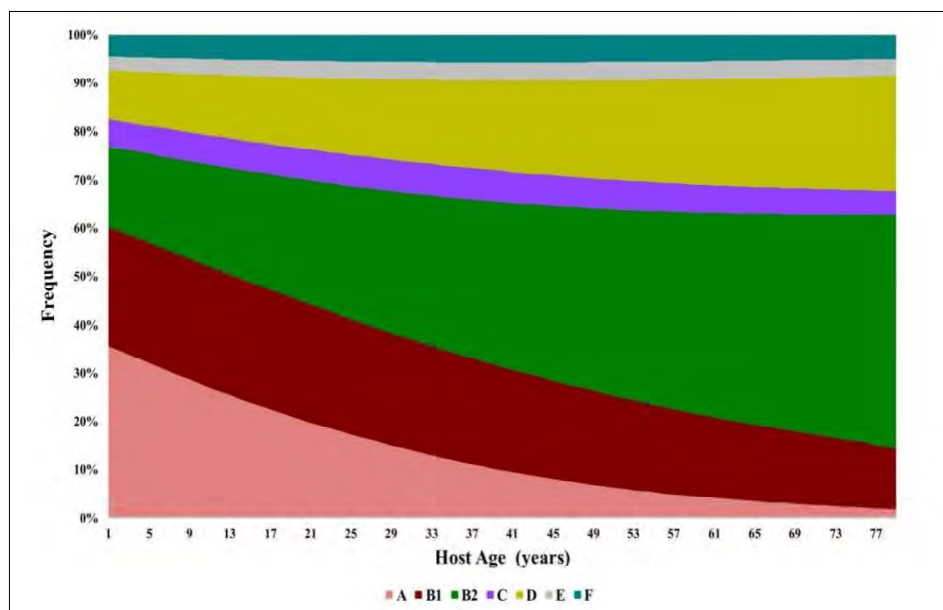


Figure 7: Change in the relative abundance of the commensal *E. coli* phylogenetic groups with respect to the age of host (n = 122 whose age was provided and phylogenetic group identified)

However, there was a tendency for the frequency of phylogroups A and B1 to decline with age, while the frequencies of phylogroups B2 and D increased. A very similar observation is reported in Bok *et al.*, (2018),

where groups A and B1 have shown a higher prevalence in young children while groups B2 and D prevailed among adults in Poland (only four phylogenetic groups were compared in that study).

Table 3: The distribution of Sequence Types (ST) and group B2 subgroups, as screened by different PCR protocols ($n_{B2} = 40$, $n_D = 20$)

ST Detected	B2 subgroup	No. of isolates detected by different PCR protocols (% of D or B2 isolates)		
		Doumith	B2 subtyping	ST Specific
69 ^a	-	4 (20.0)		4 (20.0)
131	I	1 (2.5)	2 (5.0)	0 (0.0)
73	II	4 (10.0)	2 (5.0)	
127	III		15 (37.5)	
141	IV		1 (2.5)	
144	V		8 (20.0)	
12	VI		0 (0.0)	
14	VII		0 (0.0)	
95	IX	8 (20.0)	9 (22.5)	9 (22.5)
372	X	1 (2.5)	0 (0.0)	

a - ST 69 belongs to Group D

Sequence Types and B2 subgroups

The present study investigated the distribution of the four sequence types ST 69 (within group D), ST 73, ST 95, and ST 131 (within group B2) whose involvement in extra-intestinal infections have been shown previously (Mora *et al.*, 2009; Riley, 2014). These STs differ in their antibiotic sensitivity profiles. Strains of STs 69, 73, and 95 are still susceptible to antibiotics whereas members of ST131 show increasing resistance to multiple antibiotic classes including fluoroquinolones (Giufre *et al.*, 2012; Banerjee *et al.*, 2013; Hu *et al.*, 2013; Petty *et al.*, 2014). However, the current study detected low levels in all four STs (Table 3). Only two isolates of ST 131 were detected out of the 40 group B2 isolates, despite the high level of antibiotic resistance in *E. coli* that prevail in Sri Lanka (Chandrasiri *et al.*, 2013; Jayatilleke *et al.*, 2016; Tillekeratne *et al.*, 2016; Fernando *et al.*, 2017).

Ten (I – X) phylogenetic subgroups within group B2 have been described (Le Gall *et al.*, 2007; Clermont *et al.*, 2014) and some of these subgroups have been shown to be frequently associated with extra-intestinal pathologies (Bidet *et al.*, 2007; Clermont *et al.*, 2008; Jauregui *et al.*, 2008). Le Gall *et al.*, (2007) have observed all the strains to be virulent in subgroups I, III and IV, both virulent and avirulent strains to be present in subgroups II, V, VI, VII, and IX, and all strains to be avirulent in subgroup VIII. In this study, the rapid and convenient PCR introduced by

Clermont *et al.*, 2014 to identify group B2 human extra-intestinal pathogenic *E. coli*, was followed in subtyping the group B2 isolates (strains belonging to subgroup VIII are unassignable by this PCR). Group B2 isolates fell into their respective subgroups as shown in Table 3. In North America, Europe, and Australia, ~30% of human hosts sampled harbor an isolate representing STs either 73, 95, or 131 typically (Riley, 2014). By contrast, isolates belonging to these STs represented, at best, only about 10 % (14 of 142 isolates) of all *E. coli* observed in the present study.

CONCLUSIONS

To the best of our knowledge, the current study is the first report from South Asia, on phylogenetic group distribution of human commensal *E. coli* in a human community. Group B2 predominates in the human commensal gut flora of the Sri Lankan study population of the Kandy District, followed by the groups B1, A, D, C, F and E, while the relative abundance of *E. coli* phylogenetic groups varied between male and female hosts. Further, in group B2, SG III is the predominant subgroup while the common ExPEC STs of group B2 (ST 73, 95, and 131) and group D (ST 69) are represented in low frequencies (<25 %). In this study population, the distribution of phylogroups is independent of host gender except in group D, which is significantly over-represented in males.

Future directions

The current study is limited to hosts living in the Kandy district of the country. It would be worthwhile to screen hosts from other areas of the country, to obtain the phylogroup distribution throughout the country. Also, a more precise idea about the effect of gender and/or age of the host on the distribution of *E. coli* phylogroups could have been achieved if sampling method was altered to obtain comparable numbers of individuals from different genders/age groups.

The high levels of antibiotic resistance observed among gram negative clinical bacterial isolates in Sri Lanka make it imperative to investigate antibiotic sensitivity patterns and genetic markers of virulence and pathogenicity of the different *E. coli* phylogenetic groups identified in this study. Even though they are of commensal origin, such knowledge aids in predicting and interpreting pathogenicity/virulence of clinical *E. coli* isolates, understanding the changes in human practices, particularly antibiotic usage, and more importantly, in designing the antibiotic therapy for infections.

Acknowledgement

The authors acknowledge the provision of reagents and other consumables, by the Research School of Biology, The Australian National University, Canberra. Further, the authors thank Ms. Samantha Burn of the Gordon Laboratory, Research School of Biology, The Australian National University, Canberra, and Prof. Sanath Rajapakse of the Department of Molecular Biology and Biotechnology, of the University of Peradeniya for the assistance given.

REFERENCES

- Adams-Sapper S., Diep B.A., Perdreau-Remington F. & Riley L.W. (2013). Clonal composition and community clustering of drug-susceptible and resistant *Escherichia coli* isolates from blood stream infections. *Antimicrobial Agents and Chemotherapy* **57**(1): 490–497.
DOI: <https://doi.org/10.1128/AAC.01025-12>
- Bailey J.K., Pinyon J.L., Anantham S. & Hall R.M. (2010). Distribution of human commensal *Escherichia coli* phylogenetic groups. *Journal of Clinical Microbiology* **48**(9): 3455–3456.
DOI: <https://doi.org/10.1128/JCM.00760-10>
- Banerjee R., Johnston B., Lohse C., Chattopadhyay S., Tchesnokova V., Sokurenko E.V. & Johnson J.R. (2013). The clonal distribution and diversity of extraintestinal *Escherichia coli* isolates vary according to patient characteristics. *Antimicrobial Agents and Chemotherapy* **57**(12): 5912–5917.
DOI: <https://doi.org/10.1128/AAC.01065-13>
- Bergeron C.R., Prussing C., Boerlin P., Daignault D., Dutil L., Reid-Smith R.J., Zhanel G.G. & Manges A.R. (2012). Chicken as reservoir for extraintestinal pathogenic *Escherichia coli* in humans, Canada. *Emerging Infectious Diseases* **18**(3): 415–421.
DOI: <https://doi.org/10.3201/eid1803.111099>
- Bert F., Johnson J.R., Ouattara B., Leflon-Guibout V., Johnston B., Marcon E., Valla D., Moreau R. & Nicolas-Chanoine M.H. (2010). Genetic diversity and virulence profiles of *Escherichia coli* isolates causing spontaneous bacterial peritonitis and bacteremia in patients with cirrhosis. *Journal of Clinical Microbiology* **48**(8): 2709–2714.
DOI: <https://doi.org/10.1128/JCM.00516-10>
- Bidet P., Metais A., Mahjoub-Messai F., Durand L., Dehem M., Aujard Y., Bingen E., Nassif X. & Bonacorsi S. (2007). Detection and identification by PCR of a highly virulent phylogenetic subgroup among extraintestinal pathogenic *Escherichia coli* B2 strains. *Applied and Environmental Microbiology* **73**(7): 2373–2377.
DOI: <https://doi.org/10.1128/AEM.02341-06>
- Bingen E., Picard B., Brahimi N., Mathy S., Desjardins P., Elion J. & Denamur E. (1998). Phylogenetic analysis of *Escherichia coli* strains causing neonatal meningitis suggests horizontal gene transfer from a predominant pool of highly virulent B2 group strains. *Journal of Infectious Diseases* **177**(3): 642–650.
DOI: <https://doi.org/10.1086/514217>
- Bok E., Mazurek J., Myc A., Stosik M., Wojciech M. & Baldy-Chudzik K. (2018). Comparison of commensal *Escherichia coli* isolates from adults and young children in Lubuskie province, Poland: virulence potential, phylogeny and antimicrobial resistance. *International Journal of Environmental Research and Public Health* **15**(4): 617.
DOI: <https://doi.org/10.3390/ijerph15040617>
- Boyd E.F. & Hartl D.L. (1998). Chromosomal regions specific to pathogenic isolates of *Escherichia coli* have a phylogenetically clustered distribution. *Journal of Bacteriology* **180**(5): 1159–1165.
DOI: <https://doi.org/10.1128/jb.180.5.1159-1165.1998>
- Carlos C., Pires M.M., Stoppe N.C., Hachich E.M., Sato M.I., Gomes T.A., Amaral L.A. & Ottoboni, L.M. (2010). *Escherichia coli* phylogenetic group determination and its application in the identification of the major animal source of fecal contamination. *BMC Microbiology* **10**(1): 1–10.
DOI: <https://doi.org/10.1186/1471-2180-10-161>
- Caugant D.A., Levin B.R. & Selander R.K. (1981). Genetic diversity and temporal variation in the *E. coli* population of a human host. *Genetics* **98**(3): 467–490.
- Chakraborty A., Saralaya V., Adhikari P., Shenoy S., Baliga S. & Hegde A. (2015). Characterization of *Escherichia coli* phylogenetic groups associated with extraintestinal infections in South Indian population. *Annals of Medical and Health Sciences Research* **5**(4): 241–246.
DOI: <https://doi.org/10.4103/2141-9248.160192>
- Chandran S.P., Sarkar S., Diwan V., Pathak A., Shah H., Tamhankar A.J., Macaden R. & Stålsby-Lundborg C.

- (2017). Detection of virulence genes in ESBL producing, quinolone resistant commensal *Escherichia coli* from rural Indian children. *The Journal of Infection in Developing Countries* **11**(5): 387–392.
DOI: <https://doi.org/10.3855/jidc.8574>
- Chandrasiri P., Elwitigala J., Nanayakkara G., Chandrasiri S., Patabendige G., Karunanayaka L., Perera J., Somaratne P. & Jayathilleke K. (2013). A multi centre laboratory study of Gram negative bacterial blood stream infections in Sri Lanka. *Ceylon Medical Journal* **58**(2): 56–61.
DOI: <http://doi.org/10.4038/cmj.v58i2.5680>
- Chaudhuri R.R. & Henderson I.R. (2012). The evolution of the *Escherichia coli* phylogeny. *Infection, Genetics and Evolution* **12**(2): 214–226.
DOI: <https://doi.org/10.1016/j.meegid.2012.01.005>
- Clermont O., Christenson J.K., Daubie A.S., Gordon D.M. & Denamur E. (2014). Development of an allele-specific PCR for *Escherichia coli* B2 sub-typing, a rapid and easy to perform substitute of multilocus sequence typing. *Journal of Microbiological Methods* **101**: 24–27.
DOI: <https://doi.org/10.1016/j.mimet.2014.03.008>
- Clermont O., Christenson J.K., Denamur E. & Gordon D.M. (2013). The Clermont *Escherichia coli* phylo-typing method revisited: improvement of specificity and detection of new phylo-groups. *Environmental Microbiology Reports* **5**(1): 58–65.
DOI: <https://doi.org/10.1111/1758-2229.12019>
- Clermont O., Lavollay M., Vimont S., Deschamps C., Forestier C., Branger C., Denamur E. & Arlet G. (2008). The CTX-M-15-producing *Escherichia coli* diffusing clone belongs to a highly virulent B2 phylogenetic subgroup. *Journal of Antimicrobial Chemotherapy* **61**(5): 1024–1028.
DOI: [10.1093/jac/dkn084](https://doi.org/10.1093/jac/dkn084)
- Clermont O., Dixit O.V.A., Vangchhia B., Condamine B., Dion S., Bridier-Nahmias A., Denamur E. & Gordon D. (2019). Characterization and rapid identification of phylogroup G in *Escherichia coli*, a lineage with high virulence and antibiotic resistance potential. *Environmental Microbiology* **21**(8): 3107–3117.
DOI: <https://doi.org/10.1111/1462-2920.14713>
- Diard M., Garry L., Selva M., Mosser T., Denamur E. & Matic I. (2010). Pathogenicity-associated islands in extraintestinal pathogenic *Escherichia coli* are fitness elements involved in intestinal colonization. *Journal of Bacteriology* **192**(19): 4885–4893.
DOI: <https://doi.org/10.1128/JB.00804-10>
- Dissanayake D.R.A., Octavia S. & Lan R. (2014). Population structure and virulence content of avian pathogenic *Escherichia coli* isolated from outbreaks in Sri Lanka. *Veterinary Microbiology* **168**(2): 403–412.
DOI: <https://doi.org/10.1016/j.vetmic.2013.11.028>
- Doumith M., Day M., Ciesielczuk H., Hope R., Underwood A., Reynolds R., Wain J., Livermore D.M. & Woodford N. (2015). Rapid identification of major *Escherichia coli* sequence types causing urinary tract and bloodstream infections. *Journal of Clinical Microbiology* **53**(1): 160–166.
DOI: <https://doi.org/10.1128/JCM.02562-14>
- Duriez P., Clermont O., Bonacorsi S., Bingen E., Chaventré A., Elion J., Picard B. & Denamur E. (2001). Commensal *Escherichia coli* isolates are phylogenetically distributed among geographically distinct human populations. *Microbiology* **147**(6): 1671–1676.
DOI: <https://doi.org/10.1099/002221287-147-6-1671>
- Escobar-Páramo P. et al., (12 authors) (2004). Large-scale population structure of human commensal *Escherichia coli* isolates. *Applied and Environmental Microbiology* **70**(9): 5698–5700.
DOI: <https://doi.org/10.1128/AEM.70.9.5698-5700.2004>
- Fernando M.M.P.S.C., Luke W.A.N.V., Miththinda J.K.N.D., Wickramasinghe R.D.S.S., Sebastianpillai B.S., Gunathilake M.P.M.L., Silva F.H.D.S. & Premaratna R. (2017). Extended spectrum beta lactamase producing organisms causing urinary tract infections in Sri Lanka and their antibiotic susceptibility pattern – A hospital based cross sectional study. *BMC Infectious Diseases* **17**(1): 138.
DOI: <https://doi.org/10.1186/s12879-017-2250-y>
- Giufre M., Graziani C., Accogli M., Luzzi I., Busani L. & Cerquetti M., on behalf of the *Escherichia coli* Study Group. (2012). *Escherichia coli* of human and avian origin: detection of clonal groups associated with fluoroquinolone and multidrug resistance in Italy. *Journal of Antimicrobial Chemotherapy* **67**(4): 860–867.
DOI: <https://doi.org/10.1093/jac/dkr565>
- Gordon D.M., Stern S.E. & Collignon P.J. (2005). Influence of the age and sex of human hosts on the distribution of *Escherichia coli* ECOR groups and virulence traits. *Microbiology* **151**(1): 15–23.
DOI: <https://doi.org/10.1099/mic.0.27425-0>
- Hilali F., Ruimy R., Saulnier P., Barnabé C., Lebouguénec C., Tibayrenc M. & Andremon A. (2000). Prevalence of virulence genes and clonality in *Escherichia coli* strains that cause bacteremia in cancer patients. *Infection and Immunity* **68**(7): 3983–3989.
DOI: <https://doi.org/10.1128/iai.68.7.3983-3989.2000>
- Hu Y.Y., Cai J.-C., Zhou H.-W., Chi D., Zhang X.-F., Chen W.-L., Zhang R. & Chen G.-X. (2013). Molecular typing of CTX-M-producing *Escherichia coli* isolates from environmental water, swine feces, specimens from healthy humans, and human patients. *Applied and Environmental Microbiology* **79**(19): 5988–5996.
DOI: <https://doi.org/10.1128/aem.01740-13>
- Jauregui F. et al., (13 authors) (2008). Phylogenetic and genomic diversity of human bacteremic *Escherichia coli* strains. *BMC Genomics* **9**(1): 560.
DOI: [10.1186/1471-2164-9-560](https://doi.org/10.1186/1471-2164-9-560)
- Jayathilleke S. K. et al., (11 authors) (2016) Analysis of urine culture isolates from seven laboratories of Sri Lanka: National laboratory based surveillance of Sri Lanka College of Microbiologists in 2014. *Sri Lankan Journal of Infectious Diseases* **6**(1): 17–24.
DOI: <http://dx.doi.org/10.4038/sljid.v6i1.8105>
- Johnson J.R., Delavari P., Kuskowski M. & Stell A.L. (2001). Phylogenetic distribution of extraintestinal virulence-associated traits in *Escherichia coli*. *Journal of Infectious Diseases* **183**(1): 78–88.

- DOI: <https://doi.org/10.1086/317656>
- Johnson J.R., Menard M., Johnston B., Kuskowski M.A., Nichol K. & Zhanel G.G. (2009). Epidemic clonal groups of *Escherichia coli* as a cause of antimicrobial-resistant urinary tract infections in Canada, 2002 to 2004. *Antimicrobial Agents and Chemotherapy* **53**(7): 2733–2739.
DOI: <https://doi.org/10.1128/AAC.00297-09>
- Johnson J.R., Oswald E., O'Bryan T.T., Kuskowski M.A. & Spanjaard L. (2002). Phylogenetic distribution of virulence-associated genes among *Escherichia coli* isolates associated with neonatal bacterial meningitis in the Netherlands. *Journal of Infectious Diseases* **185**(6): 774–784.
DOI: <https://doi.org/10.1086/339343>
- Le Gall T., Clermont O., Gouriou S., Picard, B. Nassif X., Denamur, E. & Tenaillon O. (2007). Extraintestinal virulence is a coincidental by-product of commensalism in B2 phylogenetic group *Escherichia coli* strains. *Molecular Biology and Evolution* **24**(11): 2373–2384.
DOI: <https://doi.org/10.1093/molbev/msm1172>
- Massot M. *et al.*, (14 authors) (2016). Phylogenetic, virulence and antibiotic resistance characteristics of commensal strain populations of *Escherichia coli* from community subjects in the Paris area in 2010 and evolution over 30 years. *Microbiology* **162**(4): 642–650.
DOI: <https://doi.org/10.1099/mic.0.000242>
- Matsukawa M., Igarashi M., Watanabe H., Qin L., Ohnishi M., Terajima J., Iyoda S., Morita-Ishihara T., Tateda K. & Ishii Y. (2019). Epidemiology and genotypic characterisation of dissemination patterns of uropathogenic *Escherichia coli* in a community. *Epidemiology and Infection* **147**.
DOI: <https://doi.org/10.1017/S0950268819000426>
- Méric G., Kemsley E.K., Falush D., Siggers E.J. & Lucchini S. (2013). Phylogenetic distribution of traits associated with plant colonization in *Escherichia coli*. *Environmental Microbiology* **15**(2): 487–501.
DOI: <https://doi.org/10.1111/j.1462-2920.2012.02852.x>
- Milkman R. (1973). Electrophoretic variation in *Escherichia coli* from natural sources. *Science* **182**(4116): 1024–1026.
DOI: <https://doi.org/10.1126/science.182.4116.1024>
- Mora A. *et al.*, (11 authors) (2009). Extraintestinal pathogenic *Escherichia coli* O1: K1: H7/NM from human and avian origin: detection of clonal groups B2 ST95 and D ST59 with different host distribution. *BMC Microbiology* **9**(1): 1–11.
DOI: <https://doi.org/10.1186/1471-2180-9-132>
- Mukherjee M., Koley S., Mukherjee S.K., Basu S., Ghosh B. & Chakraborty S. (2015) Phylogenetic background of *E. coli* isolated from asymptomatic pregnant women from Kolkata, India. *The Journal of Infection in Developing Countries* **9**(7): 720–724.
DOI: <https://doi.org/10.3855/jidc.5771>
- Mushtaq S., Irfan S., Sarma J.B., Doumith M., Pike R., Pitout J., Livermore D.M. & Woodford N. (2011). Phylogenetic diversity of *Escherichia coli* strains producing NDM-type carbapenemases. *Journal of Antimicrobial Chemotherapy* **66**(9): 2002–2005.
DOI: <https://doi.org/10.1093/jac/dkr226>
- Nowrouzian F.L., Östblom A.E., Wold A.E. & Adlerberth I. (2009). Phylogenetic group B2 *Escherichia coli* strains from the bowel microbiota of Pakistani infants carry few virulence genes and lack the capacity for long-term persistence. *Clinical Microbiology and Infection* **15**(5): 466–472.
DOI: <https://doi.org/10.1111/j.1469-0691.2009.02706.x>
- Ochman H. & Selander R.K. (1984). Standard reference strains of *Escherichia coli* from natural populations. *Journal of Bacteriology* **157**(2): 690–693.
- Petty N.K. *et al.*, (20 authors) (2014). Global dissemination of a multidrug resistant *Escherichia coli* clone. *Proceedings of the National Academy of Sciences* **111**(15): 5694–5699.
DOI: <https://doi.org/10.1073/pnas.1322678111>
- Picard B., Garcia J.S., Gouriou S., Duriez P., Brahimi N., Bingen E., Elion J. & Denamur E. (1999). The link between phylogeny and virulence in *Escherichia coli* extraintestinal infection. *Infection and Immunity* **67**(2): 546–553.
DOI: [doi:10.1128/iai.67.2.546-553.1999](https://doi.org/10.1128/iai.67.2.546-553.1999)
- Riley L.W. (2014). Pandemic lineages of extraintestinal pathogenic *Escherichia coli*. *Clinical Microbiology and Infection* **20**(5): 380–390.
DOI: <https://doi.org/10.1111/1469-0691.12646>
- Savageau M.A. (1983). *Escherichia coli* habitats, cell types, and molecular mechanisms of gene control. *American Naturalist* **122**: 732–744.
DOI: <https://doi.org/10.1086/284168>
- Sears H.J., Brownlee I. & Uchiyama J.K. (1950). Persistence of individual strains of *Escherichia coli* in the intestinal tract of man. *Journal of Bacteriology* **59**(2): 293–301.
- Selander R. & Levin B. (1980). Genetic diversity and structure in *Escherichia coli* populations. *Science* **210**(4469): 545–547.
DOI: <https://doi.org/10.1126/science.6999623>
- Singh T., Das S., Ramachandran V.G., Wani S., Shah D., Maroof K.A. & Sharma A. (2017). Distribution of integrons and phylogenetic groups among enteropathogenic *Escherichia coli* isolates from children <5 years of age in Delhi, India. *Frontiers in Microbiology* **8**(561).
DOI: <https://doi.org/10.3389/fmicb.2017.00561>
- Skurnik D. *et al.*, (16 authors) (2008). Characteristics of human intestinal *Escherichia coli* with changing environments. *Environmental Microbiology* **10**(8): 2132–2137.
DOI: <https://doi.org/10.1111/j.1462-2920.2008.01636.x>
- Stoppe N.D.C., Silva J.S., Torres T.T., Carlos C., Hachich E.M., Sato M.I.Z., Saraiva A.M. & Ottoni L.M.M. (2014). Clustering of water bodies in unpolluted and polluted environments based on *Escherichia coli* phylogroup abundance using a simple interaction database. *Genetics and Molecular Biology* **37**(4): 694–701.
DOI: <https://doi.org/10.1590/S1415-47572014005000016>
- Tenaillon O., Skurnik D., Picard B. & Denamur E. (2010). The population genetics of commensal *Escherichia coli*. *Nature Reviews Microbiology* **8**(3): 207–217.
DOI: <https://doi.org/10.1038/nrmicro2298>

- Tillekeratne L.G., Vidanagama D., Tippalagama R., Lewkebandara R., Joyce M., Nicholson B.P., Nagahawatte A., Bodinayake C.K., De Silva A.D. & Woods C.W. (2016). Extended-spectrum β -Lactamase-producing Enterobacteriaceae as a common cause of urinary tract infections in Sri Lanka. *Infection and Chemotherapy* **48**(3): 160–165.
DOI: <https://doi.org/10.3947/ic.2016.48.3.160>
- Unno T., Han D., Jang J., Lee S.N., Ko G., Choi H.Y., Kim J.H., Sadowsky M.J. & Hur H.G. (2009). Absence of *Escherichia coli* phylogenetic group B2 strains in humans and domesticated animals from Jeonnam Province, Republic of Korea. *Applied and Environmental Microbiology* **75**(17): 5659–5666.
DOI: <https://doi.org/10.1128/AEM.00443-09>
- Walk S.T., Alm E.W., Calhoun L.M., Mladonicky J.M. & Whittam T.S. (2007). Genetic diversity and population structure of *Escherichia coli* isolated from freshwater beaches. *Environmental Microbiology* **9**(9): 2274–2288.
DOI: <https://doi.org/10.1111/j.1462-2920.2007.01341.x>
- Walk S.T., Alm E.W., Gordon D.M., Ram J.L., Toranzos G.A., Tiedje J.M. & Whittam T.S. (2009). Cryptic lineages of the genus *Escherichia*. *Applied and Environmental Microbiology* **75**(20): 6534–6544.
DOI: <https://doi.org/10.1128/AEM.01262-09>
- Zhang L., Foxman B. & Marrs C. (2002). Both urinary and rectal *Escherichia coli* isolates are dominated by strains of phylogenetic group B2. *Journal of Clinical Microbiology* **40**(11): 3951–3955.
DOI: <https://doi.org/10.1128/JCM.40.11.3951-3955.2002>

RESEARCH ARTICLE

Tissue Culture

Sonication-assisted water extract of *Dendronephthya gigantea* exhibits anti-fine dust effects; attenuation of MAPK phosphorylation in macrophages

TU Jayawardena^{1,2}, IPS Fernando³, DP Nagahawatta¹, L Wang^{1,4}, HW Yang¹, JY Oh¹, KKA Sanjeewa^{1,5} and Y Jeon^{1,6*}

¹ Department of Marine Life Sciences, Jeju National University, Jeju 690-756, Republic of Korea.

² Department of Cell Biology & Anatomy, Arnie Charbonneau Cancer and Alberta Children's Hospital Research Institutes, Cumming School of Medicine, University of Calgary, Calgary, AB, Canada.

³ Department of Marine Bio-Food Sciences, Chonnam National University, Yeosu 59626, Republic of Korea.

⁴ College of Food Science and Engineering, Ocean University of China, Qingdao, 266003, China.

⁵ Department of Biosystems Technology, Faculty of Technology, University of Sri Jayewardenepura, Pitipana, Homagama.

⁶ Marine Science Institute, Jeju National University, Jeju Self-Governing Province 63333, Republic of Korea.

Submitted: 05 November 2020; Revised: 05 September 2021; Accepted: 22 October 2021


Abstract: Air pollution due to fine dust (FD) has become a global concern. Industrial effluents and traffic emissions combined with naturogenic sources influence this issue, which particularly impacts the East Asia region. Health concerns caused by this form of pollution include respiratory disorders. The development of anti-inflammatory agents requires an understanding of the underlying mechanism. This study investigated the impact of FD on RAW 264.7 macrophages and sonication-assisted water extract of soft coral *Dendronephthya gigantea* (DGE) as a potent anti-fine dust agent. Cytoprotective effects using MTT and NO production inhibition using the Griess assay were assessed. ELISA, western blotting, and RT-qPCR techniques were used to evaluate multiple molecular mediators involved in the inflammatory pathway. It was observed that iNOS, COX-2, and PGE₂, including pro-inflammatory cytokines (TNF- α , IL-1 β , and IL-6), were downregulated in a dose-dependent manner by DGE treatment. DGE inhibited the inflammatory responses initiated through FD by suppressing MAPK signaling in RAW 264.7 macrophages. This study provides insight into the protective mechanisms against FD, and suggests that *D. gigantea* could be a valuable, low-cost source of protein for potential use in the cosmeceutical and pharmaceutical sectors.

Keywords: Anti-fine dust, *Dendronephthya gigantea*, inflammation, macrophages MAPK, RT-qPCR

INTRODUCTION

Air pollution is comprised of harmful suspended contaminants in the air and is referred to as fine dust (FD) (Kim *et al.*, 2016). Concern regarding FD has increased due to its detrimental effects on humans and other organisms. Air pollution in the East Asia region, including China, Japan, and Korea, has become a major issue. This is mainly due to rapid industrialization, including coal burning, power generation, and traffic emissions consisting of hydrocarbons, oxides of nitrogen, and carbon monoxide (Pozzi *et al.*, 2003). Naturogenic sources also contribute to fine dust levels. Lee *et al.* (2015) reported that emissions released by China due to its industries are less than those released by natural sources.

The association between fine dust and health issues, including lung function issues and conditions regarding the respiratory system, has been reported previously. Nel *et al.* (1998) described allergic conditions that arise due to diesel exhaust particles. The influence of FD on human monocytes and pro-inflammatory cytokine levels

* Corresponding author (youjin2014@gmail.com  <https://orcid.org/0000-0003-3299-7266>)



This article is published under the Creative Commons CC-BY-ND License (<http://creativecommons.org/licenses/by-nd/4.0/>). This license permits use, distribution and reproduction, commercial and non-commercial, provided that the original work is properly cited and is not changed in anyway.

were described by Monn *et al.* (1999). The literature emphasizes two distinct sources of FD in the induction of inflammation. Several reports have suggested that the transition metal ion content influences inflammation via the oxidative stress pathway. According to some authors oxidative stress is caused by radicals that arise from the Fenton chemistry pathway. (Gilmour *et al.*, 1996; Knaapen *et al.*, 2002). The oxidative mechanism is most applicable to the smaller FD, which possess a higher surface area and a larger number of particles in a given volume of air. These are more toxic than their larger counterparts (Brown *et al.*, 2001). Alternatively, the bacterial-derived endotoxin bound to the surface of the particle may stimulate inflammation (Becker *et al.*, 1996; Schins *et al.*, 2004).

The anti-inflammatory potential of soft coral species has been widely studied. Chao *et al.* (2008) reported the anti-inflammatory potential of cembranoids isolated from the soft coral *Lobophytum crissum*. Ethanol extracts of soft corals collected from Jeju Island were studied by Wang *et al.* (2016) for their potential anti-inflammatory properties against LPS-stimulated RAW 264.7 macrophages. The therapeutic ability of soft coral *D. gigantea* regarding anti-inflammation in *in vivo* and *in vitro* conditions has been extensively studied by Fernando *et al.* (2018b); the compounds of interest was steroidal congeners.

The present study aimed to investigate the inflammatory stimulation of FD using macrophages as a model. *D. gigantea* sonication-assisted water extract (DGE) was evaluated for its ability to reduce the inflammatory responses that occurred in the macrophages. Inhibition of NO production, cytoprotective effect, and pro-inflammatory cytokines, including PGE₂, were also examined, including their gene expression levels, to identify the regulatory mechanism. The effects of DGE treatment on the MAPK pathway were also investigated. To the best of our knowledge, this is the first study to demonstrate that the sonication-assisted water extract from *D. gigantea* exhibits anti-fine dust effects through anti-inflammatory responses in macrophages.

MATERIALS AND METHODS

Materials

The fine dust used in the experiments was a certified reference material (CRM No. 28, National Institute for Environmental Studies, Ibaraki, Japan). RAW 264.7 macrophage cells purchased from the Korean Cell Line Bank (KCLB, Seoul, Korea) were used for experiments.

Growth media (Dulbecco's modified Eagle's medium, penicillin, and streptomycin) were purchased from GIBCO Inc. (Grand Island, NY, USA). Western blotting was performed using antibodies purchased from Santa Cruz Biotechnology (Santa Cruz, CA, USA) and Cell Signaling Technology (Beverly, MA, USA). Cytokine levels were analyzed using kits purchased from eBioscience (San Diego, CA, USA), R&D Systems (Minneapolis, MN, USA), BD Opteia (San Diego, CA, USA), and Invitrogen (Carlsbad, CA, USA). All solvents used were of analytical grade and were purchased from Sigma-Aldrich.

Extraction of *Dendronephthya gigantea*

D. gigantea samples were collected from the sea area around Jeju Island, South Korea, in May 2018. The Jeju Biodiversity Research Institute assisted with the sample identification process. Salt, sand, and epiphyte interferences were removed by washing. A sample portion (sample:water, 1:9) was extracted by assisting the sonication power (40 kHz) in an ultrasonic bath (Kodo Technical Research Co. Ltd., Hwaseong, Korea), maintaining the temperature between 20–30 °C. This solution was lyophilized and extensively dialyzed to remove salt ions. The sample was then again lyophilized, resulting in a *D. gigantea* 5 h sonication water extract (DGE), which was used in the subsequent experiments.

Analysis of proximate composition and amino acids of DGE

The moisture, ash content, and protein and lipid approximations were conducted following the methods described by the Association of Official Analytical Chemists standard methods (AOAC International, 2005). The method described by Um *et al.* (2017) was used to determine amino acid composition. HCl (6.0 M, 2 mL) was used to hydrolyze a 50 mg sample portion of DGE. It was then pre-concentrated to remove the HCl, and sodium citrate buffer was used to dissolve it (0.2 M, pH 2.2, 10 mL). Thereafter, this was successfully separated using a cation exchange column (LCA K06/Na, 4.6 × 150 mm). An amino acid analyzer was used for compositional analysis (S433-H, Sykam GmbH, Germany).

Estimation of fine dust size and morphology using SEM

The particle size and morphology of the FD specimens were determined using a field-emission electron

microscope (SEM) (JSM-670F, JEOL, Tokyo, Japan). Before SEM was introduced, the sample was sputter-coated with platinum (Q150R, Quorum Technologies, Lewes, UK) (Fernando *et al.*, 2017).

Maintenance of cell lines

Macrophage RAW 264.7 cells were cultured in DMEM medium (10 % FBS, 1 % P/S). Cell cultures were maintained in incubated conditions (5 % CO₂, 37 °C, humidified). Periodical subcultures were conducted and used for experiments during the exponential growth phase.

Analysis of cell viability and NO production

The MTT assay was used to assess cytotoxicity in FD-induced RAW macrophages (Mosmann 1983). The cells were seeded in 24 well plates (1×10^5 cells/mL), incubated, and treated with the samples. After 30 min, FD stimulation was conducted and further incubated for 30 min. This was followed by rinsing and refilling with fresh medium. The culture plates were incubated for an additional 23 h. The FD sample was first dissolved in growth media (DMEM) to obtain a stock concentration of 2.5 mg/mL and was further diluted to achieve the treatment concentrations. The MTT assay was conducted by measuring the optical density at a wavelength of 540 nm. NO production was measured using the Griess assay (Wijesinghe *et al.*, 2014).

Inflammatory mediator level assessment via ELISA

To obtain the cell culture media for the assessment of cytokine experiments, the cells were seeded, and sample treatment was performed similarly. Tumor necrosis factor α (TNF- α), interleukin (IL)-1 β , IL-6, and prostaglandin E₂ (PGE₂) levels were measured in the collected cell culture supernatants. The process was assisted with commercially available cytokine assessment kits, and the test followed the manufacturer's instructions.

Western blot analysis

Macrophage cells were seeded for the western blot analysis, and cells were harvested after sample and FD treatment. The experiment was conducted following the method explained in Jayawardena *et al.*, (2019).

RNA extraction, cDNA synthesis, and qPCR analysis

RNA extraction was performed in macrophage cells to synthesize cDNA. Total RNA was extracted, followed by purity measurement and cDNA synthesis. Synthesized

cDNA was stored at -80 °C, until use. qPCR analysis was performed using primers obtained from Bioneer (Seoul, Korea), following the method explained by Jayawardena *et al.* (2019). The method described by Livak *et al.* (2001) was used to analyze the relative expression levels.

Statistical analysis

A minimum of three trials were performed to express the data as the mean \pm standard deviation. IBM SPSS statistics using one-way ANOVA was used for the statistical comparison of significant differences. *p* values less than 0.05 ($p < 0.05$) were considered significant.

RESULTS AND DISCUSSION

Fine dust

The scanning electron microscope image of the urban aerosol (CRM No. 28) is shown in Figure 1. The sample consisted of particles with an irregular morphology. The size distribution was between 2 and 14 μ m in diameter, and most particles had diameters of $< 2 \mu$ m. The CRM No. 28 certificate contains polycyclic aromatic hydrocarbons (PAHs) and inorganic components (Mg, Ca, Ba, Sr, Mn, and Pb).

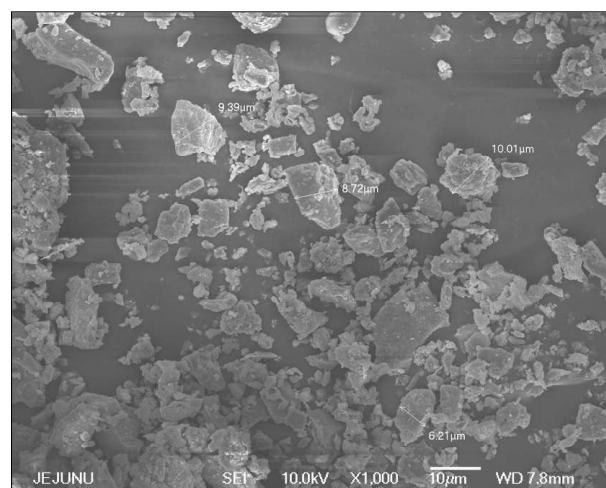


Figure 1: Fine dust subjected to scanning electron microscope (SEM) imaging (CRM No. 28 Urban Aerosols, National Institute for Environmental Studies (NIES), Ibaraki, Japan).

Fine dust air pollution has become a major issue in East Asia in recent years. Countries such as Korea, Japan, and China are the most affected. Recent publications have proposed that FD exposure is associated with respiratory complications, allergic reactions, and inflammatory skin

conditions. The FD is a complex mixture of different components. It includes various types of dust, such as tobacco smoke, pollen, and exhaust gas from traffic emissions (Kim *et al.*, 2016). In the East Asia region, this is exacerbated by anthropogenic activities; the Asian deserts are also act as a source of dust, which is transported by the wind (Choi *et al.*, 2001). FD contains both organic and inorganic components. Asian dust is reported to contain water-soluble mineral particles, such as Mg^{2+} and Ca^{2+} . Furthermore, negative ions, such as nitrate (NO_3^-) and sulfate (SO_4^{2-}), are associated with positive ions such as ammonium (NH_4^+) and potassium (K^+) (Maxwell-Meier 2004).

Proximate composition and amino acids of DGE

The 5 h sonication-assisted water extract yielded 4.3 ± 0.56 %. A higher amount of protein (68.38 ± 1.14 %) was identified compared to the lipid (5.82 ± 0.44 %) and carbohydrate (16.18 ± 0.38 %) content. The ash and moisture contents were reported as 5.14 ± 0.12 and 1.97 ± 0.16 respectively. DGE is an abundant source of protein and could potentially act as an important feature of the sample. The amino acid composition of DGE was rich in aspartic acid (11.97 %), glutamic acid (14.32 %), and proline (8.25 %). Branched-chain amino acids (BCAA; valine 6.39 %, isoleucine 4.00 %, and leucine 5.79 %), which are important in immune responses, also indicate an accountable portion of the DGE. The amino acid composition was as follows: Asp, 11.97; Glu, 14.32; Ser, 6.42; Gly, 5.54; His, 3.56; Arg, 5.37; Thr, 6.55; Ala, 5.14; Pro, 8.25; Tyr, 3.79; Val, 6.39; Met, 2.28; Cys, 2.20; Ile, 4.00; Leu, 5.79; Phe, 4.23; Lys, 4.12.

The present study evaluated the physical parameters of the FD via SEM, followed by its biological effect, using macrophages as a model. The relative effectiveness of time-dependent extraction methods in the marine soft coral *D. gigantea*, which could counter FD toxicity, was evaluated. Among them, the 5 h water extract (DGE) was found to be most effective (** $p < 0.01$).

Potential anti-fine dust effect of DGE in the inflammatory responses

The data presented in Figure 2a and 2b show that the viability of macrophages exposed to LPS and FD decreased while NO production increased. However, DGE treatment dose-dependently and substantially attenuated the cytotoxicity induced by LPS and FD. NO production, which was significantly upregulated by FD treatment, was successfully restored by treatment with DGE (Figure 2). This study demonstrates the significance of increasing levels of inflammatory regulators, including PGE_2 , and hence the levels of cyclooxygenase-2 (COX-2) and pro-inflammatory cytokines (IL-1 β and IL-6) against lipopolysaccharide (LPS; $1 \mu g mL^{-1}$) and FD stimulation ($125 \mu g/mL$). The use of LPS as an inflammatory stimulator provides a reference for the inflammatory induction that occurs via FD. DGE downregulates the expression of inflammatory mediators (Figure 3). TNF- α downregulation was notable but not significant, while IL-1 β and IL-6 levels declined significantly. Western blot analysis showed that the levels of iNOS and COX-2 (Figure 4a and b) increased with the stimulation of FD, whereas co-treatment with DGE dose-dependently downregulated the protein levels.

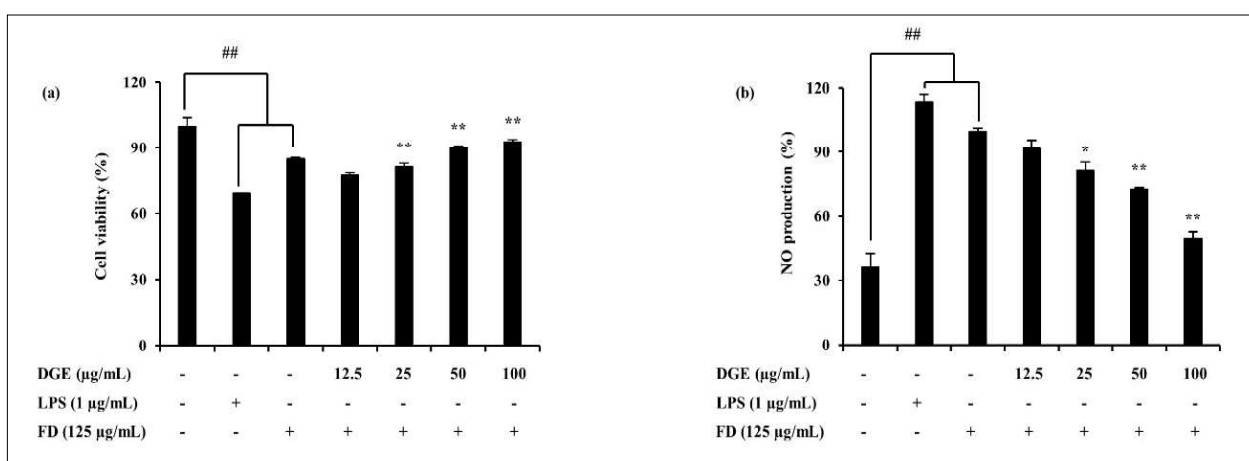


Figure 2: FD-induced RAW 264.7 macrophages, (a) cell viability and (b) NO production. LPS stimulation ($1 \mu g/mL$) or FD ($125 \mu g/mL$). Triplicated experiments; mean value is expressed with \pm SD. * $p < 0.05$, ** $p < 0.01$ vs. the FD treated group; # $p < 0.05$, ## $p < 0.01$ vs. the un-stimulated group.

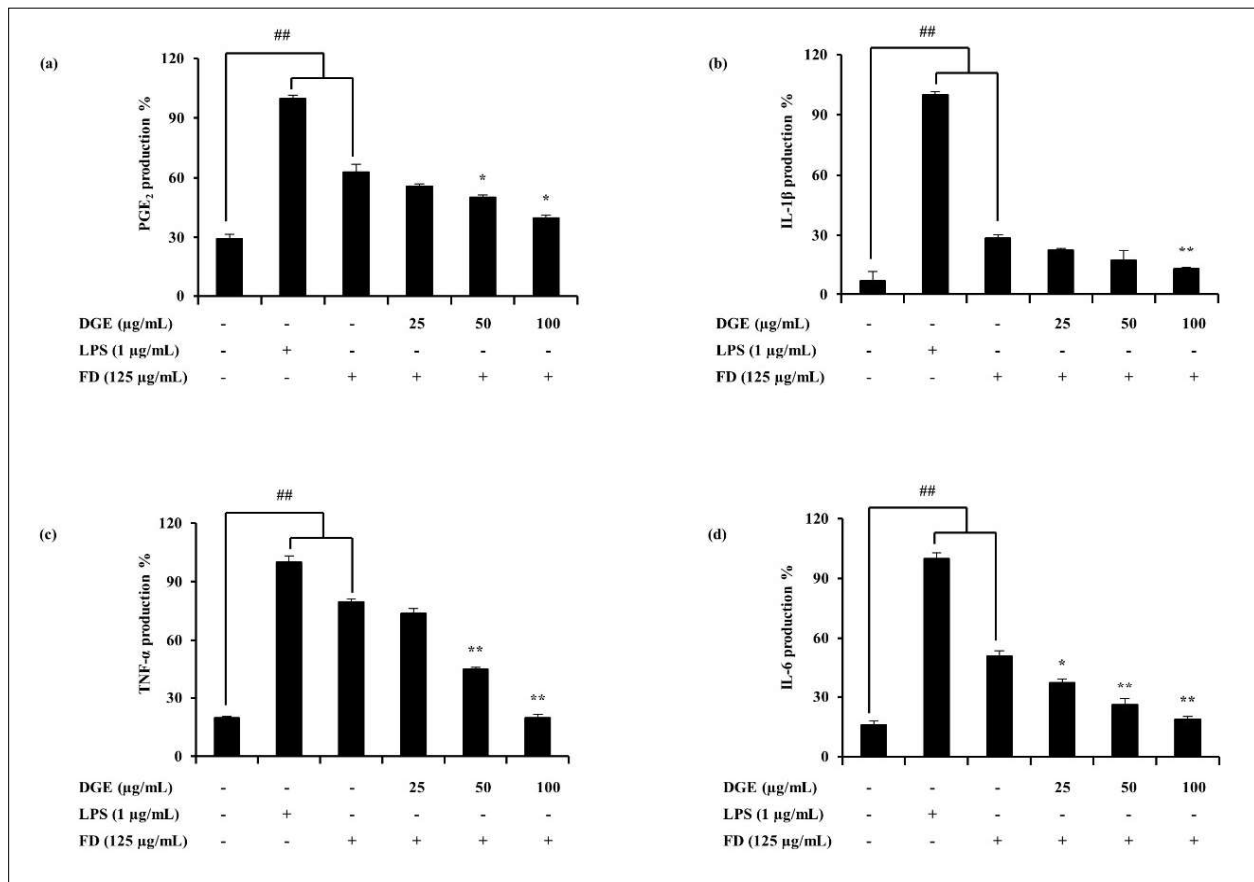


Figure 3: ELISA experiments performed using FD-induced RAW 264.7 cell supernatants. Potential of DGE to inhibit PGE₂ and pro-inflammatory cytokines (IL-1β, IL-6, and TNF-α) production. Triplicated experiments; mean value is expressed with \pm SD. *p < 0.05, **p < 0.01 vs. the FD treated group; #p < 0.05, ##p < 0.01 vs. the un-stimulated group.

Inflammation is directly associated with macrophage cells and is regulated via different mechanisms, such as phagocytosis, antigen presentation, and the production of various cytokines and chemokines. Although the activation of macrophages is essential to counteract inflammation, their over-activation could lead to detrimental effects. Hence, the regulation of these cells is important for the treatment of inflammation. Important mediators in this process are NO, iNOS, COX-2, PGE₂, and pro-inflammatory cytokines, including TNF-α, IL-1β, and IL-6 (Fernando *et al.*, 2017). The results indicate the upregulation of these mediators upon LPS and FD stimulation in macrophages. Their gradual downregulation is ensured via the dose-dependent treatment of DGE, verifying its ability to act as a potent anti-fine dust agent via anti-inflammatory mechanisms. Furthermore, the results indicated that DGE suppressed

the mRNA expression of the above mediators, leading to a decline in the production of inflammatory mediators required for inflammation, thus inhibiting inflammation. NO plays a vital role as a vascular dilator, neurotransmitter, and a key component of the immunological system. It is synthesized from arginine via nitric oxide synthase (NOS) (Nakagawa *et al.*, 2002). Under obsessive conditions, NO production is inclined due to the activity of inducible NOS (iNOS), leading to cytotoxicity and tissue damage (Kim *et al.*, 1999). COX-2 is another protein closely related to this pathway. This helps in generating another inflammatory mediator, PGE₂, by catalyzing the process. Different cytokines and growth factors stimulate COX-2 expression (Park *et al.*, 2006). Hence, cytokine production may ultimately attenuate NO production in the inflammatory pathway.

Ability of DGE to reduce the FD induced inflammatory responses via the p38-MAPK pathway

In the process of evaluating the activity of DGE as an anti-fine dust agent, we subsequently assessed whether the inhibition of inflammatory responses is mediated via through p38-MAPK pathway. The FD-induced phosphorylation of p38, ERK1/2, and JNK MAPKs in macrophages was evaluated by western blotting. As shown in Figure 4, LPS encouraged phosphorylation, whereas FD stimulation lagged behind it. DGE treatment (25, 50, and 100 µg/mL) gradually downregulated the phosphorylation of p38, ERK1/2, and JNK. Among the MAPKs, p38 exhibited drastic down-regulation, whereas ERK1/2 remained the least affected by all three. Thus, the results indicate the potential of DGEs to inhibit MAP kinase phosphorylation against FD stimulation.

This study focused on MAP kinases, a highly conserved family of proteins that comprise serine/threonine. This includes three subfamilies: ERKs, JNKs, and p38 MAPKs (Ruland *et al.*, 2003). The MAPK signaling pathway can be triggered by various extracellular signals, including cell proliferation, apoptosis, and inflammation. LPS is a potential activator of all three types of MAPKs (Hommes *et al.*, 2003). Fernando *et al.* (2018a) described MAP kinase activation via stimulation of FD in keratinocytes and macrophages. Activated p38 is thought to exhibit significant activities in regulating inflammatory mediators, such as iNOS, COX-2, and TNF-α gene expression. Activated ERK is believed to increase the production of iNOS and other pro-inflammatory cytokines (Bhat *et al.*, 1998; Ajizian *et al.*, 1999). JNK is also involved in iNOS expression of the iNOS (Uto *et al.*, 2005). It was observed that the

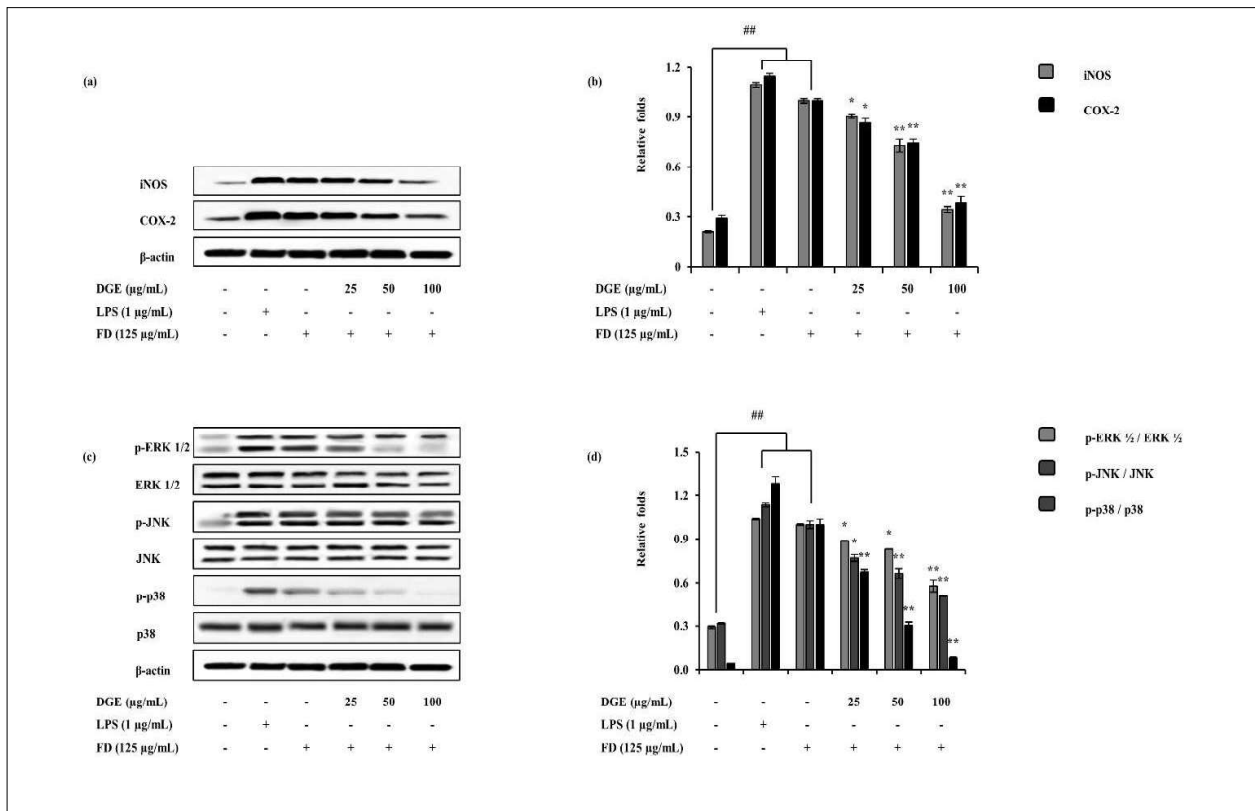


Figure 4: Potential of DGE to act upon inflammatory pathway mediators induced via FD. (a) iNOS and COX-2, (b) quantitative data, (c) ERK, JNK, and p-38 MAPKs, and relevant (d) quantitative data, determined using western blotting. β-actin was used as an internal control. Quantitative data were analyzed using ImageJ software. Results are expressed as the mean ± SD of three separate experiments. *p < 0.05, **p < 0.01 vs. the FD-treated group; #p < 0.05, ##p < 0.01 vs. the unstimulated group.

DGE dose-dependently inhibited the phosphorylation of MAPKs. This may lead to the anti-inflammatory activity of DGE in FD-stimulated macrophage cells.

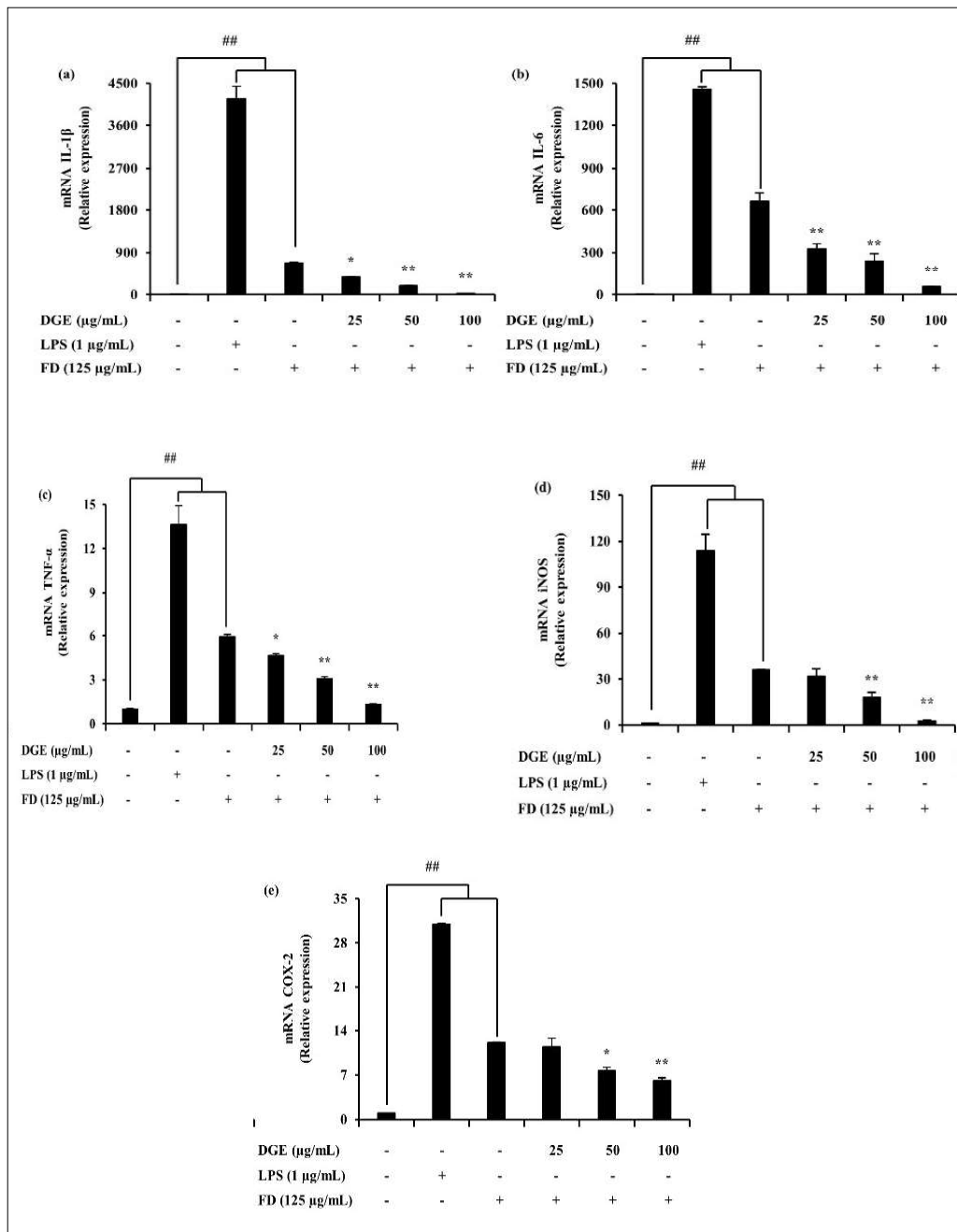


Figure 5: DGE inhibits inflammation-associated gene expression levels in FD-induced RAW 264.7 macrophages. (a) IL-1 β , (b) IL-6, (c) TNF- α , (d) iNOS and (e) COX-2. The 2- $\Delta\Delta$ Ct method was used to calculate the relative mRNA levels. GAPDH was used as an internal reference. Experiments were triplicated. mRNA significance relative to non-treated control was calculated using the Mann-Whitney U test. * $p < 0.05$, ** $p < 0.01$ vs. the FD treated group; # $p < 0.05$, ## $p < 0.01$ vs. the un-stimulated group.

Effect of DGE to attenuate FD-stimulated gene expression

DGE treatment downregulated the mRNA expression levels of iNOS and COX-2 and was observed with a similar trend to the western blot results. A significant decline in pro-inflammatory cytokine levels was also observed. The potential of DGE as an anti-fine dust agent in anti-inflammatory mechanisms was confirmed by the results.

It has been discovered that amino acids are involved in cell signaling and play an important role in gene expression regulation and protein phosphorylation cascades (Wu, 2009). It also involves the activation of natural killer cells (macrophages) and the production of cytokines. Arginine is a conditionally essential amino acid, and its major functions include regulation of cytokine production and acting as a mediator for autoimmune diseases. Glutamic acid and proline, which are abundant amino acids in DGE, are important for arginine synthesis (Li *et al.*, 2007). Similarly, the three BCAAs are vital for the regulation of immune responses. The anti-inflammatory potential of BCAAs in RAW 264.7 macrophages under LPS-stimulated conditions was evaluated recently by Lee *et al.* (2017). As DGE contains many amino acids involved in immune responses, it is potentially suitable as an anti-inflammatory agent.

CONCLUSIONS

This study reveals that DGEs have potential as anti-fine dust agents and their ability to regulate the production of important inflammatory mediators such as NO, PGE₂, and cytokines via the modulation of MAPK phosphorylation in macrophages. Hence, *D. gigantea* could be a valuable, low-cost source of protein for potential use in the cosmeceutical and pharmaceutical sectors. This study provides insight into the protective mechanisms against FD. As *D. gigantea* is a rapidly growing species due to the ocean temperature increment in the vicinity of Jeju Island, harvesting these soft coral species would not alter the diversity of its natural habitat.

REFERENCES

- Ajizian S.J., English B.K. & Meals E.A. (1999). Specific inhibitors of p38 and extracellular signal-regulated kinase mitogen-activated protein kinase pathways block inducible nitric oxide synthase and tumor necrosis factor accumulation in murine macrophages stimulated with lipopolysaccharide and interferon-gamma. *The Journal of Infectious Disease* **179**(4): 939–944.
- DOI: <https://doi.org/10.1086/314659>
- AOAC International (2005). *Official Methods of Analysis of AOAC International*, 18th edition. AOAC International. Rockville, Maryland, USA.
- Becker S., Soukup J.M. Gilmour M.I. & Devlin R.B.(1996). Stimulation of human and rat alveolar macrophages by urban air particulates: effects on oxidant radical generation and cytokine production. *Toxicology and Applied Pharmacology* **141**(2): 637–648.
- DOI: <https://doi.org/10.1006/taap.1996.0330>
- Bhat N.R., Zhang P., Lee J.C. & Hogan E.L. (1998). Extracellular signal-regulated kinase and p38 subgroups of mitogen-activated protein kinases regulate inducible nitric oxide synthase and tumor necrosis factor- α Gene Expression in Endotoxin-Stimulated Primary Glial cultures. *The Journal of Neuroscience* **18**(5): 1633–1641.
- DOI: <https://doi.org/10.1523/jneurosci.18-05-01633.1998>
- Brown D.M., Wilson M.R., MacNee W., Stone V. & Donaldson K. (2001). Size-dependent proinflammatory effects of ultrafine polystyrene particles: a role for surface area and oxidative stress in the enhanced activity of ultrafines. *Toxicology and Applied Pharmacology* **175**(3): 191–199.
- DOI: <https://doi.org/10.1006/taap.2001.9240>
- Chao C.H., Wen Z.H., Wu Y.C, Yeh H.C. & Sheu J.H. (2008). Cytotoxic and anti-inflammatory cembranoids from the soft coral *Lobophytum crassum*. *Journal of Natural Products* **71**(11): 1819–1824.
- DOI: <https://doi.org/10.1021/np8004584>
- Choi J.C., Lee M., Chun Y., Kim J. & Oh S. (2001). Chemical composition and source signature of spring aerosol in Seoul, Korea. *Journal of Geophysical Research-Atmospheres* **106**(D16): 18067–18074.
- DOI: <https://doi.org/10.1029/2001jd900090>
- Fernando I.P.S., Jayawardena T.U., Sanjeeva K.K.A., Wang L., Jeon Y.J. & Lee W.W. (2018a). Anti-inflammatory potential of alginic acid from *Sargassum horneri* against urban aerosol-induced inflammatory responses in keratinocytes and macrophages. *Ecotoxicology and Environmental Safety* **160**: 24–31.
- DOI: <https://doi.org/10.1016/j.ecoenv.2018.05.024>
- Fernando I.P.S., Kim H.-S., Sanjeeva K.K.A, Oh J.-Y., Jeon Y.-J. & Lee W.W. (2017). Inhibition of inflammatory responses elicited by urban fine dust particles in keratinocytes and macrophages by diphlorethohydroxycarmalol isolated from a brown alga *Ishige okamurae*. *Algae* **32**(3): 261–273.
- DOI: <https://doi.org/10.4490/algae.2017.32.8.14>
- Fernando I.S., Lee W.W., Jayawardena T.U., Kang M.-C., Ann Y.-S., Ko C.-i., Park Y.J. & Jeon Y.-J. (2018b). 3 β -Hydroxy- Δ 5-steroidal congeners from a column fraction of *Dendronephthya puetteri* attenuate LPS-induced inflammatory responses in RAW 264.7 macrophages and zebrafish embryo model. *RSC Advances* **8**(33): 18626–18634.
- DOI: <https://doi.org/10.1039/C8RA01967C>
- Gilmour P.S., Brown D.M., Lindsay T.G., Beswick P.H., MacNee W. & Donaldson K. (1996). Adverse health effects of PM10 particles: involvement of iron in generation of hydroxyl radical. *Occupational and Environmental*

- Medicine* **53**(12): 817–822.
DOI: <https://doi.org/10.1136/oem.53.12.817>
- Hommers D.W., Peppelenbosch M.P. & van Deventer S.J. (2003). Mitogen activated protein (MAP) kinase signal transduction pathways and novel anti-inflammatory targets. *Gut* **52**(1): 144–151.
DOI: <https://doi.org/10.1136/gut.52.1.144>
- Jayawardena T.U., Kim H.-S., Sanjeeva K.K.A., Kim S.-Y., Rho J.-R., Jee Y., Ahn G. & Jeon Y.-J. (2019). Sargassum horneri and isolated 6-hydroxy-4,4,7a-trimethyl-5,6,7,7a-tetrahydrobenzofuran-2(4H)-one (HTT); LPS-induced inflammation attenuation via suppressing NF- κ B, MAPK and oxidative stress through Nrf2/HO-1 pathways in RAW 264.7 macrophages. *Algal Research* **40**: 101513.
DOI: <https://doi.org/10.1016/j.algal.2019.101513>
- Kim H.K., Cheon B.S., Kim Y.H., Kim S.Y. & Kim H.P. (1999). Effects of naturally occurring flavonoids on nitric oxide production in the macrophage cell line RAW 264.7 and their structure–activity relationships. *Biochemical Pharmacology* **58**(5): 759–765.
DOI: [https://doi.org/10.1016/s0006-2952\(99\)00160-4](https://doi.org/10.1016/s0006-2952(99)00160-4)
- Kim K.E., Cho D. & Park H.J. (2016). Air pollution and skin diseases: Adverse effects of airborne particulate matter on various skin diseases. *Life Sciences* **152**: 126–134.
DOI: <https://doi.org/10.1016/j.lfs.2016.03.039>
- Knaapen A.M., Shi T., Borm P.J.A. & Schins R.P.F. (2002). Soluble metals as well as the insoluble particle fraction are involved in cellular DNA damage induced by particulate matter. In: *Oxygen/Nitrogen Radicals: Cell Injury and Disease* (eds. V. Vallyathan, X. Shi & V. Castranova), pp. 317–326. Springer US, Boston, USA.
DOI: https://doi.org/10.1007/978-1-4615-1087-1_36
- Lee J.H., Park E., Jin H.J., Lee Y., Choi S.J., Lee G.W., Chang P.S. & Paik H.D. (2017). Anti-inflammatory and antigenotoxic activity of branched chain amino acids (BCAA) in lipopolysaccharide (LPS) stimulated RAW 264.7 macrophages. *Food Science and Biotechnology* **26**(5): 1371–1377.
DOI: <https://doi.org/10.1007/s10068-017-0165-4>
- Lee Y.G., Ho C.H., Kim J.H. & Kim J. (2015). Quiescence of Asian dust events in South Korea and Japan during 2012 spring: dust outbreaks and transports. *Atmospheric Environment* **114**: 92–101.
DOI: <https://doi.org/10.1016/j.atmosenv.2015.05.035>
- Li P., Yin Y.L., Li D., Kim S.W. & Wu G. (2007). Amino acids and immune function. *British Journal of Nutrition* **98**(2): 237–252.
DOI: <https://doi.org/10.1017/S000711450769936X>
- Livak K.J. & Schmittgen T.D. (2001). Analysis of relative gene expression data using real-time quantitative PCR and the 2(-Delta Delta C(T)) Method. *Methods* **25**(4): 402–408.
DOI: <https://doi.org/10.1006/meth.2001.1262>
- Maxwell-Meier K. (2004). Inorganic composition of fine particles in mixed mineral dust–pollution plumes observed from airborne measurements during ACE-Asia. *Journal of Geophysical Research: Atmospheres* **109**(D19).
DOI: <https://doi.org/10.1029/2003jd004464>
- Monn C. & Becker S. (1999). Cytotoxicity and induction of proinflammatory cytokines from human monocytes exposed to fine (PM_{2.5}) and coarse particles (PM_{10-2.5}) in outdoor and indoor air. *Toxicology and Applied Pharmacology* **155**(3): 245–252.
DOI: <https://doi.org/10.1006/taap.1998.8591>
- Mosmann T. (1983). Rapid colorimetric assay for cellular growth and survival: application to proliferation and cytotoxicity assays. *Journal of Immunological Methods* **65**(1-2): 55–63.
DOI: [https://doi.org/10.1016/0022-1759\(83\)90303-4](https://doi.org/10.1016/0022-1759(83)90303-4)
- Nakagawa T. & Yokozawa T. (2002). Direct scavenging of nitric oxide and superoxide by green tea. *Food and Chemical Toxicology* **40**(12): 1745–1750.
DOI: [https://doi.org/10.1016/s0278-6915\(02\)00169-2](https://doi.org/10.1016/s0278-6915(02)00169-2)
- Nel A.E., Diaz-Sanchez D., Ng D., Hiura T. & Saxon A. (1998). Enhancement of allergic inflammation by the interaction between diesel exhaust particles and the immune system. *Journal of Allergy and Clinical Immunology* **102**(4): 539–554.
DOI: [https://doi.org/10.1016/S0091-6749\(98\)70269-6](https://doi.org/10.1016/S0091-6749(98)70269-6)
- Park J.Y., Pillinger M.H. & Abramson S.B. (2006). Prostaglandin E₂ synthesis and secretion: the role of PGE₂ synthases. *Clinical Immunology* **119**(3): 229–240.
DOI: <https://doi.org/10.1016/j.clim.2006.01.016>
- Pozzi R., De Berardis B., Paoletti L. & Guastadisegni C. (2003). Inflammatory mediators induced by coarse (PM_{2.5-10}) and fine (PM_{2.5}) urban air particles in RAW 264.7 cells. *Toxicology* **183**(1-3): 243–254.
DOI: [https://doi.org/10.1016/s0300-483x\(02\)00545-0](https://doi.org/10.1016/s0300-483x(02)00545-0)
- Ruland J. & Mak T.W. (2003). Transducing signals from antigen receptors to nuclear factor kappaB. *Immunological Reviews* **193**(1): 93–100.
DOI: <https://doi.org/10.1034/j.1600-065x.2003.00049.x>
- Schins R.P., Lightbody J.H., Borm P.J., Shi T., Donaldson K. & Stone V. (2004). Inflammatory effects of coarse and fine particulate matter in relation to chemical and biological constituents. *Toxicology and Applied Pharmacology* **195**(1): 1–11.
DOI: <https://doi.org/10.1016/j.taap.2003.10.002>
- Um J.H., Kim E.-A., Lee W.W., Kang N., Han E.J., Oh J.Y., Park S.Y., Jeon Y.-J., Lee S.-H. & Ahn G. (2017). Protective effects of an enzymatic hydrolysate from *octopus ocellatus* meat against hydrogen peroxide-induced oxidative stress in Chang liver cells and zebrafish embryo. In: *Taurine 10. Advances in Experimental Medicine and Biology* (eds. S. S. W. DH Lee., Park E., H.W. Kim), pp. 603–620. Springer Dordrecht, Netherlands.
DOI: https://doi.org/10.1007/978-94-024-1079-2_47
- Uto T., Fujii M. & Hou D.X. (2005). 6-(Methylsulfinyl) hexyl isothiocyanate suppresses inducible nitric oxide synthase expression through the inhibition of Janus kinase 2-mediated JNK pathway in lipopolysaccharide-activated murine macrophages. *Biochemical Pharmacology* **70**(8): 1211–1221.
DOI: <https://doi.org/10.1016/j.bcp.2005.07.011>

- Wang L., Oh J.Y. , Fernando I.P.S., Sanjeewa K.K.A., Kim E.-A., Lee W. & Jeon Y.-J. (2016). Soft corals collected from Jeju Island; a potential source of anti-inflammatory phytochemicals. *Journal of Chitin and Chitosan* **21**(4): 247–254.
DOI: <https://doi.org/10.17642/jcc.21.4.4>
- Wijesinghe W.A.J.P., Kang M.C., Lee W.W., Lee H.S., Kamada T., Vairappan C.S. & Jeon Y.J. (2014). 5 beta-Hydroxypalisadin B isolated from red alga *Laurencia snackeyi* attenuates inflammatory response in lipopolysaccharide-stimulated RAW 264.7 macrophages. *Algae* **29**(4): 333–341.
DOI: <https://doi.org/10.4490/algae.2014.29.4.333>
- Wu G. (2009). Amino acids: metabolism, functions, and nutrition. *Amino Acids* **37**(1): 1–17.
DOI: <https://doi.org/10.1007/s00726-009-0269-0>

RESEARCH ARTICLE

Renewable Energy

A novel approach for energy and exergy analysis of a flat plate solar collector with energy storage

M Hanif*, M K Khattak, I Ul Haq, R Uddin and K Ullah

Department of Agricultural Mechanization and Renewable Energy Technologies, Faculty of Crop Production Sciences, The University of Agriculture Peshawar, Peshawar, Pakistan - 25130.

Submitted: 13 November 2020; Revised: 03 September 2021; Accepted: 22 October 2021

Abstract: Experiments were conducted to evaluate the performance of a flat plate solar collector in terms of its energy, exergy, and efficiency. The data were analyzed using three factors in a Completely Randomized Design. The first factor was tilt angle with three levels, the second was air mass flow rates with four levels, and the third was heat storage fluid with four levels, making a 4 x 3 x 4 factorial experiment. The least significant difference between means was calculated with Alfa (α) < 0.01. The results showed that the maximum energy of 1509.74 kJ hr⁻¹ was gained by the flat plate solar collector when a polyethylene glycol solution was used in head raised pipes at 11.76 kg min⁻¹ air flow rates with a 30° collector tilt. The maximum exergy of 46.0 % was gained by the flat plate solar collector when air was used in head raised pipes at 4.67 kg min⁻¹ air flow rates, with 30° collector tilt angle, while the minimum exergy gain of 32.67 % was recorded for a polyethylene glycol solution in the solar collector at 1.78 kg min⁻¹ air flow rates with collector tilting at 30°. The maximum efficiency of 39.71 % was gained by the flat plate solar collector when a polyethylene glycol solution was used in head raised pipes at 9.69 kg min⁻¹ air flow rates with 40° collector tilt angle. The storage medium showed that the maximum energy of 40,207 kJ day⁻¹ was stored in the energy storage unit per day, followed by 33,291 kJ day⁻¹ stored in salt solution while minimum energy of 29,640 kJ day⁻¹ was stored with water.

Keywords: Efficiency, energy storage, exergy, flat plate, solar collector, solar energy

INTRODUCTION

Energy is the engine of economic growth and social development. The increasing demand for energy and

depletion of fossil fuel reservoirs is a serious global issue. An increase in the demand for energy production and the adverse impact of fossil fuels on the global environment has led to a significantly enhanced interest in acquiring environment-friendly renewable energy resources. Renewable energy sources have the potential to fulfill energy demand and alleviate environment destruction by greenhouse gases emitted via the use of fossil fuels. It is therefore widely realized that renewable energy can play a vital role in any field where energy is a primary source. Renewable energy resources have the potential to replace the non-renewable energy resources if properly planned and installed according to the demand, with all the engineering aspects needed for their maximum output (Bellos *et al.*, 2016).

Renewable energy has many sources; among them, solar energy is a clean, abundant, and environment-friendly source which has received considerable attention for generating heat and electricity. It is playing a vital role in maintaining the environment of this green planet. This energy from the sun reaches the earth in the form of solar irradiance. Solar irradiance is the energy given by sunlight per unit area in unit time. It can be converted into heat and electricity using different solar conversion technologies, namely flat plate solar collectors, concentrating solar collectors and photovoltaic technologies. Flat plate and parabolic trough solar collectors are the main types of solar thermal heating systems. The flat plate solar collectors are used mainly for low thermal systems for agricultural and domestic

* Corresponding author (hanif_mechanization@aup.edu.pk;  <https://orcid.org/0000-0003-1698-8802>)



This article is published under the Creative Commons CC-BY-ND License (<http://creativecommons.org/licenses/by-nd/4.0/>). This license permits use, distribution and reproduction, commercial and non-commercial, provided that the original work is properly cited and is not changed in anyway.

heating requirements. Alternately the parabolic trough concentrating solar collector technology is used for high thermal systems like steam and power generation (Soteris *et al.*, 2016).

The efficiency of a solar thermal system is critical to its maximum performance. However, the efficiency equation alone does not determine the internal losses from the solar collectors. For this purpose, an analysis based on the second law of thermodynamics is best to determine the exergy analysis or potential energy of the solar collector system. Exergy analysis is both vital and the most important parameter for optimization of design and the future operation of solar thermal collectors. Solar thermal collectors must have been examined in terms of their energy and exergy, efficiency, and entropy generation for peak performance (Boukelia *et al.*, 2015). Fahad *et al.* (2013) discussed the optimal and critical operations of different solar collectors by means of energy and exergy analysis. They concluded that an optimal operational model at any state is not useful for performance analysis because it is not a complete setup for generalizing and optimizing the solar collector performance. Therefore, an advanced model incorporating solutions to common errors for energy and exergy analysis is required for computing efficiencies of solar collectors.

Farhat *et al.* (2009) and Frances *et al.* (2012) studied the performance of a thermal solar collector. They stated that the performance must be tested in dynamic models, and energy and exergy analysis must be carried out in transient states. Many authors reported their work on optimizing the performance of solar collectors and they have concluded that solar collectors showed multiple difficulties under steady state conditions. Thus, it is recommended to develop and test the solar thermal collectors in transient states for achieving better results of energy and exergy analysis.

Air turbidity is playing a significant role in energy and exergy analysis of solar collectors. To carry out energy and exergy analysis of a solar collector, it is necessary to keep in mind that the sky must be clear, the flow rate must be constant, the assumption must be made that the properties of the material of construction of the solar collector are constant, the glazing must have more than 85% transmittance, the fluid velocity must be uniform, the losses by reflection are assumed to be negligible, and the air gap between the absorber and glazing must be transparent (Jafarkazmi & Ahmadifard, 2013). The aim of the study was to evaluate the energy, exergy, and efficiency of a flat plate solar collector as affected by both the sole and the combined or interaction effect of air mass

flow rate, tilt angle, and heat storing fluid in the flat plate solar collector, and to study the role of the energy storage unit in enhancing the solar collector performance.

MATERIALS AND METHODS

Site selection

The collector was installed on the roof of the Department of Agricultural Mechanization, The University of Agriculture Peshawar, Khyber Pakhtunkhwa, Pakistan. The latitude, longitude and elevation of the site are 34.02°, 71.48° and 448.36 m, respectively. The site is ideal for this purpose as it receives maximum solar irradiance from dawn to dusk without the interference of any shadow of a structure (Francesco *et al.*, 2016).

The thermal solar collector

The flat plate solar collector that was used in the experiment is shown in Figure 1. The solar collector was developed in the Department of Agricultural Mechanization, The University of Agriculture Peshawar. The design and other parameters of construction are given in Table 1.



Figure 1: Design specifications of the flat plate solar collector

Recording solar irradiance

The data of daily solar irradiance were recorded with the help of a digital Pyranometer (Solar Power Meter, TES-1333, Taiwan)

Energy and exergy analysis

When the solar collector is in equilibrium with the surroundings, then the general form of the energy balance equation (1) given by Govindaraj *et al.* (2012), can be applied:

Table 1: Design specifications of the flat plate solar collector

Parameters/Conditions	Value
Collector's length, width and depth	3.40, 2.46 & 0.66 m respectively
Area	8.365 m ²
Volume of the solar collector	5.520 m ³
Absorber	V-corrugated, black painted galvanized steel with header raiser pipes
Absorber area	8.360 m ²
Absorbance and transmittance of absorber	0.92 and 0.88
Glazing (single glass)	0.008 m (8 mm)
Agent fluids	Air, Water, salt solution and polyethylene glycol solution
Air velocity range	0.1 – 3.31 m s ⁻¹
Collector tilt angles	30°, 35° and 40°
Ambient temperature range	275 – 315 K
Apparent sun temperature	5777 K (Yadav <i>et al.</i> , 2014)
Absorber thickness	0.0024 m (2.4 mm)
Optical efficiency	0.88
Transmittance of glazing	0.89
Thickness of insulation (Wood of deodar + polystyrene)	0.15 m
Thermal conductivity of absorber	380 W m ⁻¹ . °C ⁻¹
Solar irradiance range	0 – 950 W m ⁻²
Tubes/ pipes diameter (steel)	0.025 m
Air mass flow rates	3.56 – 12.46 kg min ⁻¹
Volume of storage tank	0.12 m ³
Mass of water in storage tank	120 kg
Volume of the head raised pipes	0.086 m ³
Mass of water in pipes	86 kg
Total volume of water in solar collector	206 kg
Parts of the the solar collector/materials Used for construction	Cost
Insulation box	\$ 500
Absorber	\$ 120
Glazing	\$ 110
Water pipes, fluids and storage tank	\$ 130
Total cost	\$ 860

$$E_{in} - E_s - E_{L1} - E_{L2} - E_{ex} = 0 \quad \dots(1)$$

Where E_{in} is energy input to the solar collector (kJ), E_s is the energy stored by the solar collector (kJ), E_{ex} is the exergy of the solar collector (kJ), E_{L1} is the heat lost

by glazing due to transmittance and absorbance of the absorber plate (kJ), and E_{L2} is heat lost due to insulation characteristics of the solar collector (kJ). Now we have to calculate each and every component of equation (1) in detail to develop an equation for finding the efficiency of the solar collector.

Energy analysis of a thermal solar collector

The Energy available to the solar collector is the amount of solar irradiance per unit area of the collector. It is the energy given by sun radiation to the solar collector and can be calculated using equation (2) given by Hanif *et al.* (2015),

$$E_{in} = I A_c \left(1 - \frac{T_a}{T_s}\right) \quad \dots(2)$$

where E_{in} is the rate of energy given by sunlight to the solar collector (kJ hr^{-1}), I is solar irradiance (kJ m^{-2}), A_c is area of the solar collector (m^2), T_a is ambient air temperature ($^{\circ}\text{C}$), T_s is the apparent the sun surface temperature, which is 4077 ($^{\circ}\text{C}$). Since both I and T_a changes with time of the day, the total energy should be calculated by integrating solar irradiance over small time intervals.

Exergy analysis of a thermal solar collector

Exergy is defined as the heat energy that can be used from the solar collector with the help of the fluids (air, water) flowing inside the solar collector. Before calculating the exergy we have to calculate the energy stored and lost in the process.

Energy stored in the solar collector

The energy stored in solar collector will be the energy gained by the absorber plate, energy gained by the water present in the storage tanks and energy gained by the air present inside the solar collector. The stored energy can be calculated using equation (3) given by Hanif *et al.* (2018).

$$E_s = E_{abs} + E_w + E_a \quad \dots(3)$$

Where E_s represents the energy stored in solar collector (kJ), E_{abs} represents the energy stored by the absorber plate (kJ), E_w represents the energy stored by the water (kJ), and E_a represents the energy stored in the air inside the solar collector (kJ). Now we can determine each component in detail using a separate equation for the energy gained at each place. Firstly, we determine the energy gained by the absorber which can be calculated using equation (4) (Hanif *et al.*, 2015)

$$E_{abs} = m_{abs} C_{abs} \Delta T \quad \dots(4)$$

where E_{abs} represents the energy stored by the absorber plate (kJ), m_{abs} represents the mass of the absorber plate (kg), C_{abs} represents the specific heat of the absorber plate

($\text{kJ } ^{\circ}\text{C}^{-1} \text{ kg}^{-1}$), and ΔT is the difference between ambient and absorber temperature ($^{\circ}\text{C}$).

Secondly, the energy gained by the water is calculated using equation (5), given by Hanif *et al.* (2016),

$$E_w = m_w C_{pw} \Delta T \quad \dots(5)$$

where E_w represents the energy stored by water (kJ), m_w represents the mass of water (kg), C_w represents the specific heat of water ($\text{kJ } ^{\circ}\text{C}^{-1} \text{ kg}^{-1}$), and ΔT is the temperature rise of the water inside the solar collector ($^{\circ}\text{C}$).

Thirdly, the energy gained by the air inside the solar collector is given by equation (6) given by Islam *et al.* (2015),

$$E_a = m_a C_a \Delta T \quad \dots(6)$$

where E_a represents the energy stored by air (kJ), m_a represents the mass of air (kg), C_a represents the specific heat of air ($\text{kJ } ^{\circ}\text{C}^{-1} \text{ kg}^{-1}$), and ΔT is the temperature difference between ambient air and the air inside the solar collector ($^{\circ}\text{C}$).

Energy lost from the solar collector

Energy is lost from the solar collector in two ways. The first is due to the optical efficiency of the glazing and acceptance of the absorber plate and can be calculated using equation (7), given by Hanif *et al.* (2018),

$$E_{L1} = (\tau\alpha) I A_c T_a \left(\frac{1}{T_a} - \frac{1}{T_{abs}}\right) \quad \dots(7)$$

where E_{L1} is the energy lost by glazing due to transmittance and absorbance of the absorber plate (kJ), τ is the transmittance of the glazing, α is the absorbance of the absorber plate, I is solar irradiance (kJ. m^{-2}), A_c is area of the solar collector (m^2), T_a is the ambient air temperature ($^{\circ}\text{C}$), and T_{abs} is absorber temperature ($^{\circ}\text{C}$).

The second factor that affects the heat lost is the insulation characteristic. The heat lost through insulation can be calculated using equation (8) given by Jafarkazemi *et al.* (2013),

$$E_{L2} = \{U_i A_{abs} (T_{abs} - T_a) \left(1 - \frac{T_a}{T_{abs}}\right)\} \quad \dots(8)$$

where E_{L2} is energy lost by the solar collector due to insulation characteristics (kJ), U_i is the coefficient of the rate of energy lost from the insulation to the surroundings ($\text{kJ m}^{-2} \text{ } ^{\circ}\text{C}^{-1}$), A_{abs} is an area of the absorber

(m²), T_a is ambient air temperature (°C), and T_{abs} is absorber temperature (°C)

Exergy of the solar collector

The exergy of a solar collector can be calculated using equation (9) given by Koca *et al.* (2008),

$$E_{ex} = m_f C_{pa} \Delta T \quad \dots(9)$$

where E_{ex} is the rate of exergy of the solar collector (kJ hr⁻¹), m_f is the mass flow rate of air delivered by the blower (kg hr⁻¹), C_{pa} is the specific heat of air (kJ °C⁻¹ kg⁻¹), and T is the difference in the temperatures of ambient air and air at the outlet (°C).

Mass flow rates were determined using the continuity equation as used by Hanif *et al.*, (2018). Mass flow rates are obtained by taking the product of air velocity at outlet, density of air and outlet area. To find the mass flow rate (m_p), an anemometer (Extech, AN100, USA) will be used to find the velocity of air at the outlet.

Efficiency of a thermal solar collector

The Performance of the solar collector is measured in terms of its energy and exergy. It is the ratio of energy and exergy of the solar collector. Equation (10) is used to find the efficiency of the solar collector and is given by Hanif *et al.* (2018),

$$\eta = x \times 100 \quad \dots(10)$$

where η represents the efficiency of the solar collector (%), m_f is the mass flow rate of air (kg hr⁻¹), C_{pa} is the specific heat of air (kJ °C⁻¹ kg⁻¹), ΔT is the difference between the temperatures of ambient air and air at the outlet, (°C), I is solar irradiance (kJ m⁻² hr⁻¹), A_c is the area of the solar collector (m²), T_a is the ambient air temperature (°C), and T_s is the apparent surface temperature of the Sun, which is 4077 °C.

Data loggers

Data loggers (Mastech, MS6514, USA) that will record the air temperature at the inlet, outlet, and absorber plate were installed on the solar collector. The water temperature in the storage tank and drying chamber tank was measured with the help of mercury thermometers. The data were collected during a clear sky having a C.S.I (Clear Sky Index) of more than 70000 Lux at the time of data recording, with the help of a Luxmeter

(Extech, 401025, USA). After evaluating the optimum combination of all the factors for maximum efficiency of the solar collector, the setup was installed and tested.

Statistical analysis

The data were analyzed using three factors in a completely randomized design. The first factor was tilt angle with three levels, second factor was air mass flow rates with four levels and third was heat storage fluid with four levels, making a 4 x 3 x 4 factorial experiment. All the treatments were replicated three times. Least significant difference between means was calculated with $\alpha < 0.01$. The experimental factor and their levels are as given below.

- a. Factor 1: Flow rates (F)
F1(natural or passive) 0.1 m.s⁻¹, F2 1.31 m.s⁻¹, F3 2.72 m.s⁻¹ and F4 3.31 m.s⁻¹
- b. Factor 2: Tilt angles (T)
T1 (30°), T2 (35°), and T3 (40°)
- c. Factor 3: Heat storage fluid (H)
H1 (air or control), H2 (water), H3 (concentrated salt solution), and H4 (polyethylene glycol)

RESULTS AND DISCUSSIONS

Diffused daily solar irradiance

Mean daily diffused solar irradiance at the site for the experimental period is shown in Figure 4. During day time, maximum solar irradiance was recorded at noon. The data show that mean maximum solar irradiance of 902 W m⁻² were recorded at noon followed by 891 W m⁻² at 1:00 pm while the minimum solar irradiance of 209 W m⁻² was recorded at 6:00 pm followed by 212 W m⁻² at 6:00 am. From the mean values of solar irradiance, the solar noon was found to be around 12:35 to 12:37 pm. The correlation equation showed a positive correlation with $R^2 = 0.950$. The R^2 showed that there is a strong relationship of solar irradiance with time of the day. The reduced Chi Square test showed that there is a perfect correlation found between solar irradiance and time of the day. The test also showed that the shape of the solar irradiance is nearly a bell shaped structure having a σ (sigma) value of 0.91. The results are in line with the findings of Mouna *et al.* (2014). The results are 1.1% less than the findings of Hanif *et al.* (2018). This may be due to air turbidity which increased in 2017 and 2018 as reported by Mamata *et al.* (2017).

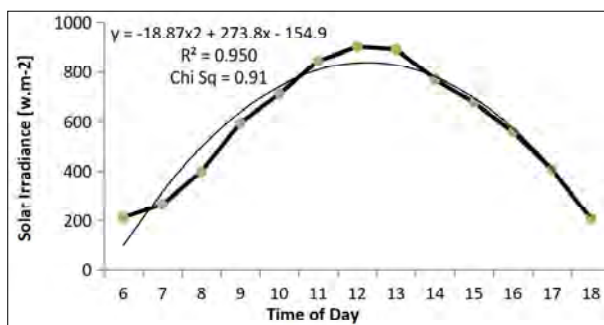


Figure 4: Daily diffused solar irradiance at the site

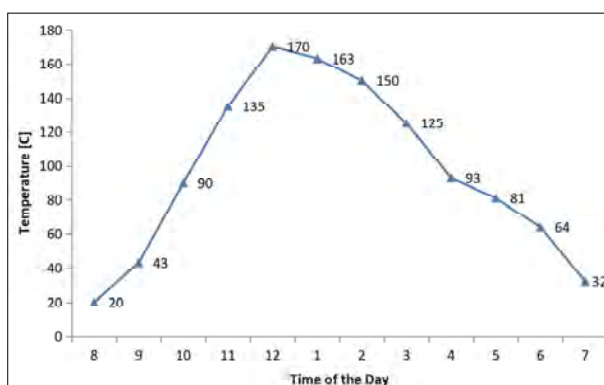


Figure 5: Average temperature of the absorber plate

Temperature of absorber plate

The average temperature data of the absorber plate and the dryer assembly is given in Figure 5. The minimum absorber plate temperature of 20 °C was recorded at 8:00 am followed by 32 °C at 7:00 pm while a maximum temperature of 170 °C was recorded at 12:00 noon followed by 163 °C recorded at 1:00 pm. Hanif *et al.* (2018) reported the same increase in temperature of the absorber plate. Hanif *et al.* (2016; 2018) reported 33 and 30% less values of absorber temperature. The fact is that they used small collectors having absorber area of 3.1 and 4.23 m².

Energy gained by the flat plate solar collector

Statistical analysis of the data showed that all three factors, *i.e.*, tilt angle, collector air flow rates, and collector fluid used as medium, have a significant ($\alpha \leq 0.05$) effect on the energy gained by the flat plate solar collector. All the interaction between the tilt angle and air flow rates, tilt

angle and collector fluids, air flow rates and collector fluids, and tilt angle, air flow rates, and collector fluids also significantly affected the energy gained by the flat plate solar collector.

The results of the energy gained (kJ hr⁻¹) by the flat plate solar collector as affected by tilt angles (degrees), air flow rates (kg min⁻¹), collector fluids and all the interaction between these factors is given in Table 2. The results of the means of tilt angle showed that the maximum energy of 1156.02 kJ hr⁻¹ was recorded at a tilt of 35° followed by 1153.20 kJ hr⁻¹ at 30° while the minimum energy of 1150.33 kJ hr⁻¹ was recorded at tilting the collector at 40°. The results of the means of air flow rates showed that the maximum energy of 1325.02 kJ hr⁻¹ was recorded for an air flow rate of 11.76 kg min⁻¹ followed by 1292.81 kJ hr⁻¹ of energy at 9.69 kg min⁻¹ while the minimum energy gained of 950.17 kJ hr⁻¹ was recorded for an air flow rate of 1.78 kg min⁻¹. The results of means of fluids flowing in the raiser head pipes of the flat plate solar collector showed that the maximum energy gained by the collector of 1297.31 kJ hr⁻¹ was recorded for polyethylene glycol, followed by 1233.61 kJ hr⁻¹ for salt solution, while the minimum energy gained of 941.93 kJ hr⁻¹ was recorded for air as the flowing medium without any fluid in the head riser pipes.

With regard to interaction effects, the means of interaction between tilt angles and air flow rates (T x F) showed that the maximum energy of 1331.11 kJ hr⁻¹ was gained by the flat plate solar collector at 11.76 kg min⁻¹ air flow rate with a 35° collector tilt angle, while the minimum energy gained of 947.63 kJ hr⁻¹ was recorded at 1.78 kg min⁻¹ air flow rate with the collector tilting at 35°. The means of interaction between air flow rates and collector fluid (F x H) showed that the maximum energy of 1500.33 kJ hr⁻¹ was gained by the flat plate solar collector at 11.76 kg min⁻¹ air flow rate with polyethylene glycol solution used as collector fluid while the minimum energy gained of 756.07 kJ hr⁻¹ was recorded at 1.78 kg min⁻¹ air flow rate with no fluids in the collector head riser pipe. The means of interaction between tilt angles and collector fluid (T x H) showed that the maximum energy of 1301.99 kJ hr⁻¹ was gained by the collector when polyethylene glycol solution was used in head riser pipes with a 30° collector tilt angle, while the minimum energy gained of 938.38 kJ hr⁻¹ was recorded with air only flowing in the solar collector without any fluids in head raised pipes, and with the collector tilting at 40°. The means of overall interaction between tilt angles, flow rates and collector fluid (T x F x H) showed that the maximum energy of 1509.74 kJ hr⁻¹ was gained

by the collector when polyethylene glycol solution was used in head raised pipes at $11.76 \text{ kg min}^{-1}$ air flow rates with a 30° collector tilt angle, while the minimum energy gained of $751.39 \text{ kJ hr}^{-1}$ was recorded with air only flowing in the solar collector, without any fluids in head raised pipes, at 1.78 kg min^{-1} with the collector

tilting at 35° . Hanif *et al.* (2018) reported results in line with the findings of this research. Sabet *et al.* (2014) also reported results in line with the findings of this research. Hanif *et al.* (2016) reported results of energy less than the findings of this research because of the fact that they have not used any energy storage medium.

Table 2: Energy gained (kJ hr^{-1}) by the flat plate solar collector as affected by tilt angles (degrees), air flow rates (kg min^{-1}) and collector fluids.

		Collector fluids				Mean
		Air/control	Water	Salt solution	Polyethileneglycol	
Tilt Angles	Flow rates		T x F x H		T x F	
30°	1.78	760.07	964.05	1001.52	1082.97	952.15
	4.67	839.64	1020.47	1145.18	1162.25	1041.88
	9.69	1091.22	1249.05	1370.57	1453.02	1290.96
	11.76	1077.04	1315.02	1409.34	1509.74	1327.78
35°	1.78	751.39	985.03	1007.02	1047.09	947.63
	4.67	871.03	1011.65	1145.90	1169.05	1049.41
	9.69	1075.59	1275.67	1366.52	1465.90	1295.92
	11.76	1083.55	1325.14	1417.44	1498.31	1331.11
40°	1.78	756.75	936.71	1030.75	1078.63	950.71
	4.67	868.28	1017.4	1122.03	1163.84	1042.90
	9.69	1070.67	1253.97	1397.62	1443.91	1291.54
	11.76	1057.80	1324.56	1389.37	1492.96	1316.17
Tilt Angles			T x H			
	30°	941.99	1137.15	1231.65	1301.99	1153.20b
	35°	945.39	1149.37	1234.22	1295.09	1156.02a
	40°	938.38	1133.17	1234.94	1294.83	1150.33c
Flow rates (kg min^{-1})			F x H			
	1.78	756.07	961.93	1013.10	1069.56	950.17d
	4.67	859.65	1016.52	1137.70	1165.04	1044.73c
	9.69	1079.16	1259.56	1378.23	1454.28	1292.81b
	11.76	1072.81	1321.57	1405.38	1500.33	1325.02a
Mean		941.93d	1139.90c	1233.61 b	1297.31a	

Means followed by different letter (s) within each category are significantly ($\alpha \leq 0.05$) different using the LSD test

LSD_(0.05) for T = 1.09, LSD_(0.05) for F = 45.61, LSD_(0.05) for H = 43.21

T x F = * ; T x H = * ; F x H = * ; T x F x H = *

* Significant at 1% level of probability

Exergy analysis of the flat plate solar collector

Statistical analysis of the data showed that all three factors, *i.e.*, tilt angle, collector air flow rates, and collector fluid used as medium, have a significant ($\alpha \leq 0.05$) effect on the total potential or exergy efficiency of the flat plate

solar collector. All the interactions, between the tilt angle and air flow rates, tilt angle and collector fluids, air flow rates and collector fluids, and tilt angle, air flow rates, and collector fluids—also significantly affected the exergetic efficiency of the flat plate solar collector.

Table 3: Exergy efficiency (%) of flat plate solar collector as affected by tilt angles (degrees), air flow rates (kg min^{-1}) and collector fluids

		Collector fluids				
		Air/control	Water	Salt solution	Polyethylene glycol	Mean
Tilt angles	Flow rates	T x F x H	T x F			
30°	1.78	42.33	36.07	33.94	32.67	36.25
	4.67	46.00	45.00	37.33	35.67	41.00
	9.69	44.17	40.53	35.64	34.17	38.63
	11.76	44.17	40.53	35.64	34.17	38.63
35°	1.78	44.78	42.02	36.20	34.67	39.42
	4.67	44.37	41.03	35.83	34.33	38.89
	9.69	44.44	41.20	35.89	34.39	38.98
	11.76	44.53	41.42	35.97	34.46	39.09
40°	1.78	44.45	41.21	35.90	34.40	38.99
	4.67	44.47	41.27	35.92	34.42	39.02
	9.69	44.48	41.30	35.93	34.42	39.03
	11.76	44.47	41.26	35.91	34.41	39.01
Tilt angles		T x H				
	30°	44.17	40.53	35.64	34.17	38.63c
	35°	44.53	41.42	35.97	34.46	39.09a
	40°	44.47	41.26	35.91	34.41	39.01b
Flow rates (kg min ⁻¹)		F x H				
	1.78	43.85	39.77	35.35	33.91	38.22c
	4.67	44.95	42.43	36.36	34.81	39.64a
	9.69	44.36	41.01	35.82	34.33	38.88b
	11.76	44.37	41.11	35.84	34.35	38.91ab
Mean		44.39 a	41.07b	35.81c	34.32d	

Means followed by different letter (s) within each category are significantly ($\alpha \leq 0.05$) different using the LSD test

LSD_(0.05) for T = 0.03, LSD_(0.05) for F = 0.16, LSD_(0.05) for H = 3.01

T x F = *; T x H = *; F x H = *; T x F x H = *; T x F x H = *

* Significant at 1% level of probability

The results of the exergy analysis of the flat plate solar collector as affected by tilt angles (degrees), air flow rates (kg min^{-1}), collector fluids and all the interaction between these factors is given in Table 3. The results of the means of tilt angle showed that the maximum exergy efficiency of 39.09 % was recorded at the tilt of 35° followed by 39.01 % at 40° , while the minimum exergy efficiency of 38.63 % was recorded at tilting the collector at 30° . The results of the means of air flow rates showed that the maximum exergy efficiency of 39.64 % was recorded for an air flow rate of 4.67 kg min^{-1} followed by 38.91% at $11.76 \text{ kg min}^{-1}$, while the minimum exergy efficiency of 38.22 % was recorded for an air flow rate of 1.78 kg min^{-1} . The results of means of fluids flowing in the head riser pipes of the collector showed that the maximum exergy efficiency gained by the collector was 44.39 % recorded for air without any medium in the pipes, followed by 41.07 % for water, while the minimum exergy efficiency of 38.22 % was recorded for polyethylene glycol solution as a flowing medium in the head riser pipes.

With regard to interaction effects, the means of interaction between tilt angles and air flow rates (T x F) showed that the maximum exergy of 41.0 % was gained by the flat plate solar collector at a 4.67 kg min^{-1} air flow rate with a 30° collector tilt angle, while the minimum exergy gained of 36.25 % was recorded at a 1.78 kg min^{-1} air flow rate with the collector tilting at 30° . The means of interaction between air flow rates and collector fluid (F x H) showed that the maximum exergy of 44.95 % was gained by the flat plate solar collector at a 4.67 kg min^{-1} air flow rate with air used as the collector fluid while the minimum exergy efficiency gained of 33.91 % was recorded at 1.78 kg min^{-1} air flow rate with polyethylene glycol used as the fluid in the flat plate solar collector head riser pipe. The means of interaction between tilt angles and collector fluid (T x H) showed that the maximum exergy of 44.53 % was gained by the flat plate solar collector when air was used with a 35° collector tilt angle, while the minimum exergy efficiency gained of 34.17 % was recorded for polyethylene glycol flowing in the solar collector head riser pipes with the collector tilting at 30° . The means of overall interaction between tilt angles, flow rates and collector fluid (T x F x H) showed that maximum exergy of 46.0 % was gained by the flat plate solar collector when air was used in the head riser pipes at 4.67 kg min^{-1} air flow rates with a 30° collector tilt angle, while the minimum exergy gained of 32.67% was recorded for a polyethylene glycol solution in the solar collector at 1.78 kg min^{-1} with the collector tilting at 30° . Silva *et al.* (2013) reported results in line with the findings of this research. Soteris *et al.* (2016) reported that exergy increase was a function of collector fluids,

which was confirmed by the results of the solar collector exergy gained in this research. Siva *et al.* (2012) reported less exergy gained by the flat plate solar collector. This was due to the smaller size of the solar collector used in their experiment.

Efficiency of the flat plate solar collector

Statistical analysis of the data showed that all three factors, *i.e.*, tilt angle, collector air flow rates, and collector fluid used as medium, have a significant ($\alpha \leq 0.05$) effect on the efficiency of the flat plate solar collector. All the interactions between the tilt angle and air flow rates, tilt angle and collector fluids, air flow rates and collector fluids, and tilt angle, air flow rates, and collector fluids also significantly affected the efficiency of the flat plate solar collector.

The results of the performance evaluation of the flat plate solar collector as affected by tilt angles (degrees), air flow rates (kg min^{-1}), collector fluids, and all the interaction between these factors are given in Table 4. The results of the means of tilt angle showed that the maximum efficiency of 29.74 % was recorded at the tilt of 40° followed by 28.16 % at 35° tilt while the minimum efficiency of 21.77 % was recorded when tilting the collector at 30° . The results of the means of air flow rates showed that the maximum efficiency of 28.28% was recorded for air flow rate of $11.76 \text{ kg min}^{-1}$ followed by 27.64 % at 9.69 kg min^{-1} , while the minimum efficiency of 25.01 % was recorded for air flow rates of 1.78 kg min^{-1} . The results of means for fluids flowing in the head riser pipes of the collector showed that the maximum efficiency obtained by the collector was 29.90 % recorded for polyethylene glycol solution used as a medium in the pipes, followed by an efficiency of 28.36 % for salt solution, while the minimum efficiency of 21.70 % was recorded for air or without any medium in the head riser pipes.

With regard to interaction effects, the means of interaction between tilt angles and air flow rates (T x F) showed that the maximum efficiency of 36.17 % was gained by the flat plate solar collector at a $11.76 \text{ kg min}^{-1}$ air flow rate with 35° collector tilt angle while the minimum efficiency gained of 18.54 % was recorded at 1.78 kg min^{-1} air flow rate with the collector tilting at 30° . The means of interaction between air flow rates and collector fluid (F x H) showed that the maximum efficiency of 31.08% was recorded by the flat plate solar collector at $11.76 \text{ kg min}^{-1}$ air flow rate when polyethylene glycol solution was used as the collector fluid, while the minimum efficiency gained of 18.61% was recorded

at a 1.78 kg min^{-1} air flow rate when air was used as the fluid in the flat plate solar collector. The means of interaction between tilt angles and collector fluid (T x H) showed that maximum efficiency of 34.14 % was gained by the flat plate solar collector when polyethylene glycol solution was used with a 40° collector tilt angle, while the minimum efficiency gained of 17.92 % was recorded for air flowing in the solar collector with the collector tilting at 30° . The means of overall interaction between tilt angles, flow rates and collector fluid (T x F x H) showed that the maximum efficiency of 39.71% was gained by the flat plate solar collector when polyethylene

glycol solution was used in the head riser pipes at a 9.69 kg min^{-1} air flow rate, with a 40° collector tilt angle, while the minimum efficiency gained of 13.71 % was recorded for air in the solar collector at 1.78 kg min^{-1} with the collector tilting at 30° . Tian *et al.* (2013) and Wang *et al.* (2008) reported results in line with the findings of this research. However, Hanif *et al.* (2018) reported efficiency results with the fluids used in contradiction of the results obtained in this research. The fact was that they used a lower concentration of salt in the solution, while using tap water with high impurities.

Table 4: Overall efficiency (%) of flat plate solar collector as affected by tilt angles (degree), air flow rates (kg min^{-1}) and collector fluids

		Collector Fluids				
		Air/control	Water	Salt solution	Polyethyleneglycol	Mean
Tilt angles	Flow rates	T x F x H				T x F
30°	1.78	13.71	19.18	19.39	21.89	18.54
	4.67	19.18	24.84	27.6	28.63	25.06
	9.69	19.38	22.47	23.04	23.53	22.10
	11.76	19.41	20.97	22.09	23.12	21.39
35°	1.78	20.49	28.22	33.27	33.89	28.96
	4.67	19.52	21.02	23.28	23.53	21.83
	9.69	23.18	22.44	28.77	28.31	25.67
	11.76	29.78	37.42	38.13	39.36	36.17
40°	1.78	21.63	27.24	28.37	32.85	27.52
	4.67	23.26	29.66	29.9	33.25	29.01
	9.69	28.86	33.71	38.28	39.71	35.14
	11.76	22.04	28.00	28.27	30.75	27.26
Tilt Angles		T x H				
	30°	17.92	21.86	23.03	24.29	21.77 c
	35°	23.24	27.27	30.86	31.27	28.16 b
	40°	23.94	29.65	31.21	34.14	29.74 a
Flow rates (kgmin^{-1})		F x H				
	1.78	18.61	24.88	27.01	29.54	25.01 d
	4.67	20.65	25.17	26.93	28.47	25.31 c
	9.69	23.81	26.21	30.03	30.52	27.64 b
	11.76	23.74	28.80	29.49	31.08	28.28 a
Mean		21.70d	26.26c	28.36b	29.90a	

Means followed by different letter(s) within each category are significantly ($\alpha \leq 0.05$) different using the LSD test

LSD_(0.05) for T = 0.023, LSD_(0.05) for F = 0.011, LSD_(0.05) for H = 0.021

T x F = * ; T x H = * ; F x H = * ; T x F x H = *

* Significant at 1% level of probability

The role of the energy storage unit in storing energy in the solar collector

The role of the energy storage unit to store energy in the flat plate solar collector is shown in Figure 6. The statistical analysis of the data (Appendix E) showed that there is significant ($\alpha \leq 0.05$) difference found in the values of energy stored by different fluids. The results showed that the maximum energy of 40,207 kJ day⁻¹ was stored in the energy storage unit followed by 33,291 kJ day⁻¹ stored by the salt solution, while the minimum energy of 29,640 kJ day⁻¹ was stored with water. Energy storing ability varies for each fluid used in the solar collector. They play a vital role in increasing the efficiency and exergy. This energy stored by the energy storage unit helped the solar collector to achieve higher performance, less energy loss, and more drying time. The results are in accordance with the findings of Zhong *et al.* (2014). The results are more significant than those of Yahya *et al.* (2000) and Hanif *et al.* (2018), because of the fact that a larger collector absorber was used as compared to the size of their solar collectors. Tian *et al.* (2013) reported results in accordance with the findings of this research. They stated that energy storage can be increased with increasing flow rates of the solar collectors.

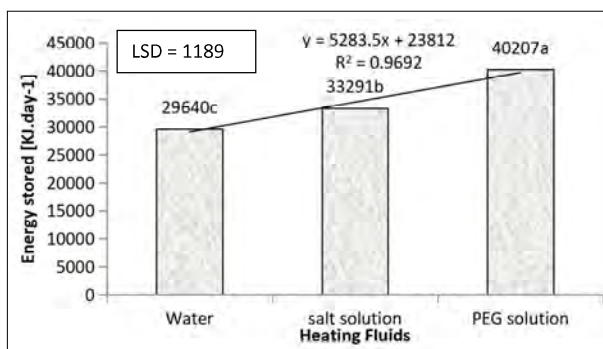


Figure 6: The energy stored by the fluids in the flat plate solar collector

CONCLUSIONS

From the results of the research study it was concluded that

1. Tilt angle, air mass flow rates and heat storage fluid played a vital role in increasing the efficiency of the solar collector when analyzed as factors in three factors in a completely randomized design.
2. A solar collector with fluids used as a medium of storage gives higher efficiencies of energy and exergy as compared to air used as a medium.

3. Polyethylene glycol is the best solution to increase performance of a solar collector.
4. The flat plate solar collector must be operated at higher air flow rates with 40° tilt to achieve maximum performance with higher exergetic values.
5. More energy is stored by polyethylene glycol when used as fluid in the flat plate solar collector.

REFERENCES

- Bellos E., Christos T. & Antonopolus A. (2016). Exergetic, energetic and financial evaluation of a solar driven absorption cooling system with various collector types. *Journal of Applied Thermal Engineering* **102**(3): 749–759. DOI: <https://doi.org/10.1016/j.applthermaleng.2016.04.032>
- Boukelia T., Macibah M. & Reddy S. (2015). Investigation of solar parabolic trough power plants with and without integrated TES (thermal energy storage) and FBS (fuel backup system) using thermic oil and solar salt. *Energy* **88**(1): 292–303. DOI: <https://doi.org/10.1016/j.energy.2015.05.038>
- Fahad A & Sulaiman A.L. (2013). Exergy analysis of parabolic trough solar collectors integrated with combine steam and organic Rankine cycle. *Energy Conversion and Management* **77**(2): 441–449. DOI: <https://doi.org/10.1016/j.enconman.2013.10.013>
- Farhat S., Sarhadi F. & Ajam. H. (2009). Exergetic optimization of flat plate solar collectors. *Renewable Energy* **34**(3): 1169–1174. DOI: <https://doi.org/10.1016/j.renene.2008.06.014>
- Frances C., Polombo A. & Vanoli L. (2012). A finite-volume model of a parabolic trough photovoltaic/thermal collector: Energetic and exergetic analyses. *Energy* **46**(1): 283–294. DOI: <https://doi.org/10.1016/j.energy.2012.08.021>
- Francesco D., Massimo D. & Adriano M. (2016). Exergetic and exergoeconomic analysis of a novel hybrid solar-geothermal poly generation system producing energy and water. *Energy Conversion and Management* **115**(1) : 200–220. DOI: <https://doi.org/10.1016/j.enconman.2016.02.029>
- Govindaraj K., Rahulram S. & Vilraj R. (2012). Performance studies of a solar parabolic trough collector with a thermal energy storage system. *Energy* **47**(2): 395–402. DOI: <https://doi.org/10.1016/j.energy.2012.09.036>
- Hanif M., Khattak M.K., Ali S.A., Khan M., Ramzan M., Amin M. & Aamir M. (2015). Impact of drying temperature and slice thickness on retention of vitamin C in persimmons (*Diospyros Kaki*. L) Dried by a flat plate solar collector. *Pakistan Journal of Food Sciences* **25**(2): 66–70.
- Hanif M., Khattak M.K., Amin M., Ramzan M., Zakir S., Ullah S. & Khan Z. (2016). Developing a flat plate solar collector for drying and water heating purposes. *Sains Malaysiana* **45**(3): 89–497.
- Hanif M., Khattak M.K., Ramzan M. & Maazullah K. (2018). Energy, exergy and efficiency analysis of a flat plate solar collector. *Sains Malaysiana* **47**(6): 1061–1067. DOI: <https://doi.org/10.17576/jsm-2018-4705-24>

- Islam S., Ibrahim D. & Sami Y. (2015). Energetic and exergetic performance analyses of a solar energy-based integrated system for multi generation including thermoelectric generators. *Energy* **93**(6): 1246–1258.
DOI: <https://doi.org/10.1016/j.energy.2015.09.111>
- Jafarkazemi F. & Ahmadifard E. (2013). Energetic and exergetic evaluation of flat plate solar collectors. *Renewable Energy*. **56**(1): 55–63.
DOI: <https://doi.org/10.1016/j.renene.2012.10.031>
- Koca A., Hakan F., Koyun T. & Varol Y. (2008). Energy and exergy analysis of a latent heat storage system with phase change material for a solar collector. *Renewable Energy* **33**(4): 567–574.
DOI: <https://doi.org/10.1016/j.renene.2007.03.012>
- Mamta S., Singha G.K. and Sainib R.P. (2017). Effects of air pollution for estimating global solar radiation in India. Effects of air pollution for estimating global solar radiation in India. *International Journal of Sustainable Energy* **36**(1): 20–27.
DOI: <https://doi.org/10.1080/14786451.2014.979348>
- Mouna H., Snoussi A. & Brahim A.B. (2014). Energy and exergy analysis of flat plate solar collectors in transient behaviors. *The fifth International Renewable Energy Congress IREC*. 2014. March 25-27, Hammamet, Tunisia. Applied Thermodynamic Research Unit, Engineers National School of Gabes, University of Gabes, 6072 Gabes, Tunisia.
- Sabet A., Rahini A. & Hatamipour M.S. (2014). An experimental study on drying characteristics and kinetics of figs. *Polish Journal of Chemical Technology* **16**(1): 60–65.
DOI: <https://doi.org/10.2478/pjct-2014-0071>
- Silva R., Berenguel M., Perez M. & Fernandez A. (2013). Thermo-economic design optimization of parabolic trough solar plants for industrial process heat applications with memetic algorithms. *Applied Energy* **113**(3): 603–614.
DOI: <https://doi.org/10.1016/j.apenergy.2013.08.017>
- Siva V., Kaushik S.C. & Tyagi S.K. (2012). Exergetic analysis and performance evaluation of parabolic trough concentrating solar thermal power plant. *Energy* **39**(1): 258–273.
DOI: <https://doi.org/10.1016/j.energy.2012.01.023>
- Soteris A.K., Karellas S., Badescu V. & Braimakis K. (2016). Exergy analysis on solar thermal systems: A better understanding of their sustainability. *Renewable Energy* **85**(6): 1328–1333.
DOI: <https://doi.org/10.1016/j.renene.2015.05.037>
- Tian Y. & Zhao C.Y. (2013). A review of solar collectors and thermal energy storage in solar thermal applications. *Applied Energy* **104**(3): 538–553.
DOI: <https://doi.org/10.1016/j.apenergy.2012.11.051>
- Wang Z., Sun J., Liao X., Chen F., Zhao G., Wu J. & Hu X. (2008). Mathematical modeling of hot air drying of thin layer apple. *Food Research International* **40**(1): 39–46.
DOI: <https://doi.org/10.1016/j.foodres.2006.07.017>
- Yadav S., Kaushal M., Varun M. & Siddhartha S. (2014). Exergetic performance evaluation of solar air heater having arc shape oriented protrusions as roughness element. *Solar Energy* **105**(1): 181–189.
DOI: <https://doi.org/10.1016/j.solener.2014.04.001>
- Yahya M.G., Yahya S.A. & Faiz K.B. (2000). Preservation of fruits and vegetables using solar drier. *Renewable Energy* **19**(1): 203–212.
DOI: [https://doi.org/10.1016/S0960-1481\(99\)00032-4](https://doi.org/10.1016/S0960-1481(99)00032-4)
- Zhong G., Wang H., Hua W., Zhang S. & Guan X. (2014). Exergy analysis of flat plate solar collectors. *Entropy* **16**(6): 2549–2567.
DOI: <https://doi.org/10.3390/e16052549>



JOURNAL OF THE NATIONAL SCIENCE FOUNDATION OF SRI LANKA

GUIDANCE TO CONTRIBUTORS

GENERAL INFORMATION

Scope

The Journal of the National Science Foundation of Sri Lanka publishes the results of research in all aspects of Science and Technology. It is open for publication of Research Articles, Reviews, Research Communications and Correspondence.

Categories of manuscripts

Research Articles: Research Articles are papers that present complete descriptions of original research. Research Articles should include an Abstract, Keywords, Introduction, Methodology, Results and Discussion, Conclusion and Recommendations where relevant. References should be prepared according to the “Guidelines for the preparation of manuscripts”. Maximum length of the article should be limited to 25 pages with a word count of 10,000 including references, figures and tables. Any articles above this limit will be returned.

Reviews: Reviews are critical presentations on selected topics of Science or Technology. They should be well focused and organized and avoid general “textbook” style. As reviews are intended to be critical presentations on selected topics, reviewers need to have had substantial leadership in research supported by a publication track record in the areas covered by the review. A person/s wishing to submit a Review Article should obtain prior approval from the Editorial Board by submitting a concise summary of the intended article, along with a list of the author’s publications in the related area (jnsf@nsf.gov.lk). Maximum length of the article should be limited to 40 pages with a word count of 12,000 including references, figures and tables. Any articles above this limit will be returned.

Research Communications: Research Communications are intended to communicate important new findings in a specific area of limited scope that are worthy of rapid dissemination among the scientific community. The article should include an Abstract, Keywords, Introduction, Methodology, Results & Discussion, Conclusion and References. Maximum length of the article should be limited to 10 pages with a word count of 2,500 including references, figures and tables. Any articles above this limit will be returned.

Correspondence: Correspondence will be accepted regarding one or more articles in the preceding four issues of the Journal, as well as Letters to the Editor. Articles covering important scientific events or any other news of interest to scientists, reviews of books of scientific nature, articles presenting views on issues related to science and scientific activity will also be considered. Publication will be made at the discretion of the Editor-in-Chief. Maximum length of the article should be limited to 05 pages with a word count of 1,500 including references, figures and tables. Any articles above this limit will be returned.

SUBMISSION OF MANUSCRIPT

Authors submitting articles to the JNSF should first create an account in the Sri Lanka Journals Online System (<https://jnsfsl.sljol.info/>). All manuscripts in MS Word format must be electronically submitted to the journal’s online platform at <https://jnsfsl.sljol.info/submit/start/>. Submissions via emails are not encouraged. Please make sure that no author information is mentioned in the article submitted. The names and details of affiliations of all authors and contact information of the corresponding author must be fed into the system during the online submission process. Authors (at least the corresponding author) are required to provide their personal, validated ORCID ID (by obtaining an ORCID ID from <https://orcid.org/>) when submitting the manuscript. No change to the authors or order of authors will be accepted after the submission. All those who have made significant contributions should be listed as co-authors. The corresponding author should ensure that all contributing co-authors are included in the author list and have approved the final version of the paper and have agreed to its submission for publication.

All submissions should be in English. If the manuscript conforms to the guidelines specified, the date received will be the date that the manuscript was submitted to the online system.

Submissions are accepted for processing on the understanding that they will be reviewed and that they have not been submitted for publication elsewhere (including publication as a full paper or extended abstract as a part of Conference Proceedings). The JNSF does not accept manuscripts that have already been submitted to pre-print servers.

Suggesting potential reviewers by authors

The authors may suggest up to three names of referees when submitting their manuscript, in the Cover Letter space provided at the bottom of the page in the first stage of online submission. Referees should not be from the institution where the work was carried out and should not have been co-authors in previous publications. The address, institutional affiliation and e-mail of the suggested referees should be supplied. Please note that the JNSF is not bound to select all or any of the suggested referees for sending the manuscript for reviewing

Authorship

All authors designated as authors should be eligible for authorship. Those who have made a substantial contribution to the concept or design of the work; or acquisition, analysis or interpretation of data are recognized as Authors.

The corresponding author should be prompt and ensure adherence to timelines when responding to requests, queries and recommendation of reviewers conveyed by or on behalf of the Editor-in Chief and Editorial Board.

Supplementary materials

Any experimental data necessary to evaluate the claims made in the paper but not included in the paper should be provided as supplementary materials. Supplementary materials will be sent to the reviewers and published online with the manuscript if accepted. The supplementary materials should conform to Journal guidelines and should be uploaded as separate files. Authors should number Supplementary Tables and Figures as, for example, 'Supplementary Table S1'. Refer to each piece of supplementary material at the appropriate point(s) in the main article. Supplementary Materials may include description of the materials and methods, controls, or tabulated data presented in Tables or Figures, and programming codes.

Peer review

The manuscripts submitted to the JNSF will initially be screened by the Editorial Board and, if suitable, will be referred to at least two subject experts in the relevant field. The peer-review process of the JNSF is double-blind.

When revision of a manuscript has been requested, the revised manuscript should be submitted on or before the stated deadline. If the revised manuscript is not received on time, the manuscript will not be processed further. The authors' response to the comments of referees should be tabulated with the comment, response and the line number/s for reference. The decision of the Editorial Board shall be final.

Accepted papers are subject to editing. The date of acceptance will be the date when the Editorial Board has decided it to be acceptable for publication.

Article publication fee and complementary copies

A publication fee of US\$ 150 will be levied for each manuscript other than where the corresponding author is affiliated to a Sri Lankan Institute, to cover the publication cost.

A complimentary copy of the Journal issue carrying the respective article will be supplied to each of the authors.

Authors' declaration

When an article is accepted for publication, the authors are required to submit the Authors' Declaration signed by all the authors.

Copyright

Articles in JNSF are published under the Creative Commons License CC-BY-ND. This license permits use, distribution and reproduction of articles for commercial and non-commercial purposes, provided that the original work is properly cited and is not changed in anyway. The copyright of the article is with the National Science Foundation of Sri Lanka. Therefore, authors are requested to check with institution's copyright and publication policy before submitting an article to the JNSF. Authors secure the right to reproduce any material that has already been published or copyrighted elsewhere. When an article is accepted for publication, the authors are required to submit the Transfer of Copyright document signed by all the authors.

Post-publication corrections

The Editorial Board reserves the right to take action on publishing an erratum or corrigendum. If serious errors are identified in a published article, the Journal may consider a retraction or publishing a correction.

STRUCTURE OF MANUSCRIPT

Manuscript

The manuscript should be free of errors and prepared in single column, using double-spaced text of Times New Roman 12 font throughout with line numbers, leaving at least 2 cm margins on both sides, and liberal spacing at the top and bottom of each page. Pages should be numbered consecutively.-

a. Style

The paper should be written clearly and concisely. The style of writing should conform to scholarly writing. Slang, jargon, unauthorized abbreviations, abbreviated phrasings should not be used. In general, the impersonal form should be used. Poor usage of language will result in rejection of the manuscript during initial screening.

b. Layout

Manuscripts other than review articles should be generally organized as follows: Title, Abstract, Keywords, Introduction, Methodology, Results and Discussion, Conclusions and Recommendations (where relevant), Acknowledgements and References. Pages should be arranged in the following order:

Title page should include the title of manuscript, and no author information should be mentioned in the title page. If a major part of the research has been published as an abstract in conference proceedings, it should be cited as a footnote on the title page. Authors must also indicate the **general and specific research area** of the manuscript in the title page. In order to highlight the significance of the manuscript, authors are required to provide the following highlights in brief. (1) Why was this study conducted? (2) What are the new findings? (3) Possible applications of the findings. Please limit your answers to 25-30 words for each.

Title: Should accurately and concisely reflect the contents of the article.

Running title: Should be a shortened title (limited to a maximum of 50 characters) that could be printed at the top of every other page of the Journal article.

Abstract: Should be between 200 - 250 words for full length articles and written as a single paragraph. It should not contain any references and should be able to stand on its own. It should outline objectives and methodology together with important results and conclusions. A Review Article should carry a summary of not more than 300 words.

Keywords: Include a maximum of six keywords, which may include the names of organisms (common or scientific), methods or other important words or phrases relevant to the study.

Introduction: This should state the reasons for performing the work with a brief review of related research studies in the context of the work described in the paper. Objectives of the study should be clearly stated.

Materials and Methods: This section should give the details of how you conducted your study. New methods may be described in detail with an indication of their limitations. Established methods can be mentioned with appropriate references. Sufficient details should be included to allow direct repetition of the work by others. Where human subjects are involved, they should be referred to by numbers or fictitious names. A paper reporting the results of investigations on human subjects or on animals must include a statement to the effect that the relevant national or other administrative and ethical guidelines have been adhered to, and a copy of the ethical clearance certificate should be submitted. Methods of statistical analyses used should be mentioned where relevant.

Results and Discussion: Results: the results should be concisely and logically presented. Repetition of the same results in figures, tables or text should be avoided.

Discussion: data essential for the conclusions emerging from the study should be discussed. Long, rambling discussions should be avoided. The discussion should deal with the interpretation of results. It should logically relate new findings to earlier ones. Unqualified statements and conclusions not completely supported by data should be avoided.

Molecular sequence data, such as gene or rDNA sequences, genome sequences, metagenomic sequences etc. must be deposited in a public molecular sequence repository, such as GenBank, that is part of the International Nucleotide Sequence Database Collaboration (INSDC). The accession numbers obtained must be cited in the text, Table or on Figures of phylogenetic trees of the manuscript.

Conclusion: The conclusion should be brief, highlight the outcomes of the study and should be aligned with the objectives of the study. It should not contain references.

Conflict of interest statement: All authors should include a statement on conflict of interest disclosing any financial or other substantive conflicts of interest that may be construed to influence the results or interpretation of their research. All sources of financial support for the project should be disclosed.

Acknowledgement: Should be brief and made for specific scientific, financial and technical assistance only. If a significant part of the research was performed in an institution other than in those indicated by the authors' affiliations given in the title page, this fact should be acknowledged. All those who have made substantial contribution to the research but do not qualify to be authors should be acknowledged.

References :

All research work of other authors, when used or referred to or cited, should be correctly acknowledged in the text and in the References.

Citing references in the text:

- References to the literature must be indicated in the text and tables as per the Author-Year System, by the author's last name and year, in parenthesis (i.e. Able, 1997) or (Able & Thompson, 1998).
- Citation to work by more than two authors should be abbreviated with the use of *et al.* (i.e. Able *et al.*, 1997).
- Multiple publications by the same first author in the same year should be coded by letters, (i.e. Thompson, 1991a; b).
- Multiple citations should be made in chronological order and separated by a semi-colon, (i.e. Zimmerman *et al.*, 1986; Able *et al.*, 1997).
- Reference to unpublished work, work in preparation or work under review should be cited in italics as (*unpublished data*) or, with the author's initials and surname given; such works should not be included in the Reference section.
- Personal communications may be mentioned in the text with the date of communication as (*Personal communication*, 2 June 2000).

List of references:

- The list of References should be arranged in alphabetical order based on the last name of the first author.
- Names of all the authors should be given except when there are more than 10 authors. When there are more than 10 authors, only the name of the first author can be given followed by *et al.*
- All the initials of the author must be given after the last name and the year of publication should follow in parentheses.
- This should be followed by the full title of the referred publication.
- When journal articles are listed, the journal name should be given in full and in italics and followed by the volume number in bold type, issue number in parentheses and then the inclusive pages.
- Where there are several publications by the same author(s) and published in the same year they should be differentiated by adding a lower-case letter after the year. When books are listed, the order should be: author(s), year, book title, volume number, edition, pagination/ inclusive pages, publisher and place of publication. The book title should be in italics. When sections of a book are listed, the order should be: author(s) of chapter, year, title of the section, title of the book, edition, inclusive pages, publisher and place of publication.
- Digital object identifiers (DOIs) should be included for all references where available.
- References should only be cited as 'in press' if the paper has been accepted for publication.

Examples of correct forms of references are given below.

Journal Articles

Boutin C. & Harper J.L. (1991). A comparative study of the population dynamics of five species of *Veronica* in natural habitats. *Journal of Ecology* 79(01): 199 – 221.
DOI: <https://doi.org/10.2307/2260793>

Books

Burnham K.P. & Anderson D.R. (2002). *Model Selection and Multimodal Inference*, 2nd edition, pp. 488. Springer Science and Business Media, Inc., New York, USA.

Book Chapters

Hinrichsen R.A. & Holmes E.E. (2009). Using multivariate state-space models to study spatial structure and dynamics. In: *Spatial Ecology* (eds. R.S. Cantrell, C. Cosner & S. Ruan), pp. 145 – 166. CRC/ Chapman Hall, Florida, USA.
DOI: <https://doi.org/10.1201/9781420059861.ch8>

Edited Books

Kimati H., Amorim L., Rezende J.A.M., Bergamin Filho A. & Camargo L.E.A. (eds.) (2005). *Manual de Fitopatologia*, volume 2. Doenças das Plantas Cultivadas, 4th edition. Ceres, São Paulo, Brazil.

Conference Papers

Weaver D. (2002). Implementation of a learning management system using an integrated approach to professional development. In: Winds of change in the sea of learning. *Proceedings of the 19th Annual Conference of the Australasian Society for Computers in Learning and Tertiary Education (ASCILITE)* (eds. A. Williamson, C. Gunn, A. Young & T. Clear), volume 2, Auckland, New Zealand, 8-11 December. Unitec Institute of Technology, Auckland, New Zealand, pp. 711-720.

Agency Publications

U.S. Census Bureau (2009). *World Population: 1950 – 2050*. U.S. Census Bureau, Washington DC, USA.

Department of Health (2008). *Health Inequalities: Progress and Next Step* (pdf). Department of Health, London, UK. Available at http://PublicationsPolicyAndGuidance/DH_08_5307, Accessed 9 June 2008.

Other

Robinson L.J. (2003) Spatial scale and depletion models of farmland birds in a fragmented landscape. *PhD thesis*, University of Reading, Reading, UK.

Efford M.G. (2008). Density 4.3: software for spatially explicit capture-recapture. Available at <http://www.otago.ac.nz/density>, Accessed 15 March 2009.

Abbreviations and Symbols: Unless common, these should be defined when first used, and not included in the abstract. The SI System of units should be used wherever possible. If measurements were made in units other than SI, the data should be reported in the same units followed by SI units in brackets, e.g. 5290 ft (1610 m).

Formulae and Equations: Equations should be typewritten and quadruple spaced. They should be started on the left margin and the number placed in parentheses to the right of the equation.

Nomenclature: Scientific names of plants and animals should be printed in italics. In the first citation, genus, species and authority must be given. e.g. *Borassus flabellifer* Linn. In latter citations, the generic name may be abbreviated, for example, *B. flabellifer* L.

Tables and figures: Tables and Figures should be clear and intelligible and kept to a minimum, and should not repeat data available elsewhere in the paper. Any reproduction of illustrations, tabulations, pictures etc. in the manuscript should be acknowledged.

Tables: Tables should be numbered consecutively with Arabic numerals and placed at the appropriate position in the manuscript. If a Table must be continued, a second sheet should be used and all the headings repeated. The number of columns or rows in each Table should be minimized. Each Table should have a title, which makes its general meaning clear, without reference to the text. All Table columns should have explanatory headings. Units of measurement, if any, should be indicated in parentheses in the heading of each column. Vertical lines should not be used and horizontal lines should be used only in the heading and at the bottom of the table. Footnotes to Tables should be placed directly below the Table and should be indicated by superscript lower case italic letters (^a, ^b, ^c, etc.).

Figures: All illustrations are considered as figures, and each graph, drawing or photograph should be numbered consecutively with Arabic numerals and placed at the appropriate position in the manuscript. Any lettering to appear on the illustrations should be of a suitable size for reproduction and uniform lettering should be used in all the Figures of the manuscript. Scanned figures or photographs should be of high quality (**300 dpi**), to fit the proportions of the printed page (12 × 17 cm). Each figure should carry a legend so that the general meaning of the figure can be understood without reference to the text. Where magnifications are used, they should be stated.

Units of measurement

Length: km, m, mm, µm, nm

Area: ha, km², m²

Capacity: kL, L, mL, µL

Volume: km³, m³, cm³

Mass: t, kg, g, mg, µg

Time: year(s), month(s), wk(s),

d(s), h, min, s

Concentration: M, mM, N, %, g/L, mg/L, ppm

Temperature: °C, K

Gravity: x g

Molecular weight: mol wt

Others: Radio-isotopes: 32P

Radiation dose: Bq

Oxidation-reduction potential: rH

Hydrogen ion concentration: pH